ASPECTOS SEDIMENTOLÓGICOS E PETROLÓGICOS DOS *BEACHROCKS* DO ESTADO DO RIO GRANDE DO NORTE

por

MARCELA MARQUES VIEIRA

Tese apresentada ao Programa de Pós-Graduação em Geociências da UFRGS como requisito parcial para obtenção do título de Doutor

Orientador: Prof. Dr. Luiz Fernando De Ros

Banca Examinadora:

Prof. Dr[a]. Valderez P. Ferreira (UFPE/NEG-LABISE)
Dr. Rogério Schiffer de Souza (PETROBRAS/CENPES)
Prof. Dr[a]. Ana Maria Pimentel Mizusaki (UFRGS/IG/PPGGeo)

2005

"O que escrevo nasce do meu próprio amadurecimento, um trajeto de altos e baixos, pontos luminosos e zonas de sombra. Nesse curso entendi que a vida não tece apenas uma teia de perdas, mas nos proporciona uma sucessão de ganhos.
O equilíbrio da balança depende muito do que soubermos e quisermos enxergar."
Lya Luft

Aos meus pais,

Marinete e Orlando.

Aos meus filhos,

Eduardo e Fernando.

AGRADECIMENTOS

Ao **Prof. Dr. Luiz Fernando De Ros (UFRGS/IG/PPGGeo)**, pela confiança em mim depositada, pela atenção constante em todas as etapas deste trabalho e, acima de tudo, pela orientação segura e competente.

Ao **Prof. Dr. Francisco Hilário Rego Bezerra (UFRN/CCET/DG)**, pelo apoio dado em todas as etapas que antecederam o início do doutorado e pelas proveitosas sugestões feitas no decorrer do mesmo.

À **Geóloga Maria Rosilene Ferreira de Menezes (PETROBRAS/CENPES)**, pela forma afetuosa com que me acolheu em sua casa e pelo companheirismo e amizade demonstrados.

Àqueles que me ajudaram em diferentes etapas da confecção desta tese:

- **Prof. Dr. Alcides Nóbrega Sial (UFPE/DG/NEG-LABISE)**;

- **Dr. João Marcelo Medina Ketzer (PUCRS);**

- Professores Doutores **Jean Michel Legrand**, **Laécio Cunha de Souza**, **Narendra Kumar Srivastava**, **Raquel Franco de Souza Lima**, **Thomas Ferreira da Costa Campos** e **Vanildo Pereira da Fonseca (UFRN/CCET/DG)**;

- Geólogos **Adelbaldo de Oliveira Silva**, **Carlos Manuel de Assis Silva**, **Gerson José Salomoni Terra** e **Rodrigo Dias Lima (PETROBRÁS)**;

- Engenheiro **Francisco Antônio Vieira (CT-Gás);**

- Geólogos **Alexandre Ranier Dantas**, **Ivaldo Rodrigues da Trindade e Márcia Gomes da Silva**;

- Técnicos **Emanoel Maria de Morais** e **Fernando Antônio Feitosa (UFRN/CCET/DG)**;

- **Fernando Yoshizato**, aluno do Curso de Geologia da UFRN**.**

A **CAPES (Ministério da Educação)** pela concessão da bolsa PICDT.

Ao **Programa de Pós-Graduação em Geociências da UFRGS** e ao **Departamento de Geologia da UFRN** pelo apoio dado.

Àqueles que, nos momentos mais difíceis, deram a força necessária para que eu me fortalecesse e prosseguisse:

- Meus tios: **Maria José** (*in memoriam*), **Marilita**, **Marilena** e **Mário Henrique**;
- Minha irmã, **Fernanda**;
- Minha amiga, **Andréa**;
- Minha secretária, **Fátima**.

RESUMO

A maior parte dos *beachrocks* distribuídos ao longo das costas oriental e setentrional do Estado do Rio Grande do Norte (53% da espessura total) foi depositada na zona de ante-praia superior, representada pelas litofácies arenitos com estratificação cruzada tabular-planar e acanalada de média escala e arenitos conglomeráticos bioturbados por Skolithos. Conglomerados e arenitos com estratificação cruzada de baixo ângulo, depositados na zona de estirâncio, representam 31% das seções descritas. Os 16% restantes são atribuídos ao colapso de material sobrejacente como resultado de solapamento basal de falésias (conglomerados maciços), de transporte como tapetes de tração (conglomerados incipientemente estratificados) e de alto grau de alteração (arenitos maciços). Uma sucessão geral de fases diagenéticas pode ser reconhecida, nos *beachrocks* estudados, incluindo a precipitação de esmectita autigênica, cutículas micríticas, agregados radiais, franjas isópacas de cristais prismáticos, espato equante, cimento criptocristalino de preenchimento de poros e agregados pseudo-peloidais, bem como a infiltração vadosa de sedimentos micríticos, margosos ou sílticos. A ausência de estruturas orgânicas, tais como filamentos e corpos microbiais (bactérias ou fungos), dentro dos cimentos, sugere que o mecanismo por trás da cimentação é essencialmente inorgânico, muito provavelmente devido à evaporação de água do mar, em resposta às condições climáticas secas prevalecentes. Os valores de $\delta^{13}C_{VPDB}$ máximo, mínimo e médio obtidos para os cimentos são +3.57, –7.8 e +2.34‰, respectivamente. Os valores de $\delta^{18}O_{SMOW}$ e $\delta^{18}O_{VPDB}$ variam de 26.32 a 31.41 (valor médio: 30.64) e de –4.41 a 0.54‰ (valor médio: –0.22‰), respectivamente. A maior parte dos valores de $\delta^{18}O_{VPDB}$ e $\delta^{13}C_{VPDB}$ é compatível com os de cimentos marinhos. Algumas amostras apresentam valores de $\delta^{18}O$ fortemente negativos, o que provavelmente reflete uma origem a partir de uma mistura de águas marinhas e meteóricas ou recristalização do cimento marinho através da interação com águas meteóricas. As temperaturas de precipitação assumindo $\delta^{18}O_{VPDB}$ da água igual a 2,0 (água do mar modificada por evaporação) e -2,0 (água mista, em boa parte meteórica) variam de 23,3 a 34,9^{o}C (valor médio: 25,8^{o}C).

ABSTRACT

Most of the beachrocks distributed along the eastern and northern coasts of the state of Rio Grande do Norte, northeastern Brazil (53% of total thickness) were deposited on the upper shoreface zone, represented by medium-scale tabular-planar and trough cross-stratified sandstone and by skolithos-bioturbated conglomeratic sandstone. Low-angle cross-stratified conglomerates and sandstone, which were deposited on the foreshore zone, represent 31% of the sections described. The remaining 16% are attributed to collapse of overlying material as a result of sea cliff undercutting (massive conglomerate, Lithofacies 1), transport as traction-carpet deposit (weakly stratified conglomerate, Lithofacies 1), and high degree of alteration (Lithofacies 5 - Massive Sandstones). A general succession of diagenetic phases can be recognized, in the studied beachrocks, comprising the precipitation of authigenic smectite, micritic coatings, radial fibers, isopachous rims of prismatic crystals or equant spar, cryptocrystalline and pseudo-peloidal pore-filling cements, as well as the vadose infiltration of micritic, marly, or silty sediments. The absence of organic structures, such as microbial (bacteria or fungi) filaments and bodies within the cements suggests that the mechanism behind beachrock cementation is essentially inorganic, most probably the evaporation of seawater, in response to the dry climatic conditions. The maximum, minimum and average $\delta^{13}C_{VPDB}$ values for the cements are +3.57, –7.8 and +2.34‰, respectively. The $\delta^{18}O_{SMOW}$ values range from 26.32 to 31.41 and average 30.64), while the $\delta^{18}O_{VPDB}$ values range from –4.41‰ to 0.54‰ and average –0.22‰. Most of the $\delta^{18}O_{VPDB}$ and $\delta^{13}C_{VPDB}$ values of the studied beachrocks are compatible with values of marine cements. A few samples show strongly negative $\delta^{18}O$ values, which probably reflect origin from mixed marine-meteoric waters, or recrystallization of marine cements by interaction with meteoric waters. The precipitation temperatures calculated for the studied samples assuming marine waters of $\delta^{18}O_{SMOW}$ = +2,0 (marine water modified by evaporation) and –2,0 (mixed water, the bulk of it meteoric) range from 23,3 a 34,9^{o}C (mean value: 25,8^{o}C).

ÍNDICE

LISTA DE ILUSTRAÇÕES

Pág.

SUMÁRIO INTEGRADO

PRIMEIRO ARTIGO: Lithofaciology and palaeoenvironmental analysis of Holocene beachrocks in northeastern Brazil

TERCEIRO ARTIGO: Carbon and oxygen isotopic composition of beachrock cements, Rio Grande do Norte State, northeastern Brazil

TEXTO EXPLICATIVO

Sobre a estrutura desta tese:

Esta tese de Doutorado está estruturada em torno de artigos publicados em periódicos internacionais. Conseqüentemente, sua organização compreende as seguintes partes principais:

a) introdução sobre o tema e descrição do objeto de pesquisa de Doutorado, onde são sumarizados os objetivos e a filosofia de pesquisa desenvolvidos, o estado da arte sobre o tema de pesquisa, seguidos de uma discussão integradora contendo os principais resultados e interpretações deles derivadas;

b) artigos publicados ou submetidos a periódicos com corpo editorial permanente e revisores independentes, escritos pelo autor durante o desenvolvimento do seu Doutorado;

c) Anexos, compreendendo: fotos de lâminas delgadas, fotos obtidas ao microscópio eletrônico de varredura e análises de espectrocopia de energia dispersada (EDS).

SUMÁRIO INTEGRADO

JUSTIFICATIVA E OBJETIVOS

O termo *beachrock* refere-se ao sedimento litificado nas zonas de intermarés mais arrebentação, tanto em praias de alta quanto baixa energia, ou mesmo em amplas planícies de maré e canais de maré. Tendo em vista ser este tipo de litificação não restrita às praias verdadeiras, segundo a definição geomorfológica, Bricker (1971) propôs que se adotasse a denominação *rocha de intermarés* para aqueles corpos rochosos que ainda estão sob influência de água marinha e *cay rock* (ou outro termo mais apropriado) para o material litificado, atualmente sob influência exclusiva de águas meteóricas. Hopley (1986) chama atenção para o significado amplo do termo *beachrock*, o qual tem sido aplicado a um variado conjunto de materiais litificados na zona litorânea, incluindo aqueles com cimentos de ferro e sílica. Segundo este autor, o termo aplica-se exclusivamente aos sedimentos praiais cimentados por carbonato de cálcio, na zona de intermarés, limitados às baixas latitudes, significado este que será adotado na presente tese.

Embora os *beachrocks* tenham sido estudados por inúmeros pesquisadores, em diferentes regiões do mundo [Florida (Ginsburg, 1953); Hawaii (Meyers, 1987); Mediterrâneo (Sanlaville *et al.*, 1997); Mar Vermelho (Holail and Rashed, 1992); Sri Lanka (Cooray, 1968); Golfo Pérsico (Khalaf, 1988); América Central (Kindler & Bain, 1993); África (Amieux *et al.*, 1989) e Australia (Chivas *et al.*, 1986)], ainda persistem dúvidas sobre o processo específico responsável por este tipo de cimentação (evaporação, mistura de águas, desgaseificação de CO_2 ou atividade metabólica de organismos) e a taxa em que o mesmo ocorre [crescimento contínuo e lento ou rápido (Alexandersson, 1972)]. Acrescenta-se a estes aspectos o fato de que, tendo em vista a natureza extremamente precoce desta cimentação, o estudo destes arenitos quaternários torna-se extremamente importante para compreensão dos ambientes sedimentares e diagenéticos de rochas mais antigas cimentadas por carbonatos em ambientes eodiagenéticos.

No caso específico do Estado do Rio Grande do Norte, tanto o litoral setentrional quanto oriental caracterizam-se pela presença de inúmeras exposições de *beachrocks*. A despeito da grande extensão das mesmas (dezenas de metros a alguns quilômetros), incluindo linhas de diferentes idades (7460 a 110 anos calibrados A.P; Bezerra *et al.*, 2003) e posições em relação ao perfil de praia atual (maior parte localiza-se na atual zona de intermarés, enquanto alguns corpos encontram-se permanentemente submersos ou emersos), existe uma escassez de trabalhos sobre o tema, principalmente no que diz respeito aos seus aspectos diagenéticos. Consequentemente, a presente tese propõe-se a: (a) fazer uma descrição detalhada das diferentes litofácies identificadas nestas rochas; (b) identificar em que porções do perfil praial as mesmas foram originalmente depositadas; (c) estabelecer possíveis relações entre a deposição dos *beachrocks* e curvas de variação local do nível do mar; (d) descrever as feições diagenéticas atuantes durante a litificação dos mesmos e

investigar sua distribuição quanto à fácies deposicional, idade e posição em relação à atual zona de intermarés; (e) elucidar a evolução da química dos fluidos percolantes nos *beachrocks*, desde o momento de sua deposição, através da assinatura isotópica dos cimentos carbonáticos; (f) comparar as ocorrências estudadas com casos da literatura internacional sobre o tema.

METODOLOGIA

A fim de atender aos objetivos propostos, as seguintes etapas de trabalho foram empreendidas:

a) **Pesquisa bibliográfica** visando a fornecer o embasamento teórico necessário à pesquisa a ser empreendida. Mais especificamente, foram enfocados os seguintes temas:

- *beachrocks*, no Brasil e em outros países: metodologia de estudo e resultados obtidos;
- sedimentos praiais atuais: aspectos texturais e estruturas sedimentares;
- cimentação carbonática: principais texturas, composições químicas e ambientes geoquímicos de precipitação;
- preparação, utilização e limitações dos diversos métodos a serem empregados (tingimento, microscopia eletrônica de varredura, microssonda EDS, geoquímica isotópica estável e datação pelo método ^{14}C);

b) **Pré-seleção** dos trechos mais expressivos, nas diversas linhas de *beachrocks,* tanto no litoral oriental quanto setentrional, os quais foram detalhadamente descritos e amostrados. Priorizaram-se aqueles com melhores exposições de feições sedimentológicas e que já possuíssem dados confiáveis de idade obtidos pelo Método do ^{14}C;

c) **Individualização de litofácies** em 36 seções estratigráficas feitas nos corpos de *beachrock* pré-selecionados, tomando-se como base a textura, geometria dos *sets*, estruturas sedimentares e conteúdo fossilífero, incluindo-se a retirada de amostras por litofácies, para posterior análise microscópica. A espessura total de rochas descritas foi de aproximadamente 41m. Corpos de *beachrocks* permanentemente submersos não foram descritos (Fig. 1);

d) **Descrição petrográfica quantitativa** de 112 lâminas delgadas (Anexo 1) impregnadas e tingidas através de técnicas padronizadas de identificação da mineralogia dos cimentos carbonáticos (Warne, 1962; Friedman, 1971), visando à determinação dos aspectos texturais básicos, identificação dos componentes detríticos, individualização de feições diagenéticas e reconhecimento de uma sequência de ocorrência das mesmas;

e) Seleção de amostragem vinculada para análises especiais:

- **Microscopia eletrônica de varredura (MEV),** visando à observação detalhada da morfologia dos cristais e relações texturais do cimento carbonático (Anexo 2). As amostras receberam uma dupla cobertura de carbono e ouro, tendo sido analisadas em um microscópio da marca SHIMADZU SSX-550 (voltagem: 20kV), complementado pela determinação dos elementos maiores e traços por espectroscopia de energia dispersada (EDS, Anexo 3);

- **Análise isotópica ($\delta^{13}C$ e $\delta^{18}O$)** dos diferentes tipos de cimento carbonático, visando à determinação do ambiente geoquímico em que os mesmos foram formados. Trinta amostras, caracterizadas pela presença de uma grande quantidade de um único tipo de cimento ao redor dos grãos, foram selecionadas. Vinte a cinquenta miligramas de pó das mesmas reagiram com ácido ortofosfórico a 100%, sob condições de alto vácuo, a 25^{o}C, por um dia. O gás carbônico liberado, após criogenicamente limpo, foi analisado em um espectrômetro de massa da marca VG-ISOTECH SIRA II, no Laboratório de Isótopos Estáveis (LABISE) da Universidade Federal de Pernambuco. Todos os valores são fornecidos em partes por mil (‰) relativamente ao padrão internacional VPDB (Vienna Pee Dee Belemnite; Urey *et al*., 1951; Craig, 1957). No caso de $\delta^{18}O$, o padrão SMOW (Standard Mean Ocean Water) também é usado (Craig, 1961).

f) **Integração de todos os dados obtidos,** objetivando fazer uma análise comparativa entre linhas de *beachrock* de diferentes idades e posições em relação à posição atual da zona intermarés, fornecendo uma visão, em escala regional, dos processos diagenéticos que afetaram estas rochas;

g) **Elaboração e submissão** dos três artigos.

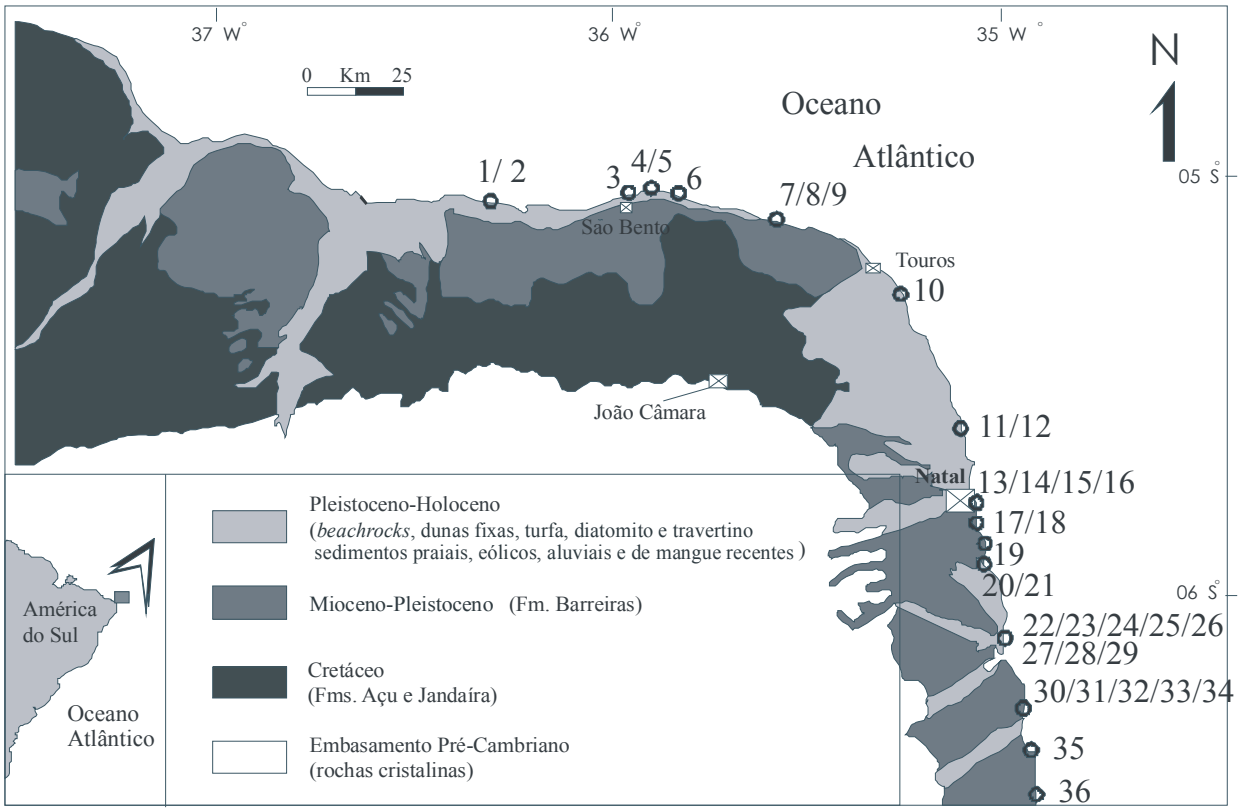

Figura 1: Mapa de localização da área estudada com localização dos pontos descritos.

ASPECTOS GERAIS DOS *BEACHROCKS*

Tomando-se como base estudos feitos em *beachrocks* localizados em diferentes pontos do planeta, Bricker (1971) lista as características gerais destes tipos de depósitos das quais serão citadas as principais, complementadas por informações obtidas em outros trabalhos:

a) A composição do arcabouço é variada [mas geralmente idêntica aos materiais da praia sobrejacente ou adjacente (Hopley, 1986)], podendo encontrar-se desde material 100% vulcânico (Tietz & Muller, 1971) a grãos inteiramente carbonáticos (Kindler & Bain, 1993), assim como quartzo mais fragmentos de rocha (Chaves & Sial, 1998);

b) O cimento pode ocorrer em três morfologias principais, envolvendo dois minerais: cutículas micríticas compostas por carbonato (aragonita ou calcita magnesiana) cripto- a microcristalino; franjas fibrosas ou prismáticas constituídas sobretudo de aragonita, sob a forma de cristais alinhados perpendicularmente à superfície dos grãos; franjas equantes de calcita magnesiana, estas últimas mais raras;

c) Contrastando com a cimentação lenta de muitos ambientes diagenéticos, a formação de um *beachrock* é excepcionalmente rápida [dezenas de anos (Holail & Rashed, 1992)], fato este evidenciado pela ocorrência de inúmeros objetos modernos cimentados nestas rochas;

d) A ocorrência destas rochas restringe-se às regiões tropicais [30^{o} norte e sul do Equador, estendendo-se um pouco além do intervalo latitudinal dos modernos recifes de coral (Hopley, 1986)], embora nem toda ilha tropical carbonática tenha *beachrocks.*

A importância dos *beachrocks* refere-se a três aspectos principais:

a) o impacto que os mesmos promovem sobre a evolução costeira;

b) o significado dos mesmos como indicadores de posição do nível do mar;

c) a oportunidade que os mesmos oferecem para a compreensão dos ambientes diagenéticos rasos onde ocorre a maior parte da cimentação e geração de porosidade, em rochas carbonáticas.

No que diz respeito ao primeiro aspecto, Cooper (1991) aponta três impactos diretos sobre a evolução costeira, resultantes da formação de *beachrocks*:

⇒ redução no volume de sedimentos litorâneos: a cimentação dos grãos de areia que constituirão o arcabouço dos *beachrocks* impede o transporte posterior pela deriva litorânea. A reintrodução no ciclo sedimentar somente pode ocorrer através da erosão pelas ondas e pelo vento, bioerosão e intemperismo;

⇒ mudança na morfologia costeira: transformação de uma linha de costa arenosa em outra subjacente ao *beachrock*; formação de baías em zeta na porção de *downdrift* dos afloramentos mais proeminentes; formação de depósitos cascalhosos resultantes da erosão de *beachrocks* pré-existentes;

⇒ potencial preservação das fácies próximas à linha de costa devido à cimentação precoce dos sedimentos de praia.

Cooper (op. cit.) destaca a pouca atenção dada ao papel exercido pelos *beachrocks* na evolução costeira, fato este que se deve, provavelmente, à maior concentração de trabalhos sobre linhas de costa, em áreas temperadas. Segundo este autor, uma boa parte das linhas de costa atuais situa-se em áreas favoráveis à formação de *beachrocks*, o que torna este fato um componente significativo em modelos de evolução costeira nestas áreas.

Quanto ao segundo aspecto, isto é, o papel exercido pelos *beachrocks* como indicadores de posição do nível do mar, o mesmo baseia-se na localização bastante específica destas rochas, atualmente (entre os limites inferior e superior da oscilação das marés), o que tem levado inúmeros pesquisadores a utilizá-los em suas interpretações a respeito da evolução da linha de costa de diversas regiões do planeta, principalmente se os níveis de cimentação estendem-se abaixo dos níveis modernos de intermarés. Hopley (1986), entretanto, chama a atenção para os cuidados que se devem ter ao utilizar-se esta ferramenta, em modelos evolutivos de regiões costeiras. Segundo este autor, a utilização dos *beachrocks* torna-se mais confiável, nas seguintes circunstâncias:

⇒ pequeno intervalo de marés;

⇒ depósitos grossos (a migração ascendente de águas subterrâneas, por ação capilar, é limitada);

⇒ regiões áridas (a água subterrânea apresenta alta salinidade);

⇒ pequenos recifes ou esporões e praias, em ilhas (gradiente hidráulico não pode desenvolver-se devido à falta de espaço).

O terceiro e último aspecto refere-se à oportunidade que os *beachrocks* oferecem de estudar alguns ambientes diagenéticos rasos, tendo em vista as taxas relativamente rápidas de cimentação carbonática neles encontradas. A importância deste fato é enfatizada por Longman (1980). Segundo este autor, em reservatórios terrígenos, cuja porosidade é usualmente intergranular, a prioridade máxima da exploração tem sido a interpretação das fácies deposicionais e da disposição espacial dos corpos de arenito, ficando a diagênese, em segundo plano. Em contraposição, nos reservatórios carbonáticos, observa-se uma diversidade de tipos de poros (intergranulares, móldicos, fratura etc), com origem algumas vezes independente das fácies deposicionais. Neste caso, em termos exploratórios, a ênfase deve ser dada, primariamente, à interpretação do controle diagenético sobre a porosidade, devendo utilizar-se a interpretação de fácies deposicionais somente se a relação entre porosidade e fábrica deposicional for clara.

Devido à importância dos processos pós-deposicionais precoces e tardios, na criação ou modificação da porosidade dos carbonatos, Choquette e Pray (1970) identificaram os seguintes estágios diagenéticos: eodiagênese, mesodiagênese e telodiagênese. Os *beachrocks* formam-se no primeiro estágio, eodiagênese, o qual corresponde à zona de influência efetiva dos processos de superfície cujo limite superior pode ser subaéreo ou subaquoso, correspondendo à interface de deposição ou superfície de não-deposição/erosão. O limite inferior, neste caso, não é tão claro, podendo os diversos processos atuantes atingir diferentes profundidades. A telodiagênese corresponde à passagem da rocha sedimentar para a zona de influência dos processos que ocorrem em uma superfície erosional.

Quatro ambientes eodiagenéticos (Fig. 2) foram identificados por Longman (op. cit), em carbonatos marinhos rasos sujeitos à diagênese precoce: freático marinho (no qual, juntamente com o ambiente vadoso marinho, formam-se os *beachrocks*), vadoso meteórico, freático meteórico e de mistura (meteórico/marinho). O primeiro ambiente (freático marinho) divide-se em duas zonas: estagnada e ativa. A zona estagnada caracteriza-se por uma pequena circulação de água, propiciando a ocorrência de micritização e cimentação intragranular incipientes. Uma boa circulação de água próxima à interface sedimento / água identifica a zona ativa a qual pode ocorrer na margem da plataforma ou na zona de ante-praia superior. Extensa cimentação intergranular e de preenchimento de cavidades ocorre nesta zona, sendo aragonita fibrosa e calcita magnesiana micrítica os cimentos dominantes (Fig. 3A). No ambiente vadoso meteórico, têm-se duas zonas: uma de solução e outra de precipitação. Na zona de solução, o CO_2 proveniente da atmosfera e do solo contribui para a dissolução, formando *vugs*, moldes e grãos alveolados, nas proximidades da

zona de solo. A zona de precipitação estabelece-se onde a água torna-se saturada em calcita e a evaporação ou a perda de CO_2 possibilitam a precipitação de calcita equante de granulometria fina, sob a forma de cimentos pendulares ou meniscos (Fig. 3B). No ambiente freático meteórico, observam-se três zonas: de solução, saturada ativa e saturada estagnada. A zona de solução caracteriza-se pela ocorrência de lixiviação; a saturada ativa, pela recristalização de grãos acompanhada de extensa cimentação calcítica intergranular, e a saturada estagnada, pelo neomorfismo sem cimentação. Crescimentos sintaxiais em fragmentos de equinodermas e cristais de calcita equante cujos tamanhos aumentam no sentido do centro dos poros ocorrem, tipicamente, na zona ativa freática meteórica (Fig. 3C). No ambiente de mistura de águas meteórica e marinha, pode formar-se dolomita, caso a água tenha salinidade relativamente baixa, ou calcita magnesiana do tipo *bladed,* se a água for relativamente salina.

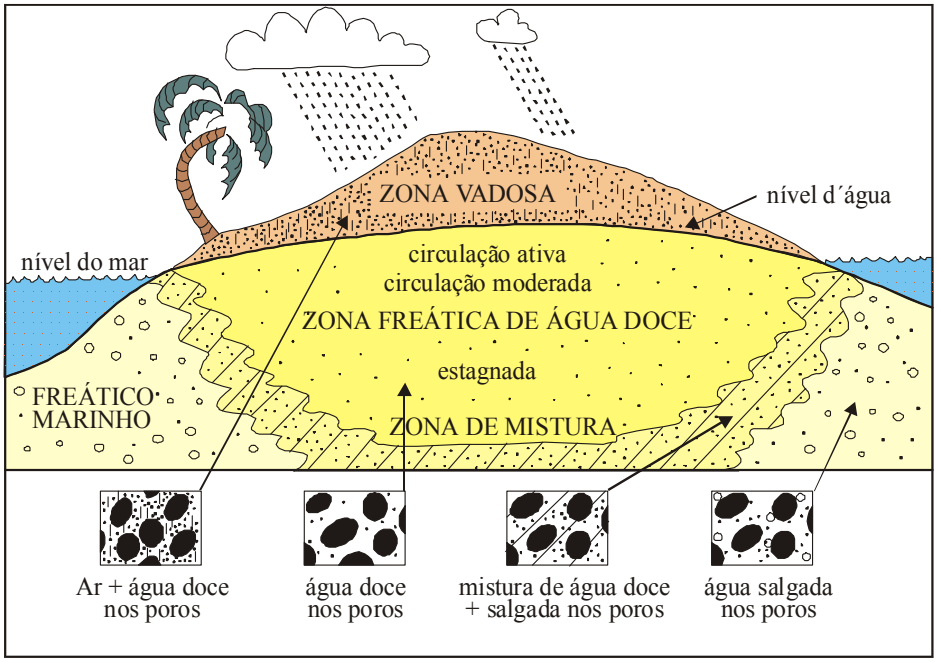

Figura 2: Distribuição dos ambientes diagenéticos, em subsuperfície rasa, em uma ilha de areia carbonática idealmente permeável (Longman, 1980).

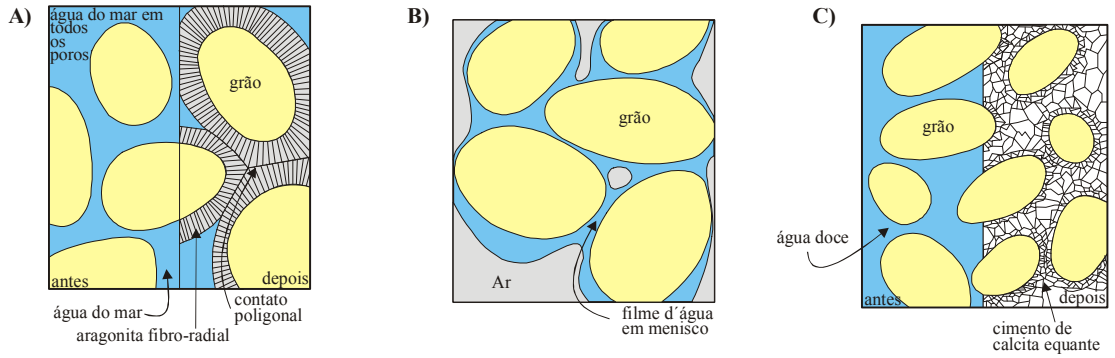

Figura 3: (A) Ambiente freático marinho; (B) Ambiente vadoso de água doce; (C) Ambiente freático de água doce (adaptada de Longman, 1980).

Além dos quatro grandes ambientes eodiagenéticos descritos anteriormente, Longman (1980) reconhece a existência de três outros: vadoso marinho, salmouras em *sabkhas* e marinho profundo. No ambiente vadoso marinho onde também ocorrem os *beachrocks*, os cimentos tendem a ser constituídos de aragonita fibrosa ou calcita magnesiana micrítica/fibrosa, sob a forma de meniscos ou cimentos pendulares.

A maior parte da cimentação marinha ocorre muito próxima à interface sedimento / água (Longman, 1980). Dentro da zona freática marinha ativa, substratos rígidos formados por bioconstruções (recifes) são mais susceptíveis à cimentação do que substratos não consolidados, devendo-se este fato, em parte, ao poder inibidor que o movimento dos grãos tem sobre a cimentação. Portanto, recifes ou grãos estabilizados por atividade orgânica são os melhores locais para cimentação marinha. Algumas barras arenosas carbonáticas, localizadas próximas à linha de costa, caracterizam-se por uma baixa taxa de sedimentação e granulometria relativamente grossa, sob condições de clima árido, sendo, também, vulneráveis à cimentação marinha. Como foi dito anteriormente, os cimentos dominantes que se precipitam no ambiente freático marinho ativo são a calcita magnesiana e a aragonita. No primeiro caso, têm-se cristais micríticos ou romboedros distribuídos como franjas isópacas ao redor dos grãos, sendo esta textura comum em recifes recentemente cimentados e em *beachrocks*. Quanto à aragonita, a mesma ocorre sob a forma de cristais fibrosos, em uma variedade de texturas, podendo ser encontrada em diversos tipos de rochas, incluindo recifes, *beachrocks* e bancos oolíticos.

Segundo Hopley (1986), as explicações para a formação dos *beachrocks* podem ser divididas em três categorias:

⇒ orgânica;

⇒ inorgânica, a partir da água doce;

⇒ inorgânica, a partir da água do mar.

Na primeira categoria, tem-se ação microbiológica, decomposição da matéria orgânica e atividade algálica como processos mais apontados. Tendo em vista a baixa quantidade de matéria orgânica normalmente encontrada nas areias e a existência de algas somente na superfície dos *beachrocks* e não em seu interior, Milliman (1974) descarta esses mecanismos; entretanto, trabalhos mais recentes têm indicado a ação direta ou indireta de organismos como os processos mais comuns responsáveis pela precipitação de cimentos em *beachrocks* (Webb *et al.*, 1999; Neumeier, 1999).

Na segunda categoria, precipitação inorgânica a partir de águas subterrâneas meteóricas, Russel (1959, 1962), ao pesquisar *beachrocks* em ilhas do Caribe sugere que a cimentação ocorra ao longo do nível freático, sob a forma de cutículas de calcita as quais são seguidas, em um estágio posterior, por um cimento marrom de origem desconhecida. Tomando-se como base a existência de *beachrocks*, em áreas excessivamente áridas, isto é, sem água subterrânea doce (ex: Mar Vermelho) e em ilhas muito pequenas para manter um nível d'água permanente, Stoddart e Cann (1965) criticam esta hipótese.

A terceira e última categoria, precipitação inorgânica a partir da água do mar, baseia-se no reconhecimento de aragonita como cimento primário em *beachrocks*, principalmente sob a forma de cristais aciculares ou fibrosos. Neste caso, a precipitação ocorreria, em profundidade rasa, após percolação, ou, em superfície, após evaporação e aquecimento da água do mar. Hanor (1978) propôs que a perda de CO_2 a partir de águas praiais saturadas em carbonato seja o processo responsável pela precipitação dos cimentos, em *beachrocks.* Segundo este autor, cálculos de transporte de massa indicam que a ascensão vertical de fluidos na zona freática, resultante da oscilação do nível freático promovida pelas marés, é suficiente para induzir a desgaseificação de CO_2 da água intersticial que flui para o mar. A perda de CO_2 seria posteriormente incrementada através do bombeamento da fase gasosa, pelas marés, na zona vadosa presente na interface sedimento-atmosfera. A medida que a precipitação do cimento prossegue, diminui a porosidade, assim como a habilidade do sistema em desgaseificar, reduzindo, portanto, a formação de novos cimentos. Hanor (op. cit) confirmou sua hipótese através de um experimento no qual estudou-se a desgaseificação de uma mistura de águas marinhas e praiais, em St. Croix (U. S. Virgin Islands), a qual foi responsável pela formação de uma crosta de calcita pouco magnesiana muito semelhante aos cimentos naturais. Cálculos termodinâmicos indicam que a precipitação não teria sido induzida pela mistura de águas meteóricas e marinhas, mas sim pela supersaturação causada pela perda de CO_2, processo este que independe de qualquer mistura.

BEACHROCKS DO ESTADO DO RIO GRANDE DO NORTE

Trabalhos Anteriores

O primeiro estudo detalhado sobre *beachrocks,* na costa brasileira, deve-se a Branner (1904) o qual descreveu as relações geológicas e geográficas dos diversos recifes que ocorrem entre os estados do Ceará e Bahia, incluindo os de corais. Este mesmo autor relaciona bibliografia sobre o tema a qual tem início no século XVII, com as observações feitas por viajantes e pesquisadores que visitavam, constantemente, a região costeira do Brasil. Nos setenta anos seguintes, os únicos trabalhos sobre *beachrocks* do Estado do Rio Grande do Norte enfocaram seu conteúdo fossilífero (Maury, 1934; Campos e Silva *et al*., 1964; Mendonça, 1966) e a interpretação de suas estruturas sedimentares (Bigarella, 1975; Oliveira, 1978).

O início da década de 90 deu origem a um período de reaquecimento nos estudos sobre *beachrocks* no estado. Neste contexto, Oliveira *et al*. (1990) produziram o único trabalho detalhado a respeito da evolução diagenética destas rochas. Estes autores estudaram os *beachrocks* localizados entre as praias do Forte, no Município de Natal, e Barra de Cunhaú, no Município de Canguaretama, tecendo considerações a respeito da geometria, petrografia, sedimentologia, diagênese e idade dos mesmos. Estudos mais recentes utilizaram os *beachrocks* na reconstrução da evolução costeira holocênica do Estado do Rio Grande do Norte (Vianna *et al*., 1993; Amaral, 1999; Caldas, 2002) e na investigação de movimentos neotectônicos (Caldas, 1998; Bezerra *et al*., 1998; Bezerra *et al*., 2003; Bezerra *et al*., 2004).

Contexto Regional

A área estudada apresenta um clima tropical, com 600 a 1000mm de chuvas por ano e temperatura média de 30^{o}C (Nimer, 1989). Fortes correntes de deriva litorânea deslocam-se para norte e para oeste, ao longo das costas oriental e setentrional, respectivamente. Predominam rios intermitentes pequenos a médios cuja descarga é insignificante na maior parte do ano, enquanto os poucos rios perenes maiores, incluindo alguns estuários, geralmente drenam para dentro de lagunas e planícies de maré (Bittencourt *et al*., 2002).

Medidas feitas no período de um ano, entre as cidades de São Bento do Norte e Caiçara do Norte mostraram que a velocidade da corrente longitudinal varia de 0.07 a 0.85 m/s e a altura da onda, entre 49.7 e 5.3cm (Tabosa, 2002). Medidas feitas durante seis meses em praias localizadas ao longo da costa oriental, indicaram que a velocidade da corrente litorânea varia de 0.863 a 0.066 m/s, enquanto os valores da altura da onda variam entre 90.3 e 20.1cm (Chaves, 2000).

As linhas de *beachrocks* estudadas são parte integrante da sedimentação quaternária que se verificou, no Rio Grande do Norte, em dois contextos geológicos distintos: a Bacia Potiguar e o prolongamento, no Rio Grande do Norte, da Bacia de Pernambuco-Paraíba.

Bacia Potiguar

A Bacia Potiguar localiza-se no extremo nordeste do Brasil, sendo quase em sua totalidade no Estado do Rio Grande do Norte e uma pequena porção no Estado do Ceará. Possui uma área total de 60.000 km^2 (Araripe & Feijó, 1994), sendo uma parte emersa e outra submersa. Geologicamente, seus limites são os seguintes: a noroeste, com a Bacia do Ceará, pelo Alto de Fortaleza; a leste, com a Bacia Pernambuco-Paraíba-Rio Grande do Norte, pelo Alto de Touros; a sul, pelas rochas do embasamento cristalino; a norte e a nordeste, pela cota batimétrica de 2000m.

A porção emersa da bacia possui uma área de 24.500km^2, compreendendo a parte nordeste do Estado do Ceará e a região norte do Estado do Rio Grande do Norte. Seu arcabouço estrutural (Fig. 4) é composto basicamente por três elementos (Bertani *et al*., 1990): grábens, altos internos e plataformas do embasamento. Falhas e/ou sistemas de falhas definem os principais limites da bacia.

Nos últimos vinte anos, vários trabalhos a respeito da litoestratigrafia da Bacia Potiguar têm sido escritos, destacando-se, primeiramente, o de Souza (1982) o qual reconheceu três sequências deposicionais principais na bacia: uma continental, uma transicional e outra marinha. A sequência continental seria representada pelos arenitos finos, siltitos e folhelhos da Formação Pendência e pelos arenitos do Membro Upanema da Formação Alagamar. A sequência transicional estaria representada, na porção *offshore* da bacia, pelos folhelhos do Membro Galinhos e arenitos do Membro Aracati da Formação Alagamar, enquanto na porção *onshore* corresponderia à parte superior da Formação Açu. A sequência marinha seria marcada por uma série de ciclos transgressivos e regressivos que resultariam na formação de duas plataformas carbonáticas representadas pelas formações Ponta do Mel e Jandaíra, separadas pelos clásticos do Membro Quebradas da Formação Ubarana. Após a deposição da Formação Jandaíra, um ciclo regressivo teve início com a sedimentação dos folhelhos e arenitos turbidíticos da porção superior da Formação Ubarana, dos calcários da Formação Guamaré e dos arenitos da Formação Tibau. Este último ciclo teria sido marcado, igualmente, pela ocorrência de vulcanismo de natureza básica representado pela Formação Macau. Esta sequência inclui, igualmente, arenitos e conglomerados da Formação Barreiras de idade cenozóica e os depósitos aluvionares e costeiros recentes, incluindo-se nestes os *beachrocks* aqui estudados.

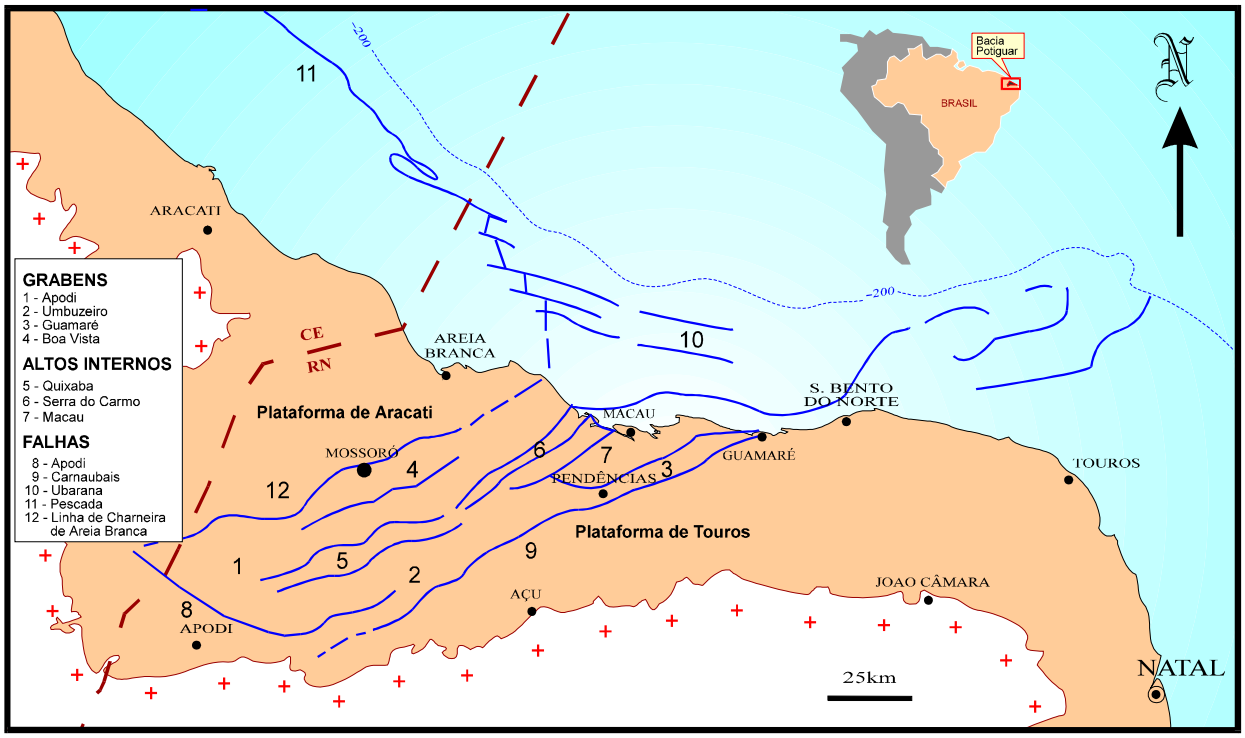

Figura 4: Arcabouço estrutural da Bacia Potiguar (modificado de Bertani *et al*., 1990).

Araripe e Feijó (1994) atualizaram a coluna proposta por Souza (1982) e a de Lima Neto (1989 *apud* Araripe & Feijó, 1994). Nesta versão mais recente, foram propostas as seguintes modificações (Fig. 5):

a) Criação de dois novos grupos: Areia Branca, de conteúdo predominantemente clástico, o qual uniria as formações Pendência, Pescada e Alagamar, e Agulha, formado por clásticos e carbonatos de alta e baixa energia, o qual reuniria as formações Ubarana, Guamaré e Tibau;

b) Inclusão, no Grupo Apodi, estratigraficamente posicionado entre os dois outros citados acima, das formações Ponta do Mel e Quebradas, esta última representando uma elevação de categoria do membro homônimo da Formação Ubarana definido por Souza (1982);

c) Subdivisão das rochas vulcânicas em três formações: Rio Ceará-Mirim, Serra do Cuó e Macau.

Segundo Araripe e Feijó (1994), o preenchimento sedimentar da Bacia Potiguar seria dividido em duas fases principais: rifte e margem passiva, separadas por uma fase de transição.

Figura 5: Coluna litoestratigráfica da Bacia Potiguar (adaptada de Araripe & Feijó, 1994).

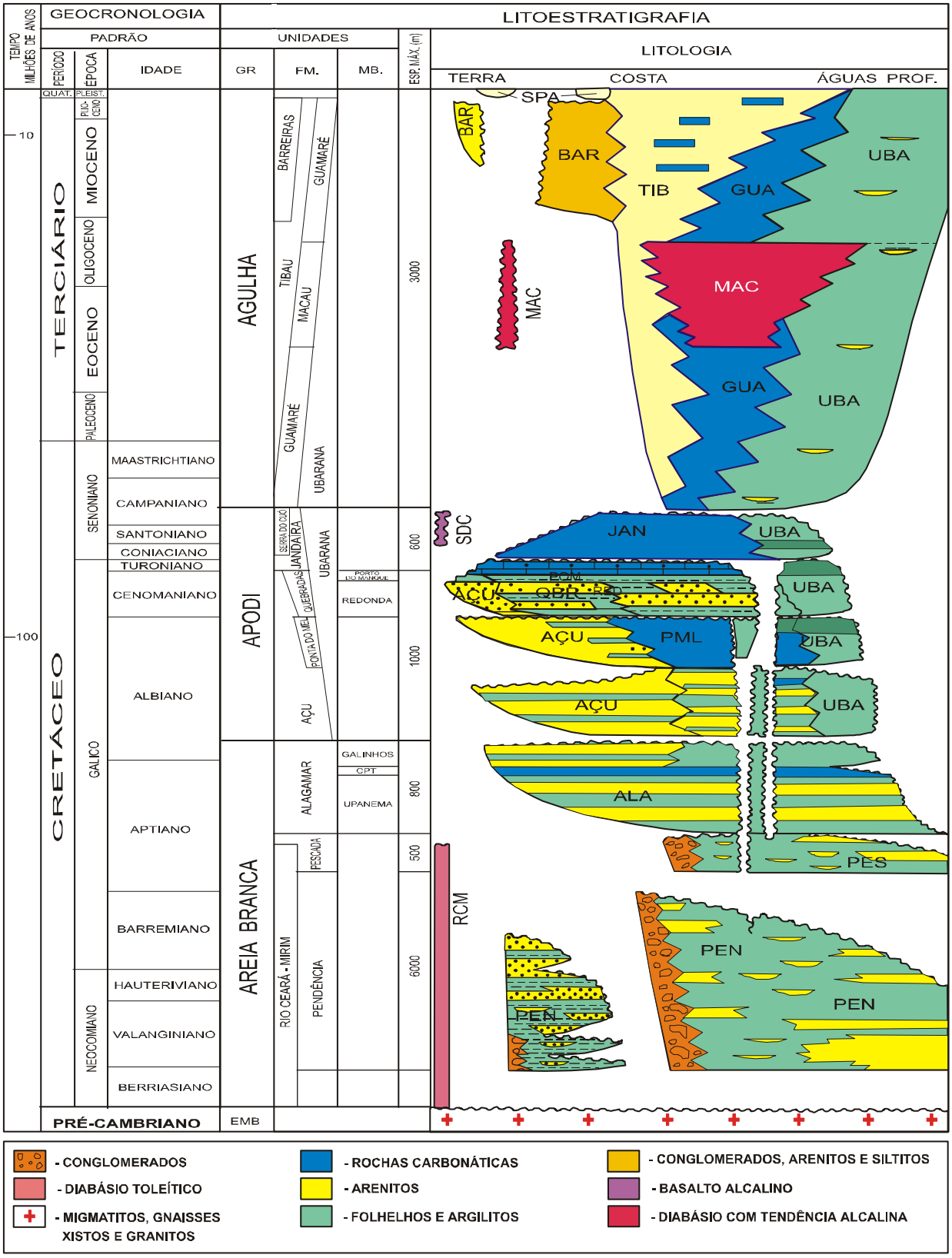

Bacia PE-PB-RN

Em revisão geológica da faixa costeira de Pernambuco, Paraiba e parte do Rio Grande do Norte, Mabesoone e Alheiros (1991) propõem uma compartimentação da porção sedimentar em sub-bacias, com base em características litológicas e estruturais (Fig. 6). O domínio da Sub-bacia Natal a qual, conforme tudo indica, constitui uma extensão da chamada Plataforma Leste, extremidade oriental da Bacia Potiguar, comporta-se como uma faixa sedimentar do tipo homoclinal, embora exista controvérsia sobre este tema. Uma estratigrafia de referência para esta região (Fig. 7) foi elaborada por Fonseca *et al.* (1997), a qual revela rochas do embasamento pré-cambriano, rochas sedimentares mesozóicas e, por fim, rochas sedimentares e sedimentos cenozóicos, incluindo os *beachrocks*.

Lacerda (1999) identificou o embasamento cristalino aflorante a oeste da bacia, no Município de Monte Alegre (RN), o qual está representado por gnaisses de composição granítica e por um corpo granítico de composição tonalítica. A sequência sedimentar cretácea, também aflorante nesse setor (já citada pelo IPT, 1982), é composta por um calcário quartzoso.

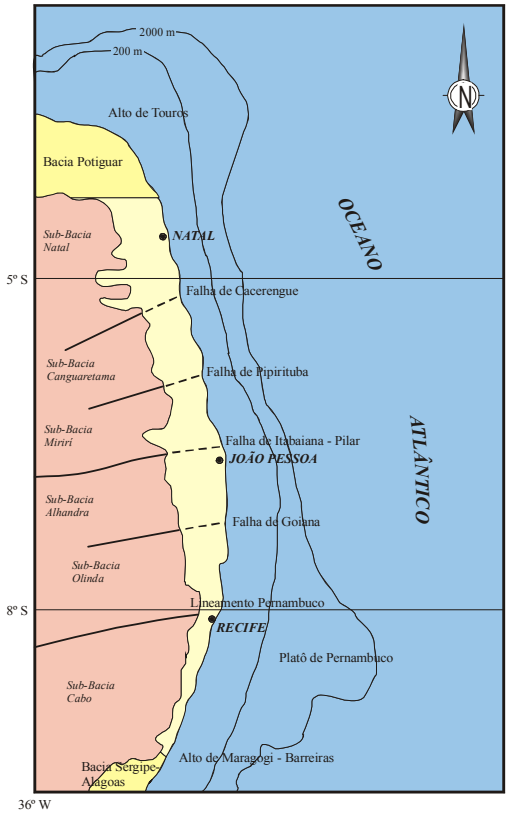

Figura 6: Subdivisão em subbacias da faixa sedimentar costeira de Pernambuco-Paraíba-Rio Grande do Norte (Mabesoone & Alheiros, 1991).

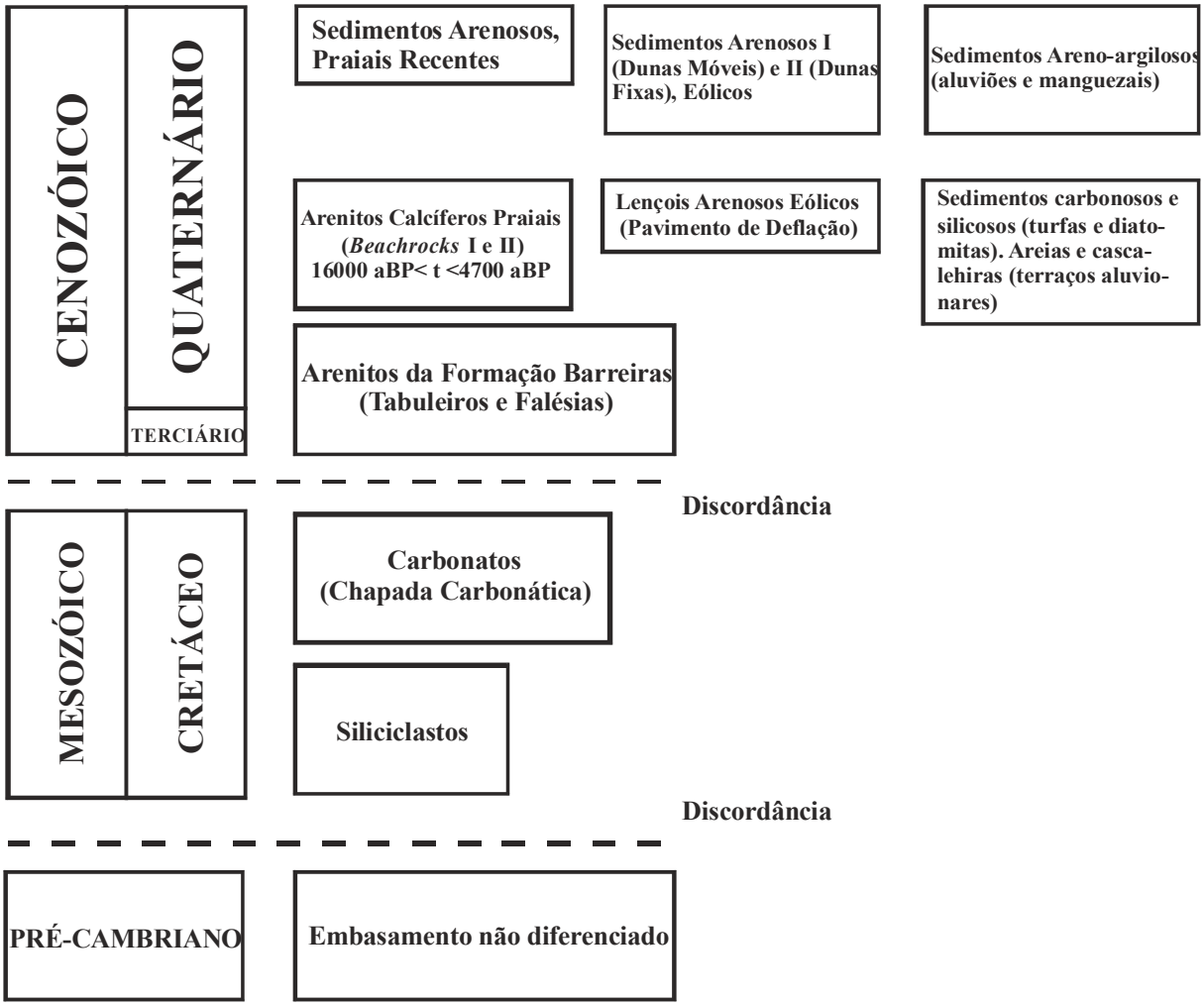

Figura 7: Coluna estratigráfica esquemática, proposta para a Região do Litoral Oriental do RN (Fonseca *et al.*, 1997).

Aspectos Gerais

Beachrocks são descontinuamente expostos ao longo das costas oriental e setentrional do Estado do Rio Grande do Norte. Alguns corpos distribuem-se por até 8 km, paralelamente à costa, enquanto outros não ultrapassam alguns metros de comprimento. Variam, em espessura, de alguns centímetros a aproximadamente 3 m e, em largura, de 2 a 50 m. A maioria dos corpos ocorre próximo à atual linha de costa; entretanto, alguns podem ser encontrados até 10 km para dentro do continente (Silva, 1991) e 5.7 km *offshore* (Vianna *et al.*, 1993).

A maior parte dos *beachrocks* compõe-se de camadas tabulares que mergulham suavemente ($<10^{o}$) no sentido do oceano, com 5 a 150 cm de espessura. Seus contatos com as camadas adjacentes são abruptos. A maioria dos corpos apresenta feições erosionais similares às descritas nos *beachrocks* e aeolianitos da África do Sul (Miller & Mason, 1994) das quais s*pitzkarren*

(pirâmides separadas por fendas ou bacias de dissolução) e depressões quase circulares (bacias de dissolução e marmitas) são as mais comuns.

No que diz respeito ao arcabouço dos *beachrocks* estudados, os mesmos são compostos de grãos de quartzo monocristalino (media: 52% do volume total da rocha; máximo: 70%), quartzo policristalino (média: 8.9%; máximo: 75.5%), feldspato (sobretudo K-feldspato; média: 0.3%; máximo: 2.3%), minerais pesados (média: 0.3%; máximo: 9.6%), bioclastos (gástropodes, bivalves, foraminíferos, algas vermelhas e equinoidermas (média: 2.2%; máximo: 29.6%) e fragmentos de arenitos cimentados por hematita oriundos da Formação Barreiras (média: 0.9%; méximo: 41.4%). Fragmentos de *beachrock* de tamanhos variados são comuns, não somente como intraclastos dentro do arcabouço dos corpos estudados (média: 0.02%; máximo: 3.6%), mas também como lajes de até 2.0 m de comprimento que se acumulam nas zonas de estirâncio e ante-praia superior, como resultado da erosão costeira e ação das ondas. As quantidades médias de grãos do arcabouço, cimento, materiais infiltrados e porosidade são 64.6% (máximo: 80%), 24.6% (máximo: 38.8%), 1.4% (máximo: 18.7%) e 10% (maximum: 30.7%), respectivamente, nas rochas estudadas.

ARTIGO 1 – LITHOFACIOLOGY AND PALAEOENVIRONMENTAL ANALYSIS OF HOLOCENE BEACHROCKS IN NORTHEASTERN BRAZIL

O primeiro artigo, submetido ao *Journal of Coastal Research*, teve como objetivos principais a descrição detalhada das litofácies identificadas em diversos corpos de *beachrocks* distribuídos ao longo da costa do Estado do Rio Grande do Norte (Fig. 1), a interpretação do paleoambiente deposicional, e a identificação das possíveis relações entre deposição e cimentação dos *beachrocks* e variações do nível do mar no Holoceno.

Cinco litofácies foram identificadas nos *beachrocks* estudados:

(1) conglomerado maciço a incipientemente estratificado;

(2) conglomerado e arenito com estratificação cruzada de baixo ângulo;

(3) arenito com estratificação cruzada tabular-planar e acanalada de média escala;

(4) arenito conglomerático bioturbado por Skolithos;

(5) arenito maciço. As características texturais e estruturas sedimentares identificadas em cada uma são indicativas de deposição em um ambiente costeiro marinho raso (Fig. 8).

A maior parte dos *beachrocks* estudados (53%) foi depositada em uma zona de ante-praia superior, representada pelas fácies com estratificação cruzada acanalada e tabular-planar (Litofácies 3), ocasionalmente com icnofósseis (Litofácies 4). Fácies depositadas na zona intertidal ou estirâncio, caracterizadas pela presença de estratificação cruzada de baixo-ângulo (Litofácies 2) são subordinadas, conforme revelado pela porcentagem de litofácies em relação à espessura total de rochas descritas (31%). Os 16% restantes são atribuídos ao colapso de material sobrejacente, em virtude do solapamento basal de falésias (Conglomerado Maciço), transporte como tapetes de tração (Conglomerado incipientemente estratificado) e alto grau de alteração (Arenito Maciço). Um resumo das principais características de cada litofácies e sua interpretação paleoambiental é mostrado na Tabela 1.

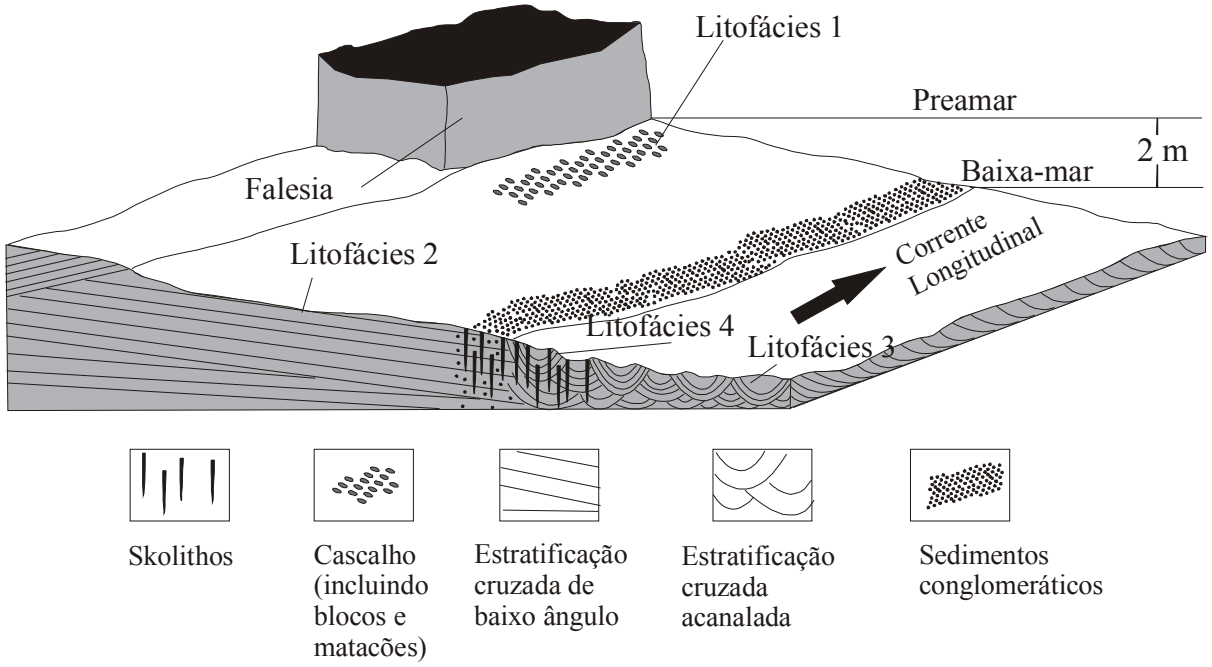

Figura 8: Representação esquemática da distribuição das litofácies identificadas ao longo de um perfil praial.

Levando-se em consideração a distribuição das amostras de *beachrock* datadas pelo Método do ^{14}C (Tabelas 2 e 3), na curva-envelope de variação do nível do mar produzida por Bezerra *et al.* (2003), observa-se que a deposição do arcabouço ocorreu sob condições extremamente variáveis, incluindo subida do nível do mar, alto nível do mar, descida do nível do mar e baixo nível do mar (Fig. 9). Ao longo da costa setentrional, os sedimentos praiais foram depositados predominantemente entre 4140 e 2190 anos calibrados AP, durante a queda do nível do mar e durante baixo nível do mar. Os depósitos praiais distribuídos ao longo da costa oriental foram preferencialmente formados entre 7460 e 4240 anos calibrados AP, durante elevação do nível do mar e alto nível de o mar. A exposição dos *beachrocks* e a geração de feições erosionais em sua superfície são devidas ao atual nível do mar baixo.

Na costa setentrional, a zona de ante-praia superior, representada pelas litofácies 3 e 4, distribui-se preferencialmente nas fases de queda do nível do mar e nível de mar baixo estacionário, enquanto a zona de estirâncio, representada pela Litofácies 2, pode ser encontrada ao longo de toda a curva. No caso da costa oriental, ambas as zonas (ante-praia superior e estirâncio) são igualmente concentradas nos primeiros estágios de elevação do nível do mar e nível de mar alto estacionário.

A distribuição de feições diagenéticas na área estudada é extremamente variável, mesmo a uma escala centimétrica, indicando que a litificação dos beachrocks ocorreu sob a influência de parâmetros físicos e químicos que variavam rapidamente. A força motora destas variações provavelmente foi a diversidade de posições do nível do mar sob as quais os *beachrocks* foram

gerados, particularmente avanços e recuos locais do mar ou oscilações de menor ordem não detectáveis na curva-envelope de variação do nível do mar. A datação por ^{14}C dos cimentos carbonáticos individualmente poderia esclarecer esta questão; entretanto, esta é uma tarefa altamente difícil e mais estudos parecem ser necessários para melhor entender a extensão e a amplitude pelas quais as mudanças do nível do mar influenciaram a variedade de texturas apresentadas pelos cimentos identificados nos *beachrocks* estudados.

Tabela 1: Resumo das principais características de cada litofácies e interpretação paleoambiental.

Litofácies	**Descrição**	**Interpretação**	**% relativa à espessura total**
1	Conglomerados maciços a incipientemente estratificados, mergulhando no sentido do oceano, pobremente a muito pobremente selecionados, com contato inferior abrupto	Depósito residual transgressivo ou tapete de tração	5%
2	Conglomerado arenoso a arenito pobremente a muito pobremente selecionados com estratificação cruzada de baixo ângulo, mergulhando no sentido do oceano	Ondas de espraiamento na zona de estirâncio ou do degrau de *backwash*	32%
3	Arenitos muito pobremente a bem selecionados, com estratificação cruzada de pequena a média escala e paleocorrentes paralelas à linha de costa	Transporte como carga de fundo por correntes de deriva litorânea na zona de ante-praia superior	51%
4	Arenitos pobremente a muito pobremente selecionados com numerosos tubos verticais densamente unidos	Abrigo escavado na zona de ante-praia superior sob condições de elevada energia de ondas e correntes	2%
5	Arenitos maciços pobremente a bem selecionados	Maior grau de alteração na base e no topo dos afloramentos	10%

Tabela 2: Idades obtidas pelo Método do ^{14}C e mostradas na figura 9A. Datações feitas por: (1) Bezerra *et al*. (1998; 2003); (2), (3), (4) e (5) Stattegger *et al*. (2004). Estas quatro últimas amostras foram retiradas dos mesmos corpos de *beachrocks* das amostras H, A, E e B, respectivamente, mas não foram utilizadas na construção das curvas. Abreviação: abm = assembléia de bivalves mortas.

Amostra	**Altura (m acima do nível médio do mar)**	**Indicador de nível do mar**	**Idade calibrada (anos AP a 2σ)**
A(1)	-0.5 ± 1.0	abm	6900-6080
B(1)	3.9 ± 1.0	abm	5730-5060
C(1)	2.1 ± 1.0	abm	4140-3760
D(1)	1.2 ± 1.0	abm	4240-3640
E(1)	1.1 ± 1.0	abm	3680-3210
F(1)	2.0 ± 1.0	abm	3640-3330
G(1)	2.1 ± 1.0	abm	2960-2720
H(1)	0.6 ± 1.0	abm	3040-2690
I(1)	0.6 ± 1.0	abm	2680-2190
J(1)	1.8 ± 1.0	abm	1250-1060
K(1)	0.2 ± 1.0	abm	160-60
KIA12334(2)	0.2	abm	2960-2900
KIA12336(3)	-2.5	abm	6830-6750
KIA 14750(4)	-1.6	abm	3235-3165
KIA14751(5)	+1.0	abm	5945-5875

Tabela 3: Idades obtidas pelo Método do ^{14}C e mostradas na figura 9B. Datações feitas por: (1) Bezerra *et al*. (1998; 2003); (2) Oliveira *et al.* (1990). Esta amostra foi retirada do mesmo corpo de *beachrock* das amostras G e H; (3) Oliveira *et al*. (1990). Estas amostras foram retiradas dos mesmos corpos de *beachrocks* das amostras B, C e D. Amostras (2) e (3) não foram utilizadas na construção das curvas. Abreviação: abm = assembléia de bivalves mortas.

Amostra	**Altura (m acima do nível médio do mar)**	**Indicador de nível do mar**	**Idade calibrada (anos AP a 2σ)**
A(1)	1.5 ± 1.0	abm	7460-6550
B(1)	0.0 ± 1.0	abm	7460-6550
C(1)	0.7 ± 1.0	abm	6730-5980
D(1)	0.2 ± 1.0	abm	6340-5600
E(1)	1.7 ± 1.0	abm	6170-5440
F(1)	0.8 ± 1.0	abm	5950-5700
G(1)	2.2 ± 1.0	abm	5310-4560
H(1)	1.8 ± 1.0	abm	4970-4380
I(1)	2.1 ± 1.0	abm	2160-1920
J(1)	-0.7 ± 1.0	abm	7240-6300
K(1)	0.5 ± 1.0	abm	5600-4840
L(1)	0.1 ± 1.0	abm	4990-4350
M(1)	1.0 ± 0.5	abm	4540-4240
AP14(2)	+3.0	abm	5310-4640
P20(3)	+1.0-2.0	abm	6690-6680
P21(3)	+1.0-2.0	abm	6600-6170
P29(3)	+3.00	abm	5050-4550

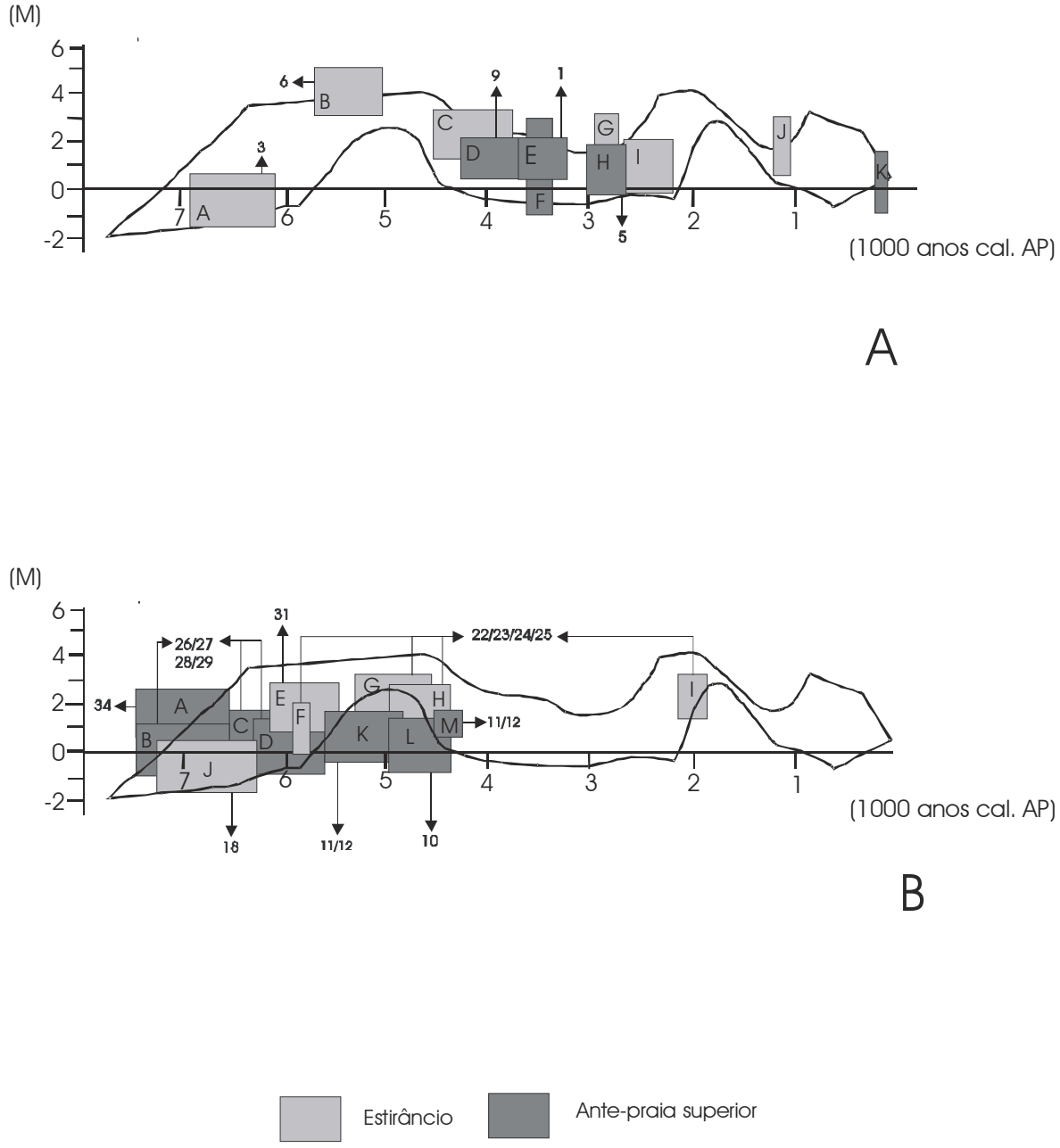

Figura 9: (A) Amostras datadas pelo Método do ^{14}C distribuídas ao longo da curva final de variação do nível do mar obtida para o litoral setentrional do Estado do Rio Grande do Norte (Bezerra *et al*., 2003). As datações foram feitas em conchas retiradas do arcabouço de *beachrocks* e a curva final resultou da interseção de duas outras obtidas para as costas E-W e N-S. Os números no interior dos retângulos referem-se às seções verticais usadas para interpretar as zonas de sedimentação predominantes (estirâncio ou ante-praia superior) do arcabouço dos *beachrocks* a partir dos quais as datações por ^{14}C foram obtidas. As letras no interior dos retângulos correspondem aos valores encontrados na Tabela 3; (B) Curva final de variação do nível do mar obtida para o litoral oriental do estado. As letras no interior dos retângulos correspondem aos valores encontrados na Tabela 4.

ARTIGO 2 - CEMENTATION PATTERNS AND GENETIC IMPLICATIONS OF HOLOCENE BEACHROCKS FROM NORTHEASTERN BRAZIL

O segundo artigo, submetido a *Sedimentary Geology,* teve como objetivos principais descrever os complexos padrões diagenéticos nos corpos de *beachrocks* distribuídos ao longo das costas oriental e setentrional do Estado do Rio Grande do Norte e investigar a distribuição destes padrões em relação às fácies deposicionais, idade máxima da cimentação e posição em relação à atual zona de intermarés.

Os *beachrocks* estudados mostram uma ampla variedade de processos, fábricas e texturas diagenéticas. Os cimentos carbonáticos são compostos exclusivamente de calcita altamente magnesiana, como revelado por tingimento e confirmado por espectroscopia de energia dispersada (EDS, Anexo 3). Eles ocorrem em sete morfologias principais:

1) cutículas criptocristalinas (Anexo 1: Prancha 1, Fig. C e E; Prancha 2, Fig. B);

2) franjas prismáticas isópacas (Anexo 1: Prancha 1, figs. C, D e E; Prancha 2, figs. A e B; Prancha 3, figs. B e C; Prancha 5, Fig. B; Anexo 2: Prancha 6 , figs. B, C e D; Prancha 7, figs. A, E e F; Prancha 8, figs. A, B, C, D, E e F; Prancha 9, figs. A, B e C);

3) espato equante (Anexo 1: Prancha 1, Fig. B; Prancha 4, Fig. E; Prancha 5, figs. C, D, E e F; Anexo 2: Prancha 6, figs. E e F; Prancha 9: figs. D, E e F);

4) preenchimento de poros criptocristalino ou micrítico (Anexo 1: Prancha 4, Fig. A; Anexo 2: Prancha 10, Fig. F);

5) agregados pseudo-peloidais (Anexo 1: Prancha 1, Fig. F; Prancha 2, Fig. E; Prancha 3, Fig, B; Prancha 4, Fig. D; Prancha 5, Fig. B; Anexo 2: Prancha 6, Fig. A; Prancha 7, Fig. C);

6) agregados radiais (Anexo 1: Prancha 4, Fig. F; Prancha 5, Fig. A; Anexo 2: Prancha 7, Fig. B; Prancha 10, figs. A, B, C, D e E);

7) agregados isolados e desorientados de cristais escalenoédricos (Anexo 1: Prancha 4, figs. C e F).

Outras feições diagenéticas incluem:

1) sedimentos infiltrados margosos híbridos (Anexo 1: Prancha 2, Fig. C e D; Prancha 3, figs. B, D e F);

2) micrita infiltrada (Anexo 1: Prancha 2, figs. E e F; Prancha 3, figs. A e F; Prancha 4, Fig. D; Prancha 5, figs. A e B; Anexo 2: Prancha 7, figs. A e D);

3) argilominerais autigênicos esmectíticos (Anexo 1: Prancha 1, Fig. A; Prancha 3, Fig. A);

4) preenchimentos de poro de calcedônia;

5) sedimento interno de silte vadoso (Anexo 1: Prancha 3, figs. C, D e E);

6) filmes orgânicos (Anexo 1: Prancha 2, Fig. A).

A Tabela 4 atesta a variabilidade no conteúdo de cada material diagenético nas litofácies 1 a 5. As franjas prismáticas isópacas, espato equante e as cutículas criptocristalinas são os produtos diagenéticos predominantes nos *beachrocks* descritos, particularmente nas litofácies 2 a 5. Na Litofácies 1, por outro lado, o material diagenético mais comum é o cimento micrítico pseudo-peloidal, seguido pela franja prismática e pelo espato equante. Outros aspectos peculiares referentes à Litofácies 1 são a presença dos maiores volumes de cimento criptocristalino de preenchimento de poros, sedimento margoso infiltrado, esmectita autigênica e cimento silicoso. A ocorrência preferencial destes constituintes nesta litofácies está provavelmente relacionado a sua maior granulometria e, conseqüentemente, maior permeabilidade original, e a uma maior exposição em comparação com as demais litofácies.

A distribuição das feições diagenéticas é extremamente variável ao longo das 36 seções verticais descritas na área estudada, não apenas em escala centimétrica, mas também em uma escala maior. Diferentes tipos de cimentos e material infiltrado ocorrem em combinação de no mínimo dois até seis elementos. Esta multiplicidade e distribuição irregular de constituintes diagenéticos indicam que a litificação dos *beachrocks* estudados ocorreu sob a influência de parâmetros que se alteram rapidamente, mesmo na escala de lâmina delgada.

As texturas dos cimentos calcíticos, juntamente com a sua composição altamente magnesiana, são indicativas de precipitação na zona freática marinha ativa. No que diz respeito à micrita infiltrada e aos infiltrados margosos híbridos, o deslocamento de águas lamosas deslocadas a partir da plataforma para o pós-praia, por tempestades, explicaria melhor a presença de feições vadosas e foraminíferos planctônicos nestes sedimentos. Argilominerais autigênicos esmectíticos podem estar relacionados à alteração meteórica de feldspatos e minerais pesados menos estáveis, no pós-praia, ou à alteração muito precoce destes mesmos minerais, sob condições marinhas. O cimento de calcedônia pode ter substituído o cimento carbonático ou preenchido poros criados pela dissolução de carbonatos, como resultado da influência de águas meteóricas. O sedimento interno de silte vadoso resultou da deposição, a partir de águas que percolantes, do silte gerado durante a exposição dos *beachrocks*. Os filmes orgânicos foram gerados em um micro-ambiente mais estagnado que propiciou a preservação de material orgânica microbial ao redor de cimentos carbonáticos.

Uma sucessão geral de fases diagenéticas pode ser proposta para os *beachrocks* estudados. De um modo geral, a cimentação por argilominerais esmectíticos foi o primeiro evento diagenético que afetou os *beachrocks* estudados, seguido da primeira geração de cutícula criptocristalina. Na maioria dos casos, os agregados radiais precipitaram-se após a formação das cutículas criptocristalinas e antes das franjas prismáticas isópacas ou do espato equante. As franjas prismáticas isópacas precipitaram-se antes do preenchimento de poros criptocristalino ou micrítico,

agregados pseudo-peloidais e micrita infiltrada. Entretanto, em alguns casos, uma única franja ocorre ao redor destes materiais de granulometria fina. A infiltração de micrita, marga ou silte, sob condições vadosas, foi o último evento a afetar as amostras.nas quais estes materiais ocorrem. Os filmes orgânicos ocorrem tipicamente ao redor de cimentos previamente precipitados.

A ausência de estruturas orgânicas sugere que o mecanismo por trás da cimentação dos beachrocks é essencialmente inorgânico, muito provavelmente através da evaporação de água do mar aprisionada nos poros, em resposta às condições climáticas secas. A variedade de texturas no cimento demonstra que os parâmetros diagenéticos mudaram através do tempo e do espaço. A força motora desta mudança de condições parece ser a diversidade de posições do nível do mar sob as quais os *beachrocks* foram gerados. Mais estudos são necessários para entender melhor a extensão e a amplitude através das quais avanços e recuos do nível do mar ou oscilações de menor ordem parecem influenciar a variedade de texturas nos cimentos.

Tabela 4: Quantidades média e máxima dos materiais diagenéticos nos *beachrocks* estudados.

Litofácies	**1**	**2**	**3**	**4**	**5**	**Máximo**	**Média**
franjas prismáticas isópacas	4.5	13.2	10.3	18.1	14.9	33.6	12.2
agregados radiais	0.4	1.0	1.9	0.0	1.8	22.8	1.0
espato equante	4.2	5.2	8.6	0.0	4.2	34.4	4.4
cutículas criptocristalinas	1.4	2.9	3.3	7.1	3.9	14.5	3.7
agregados pseudo-peloidais	5.2	0.4	0.03	0.0	1.1	38.8	1.3
preenchimento de poros micrítico	2.0	0.8	0.1	0.0	0.2	15.7	0.6
sed. infiltrados margosos híbridos	2.4	0.8	0.09	0.0	0.5	10.9	0.8
micrita infiltrada	0.6	0.9	0.09	1.6	0.0	18.7	0.6
cristais escalenoédricos	0.0	0.9	1.6	0.0	0.4	16.3	0.6
filmes orgânicos	0.0	0.0	0.1	0.0	0.0	5.0	0.02
esmectita autigênica	3.1	0.01	0.0	0.0	0.0	13.5	0.6
cimento silicoso	0.05	0.0	0.0	0.0	0.0	0.6	0.01

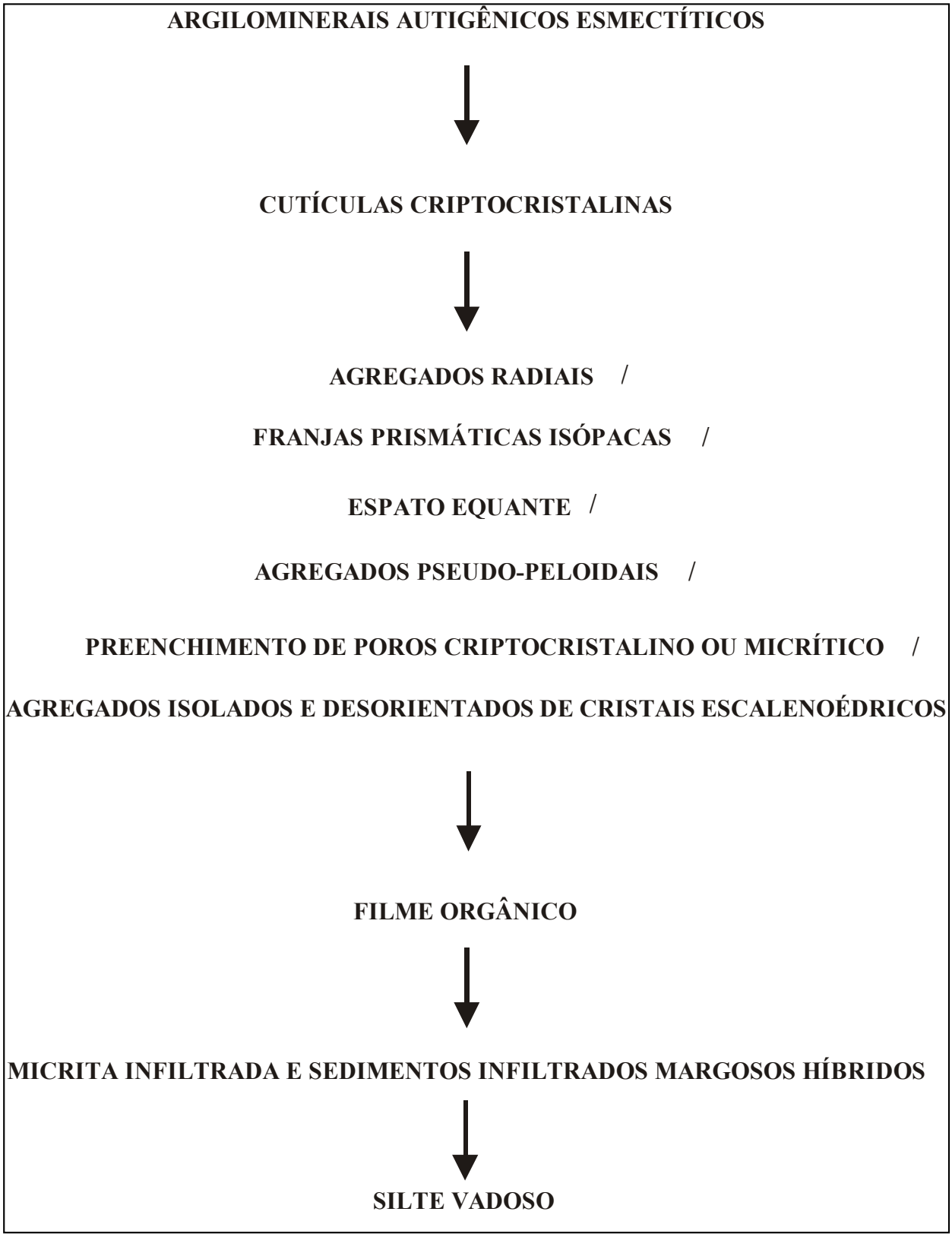

Figura 10: Sucessão geral de fases diagenéticas proposta para os *beachrocks* estudados.

ARTIGO 3 - ORIGIN OF HOLOCENE BEACHROCK CEMENTS IN NORTHEASTERN BRAZIL REVEALED BY CARBON AND OXYGEN ISOTOPES

O terceiro e último artigo, o qual foi submetido ao *Journal of Geology*, teve como objetivo principal revelar a complexa origem e evolução diagenética dos *beachrocks* estudados, tomando-se como base os valores de isótopos estáveis dos seus cimentos.

Os valores isotópicos ($\delta^{13}C_{VPDB}$ e $\delta^{18}O_{VPDB}$) obtidos para 30 amostras de *beachrocks* são mostrados na Tabela 5. Os valores de $\delta^{13}C_{VPDB}$ máximo, mínimo e médio são +3,57‰, –7,80‰ e +2,34‰, respectivamente. Os valores de $\delta^{18}O_{VPDB}$ variam de –4,41‰ a 0,54‰ (média: –0,22‰). Os valores isotópicos também foram analisados segundo o tipo predominante de cimento presente em cada amostra. O espato equante possui valores de $\delta^{13}C_{PDB}$ que variam de -7,80‰ a +3,53‰ (média: +1,57‰), valores de $\delta^{18}O_{VPDB}$ que variam de -4,41‰ a +0,54‰ (média: -0,56‰), e valores de $\delta^{18}O_{SMOW}$ que variam de +26,32‰ a +31,41‰ (média: +30,28‰). Amostras em que as franjas isópacas prismáticas predominam apresentam valores de $\delta^{13}C_{VPDB}$ entre +1,73‰ e +3,57‰ (média: +2,95‰), valores de $\delta^{18}O_{VPDB}$ entre -0,44‰ e +0,43‰ (média: +2,95‰) e valores de $\delta^{18}O_{SMOW}$ entre +30,40‰ e +31,30‰ (média: +30,94‰). Agregados isolados e desorientados de cristais escalenoédricos apresentam valores de $\delta^{13}C_{VPDB}$ que variam entre +3,15‰ e +3,52‰ (média: +3,31‰), valores de $\delta^{18}O_{VPDB}$ que variam entre +0,01‰ e +0,30‰ (média: +0,14‰) e valores de $\delta^{18}O_{SMOW}$ que variam entre +30,87‰ e +31,17‰ (média: +31,00‰). A única amostra em que os agregados pseudo-peloidais predominam possuem valores de $\delta^{13}C_{VPDB}$, $\delta^{18}O_{VPDB}$ e $\delta^{18}O_{SMOW}$ iguais a +2,89‰, 0,00‰ e +30,86‰, respectivamente.

De acordo com o gráfico $\delta^{18}O$ versus $\delta^{13}C$ (Fig. 12), a grande maioria das amostras analisadas (93% do total) apresenta valores de isótopos estáveis compatíveis com cimentos marinhos. Incluem-se nesta situação a maior parte das amostras com espato equante e todas as que possuem franjas prismáticas isópacas, agregados isolados e desorientados de cristais escalenoédricos e agregados pseudo-peloidais. Dois fatores podem ter influenciado esta assinatura isotópica uniforme: (a) a composição homogênea (calcita altamente magnesiana) dos cimentos nos *beachrocks* estudados; (b) a uniformidade nos parâmetros físico-químicos que controlam a cimentação nestas rochas, como atestado pela pequena variedade de valores de paleotemperatura calculados para as amostras estudadas. Duas amostras com predominância de espato equante apresentam valores de $\delta^{18}O$ fortemente negativos ($\delta^{13}C$ = -7.35 e -7.80 ‰; $\delta^{18}O$ = -4.41 e -4.33 ‰), provavelmente refletindo uma origem a partir de uma mistura de águas marinhas e meteóricas ou uma recristalização do cimento marinho a partir da interação com águas meteóricas.

As temperaturas de precipitação calculadas para as amostras com $\delta^{18}O_{VPDB}$ em torno de zero variam de 23,3 a 34,9ºC (valor médio: 25,8ºC), assumindo $\delta^{18}O_{VPDB}$ da água igual a 2,0 para os fluido precipitantes marinhos modificados por evaporação. Se um valor de $\delta^{18}O_{VPDB}$ igual a -2,0 for assumido para os fluidos precipitantes mistos, em boa parte meteóricos, obtêm-se temperaturas de 27.5 e 27.9ºC para os cimentos anômalos, valores estes compatíveis com as temperaturas de superfície da área. Quanto a cada tipo de cimento analisado individualmente os seguintes valores de temperatura de precipitação foram obtidos:

1) espato equante, 23,3 a 34,9ºC (valor médio: 26,1ºC);

2) franjas prismáticas isópacas, 23,8 a 28,0ºC (valor médio: 25,5ºC);

3) agregados isolados e desorientados de cristais escalenoédricos, 25,4 a 25,8ºC (valor médio: 25,6ºC).

No que diz respeito à única amostra com agregados pseudo-peloidais, a temperatura durante sua precipitação foi 25,9ºC.

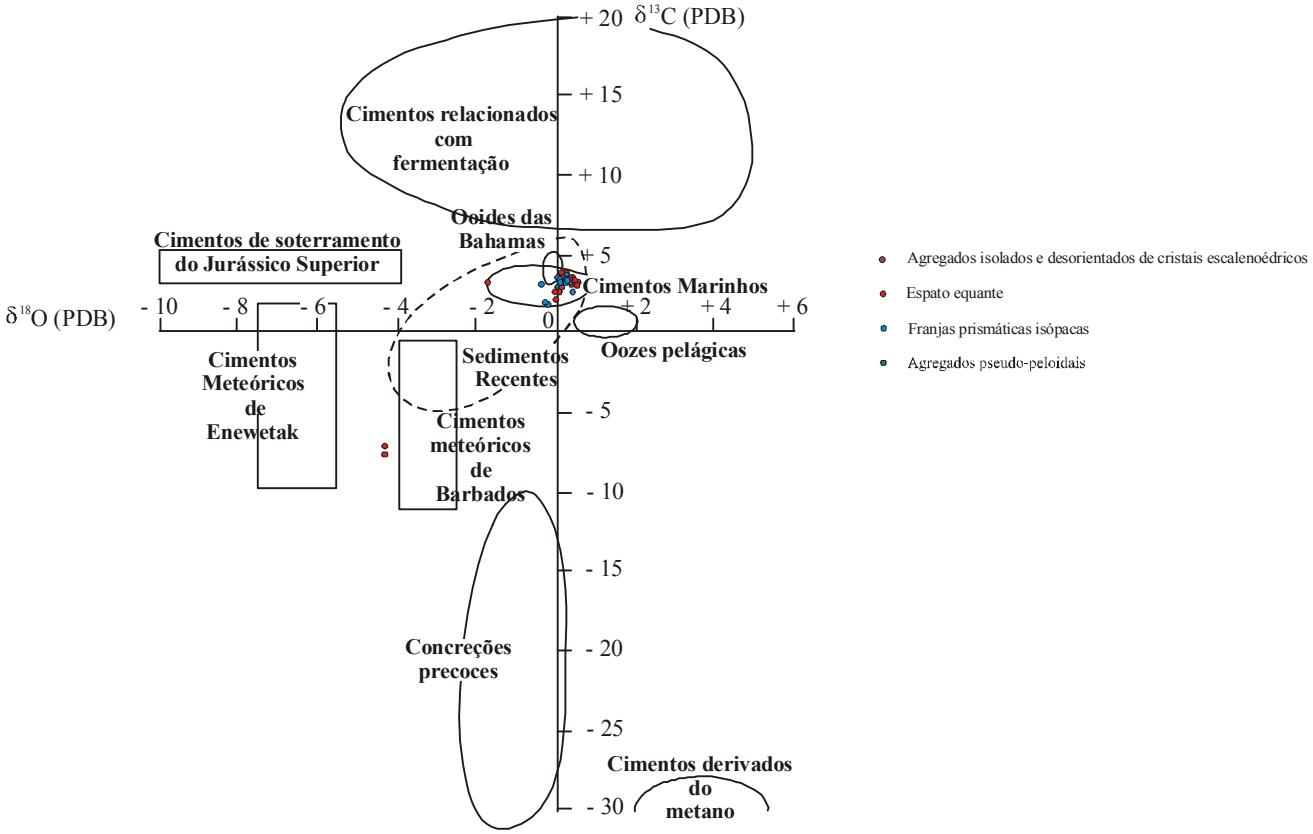

Figura 11: Gráfico $\delta^{18}O$ versus $\delta^{13}C$ (PDB, ‰) para as amostras de *beachrock* deste estudo. Ver Tabela 5 para análises. Adaptado de Moore (1989).

Tabela 5: Dados de isótopos estáveis de carbono e oxigênio para amostras de cimentos de *beachrocks* do Estado do Rio Grande do Norte. Os números das amostras correspondem à localização das mesmas de acordo com a Figura 1. Cimentos: (A) Franjas prismáticas isópacas; (B) espato equante; (C) agregados pseudo-peloidais; (D) agregados isolados e desorientados de cristais escalenoédricos. O parâmetro Z foi proposto por Keith e Weber (1964) com o objetivo de se diferenciar calcários marinhos (Z > 120) e de água doce (Z < 120), sendo o mesmo calculado a partir da equação $Z = a(\delta^{13}C + 50) + b(\delta^{18}O + 50)$ onde a=2.048 e b=0.498, respectivamente.

Amostra	Cimento	$\delta^{13}C_{VPDB}$	$\delta^{18}O_{SMOW}$	$\delta^{18}O_{VPDB}$	$\delta^{18}O$água	T (^{o}C)	Z
1	A	1,73	30,64	-0,21	2,0	26,9	130,74
2	A	1,83	30,53	-0,32	2,0	27,4	130,89
4	A	2,58	31,30	0,43	2,0	28,0	132,79
7	B	-7,35	26,32	-4,41	-2,0	27,9	110,05
8	B	2,08	30,78	-0,08	2,0	26,3	131,52
8	B	-7,80	26,40	-4,33	-2,0	27,5	109,17
12	A	3,55	31,12	0,25	2,0	24,7	134,69
13	B	3,43	31,22	0,35	2,0	24,2	134,49
13	B	3,38	31,16	0,29	2,0	24,5	134,36
14	B	3,32	31,22	0,35	2,0	24,2	134,27
15	B	3,24	29,01	-1,79	2,0	34,9	133,05
15	B	3,53	31,15	0,28	2,0	27,2	134,67
16	B	3,25	31,37	0,49	2,0	23,6	134,20
16	B	3,12	31,41	0,54	2,0	23,3	133,96
17	C	2,89	30,86	0,00	2,0	25,9	133,22
21	A	3,06	30,40	-0,44	2,0	23,8	133,35
22	A	3,05	31,01	0,15	2,0	25,2	133,62
22	A	3,42	31,15	0,28	2,0	24,6	134,44
23	A	3,25	31,22	0,35	2,0	24,2	134,13
24	A	3,57	30,87	0,01	2,0	25,8	134,61
24	D	3,27	30,97	0,11	2,0	25,4	134,05
24	A	3,03	30,94	0,08	2,0	25,5	133,55
27	A	3,20	31,13	0,26	2,0	24,6	133,98
27	D	3,52	31,17	0,30	2,0	25,7	134,66
28	D	3,15	30,87	0,01	2,0	25,8	133,75
29	A	3,12	30,97	0,10	2,0	25,4	133,74
32	B	3,07	31,21	0,34	2,0	24,3	133,76
32	B	3,47	31,04	0,17	2,0	25,1	134,49
34	B	2,72	30,92	0,06	2,0	25,6	132,90
34	B	2,48	30,74	-0,11	2,0	26,4	132,33

REFERÊNCIAS BIBLIOGRÁFICAS

Alexandersson, T. 1972. Mediterranean beachrock cementation: marine precipitation of Mg-calcite. In: Stanley, D.J. (ed.). The Mediterranean Sea: A natural sedimentation laboratory. Stroudsburg, Dowden, Hutchinson & Ross. p. 203–223.

Amaral, R.F. 1999. Contribuição ao estudo da evolução morfodinâmica do litoral oriental sul do Rio Grande do Norte, entre Ponta de Búzios e Baía Formosa. Porto Alegre. 252p. Tese de Doutorado em Geociências, Instituto de Geociências, Universidade Federal do Rio Grande do Sul.

Amieux, P.; Bernier, P.; Dalongeville, R. & Medwecki, V. 1989. Cathodoluminescence of carbonate-cemented Holocene beachrock from the Togo coastline (West Africa): an approach to early diagenesis. Sedimentary Geology, 65: 261–272.

Araripe, P.T. & Feijó, F.J. 1994. Bacia Potiguar. Boletim de Geociências da PETROBRAS, 8: 127 – 141.

Bertani, R.T.; Costa, I.G.; Mattos, R.M.D. 1990. Evolução tectono-sedimentar, estilo estrutural e habitat do petróleo na Bacia Potiguar. In: De Raja Gabaglia , G. P. & Milani, E. J. (coords.). Origem e evolução das bacias sedimentares. Rio de janeiro, PETROBRAS. p. 291 – 310.

Bezerra, F.H.R.; Lima-Filho, F.P.; Amaral, R.F.; Caldas, L.H.O. & Costa-Neto, L.X. 1998. Holocene coastal tectonics in NE Brazil. In: Stewart, I.S. & Vita-Finzi, C. (eds.). Coastal tectonics. Geol. Soc. London, Special Publication 146. p. 279–293.

Bezerra, F.H.R.; Barreto, A.M.F. & Suguio, K. 2003. Holocene sea-level history on the Rio Grande do Norte State coast, Brazil. Marine Geology, 196: 73–89.

Bezerra, F.H.R.; Amaral, R.F.; Lima-Filho, F.P.; Ferreira Jr., A.V.; Sena, E.S. & Diniz, R.F. 2004. Beachrock fracturing in Brazil. Journal of Coastal Research, Special Issue 42: 169–182.

Bigarella, J.J. 1975. Reef sandstones from northeastern Brazil (A survey on sedimentary structures). Anais da Academia Brasileira de Ciências 47: 395–409.

Bittencourt, A.C.S.P.; Martin, L.; Dominguez, J.M.L.; Silva, I.R. & Sousa, D.L. 2002. A significant longshore transport divergence zone at Northeastern Brazilian coast: implications on coastal Quaternary evolution. Anais da Academia Brasileira de Ciências, 74(3): 505–518.

Branner, J.C. 1904. The stone reefs of Brazil, their geological and geographical relations, with a chapter on the coral reefs. Museum of Comparative Zoology, Harvard College, Cambridge, Geological Series 7.

Bricker, O.P. (ed.). 1971. Carbonate cements. Johns Hopkins University, Studies in Geology 19.

Caldas, L.H.O. 1998. Estudo geológico e geofísico da Falha de Carnaubais, Bacia Potiguar – RN, e implicações tectônicas. Natal. 89p. Dissertação de Mestrado em Geodinâmica e Geofísica, Universidade Federal do Rio Grande do Norte.

Caldas, L.H.O. 2002. Late Quaternary coastal evolution of the northern Rio Grande do Norte coast, NE Brazil. Kiel. 92p. Ph.D. Thesis, University of Kiel.

Campos e Silva, A.; Silva, D.D. & Vasconcelos, M.D.T. 1964. Informação sobre a malacofauna dos beach rocks de Touros e São Bento do Norte. Arquivos do Instituto de Antropologia, 50(2): 79–90.

Chaves, M.S. 2000. Sedimentologia, morfologia praial e vulnerabilidade costeira entre as praias de Redinha e Genipabu, Natal/RN. Recife. 136p. Dissertação de Mestrado em Geociências, Centro de Tecnologia e Geociências, Universidade Federal de Pernambuco.

Chaves, N.S. & Sial, A.N. 1998. Mixed oceanic and freshwater depositional conditions for beachrocks of Northeast Brazil: evidence from carbon and oxygen isotopes. International Geology Review 40: 748–754.

Chivas, A.; Chippell, J.; Polach, H.; Pillans, B. & Flood, P. 1986. Radiocarbon evidence for the timing and rate of island development, beachrock formation and phosphatization at Lady Elliot Island, Queensland, Australia. Marine Geology, 69: 273–287.

Choquette, P.W. & Pray, L.C. 1970. Geologic nomenclature and classification of porosity in sedimentary carbonates. The American Association of Petroleum Geologists Bulletin, 54: 207 – 250.

Cooper, J.A.G. 1991. Beachrock formation in low latitudes: implications for coastal evolutionary models. Marine Geology, 98: 145 – 154.

Cooray, P.G. 1968. A note on the occurrence of beachrock along the west coast of Ceylon. Journal of Sedimentary Petrology, 38: 650–654.

Craig, H., 1957. Isotopic standards for carbon and oxygen correction factors for mass spectrometric analysis of carbon dioxide. Geochim. Cosmochem. Acta, 12: 133-149.

Craig, H. 1961. Standard for reporting concentrations of deuterium and oxygen-18 in natural water. Science, 133: 1833-1834.

Fonseca, V.P., *et al*. 1997. Mapeamento Geológico – Geomorfológico (1:250.000) do Litoral Oriental do Estado do Rio Grande do Norte: Primeiros Resultados. In: SIMPÓSIO DE GEOLOGIA DO NORDESTE , 17., 1997, Fortaleza. Boletim..., SBG. v. 15, p. 378-382.

Friedman, G.M. 1971. Staining. In: R.E. Carner (ed.). Procedures in sedimentary petrology. New York, Wiley. p. 511–530.

Ginsburg, R.N. 1953. Beachrock in south Florida. Journal of Sedimentary Petrology, 23: 85–92.

Hanor, J.S. 1978. Precipitation of beachrock cements: mixing of marine and meteoric waters *vs*. CO_2 degassing. Journal of Sedimentary Petrology, 48(2): 489–501.

Holail, H. & Rashed, M. 1992. Stable isotopic composition of carbonate-cemented recent beachrock along the Mediterranean and Red Sea Coasts of Egypt. Marine Geology, 106: 141–148.

Hopley, D. 1986. Beachrock as a sea-level indicator. In: Van de Plassche, O. (ed.). Sea-level research: a manual for collection and evaluation of data. Norwich, Geo Books. p. 157–173.

IPT. 1982. Estudos Hidrogeológico Regional Detalhado do Estado do Rio Grande do Norte. Secretaria de Indústria e Comércio do Rio Grande do Norte, vol.1, 389 p.

Keith, M.L. & Weber, J.N. 1964. Carbon and oxygen isotopic composition of selected limestones and fossils. Geochimica et Cosmochimica Acta, 28: 1787 – 1816.

Khalaf, F.I. 1988. Quaternary calcareous hard rocks and the associated sediments in the intertidal and offshore zones of Kuwait. Marine Geology, 80: 1–27.

Kindler, P. & Bain, R.J. 1993. Submerged Upper Holocene on San Salvador Island, Bahamas: implications for recent sea-level history. Geologische Rundschau, 82: 241–247.

Lacerda, A.M.A. 1999. Caracterização geológica e hidrogeológica da região de Monte Alegre – RN. Natal. 83p. Relatório de Graduação, Universidade Federal do Rio Grande do Norte.

Longman, M.W. 1980. Carbonate diagenetic textures from nearsurface diagenetic environments. The American Association of Petroleum Geologists Bulletin, 64: 461–487.

Mabessone, J.M. & Alheiros, M.M. 1991. Base Estrutural. In: Estudos Geológicos: Revisão Geológica da Faixa Costeira de Pernambuco, Paraíba e Parte do Rio Grande do Norte, Recife, UFPE, Série B, v. 10, p. 33-43.

Maury, C.J. 1934. Fossil invertebrata from northeastern Brazil. American Museum of Natural History Bulletin 67(4), 123–179.

Mendonça, M.I. 1966. O recife de arenito de Tibau. Arquivos do Instituto de Antropologia, 2: 343–346.

Meyers, J.H. 1987. Marine vadose beachrock cementation by criptocrystalline magnesian calcite–Maui, Hawaii. Journal of Sedimentary Petrology, 57: 558–570.

Miller, W.R., Mason, T.R. 1994. Erosional features of coastal beachrock and eolianite outcrops in Natal and Zululand, South Africa. Journal of Coastal Research, 10(2): 394–414.

Milliman, J.D. 1974. Marine carbonates. New York, Springer-Verlag, 375 p.

Moore, C. H. 1989. Carbonate diagenesis and porosity: Developments in Sedimentology 46, Elsevier, 301p.

Neumeier, U. 1999. Experimental modelling of beachrock cementation under microbial influence. Sedimentary Geology, 126: 35–46.

Nimer, E. 1989. Climatologia do Brasil. Rio de Janeiro, Instituto Brasileiro de Geografia e Estatística, Departamento de Recursos Naturais e Ambientais.

Oliveira, M.I.M., 1978. Os recifes de Natal. Recife. 76p. Dissertação de Mestrado em Geociências, Centro de Tecnologia e Geociências, Universidade Federal de Pernambuco.

Oliveira, M.I.M.; Bagnoli, E.; Farias, C.C.; Nogueira, A.M.B. & Santiago, M. 1990. Considerações sobre a geometria, petrografia, sedimentologia, diagênese e idades dos *beachrocks* do Rio Grande do Norte. In: CONGRESSO BRASILEIRO DE GEOLOGIA, 35., 1990, Natal. Boletim de Resumos... Natal, SBG. v. 2, p. 621–34.

Russell, R.J. 1959. Caribbean beach rock observation. Zeit. Geomorphologie, 3: 227–236.

Russell, R.J. 1962. Origin of beach rock. Zeit. Geomorphologie 6: 1–16.

Sanlaville, P.; Dalongeville, R.; Bernier, P. & Evin, J. 1997. The Syrian coast: a model of Holocene coastal evolution. Journal of Coastal Research, 13(2): 385–396.

Silva, C. G. 1991. Holocene stratigraphy and evolution of the Açu River Delta, Rio Grande do Norte State, northeastern Brazil. Durham. PhD Thesis, Duke University.

Souza, S. M. 1982. Atualização da litoestratigrafia da Bacia Potiguar. In: CONGRESSO BRASILEIRO DE GEOLOGIA, 32., 1982, Salvador. Anais...Salvador, SBG, v. 5, p. 2392 – 2406.

Stattegger, K., Caldas, L.H.O., Vital, H., 2004. Holocene coastal evolution of the northern Rio Grande do Norte Coast, NE Brazil. *Journal of Coastal Research*, Special Issue 39**.**

Stoddart, D.R.; Cann, J.R. 1965. Nature and origin of beach rock. Journal of Sedimentary Petrology, 35; 243-273.

Tabosa, W.F. 2002. Monitoramento costeiro das praias de São Bento do Norte e Caiçara do Norte, RN: implicações para o pólo petrolífero de Guamaré. Natal. 112p. Dissertação de Mestrado em Geodinâmica e Geofísica, Universidade Federal do Rio Grande do Norte.

Tietz, G., Muller, G. 1971. High magnesian calcite and aragonite cementation in recent beachrocks, Fuerteventura, Canary Islands, Spain. In: Bricker, O. P. (ed.). Carbonate cements. Johns Hopkins University Studies in Geology 19, p.5.

Urey, H.C.; Lowestam, H.A.; Epstein, S. & McKinney, C.R. 1951. Measurements of paleotemperatures and temperatures of the Upper Cretaceous of England, Denmark and the southeastern United States. Geological Society of American Bulletin, 62: 399-416.

Vianna, M.L.; Cabral, A.P. & Gherardi, D.F.M. 1993. TM-Landsat imagery applied to study of the impact of global climate change on a tropical coastal environment during the last deglaciation. International Journal of Remote Sensing, 14(14): 2971–2983.

Warne, S. St. J. 1962. A quick field or laboratory staining scheme for the differentiation of the major carbonate minerals. Journal of Sedimentary Petrology, 32(1): 29–38.

Webb, G.E.; Jell, J.S. & Baker, J.C. 1999. Cryptic intertidal microbialites in beachrock, Heron Island, Great Barrier Reef: implications for the origin of microcrystalline beachrock cement. Sedimentary Geology, 126: 317–334.

ARTIGO 1

LITHOFACIOLOGY AND PALAEOENVIRONMENTAL ANALYSIS OF HOLOCENE BEACHROCKS IN NORTHEASTERN BRAZIL

LITHOFACIOLOGY AND PALAEOENVIRONMENTAL ANALYSIS OF HOLOCENE BEACHROCKS IN NORTHEASTERN BRAZIL

Marcela Marques Vieira[a,*], Luiz Fernando De Ros[b], Francisco Hilário Rego Bezerra[a]

[a]Departamento de Geologia, Centro de Ciências Exatas e da Terra, Universidade Federal do Rio Grande do Norte, Caixa Postal: 1639, CEP: 59072-970, Natal, RN, Brazil. Fax number: ++558432153806.

[b]Instituto de Geociências, Universidade Federal do Rio Grande do Sul, Av. Bento Gonçalves, 9500, CEP: 91501-970, Porto Alegre, RS, Brazil.

*Corresponding author

E-mail adresses:

marcela@geologia.ufrn.br (M. M. Vieira)

lfderos@inf.ufrgs.br (L. F. De Ros)

bezerrafh@geologia.ufrn.br (F. H. R. Bezerra)

ABSTRACT: Five lithofacies were identified in beachrock ledges distributed along the eastern and northern coasts of the state of Rio Grande do Norte, northeastern Brazil: (1) Massive to Weakly Stratified Conglomerate; (2) Low-Angle Cross-Stratified Conglomerate and Sandstone; (3) Medium-Scale Tabular-Planar and Trough Cross-Stratified Sandstone; (4) Skolithos-Bioturbated Conglomeratic Sandstone and (5) Massive Sandstones. Most of the described beachrocks (53% relative to total thickness) were deposited on the upper shoreface zone, represented by Lithofacies 3 and 4. Lithofacies 2, which was deposited on the foreshore zone, represent 31% of the sections described. The remaining 16% are attributed to collapse of overlying material as a result of sea cliff undercutting (massive conglomerate, Lithofacies 1), transport as traction-carpet deposit (weakly stratified conglomerate, Lithofacies 1), and high degree of alteration (Lithofacies 5). The distribution of ^{14}C dated beachrock samples in a sea-level envelope curve shows that, along the northern coast, framework constituents were predominantly deposited between ~4140–2190 cal. yr BP, when sea level dropped, and during low sea-level stillstand. On the northern coast, the upper shoreface sedimentation zone is preferentially distributed during sea-level drop and low sea-level stillstand phases, while the foreshore sedimentation zone can be found along the whole sea-level curve. Conversely, the beach deposits distributed along the eastern coast were preferentially formed between ~7460–4240 cal. yr BP, during rapid sea-level rise and high sea-level stillstand. In the case of the eastern coast, both zones are equally concentrated in the first stages of rapid sea-level rise and high sea-level stillstand.

Additional Index Words: *sea-level, shoreface, foreshore, Brazil, radiocarbon dating.*

INTRODUCTION

Beachrocks are common along many littoral zones throughout the world. They are conventionally defined as friable to well-cemented sedimentary rocks, formed in the intertidal or adjacent subtidal zones, in tropical or subtropical regions, consisting of sand or gravel (detrital and/or skeletal) cemented with calcium carbonate (BATES AND JACKSON, 1987). Beachrocks form very rapidly (BRICKER, 1971), as attested by the common presence of objects from present or recent times cemented into the surrounding beach materials (FRANKEL, 1968).

The literature is replete with descriptions of beachrocks; nevertheless, their origin is not fully understood, even after many decades of investigation. Mixing of marine and meteoric waters (SCHMALZ, 1971; MOORE, 1973), evaporation (GINSBURG, 1953; TAYLOR AND ILLING, 1969; MOORE AND BILLINGS, 1971), CO_2 degassing of shallow groundwater (HANOR, 1978; BINKLEY *et al*., 1980; GISCHLER AND LOMANDO, 1997), and direct or indirect activity of organisms (MAXWELL, 1962; WEBB *et al*., 1999; NEUMEIER, 1999) have been pointed out as the most common processes responsible for the lithification of these rocks.

Two other aspects of beachrock formation have been the center of controversy. First, the exact portion of the beach profile in which the original sands have been for the most part deposited (intertidal or adjacent supratidal and subtidal zones). Second, there are some uncertainties between sea-level changes and beachrock cementation. A few authors suggest that beachrocks are formed during sea-level rise (ALEXANDERSSON, 1972), high sea-level stillstand (COORAY, 1968), sea-level drop (SIESSER, 1974), and low sea-level stillstand (KINDLER AND BAIN, 1993).

In order to give some contribution to the elucidation of these two last points, this work attempts to (a) make an accurate description of beachrock lithofacies from several locations in northeastern Brazil (Fig. 1); (b) interpret their palaeoenvironmental setting; (c) relate beachrock deposition and cementation to sea-level changes. The study area serves very well for these purposes, since several beachrock ledges, some with great continuous extension, are encountered along its eastern and northern coasts and radiocarbon dating of samples has been carried out at various sites (OLIVEIRA *et al*., 1990; BEZERRA *et al*., 2003; STATTEGER *et al*., 2004).

GEOLOGICAL AND COASTAL SETTING

The pre-Quaternary stratigraphy of the study area includes sequences that outcrop exclusively along the northern coast (Fig. 2), comprising carbonate rocks of Jandaíra Formation (Turonian-Campanian), silty/muddy sandstones of Tibau Formation (Campanian-Pliocene) and Tertiary (Eocene-Oligocene) basalts of Macau Formation. Carbonate rocks and calciferous/fossiliferous sandstones of Guamaré Formation (Campanian-Pliocene) outcrop on both the northern and eastern coasts (Fig. 3), as well as the conglomerates, sandstones, and mudrocks of the alluvial Barreiras Formation (Miocene-Pleistocene). The Barreiras Formation forms cliffs along the entire coast of the state, which are in some places overlain by raised marine terraces formed during Late Pleistocene transgressions (ages from 220 ± 2 ka to 110 ± 10 ka BP; BARRETO *et al*., 2002A). Quaternary units also include the eolian quartzose sandstones of the Potengi Formation,

beachrocks, fixed dunes, peat, diatomite, and travertine, as well as Recent beach, aeolian, alluvial, and mangrove swamp sediments (SILVA AND NOGUEIRA, 1995).

The study area has a tropical climate with typical air temperatures of 30°C and average rainfall between 600 and 1,000 mm/year (NIMER, 1989). Both northern and eastern coasts present a semidiurnal mesotidal regime in which the tide interval varies from 3.2 m to 0.8 m, along the northern coast, and from 2.7 m to 0.1 m, along the eastern coast. Throughout most of the year, trade winds result in strong southeasterly and northeasterly winds that blow towards the eastern and northern coast, respectively. As a result of this, longshore currents flow to the north along the eastern coast, and to the west along the northern coast (BITTENCOURT *et al*., 2002).

Year-long measurements taken in the towns of Caiçara do Norte (Fig. 2) show that the longshore current velocity varies from 0.07 m/s to 0.85 m/s and the wave height ranges between 49.7 cm and 5.3 cm (TABOSA, 2002). Measurements taken during six months on beaches located along the eastern coast indicated longshore current velocities between 0.863 m/s and 0.066 m/s, and wave height between 90.3 cm and 20.1 cm (CHAVES, 2000).

The study area is characterized by the predominance of intermittent medium to small rivers whose discharge is insignificant for the most part of the year, with a few perennial large rivers, including some estuaries, which commonly drain into lagoons and tidal flats.

GENERAL BEACHROCK FEATURES

The beachrocks of the State of Rio Grande do Norte are discontinuously exposed along its eastern and northern shorelines (figs. 2 and 3). Some of the ledges can be followed

for up to 8 km parallel to the beach (Fig. 4A), while others are isolated bodies a few metres long. The semidiurnal mesotidal regime has a direct effect on beachrock thickness, which attains greater values than on coasts under microtidal influence. As to the studied beachrocks, they range in thickness from a few centimetres to nearly 3 m (average value: 42 cm) and in width from 2 to 50 m. Most of beachrock ledges occur close to current sea level; nevertheless, a few can be found 10 km inland from the beach (SILVA, 1991) and 5.7 km offshore (VIANNA *et al*., 1993). Radiocarbon dating of samples collected at various sites between the towns of Macau and Baía Formosa yielded ages from c. 7460 to 110 cal. yr BP (calibrated years Before Present; BEZERRA *et al*., 2003).

Most beachrock ledges are made up of gently seaward-dipping ($<10^{o}$) tabular beds that are 5 to 150 cm thick and light-brown in color. The lower and upper contacts of these beds with adjacent ones are abrupt. The upper surface of the studied beachrocks is rarely smooth. Most of them present erosional features similar to those of beachrocks and aeolianites of South Africa (MILLER AND MASON, 1994), with spitzkarren (upward-pointing pyramids separated by clefts or solution basins, Fig. 4B) and near-circular depressions (solution basins and potholes, Fig. 4C) as the most common features.

Beachrock ledges are composed mainly of monocrystalline quartz grains (average: 52%; maximum: 70%) and, to a lesser extent, of polycrystalline quartz grains (average: 8.9%; maximum: 75.5%), feldspar grains (mainly K-feldspar; average: 0.3%; maximum: 2.3%), heavy minerals (average: 0.3%; maximum: 9.6%), bioclasts (gastropods, bivalves, foraminifers, red algae, and equinoids; average: 2.2%; maximum: 29.6%), and fragments of hematite-cemented sandstones of the Barreiras Formation (average: 0.9%; maximum: 41.4%; Fig. 5A). Reworked beachrock fragments of various sizes are commonly found, not only as framework constituents (average: 0.02%; maximum: 3.6%), but also as slabs of up

to 2.0 m long, which accumulate in the intertidal or shallow subtidal zones as a result of coastal erosion and onshore wave action (Fig. 4D).

The studied beachrocks show a wide variability in diagenetic processes, fabrics, and textures. Carbonate cements are composed exclusively of high-Mg calcite, as revealed by staining and confirmed by energy dispersive spectroscopy (EDS) techniques. Their predominant morphologies, in decreasing relative amounts, are: (1) isopachous prismatic rims (Fig. 5B); (2) equant spar (Fig. 5C); and (3) cryptocrystalline coatings (Fig. 5B). Apart from carbonate cements, other diagenetic features include: infiltrated material (silt, hybrid sediment, and micrite; Fig. 5D), non-carbonate cements (smectite and chalcedony), and organic film. The average amounts of framework, cement, infiltrated material, and porosity are 64.6% (maximum: 80%), 24.6% (maximum: 38.8%), 1.4% (maximum: 18.7%), and 9.4% (maximum: 30.7%), respectively, in the studied rocks.

LITHOFACIES

Vertical sections were constructed at 36 sites distributed along several beachrock ledges located on the eastern and northern coasts of the state of Rio Grande do Norte (Figs. 1, 2, and 3). The thickness of rock described at the various sites reached a total of approximately 40 m. Textural characteristics and sedimentary structures were used to group the examined vertical sections into five lithofacies. Descriptions were accompanied by the collection of samples, 112 of which were impregnated with blue epoxy resin, slabbed, thin-sectioned, and quantitatively analysed with a petrographic microscope. The observations made from these thin sections were integrated with field data to help in the description of the lithofacies. A summary of lithofacies description and paleoenvironmental interpretation is

shown in Table 1, which also includes the percentage of lithofacies in relation to the total thickness of beachrock described. Average and maximum content of framework grains, cement, infiltrated materials, and porosity obtained for the lithofacies separately and for the studied beachrocks as a whole are displayed in Table 2.

Lithofacies 1: Massive to Weakly Stratified Conglomerate

This lithofacies consists of massive to weakly seaward-dipping stratified, poorly to very poorly sorted, matrix- to clast-supported sharp-based conglomerates. The gravel fraction includes boulders up to 30 cm in diameter to granules. The modal size of the pebbles is 2.0 cm, but they commonly reach 5.0 cm long. The composition of this coarser-grained fraction varies from predominantly quartzose, with well-rounded to rounded quartz grains (average: 82%; maximum: 99%), to subrounded, to very angular fragments of lateritic sandstone of Barreiras Formation (average: 90.8%; maximum: 100%; Fig. 6A). Less frequently, subrounded to subangular intraclasts of beachrock are also present. The sand fraction is composed of moderately to well-sorted, coarse to very coarse, rounded to subrounded, quartz grains with subordinate amounts of other constituents (Table 2). This lithofacies represents approximately 5.2% of the total described sections (Table 1), and its thickness varies from 10 to 35 cm, with an average value of 23 cm.

Lithofacies 2: Low-Angle Cross-Stratified Conglomerate and Sandstone

This lithofacies presents a textural gradation from sandy conglomerate to sandstone. The conglomeratic strata contain mainly rounded to well-rounded pebbles up to 3.0 cm

long, with modal size of 1.0 cm, granules, and lesser amounts of subrounded to rounded, coarse to very coarse sand. These rocks range from poorly to moderately sorted. The beds richer in sand are made up of moderately to well-sorted, subrounded to subangular, coarse to very coarse sandstone, containing a few dispersed pebbles up to 1.5 cm, with modal size of 1.0 cm, and granules. They vary from moderately to well-sorted. Transitional between these two extreme types are conglomeratic sandstones in which granules and pebbles up to 3.0 cm long, with modal size of 1.0 cm, are dispersed in a coarse to very coarse subrounded to rounded sandy fraction. These rocks range from very poorly to moderately sorted and commonly constitute normally graded sequences with the sandy conglomerates at the base.

Lithofacies 2 is commonly sharp-based and ranges in thickness from 5 to 100 cm, with an average value of approximately 35.0 cm. It makes up approximately 31% of the described sections (Table 1), being encountered along both the eastern and northern coasts. A seaward-dipping low-angle ($<10^0$), occasionally incipient stratification is characteristic of this lithofacies (Fig. 6B).

Lithofacies 3: Medium-Scale Tabular-Planar and Trough Cross-Stratified Sandstone

This lithofacies comprises poorly to very poorly sorted conglomeratic sandstones and moderately to well-sorted sandstones. The sandy fraction consists of very coarse to medium-grained subangular to rounded clasts, whereas the gravel fraction, which contributes with a maximum of 15% to the described rocks, comprises granules and pebbles up to 3.0 cm long, with modal size of 1.0 cm. This may occur as granule-rich laminae, particularly in medium-grained sandstones, or in the case of conglomeratic sandstones, as dispersed grains in a sandy matrix.

Lithofacies 3 is commonly sharp-based and ranges in thickness from 5 to 150 cm, with an average value of approximately 42 cm. It makes up approximately 51.5% of the described sections (Table 1), being encountered both on the eastern and northern coasts. This facies is characterized by the predominance of small- to medium-scale trough cross-strata (7.7–94 cm sets and individual troughs 50–270 cm wide, with average values of 36 and 96.2 cm, respectively), which were identified in 92% of the units representative of Lithofacies 3 (Fig. 6C). The remaining 8% comprises tabular-planar cross-stratification (7.1–30 cm sets, with an average value of 15.9 cm), found at locations 15 and 32, occasionally arranged in a herringbone pattern (Location 6). The orientation of cross-strata is generally unimodal and consistent along each coast; that is, to the NNE, along the eastern coast, and to the WNW, along the northern coast. A few sets of trough cross-sets show orientation opposite to the dominant one (to the SW and SSE, Location 13).

Lithofacies 4: Skolithos-Bioturbated Conglomeratic Sandstone

This lithofacies is composed of coarse to very coarse sandstones with granules and pebbles up to 1.0 cm long, with modal size of 0.5 cm. Its framework is poorly to very poorly sorted, and it is made up of subrounded to rounded quartzose grains and other minor constituents (Table 2).

Numerous vertical tubes, better seen in cross-section view are characteristic of this lithofacies (Fig. 6D). These tubes are densely clustered together, and their cross-section is almost circular (1.5 to 3.0 cm in diameter). These features are interpreted as corresponding to the common burrow Ophiomorpha, which belongs to the Skolithos ichnofacies (PROTHERO AND SCHWAB, 1996). Some of the investigated tubes have a bumpy outer

surface probably caused by fecal pellet lining. The primary stratification has been completely destroyed by the great abundance of burrows. This lithofacies was described at only one site (Location 5), on the northern coast, where it has a thickness of 60 cm. It makes up 1.5% of the described beachrocks (Table 1).

Lithofacies 5: Massive Sandstone

This lithofacies comprises poorly to well-sorted, medium to very coarse-grained sandstones with rounded to subrounded grains. Dispersed granules and pebbles up to 2.0 cm long with an average size of 1.0 cm may be present, noted in less than 5% of the rocks. Its average thickness is approximately 48 cm, with a maximum of 100 cm, and it represents 10.8% of the studied beachrocks (Table 1), being encountered mostly as massive sandstones that are at either the base or the top of the described sections (Locations 15, 19, 23, 28, and 33).

DISCUSSION

Depositional Environments

Low to mid-latitude passive margins are characterized by long sandy beaches composed of fine to medium quartz sand, with carbonate sands adjacent to coral reefs and more protected and low-gradient deltaic shores usually dominated by muddy tidal flats. Low-latitude beaches are usually lower energy and reflective, except where exposed to higher ocean waves as in northeastern Brazil (SHORT, 1999A). This is confirmed in the

work by DINIZ (2002), who classified the beaches along the eastern coast of the state of Rio Grande do Norte as predominantly intermediary, in accordance with the classification proposed by WRIGHT AND SHORT (1984). The adopted parameters were wave breaking (frequently plunging), presence of beach cusps and rip currents, size of sediments (medium to coarse sand), and moderate inclination of shoreface. According to the same author, only restricted sectors of the coast present reflective beaches. Particular beach types also encountered on the eastern coast of the state include the ones with zeta morphology and others protected by beachrocks and marine-cut terraces of Barreiras Formation. The same beach types are found along the northern coasts of the state.

Intertidal and adjacent subtidal zones have been pointed out as the most common places where beachrock has been formed (TAYLOR AND ILLING, 1969; MOORE AND BILLINGS, 1971; BEIER, 1985; KHALAF, 1988; GISCHLER AND LOMANDO, 1997; CHAVES AND SIAL, 1998). In general, the structure of the swash zone along intermediate beaches is continuous longshore, tabular horizontal to seaward-dipping beach laminae (SHORT AND HESP, 1999, Fig. 7A). These usually dip seaward at 1–2^{o} and may display a transition from lower gradient, more continuous, and parallel in the upper swash zone, to steeper gradient, more discontinuous laminae, with coarser, more poorly sorted, and more carbonate-rich sediments in the lower swash zone, peaking at the step, if present. The intermediate shoreface zones are even more complex, as they contain morphologically distinct shallow bars, deeper rip channels, shore-parallel rip feeder, and longshore troughs.

Lithofacies 1

The sources and mechanisms of gravel supply to beaches have been investigated by several authors. Fluvial input, storm mobilization of shallow nearshore sources, sea cliff erosion, reworking of earlier-raised gravel beaches and redistribution along the beach by strong longshore currents have been the most cited processes in the literature. The resultant conglomeratic layer is commonly interpreted as a lag deposit that results from wave erosion acting on the sediment-starved beach foreshore and shoreface, during transgressive processes (INDEN AND MOORE, 1983). This frontal attack by waves removes fine particles from the coastal material and transports them by the strong undertow to deeper water, developing steep slopes in the backshore area. The continuous undercutting of the backshore by wave action leads to the collapse of the overlying material and the accumulation of large blocks, coarse fragments, and coarse sand at the foot of the backshore. Strong longshore currents may remove this material from the shore, leaving the backshore exposed to more frontal wave attack (EL-SAYED AND AL-BAKRI, 1994).

Descriptions of conglomeratic beachrocks can also be found in the literature. RUSSELL (1959), in St. Lucia Island (Caribbean Sea); HOPLEY (1986), in Curacoa Island (north Queensland); and GISCHLER AND LOMANDO (1997), in Belize, identified coarse-grained beachrocks, including boulders. Nevertheless, no hypothesis was put forward by these authors to account for their possible origin.

High-energy erosion involving undercutting and disruption of previously cemented beachrocks was suggested as a possible process of conglomeratic beachrock formation by MAXWELL (1962), in the Heron Island Reef (Great Barrier Reef), and by AMIEUX *et al*. (1989), along the Togo coastline (West Africa).

Undermining of a nearby cliff by wave and storm action, with collapse of the overlying beds, was proposed by SCOFFIN (1970) as the mechanism by which limestone

boulders found in the conglomeratic beachrock of Bimini (Bahamas) were generated. The same origin was suggested by STRASSER AND DAVAUD (1986) for the blocks incorporated into the basal part of a limestone sequence, on Joulter Cays (Bahamas), which also presents beachrock relicts.

In light of these previous works, Lithofacies 1 is interpreted to represent an erosional lag resulting from high-energy erosive flows of possible storm-related origin, during a marine transgression. Its high gravel content, frequently including blocks and boulders, poor to very poor sorting, absence of structures in most outcrops, sharp basal contact, and composition richer in material eroded from adjacent sea cliffs provide good evidence for this interpretation. In the case of vertical sections 16, 17, 19, 20, 21, and 35, their close proximity to the lateritic outcrops of Barreiras Formation casts no doubt on the origin of Lithofacies 1 by undercutting of sea cliffs and collapse of the overlying material (Fig. 8). The smaller roundness of these lateritic fragments confirms its proximal source. These gravel erosional lags are associated not only with trough cross-stratified layers, typical of the shoreface zone, but also with seaward-dipping plane beds characteristic of the foreshore zone.

At two other locations—vertical sections 36 (at the mouth of the Guaju River) and 7 (flanked by a wide coastal plain)—there is no apparent nearby source of lateritic sediment. In the first case, the Guaju River, which drains through a coastal tableland composed of Barreiras Formation, is interpreted to have delivered its bedload, including the gravel portion, to the coast during flood stages. This fact, together with the reflective character of the beach in front of the river mouth (DINIZ, 2002), which can be the same existent during beachrock formation, would account for the deposition of coarser-grained, occasionally conglomeratic sediments. This type of beach is characterized by a relatively

steep beachface, with waves breaking over the base of the beach and running up and down it as a strong uprush and backwash (SHORT, 1999b). In the second case (location 7), westward longshore currents related to large storm waves were the possible mechanism for gravel input to the beach. The source for the lateritic clasts would be the outcrops of the Barreiras Formation located in the east (BARROS, 2001). In both cases, high-energy flows transported the gravel sediment that constituted Lithofacies 1 as traction carpet deposits.

Lithofacies 2

The presence of a gentle seaward-dipping stratification in Lithofacies 2, together with its comparatively better sorting and finer grain size, are indicative of deposition in the foreshore zone (Fig. 8), which is dominated by high-energy wave swash and related processes (INDEN AND MOORE, 1983). Low-angle cross-stratification has been the most commonly recognized sedimentary structure in beachrocks from different parts of the world: Qatar (TAYLOR AND ILLING, 1969), Bermuda (Land, 1970), Kuwait (KHALAF, 1988), Togo (AMIEUX *et al*., 1989), San Salvador Island (Bahamas; KINDLER AND BAIN, 1993), Tunisia (STRASSER *et al*., 1989), and Tonga Island (Polynesia; DICKINSON *et al*., 1999). In the case of the Brazilian beachrocks, the presence of low-angle cross-stratification was interpreted as indicative of deposition on the foreshore zone by OLIVEIRA *et al*. (1990) and BEZERRA *et al*. (1998), in Rio Grande do Norte State, and by ASSIS *et al*. (1990), in the State of Pernambuco.

The grain size variability presented by Lithofacies 2 may result from differences in its relative position to the transition zone between the foreshore and shoreface. In intermediate (bar-trough) beaches, which is the case of northeastern Brazil, the foreshore

laminae may display a transition from lower gradient, more continuous, and parallel, in the upper foreshore zone, to steeper gradient, more discontinuous, and coarser, with more poorly sorted sediments, on the lower foreshore.

At the transition to the shoreface zone, around low-water level, a step composed of coarse-grained, poorly sorted, steeply seaward-dipping (20^{o}), thick laminae is encountered (SHORT AND HESP, 1999). In profile, this feature resembles a submerged scarp at the base of the foreshore. Its geometry and height appear to be sustained by the action of a backwash vortex that is best developed on steep reflective beaches and when surf-swash conditions are at the surging-plunging transition (BAUER AND ALLEN, 1995).

The predominant features presented by the sandier beds of Lithofacies 2 (better sorted coarse-grained sands with a small percentage of pebbles) are indicative of deposition on the upper foreshore. On the other hand, the higher gravel content and poorer sorting of the conglomeratic strata are interpreted to be a consequence of their deposition on the lower foreshore (Fig. 7B), in close proximity to the mean low-water level, or they may represent the step itself, particularly at locations where the laminae dip at a higher angle (vertical section 17). Another possibility is that these coarse-grained gravel-rich beds were deposited during a phase in which more reflective conditions prevailed on the coast or that they took place mainly during declining stages of high-energy events (READING AND COLLINSON, 1996).

Lithofacies 3

The presence of medium to very coarse, commonly conglomeratic sand, together with the conspicuous occurrence of trough cross-stratification, suggests that Lithofacies 3

was deposited on the upper shoreface zone (Fig. 8), as a result of intense winnowing that removed the fine sediment (SEMENIUK AND JOHNSON, 1982). Unidirectional longshore currents, produced by oblique wave approach, were the dominant process during its deposition, as attested by the predominance of shore-parallel-directed paleocurrents pointing to the north, in the case of the eastern coast, and to the west, along the northern coast. The same current-flow directions are found in modern beaches of Rio Grande do Norte. Minor opposite values (Location 13) may be due to local reversals in the oblique wave approach. Rare periods in which northeasterly winds exerted a major influence would best explain the occurrence of north to south currents (DINIZ, 2002). Evidence for tidal flows is sporadic, as attested by the rare arrangement of tabular cross-stratification in a herringbone pattern (Location 6).

The characteristic bedforms that occur on the upper shoreface are plane beds in bars, current ripples to megaripples in channels, and wave ripples in longshore troughs and mixtures thereof (SHORT AND HESP, 1999). Because of the mobility of the bars, their structures have less potential of preservation than the medium-scale cross-bedding in the longshore troughs and rip channels. Taking this into consideration, Lithofacies 3 is interpreted to have been deposited from bedload traction, during the migration of unidirectional sinuous- and straight-crested current ripples, in the runnels, resulting in the formation of trough and tabular cross-stratification, respectively.

Cross-stratification accentuated by thin ilmenite-rich layers and similar to the structures found in the Recent beaches was identified by COORAY (1968) in beachrocks in Sri Lanka. In northeastern Brazil, OLIVEIRA *et al*. (1990) interpreted the trough cross-stratification found in beachrocks situated along the eastern coast of the state of Rio Grande do Norte as a product of deposition on the lower foreshore and upper shoreface zones. The

same interpretation was given by BEZERRA *et al*. (1998) to the beachrocks investigated along both the eastern and northern coasts of the state. According to these authors, the trough cross-strata resulted from the migration of sinuous-crested bedforms whose paleocurrent patterns are similar to those observed on the present coastline and which are mainly influenced by longshore currents. ASSIS *et al*. (1990) and CHAVES AND SIAL (1998) identified cross-stratification in beachrocks from Pernambuco State, interpreting this structure as characteristic of the partially submerged beach deposit under low-tide conditions.

Lithofacies 4

The Skolithos ichnofacies, which includes the vertical tubes present in Lithofacies 4, is characteristic of rapidly shifting substrates in shallow marine environments (PROTHERO AND SCHWAB, 1996). It is typically encountered in clean, well-sorted near-shore sands with a high level of wave and current energy, which prompt resident organisms to dig deep vertical burrows for shelter.

In Rio Grande do Norte State, similar trace fossils were described by BARRETO *et al*. (2002b) in Pleistocenic coastal sedimentary rocks outcropping in cliffs, both on the N-S and E-W trending coasts. They were classified as Ophiomorpha nodosa LUNDGREN (1891) and correspond to a predominantly vertical gallery system larger than that previously recorded in Brazil. According to BARRETO *et al*., the prominent parallelism and verticality of these galleries are indicative of a high sedimentation-rate environment, inhabited by quickly escapable organisms. Considering the high-energy and frequent erosional processes that characterize the environment where these tubes are most

commonly found, the upper shoreface zone is the most suitable site of deposition for Lithofacies 4 (Fig. 8).

Lithofacies 5

The exclusive distribution of massive sandstones at the top or at the base of the described vertical sections is probably due to the higher degree of alteration that is characteristic of both parts. This is attested by the high frequency of erosional features present on the upper surface of the beachrocks, which may have been generated by physical, chemical, or bioerosion, plus bioarmouring and algal induration (MILLER AND MASON, 1994), and by the high degree of friability at the bottom of the sequence, which is in more frequent contact with marine water.

Beachrock deposition relative to sea-level variation

Concerning the study area, the lithofacies distribution at each site (Figs. 2 and 3) indicates that most of the vertical sections of the same ledge were deposited in only one of the two predominant sedimentation beach zones: (1) upper shoreface (53% relative to total thickness, according to Table 1), represented by facies with trough and tabular cross-stratification, occasionally with ichnofossils; and (2) upper and lower foreshore (31% relative to total thickness), characterized by the presence of low-angle cross-stratification in sandy and conglomeratic strata, respectively. Short-term sea-level changes, also referred to as minor sea-level oscillations in the literature, are detectable in only a few of the vertical sections where transition from one beach zone to another is present. Regressive sequences

are found at locations 2 and 15 where the distribution of facies from bottom to top shows a transition from the shoreface to the foreshore zone. Transgressive sequences are displayed at locations 16 and 23. A regressive sequence followed by a transgressive one can be seen at Location 1.

The short thickness of the constructed vertical sections prevents any attempt to draw a conclusion about long-term sea-level changes from the sequence of textural characteristics and sedimentary structures recorded in the beachrocks. These changes can be seen in the sea-level envelope curve constructed by BEZERRA *et al*. (2003) for the state of Rio Grande do Norte (Fig. 9). The rectangles shown in this curve represent the samples of the northern (Fig. 9A) and eastern (Fig. 9B) coasts. Radiocarbon ages used in the construction of both figures are displayed in tables 3 and 4. They were obtained from sea-level indicators found on beachrocks (death assemblage of bivalve shells, vermetid, and coral reef); peat deposits (bivalve shell in living position, fragments of wood, and oyster); Barreiras Formation outcrops (oyster and coral reef); and tidal flats (death assemblage of bivalve shells and oyster).

Beachrocks have been commonly used in studies of sea-level changes elsewhere (RAMSAY, 1991; RAMSAY, 1995; OMOTO, 2001); nevertheless, certain procedures should be adopted so as to minimize problems in the use of these rocks as sea-level indicators. Seeking of beach structures in the outcrop, careful examination of the cement, and intensive dating of both biogenic constituents and cements are some of the guidelines that should be followed (HOPLEY, 1986). With the purpose of detecting contamination by old and young carbon and identifying appropriate pretreatment procedures, special techniques such as microscopic inspection, X-ray diffraction, scanning electron microscopy, and stable isotope analysis were applied to the samples shown in Figure 9

(BEZERRA *et al*., 1998; BEZERRA *et al*., 2000). Furthermore, there is good agreement between the radiocarbon ages used by BEZERRA *et al*. (2003) in the construction of the sea-level envelope curve and the ones obtained in other studies for the same beachrock ledges (OLIVEIRA *et al*., 1990; STATTEGER *et al*., 2004). These latter ages were also included in tables 3 and 4, although they were not used in the construction of the time-depth diagrams.

Regarding both curves altogether, it is observed that beachrock deposition, in the same way as the examples described in the literature, occurred under extremely variable conditions (rapid sea-level rise, high sea-level stillstand, sea-level drop, and low sea-level stillstand); that is, there is no apparent connection with sea-level variations of great wave length. Most probably, minor sea-level oscillations, not seen in the curve, should play a role in this process. Regarding each curve separately, the following tendencies can be detected: along the northern coast, beach sediments were predominantly deposited between ~4140–2190 cal. yr BP, when sea level dropped, and during low sea-level stillstand. Conversely, the beach deposits distributed along the eastern coast were preferentially formed between ~7460–4240 cal. yr BP, during rapid sea-level rise and high sea-level stillstand. No matter in which stage of the final sea-level curve their constituents were deposited, beachrocks owe their exposure and generation of erosional features to the present low sea level.

The combination of the lithofacies identified in this study (Table 1) with the sea-level envelope curve shown in Figure 9 suggests that, on the northern coast, the upper shoreface sedimentation zone, represented by lithofacies 3 and 4, is preferentially distributed during sea-level drop and low sea-level stillstand phases (Fig. 9A), while the upper and lower foreshore sedimentation zones, represented by Lithofacies 2, can be found along the whole curve (Fig. 9B). In the case of the eastern coast, both preferential

sedimentation zones (upper shoreface and foreshore) are equally concentrated in the first stages of rapid sea-level rise and high sea-level stillstand.

Beachrock cementation relative to sea-level variation

There is an agreement among various studies on beachrocks upon their formation during progradation of a sedimentary body (RUSSELL, 1962; BEIER, 1985; AMIEUX *et al*., 1989; BERNIER *et al*., 1997). Nevertheless, the rate of progradation exerts great influence on cementation, which may be reduced or even prevented under high rates, as attested by BEIER (1985) and VOLLBRECHT AND MEISCHNER (1993). In the former work, beachrock is virtually absent on the east side of San Salvador Island, where the larger distance from the shoreline to inland vegetation indicate that beaches may be prograding more rapidly than in other areas where beachrocks are common. In the latter work, the precipitation of marine cements within Pleistocene beaches of Whalebone Bay (Bermuda) seemed to be controlled by the thickness of sediment cover; that is, the more sediment accumulates on top of an older sedimentary rock, the less complete were post-depositional pore water changes, as a result of flow restriction of marine pore water.

Whether necessary conditions for progradation and resulting beachrock formation are attained during sea-level rise, fall, or stillstand is a question still not definitely answered. ALEXANDERSSON (1972) observed that beachrocks occurred in Mediterranean offshore positions, in places forming a series of layers that probably represented repeated beachrock cementation during a rise in sea level. SIESSER (1974) suggested that the False Bay relict beachrock in South Africa formed in the intertidal zones of falling sea level by cementation of beach sands during and after a worldwide regression

from the Würm I/II high sea level. RUSSELL (1959) investigated beachrocks of Caribbean Islands (Puerto Rico, Antigua, Guadeloupe, and St. Lucia) and concluded that they probably formed along straight and cove beaches at various levels during halting stages of the latest rise in sea level. COORAY (1968) suggested that the submerged sandstone shoals parallel to the present strand line at Negombo (west coast of Sri Lanka) probably represented temporary phases of stillstand, or at least stages during which the rise in sea level was slower, so that they were not reworked but rather cemented. The conclusion from a study on Joulter's Cay (Bahamas) made by FRIEDMAN (1998) shows that marine carbonate lithification in highstand tracts is so rapid that these deposits are stabilized, inhibiting their removal as unconsolidated sediment into adjacent deeper water. In that author's opinion, the historical debate over highstand versus lowstand shedding of platform carbonate sediments is not yet over, taking into consideration that rapid cementation occurs on both highstand and lowstand facies tracts.

From the works cited above, there appears to be no doubt concerning the relationship between beachrock generation and sea-level change. Regarding the study area, the sea-level envelope curves shown in Figure 9 provide a minimum age of deposition for each beachrock ledge. To what extent the time difference between the deposition of a beach sediment and its subsequent cementation can be considered negligible is still controversial. Provided the suitable conditions occur [stability, supersaturation in the pores, and supply of material in solution (TAYLOR AND ILLING, 1969)], cementation in beachrock can be a rapid process, as pointed out by several authors (GINSBURG, 1953; RUSSELL, 1959; FRIEDMAN, 1998). Although authentic cases of fast cementation rate in beachrocks have actually occurred, as attested by the presence of modern artifacts, caution must be taken when applying this information to beachrock studies. First of all, the time difference

between the death of an organism and the cementation of a beachrock may be hundreds and even thousands of years (HOPLEY, 1986). Second, the cement may form by slow continuous growth at levels of moderate supersaturation or grow only occasionally, under extremely favorable conditions (ALEXANDERSSON, 1972).

Concerning the study area, distribution of diagenetic features is extremely variable, along each vertical section, even at a centimetric scale, as well as in large scale (VIEIRA AND DE ROS, forthcoming). This indicates that their lithification occurred under the influence of rapidly shifting parameters that have changed even in the thin-section scale. Temporal and spatial changes of the parameters controlling beachrock cementation have been advocated as the main cause of their complex cementation patterns (e.g., TAYLOR AND ILLING, 1971; STRASSER *et al*., 1989; HOLAIL AND RASHED, 1992). Data presented previously suggest that the driving force of these changeable conditions should be the diversity of sea-level positions under which the beachrocks have been generated, particularly local advances and retreats of the sea, or minor-order sea-level oscillations not detectable in the sea-level envelope curve. Radiocarbon dating of carbonate cements individually could shed some light on this question; nevertheless, difficulties in obtaining sufficient cement without fine-grained beach materials, as well as contamination by younger fluids, make the precise dating of beachrock cementation a highly difficult task (HOPLEY, 1986). In summary, further investigation appears to be necessary to better understand the extension and amplitude by which sea level changes have influenced the variety of cement textures detected in the studied beachrocks.

CONCLUSIONS

1) Five lithofacies, named 1 to 5, were identified in beachrock ledges along the eastern and northern coasts of Rio Grande do Norte State, Brazil. They are: (1) Massive to Weakly Stratified Conglomerate; (2) Low-Angle Cross-Stratified Conglomerate and Sandstone; (3) Medium-Scale Tabular-Planar and Trough Cross-Stratified Sandstone; (4) Skolithos-Bioturbated Conglomeratic Sandstone; and (5) Massive Sandstone.

2) The textural characteristics and sedimentary structures described are diagnostic of lithofacies formed in the shallow marine coastal environment. Most of the described beachrocks (53%) were deposited on the upper shoreface zone, represented by facies with trough and tabular cross-stratification (Lithofacies 3), occasionally with ichnofossils (Lithofacies 4). Facies deposited on the upper and lower foreshore zone, which are characterized by the presence of low-angle cross-stratification (Lithofacies 2), in sandy and conglomeratic strata, respectively, represent 31% of the total described. The remaining 16% are attributed to collapse of overlying material as a result of sea-cliff undercutting (massive conglomerate), transport as traction-carpet deposit (weakly stratified conglomerate), and a high degree of alteration (massive sandstone).

3) Taking into consideration the distribution of ^{14}C dated beachrock samples in a sea-level envelope curve, the following tendencies can be detected: along the northern coast, beach sediments were predominantly deposited between ~4140–2190 cal. yr BP, when sea level dropped, and during low sea-level stillstand. Conversely, the beach deposits distributed

along the eastern coast were preferentially formed between ~7460–4240 cal. yr BP, during rapid sea-level rise and high sea-level stillstand.

4) On the northern coast, the shoreface sedimentation zone, represented by lithofacies 3 and 4, is preferentially distributed during sea-level drop and low sea-level stillstand phases, while the foreshore sedimentation zone, represented by Lithofacies 2, can be found along the whole sea-level curve. In the case of the eastern coast, both preferential sedimentation zones (shoreface and foreshore) are equally concentrated in the first stages of rapid sea-level rise and high sea-level stillstand.

5) Distribution of diagenetic features in the study area is extremely variable, even at a centimetric scale, indicating that their lithification occurred under the influence of rapidly shifting physical and chemical parameters. The driving force of these changeable conditions should be the diversity of sea-level positions under which the beachrocks have been generated, particularly local advances and retreats of the sea or lower-order sea-level oscillations not detectable in the sea-level envelope curve. Radiocarbon dating of carbonate cements individually could shed some light on this question; nevertheless, this is a highly difficult task and further investigation appears to be necessary to better understand the extension and amplitude by which sea-level changes have influenced the variety of cement textures detected in the studied beachrocks.

ACKNOWLEDGMENTS

This work is part of M.M.Vieira's Ph.D. thesis research carried out at the Instituto de Geociências of the Universidade Federal do Rio Grande do Sul, Porto Alegre, Brazil. M.M.Vieira thanks the funding provided by a scholarship granted by CAPES, an organ of the Ministry of Education and Culture of Brazil. The authors would like to thank Drs. C.M.S. Scherer and E. E. Toldo, Jr., for reviewing the earlier version of this manuscript and F.A.A. Feitosa for his assistance in the field. Thanks are extended to the Geology Department of the Universidade Federal do Rio Grande do Norte for providing equipment and support.

LITERATURE CITED

ALEXANDERSSON, T., 1972. Mediterranean beachrock cementation: marine precipitation of Mg-calcite. *In*: Stanley, D.J. (ed.), *The Mediterranean Sea: A natural sedimentation laboratory* Dowden. Stroudsburg: Hutchinson & Ross, pp. 203–223.

AMIEUX, P., BERNIER, P., DALONGEVILLE, R., MEDWECKI, V., 1989. Cathodoluminescence of carbonate-cemented Holocene beachrock from the Togo coastline (West Africa): an approach to early diagenesis. *Sedimentary Geology,* 65, 261–272.

ASSIS, H.M.B., AMARAL, R.F., MANSO, V.A.V., 1990. Caracterização dos "beach rocks" do litoral sul de Pernambuco com base em evidências petrográficas e isotópicas. *XXXIV Congresso Brasileiro de Geologia* (Natal, RN, Brazil, Sociedade Brasileira de Geologia), Expanded Abstract 2, pp. 635–646.

BARRETO, A.M.F., BEZERRA, F.H.R., SUGUIO, K., TATUMI, S.H., YEE, M., PAIVA, R.P., MUNITA, C.S., 2002a. Late Pleistocene marine terrace deposits in northeastern Brazil: sea-level change and tectonic implications. *Palaeogeography, Palaeoclimatology, Palaeoecology,* 179, 57–69.

BARRETO, A.M.F., SUGUIO, K., ALMEIDA, J.A.C., BEZERRA, F.H.R., 2002b. A presença da icnoespécie *Ophiomorpha nodosa* em rochas sedimentares pleistocênicas da costa norte-riograndense e suas implicações paleoambientais. *Revista Brasileira de Paleontologia*, Jan./Jun., 17–23.

BARROS, J.J.A., 2001. Mapeamento de coberturas Supra-Barreiras no litoral do Rio Grande do Norte. Relatório de Graduação. Natal, RN: Universidade Federal do Rio Grande do Norte.

BATES, R.L., JACKSON J.A., 1987. *Glossary of geology*, 3rd ed. Alexandria, VA: American Geological Institute.

BAUER, B.O., ALLEN, J.R., 1995. Beach steps: an evolutionary perspective. *Marine Geology,* 123, 143–166.

BEIER, J.A., 1985. Diagenesis of Quaternary Bahamian beachrock: petrographic and isotopic evidence. *Journal of Sedimentary Petrology,* 55(5), 755–761.

BERNIER, P., GUIDI, J.B., BÖTTCHER, M.E., 1997. Coastal progradation and very early diagenesis of ultramafic sands as a result of rubble discharge from asbestos excavations (northern Corsica, western Mediterranean). *Marine Geology,* 144, 163–175.

BEZERRA, F.H.R., LIMA-FILHO, F.P., AMARAL, R.F., CALDAS, L.H.O., COSTA-NETO, L.X., 1998. Holocene coastal tectonics in NE Brazil. *In*: Stewart, I.S., Vita-Finzi, C. (eds.), *Coastal tectonics*. Geol. Soc. London, Special Publication No. 146, 279–293.

BEZERRA, F.H.R., VITA-FINZI, C., LIMA-FILHO, F.P., 2000. The use of marine shells for radiocarbon dating of coastal deposits. *Revista Brasileira de Geociências,* 30(1), 211–213.

BEZERRA, F.H.R., BARRETO, A.M.F., SUGUIO, K., 2003. Holocene sea-level history on the Rio Grande do Norte State coast, Brazil. *Marine Geology,* 196, 73–89.

BINKLEY, K.L., WILKINSON, B.H., OWEN, R.M., 1980. Vadose beachrock cementation along a southeastern Michigan Marl lake. *Journal of Sedimentary Petrology,* 50(3), 953–962.

BITTENCOURT, A.C.S.P., MARTIN, L., DOMINGUEZ, J.M.L., SILVA, I.R., SOUSA, D.L., 2002. A significant longshore transport divergence zone at Northeastern Brazilian coast: implications on coastal Quaternary evolution. *Anais da Academia Brasileira de Ciências*, 74(3), 505–518.

BRICKER, O.P. (ed.), 1971. *Carbonate cements*. Johns Hopkins University, Studies in Geology No. 19.

CHAVES, M.S., 2000. Sedimentologia, morfologia praial e vulnerabilidade costeira entre as praias de Redinha e Genipabu, Natal/RN. Recife, PE: Universidade Federal de Pernambuco, Master's thesis.

CHAVES, N.S., SIAL, A.N., 1998. Mixed oceanic and freshwater depositional conditions for beachrocks of Northeast Brazil: evidence from carbon and oxygen isotopes. *International Geology Review,* 40, 748–754.

COORAY, P.G., 1968. A note on the occurrence of beachrock along the west coast of Ceylon. *Journal of Sedimentary Petrology,* 38, 650–654.

DICKINSON, W.R., BURLEY, D.V., SHUTLER, R., JR., 1999. Holocene Paleoshoreline record in Tonga: geomorphic features and archaeological implications. *Journal of Sedimentary Research,* 15(3), 682–700.

DINIZ, R.F., 2002. A erosão costeira ao longo do litoral oriental do Rio Grande do Norte: causas, conseqüências e influência nos processos de uso e ocupação da região costeira. Salvador, BA: Universidade Federal da Bahia, Ph.D. thesis.

EL-SAYED, M.I., AL-BAKRI, D., 1994. Geomorphology and sedimentary/biosedimentary structures of the intertidal environment along the coast of Kuwait, north-western Arabian Gulf. *Geologische Rundschau,* 83, 448–463.

FRANKEL, E., 1968. Rate of formation of beachrock. *Earth and Planetary Science Letters,* 4, 439–440.

FRIEDMAN, G.M., 1998. Rapidity of marine carbonate cementation—implications for carbonate diagenesis and sequence stratigraphy: perspective. *Sedimentary Geology,* 119, 1–4.

GINSBURG, R.N., 1953. Beachrock in south Florida. *Journal of Sedimentary Petrology*, 23, 85–92.

GISCHLER, E., LOMANDO, A.J., 1997. Holocene cemented beach deposits in Belize. *Sedimentary Geology,* 110, 277–297.

HANOR, J.S., 1978. Precipitation of beachrock cements: mixing of marine and meteoric waters *vs*. CO_2 degassing. *Journal of Sedimentary Petrology*, 48(2), 489–501.

HOLAIL, H. RASHED, M., 1992. Stable isotopic composition of carbonate-cemented recent beachrock along the Mediterranean and Red Sea Coasts of Egypt. *Marine Geology,* 106, 141–148.

HOPLEY, D., 1986. Beachrock as a sea-level indicator. *In*: Van de Plassche, O. (ed.), *Sea-level research: a manual for collection and evaluation of data*. Norwich: Geo Books, pp. 157–173.

INDEN, R.F., MOORE, C.H., 1983. Beach environment. *In*: Scholle, P.A., Bebout, D.G., Moore, C.H. (eds.), *Carbonate depositional environment*. American Association of Petroleum Geologists, Memoir 33, pp. 211–265.

JARDIM DE SÁ, E.F., MATTOS, R.M.D., OLIVEIRA, D.C., REGO, J.M., MONTEIRO, E.T., DANTAS, J.R.A., XAVIER, C.B., HOLLANDA, M.H.B.M, 1998. *Mapa geológico do Estado do Rio Grande do Norte*. Natal, RN: DNPM/UFRN/PETROBRAS/CRM (RN), esc. 1:500000.

KHALAF, F.I., 1988. Quaternary calcareous hard rocks and the associated sediments in the intertidal and offshore zones of Kuwait. *Marine Geology,* 80, 1–27.

KINDLER, P., BAIN, R.J., 1993. Submerged Upper Holocene on San Salvador Island, Bahamas: implications for recent sea-level history. *Geologische Rundschau,* 82, 241–247.

LAND, L., 1970. Phreatic versus vadose meteoric diagenesis of limestones: evidence from a fossil water table. *Sedimentology,* 14, 175–185.

MAXWELL, W.G.H., 1962. Lithification of carbonate sediments in the Heron Island Reef, Great Barrier Reef. *Journal of the Geological Society of Australia,* 8, 217–238.

MILLER, W.R., MASON, T.R., 1994. Erosional features of coastal beachrock and eolianite outcrops in Natal and Zululand, South Africa. *Journal of Coastal Research*, 10(2), 394–414.

MOORE, C.H., 1973. Intertidal carbonate cementation, Grand Cayman, West Indies. *Journal of Sedimentary Petrology*, 43, 591–602.

MOORE, C.H., JR., BILLINGS, G.K., 1971. Preliminary model of beachrock cementation, Grand Cayman Island, British West Indies. *In*: Bricker, O.P. (ed.), *Carbonate cements*. Johns Hopkins University, Studies in Geology No.19, 40–43.

NEUMEIER, U., 1999. Experimental modelling of beachrock cementation under microbial influence. *Sedimentary Geology,* 126, 35–46.

NIMER, E., 1989. *Climatologia do Brasil*. Rio de Janeiro, RJ: Instituto Brasileiro de Geografia e Estatística, Departamento de Recursos Naturais e Ambientais.

OLIVEIRA, M.I.M., BAGNOLLI, E., FARIAS, C.C., NOGUEIRA, A.M.B., SANTIAGO, M., 1990. Considerações sobre a geometria, petrografia, sedimentologia, diagênese e idades dos *beachrocks* do Rio Grande do Norte. *XXXIV Congresso Brasileiro de Geologia* (Natal, RN, Brazil, Sociedade Brasileira de Geologia), Expanded Abstract 2, pp. 621–634.

OMOTO, K., 2001. Radiocarbon ages of beach rocks and Late Holocene sea-level changes in the southern part of the Nansei Islands, southwest of Japan. *In*: Carmi, I., Boaretto, E. (eds.), *Proceedings of the 17th International ^{14}C Conference* 43, 887–898.

PROTHERO, D.R., SCHWAB, F., 1996. *An introduction to sedimentary rocks and stratigraphy-sedimentary geology*. New York: Freeman.

RAMSAY, P.J., 1991. Holocene sea-level changes along the southern African coastline. *XXXIV International Sedimentological Congress* (Recife, PE, Brazil), Abstracts, E-22.

RAMSAY, P.J., 1995. 9000 years of sea-level change along the southern African coastline. Holocene sea-level changes along the southern African coastline. *Quaternary International*, 31, 71–75.

READING, H.G., COLLINSON, J.D., 1996. Clastic coasts. *In*: Reading, H.G. (ed.), *Sedimentary environments*: *processes, facies and stratigraphy*, 3rd ed., Cambridge: Blackwell Science, pp. 154–231.

RUSSELL, R.J., 1959. Caribbean beach rock observation. *Zeit. Geomorphologie,* 3, 227–236.

RUSSELL, R.J., 1962. Origin of beach rock. *Zeit. Geomorphologie*, 6, 1–16.

SCHMALZ, R.F., 1971. Formation of beachrock at Eniwetok Atoll. *In*: Bricker, O.P. (ed.), *Carbonate cements*. Johns Hopkins University, Studies in Geology No.19, 17–24.

SCOFFIN, T.P., 1970. A conglomeratic beachrock in Bimini, Bahamas. *Journal of Sedimentary Petrology,* 40, 756–759.

SEMENIUK, V., JOHNSON, D.P., 1982. Recent and Pleistocene beach/dune sequence, Western Australia. *Sedimentary Geology*, 32, 301–328.

SHORT, A.D., 1999a. Global variation in beach systems. *In*: Short, A. (ed.), *Handbook of beach and shoreface morphodynamics.* Chichester: Wiley, pp. 21–35.

SHORT, A.D., 1999b. Beach hazards and safety. *In*: Short, A. (Ed.), *Handbook of beach and shoreface morphodynamics.* Chichester: Wiley, pp. 293–304.

SHORT, A.D., HESP, P.A., 1999. Beach and dune stratification. *In*: Short, A. (ed.), *Handbook of beach and shoreface morphodynamics*. Chichester: Wiley, pp. 279–291.

SIESSER, W.G., 1974. Relict and recent beachrock from Southern Africa. *Geological Society of America Bulletin,* 85, 1,849–1,854.

SILVA, C. G., 1991. Holocene stratigraphy and evolution of the Açu River Delta, Rio Grande do Norte State, northeastern Brazil. Durham, NC: Duke University, PhD thesis.

SILVA, R.L.C., NOGUEIRA, A.M.B., 1995. Estratigrafia da porção emersa da costa do Rio Grande do Norte. *1º Simpósio sobre Processos Sedimentares e Problemas Ambientais na Zona Costeira Nordeste do Brasil* (Recife, Pernambuco, Brazil), pp. 144–147.

STATTEGGER, K., CALDAS, L.H.O., VITAL, H., 2004. Holocene coastal evolution of the northern Rio Grande do Norte Coast, NE Brazil. *Journal of Coastal Research*, Special Issue 39.

STRASSER, A., DAVAUD, E., 1986. Formation of Holocene limestone sequences by progradation, cementation, and erosion: two examples from the Bahamas. *Journal of Sedimentary Petrology,* 56(3), 422–428.

STRASSER, A., DAVAUD, E., JEDOUI, Y., 1989. Carbonate cements in Holocene beachrock: example from Bahiret el Biban, southeastern Tunisia. *Sedimentary Geology,* 62, 89–100.

TABOSA, W.F., 2002. Monitoramento costeiro das praias de São Bento do Norte e Caiçara do Norte, RN: implicações para o pólo petrolífero de Guamaré. Natal, RN: Universidade Federal do Rio Grande do Norte, Master's thesis.

TAYLOR, J.C.M., ILLING, L.V., 1969. Holocene intertidal calcium carbonate cementation, Qatar, Persian Gulf. *Sedimentology,* 12, 69–107.

TAYLOR, J.C.M., ILLING, L.V., 1971. Variation in recent beachrock cements, Qatar, Persian Gulf. *In*: Bricker, O.P. (ed.), *Carbonate cements*. Johns Hopkins University, Studies in Geology No. 19, 40–43.

VIANNA, M.L., CABRAL, A.P., GHERARDI, D.F.M., 1993. TM-Landsat imagery applied to study of the impact of global climate change on a tropical coastal environment during the last deglaciation. *International Journal of Remote Sensing,* 14(14), 2,971–2,983.

VIEIRA, M.M., DE ROS, L.F., forthcoming. Cementation patterns and genetic implications of Holocene beachrocks from northeastern Brazil. Submitted to *Sedimentary Geology*.

VOLLBRECHT, R., MEISCHNER, D., 1993. Sea level and diagenesis: a case study on Pleistocene beaches, Whalebone Bay, Bermuda. *Geologische Rundschau,* 82, 248–262.

WEBB, G.E., JELL, J.S., BAKER, J.C., 1999. Cryptic intertidal microbialites in beachrock, Heron Island, Great Barrier Reef: implications for the origin of microcrystalline beachrock cement. *Sedimentary Geology,* 126, 317–334.

WRIGHT, L.D., SHORT, A.D., 1984. Morphodynamics of beach and surf zone in Australia. *In*: Komar, P.O. (ed.), *C.R.C. Handbook of coastal processes and erosion*. London: C.R.C. Press, pp. 35–64.

FIGURE CAPTIONS

Figure 1: Map of Rio Grande do Norte State showing location of study area (rectangles).

Figure 2: Geological map of part of the E-W trending littoral zone and adjoining areas, compiled and simplified according to Jardim de Sá et al. (1998). Black dots and adjacent numbers correspond to the constructed vertical sections.

Figure 3: (A) Geological map of the N-S trending littoral zone and adjoining areas, compiled and simplified according to Jardim de Sá et al. (1998). Black dots and adjacent numbers correspond to the constructed vertical sections. Legend is the same as in Figure 2. Rectangle corresponds to Fig. 3B; (B) A chart of Fig. 3A with part of the constructed vertical sections.

Figure 4: Beachrock mesoscopic features: (A) Beachrock ledge approximately 8 km long and parallel to the present-day beach (Barra do Cunhaú, Location 32); (B) Highly irregular surfaces of *spitzkarren* on Barreta Beach (Location 26) similar to the ones described by Miller and Mason (1994); (C) Potholes filled with well-rounded pebbles on Marcos Beach (Location 7); (D) Numerous disrupted slabs of beachrock on Jacumã Beach (Location 11).

Figure 5: Beachrock microscopic features: (A) Fragment of hematite-cemented sandstones of the Barreiras Formation cemented by ryptocrystalline or micritic pore-filling cement. A garnet grain can be seen on its left. Thin section, uncrossed polarizers (//P), Location 35; (B) Monocrystalline and polycrystalline quartz grains cemented by an inner band of thick,

dark micrite envelope and an outer, lighter band of elongated crystal fringe. Note irregular thickness and discontinuity of the fine-grained coating. Thin section, //P, Location 27; (C) Mesocrystalline anhedral to subhedral equant spar completely fillling the pore space between quartz grains. Thin section, //P, Location 34; (D) Porosity between quartz grains partially occupied by irregular masses of infiltrated marl hybrid sediment. Note the presence of foraminifer on the upper part of the photograph. Thin section, //P, Location 18.

Figure 6: Beachrock sedimentary structures: (A) Large angular laterite pebbles from Barreiras Formation (L) embedded in a coarse quartzose sand and gravel matrix (Lithofacies 1, Location 35, Baía Formosa Beach); (B) Detail of low-angle cross-stratification (Lithofacies 2, Location 19, Ponta Negra Beach); (C) Trough cross-stratification in plan view (Lithofacies 3, Barreta Beach); (D) Vertical tubes of Skolithos ichnofacies (Lithofacies 4, Location 5, Ponta dos Três Irmãos Beach).

Figure 7: Sedimentary structures in modern beaches: (A) Swash-cross stratification accentuated by thin heavy-mineral layers; (B) Higher gravel content (mainly hematite-cemented sandstones of Barreiras Formation) on the lower foreshore in close proximity to the mean low-water level.

Figure 8: Schematic illustration of the distribution of identified lithofacies across a beach profile. HWL: high-water level; LWL: low-water level; LC: longitudinal current.

Figure 9: (A) ^{14}C samples of the E-W trending littoral zone distributed along the final sea-level curve for Rio Grande do Norte State (Bezerra et al., 2003). Radiocarbon data were

obtained from shells with beachrocks as host rocks, and this final curve resulted from the intersection of two others obtained for the E-W and N-S coasts. Numbers in rectangles refer to the vertical sections used to interpret the predominant cementation zone (foreshore or shoreface) of the beachrock ledges from which the ^{14}C samples were obtained. Letters in rectangles correspond to the values found in Table 3; (B) ^{14}C samples of the N-S trending littoral zone. Letters in rectangles correspond to the values found in Table 4.

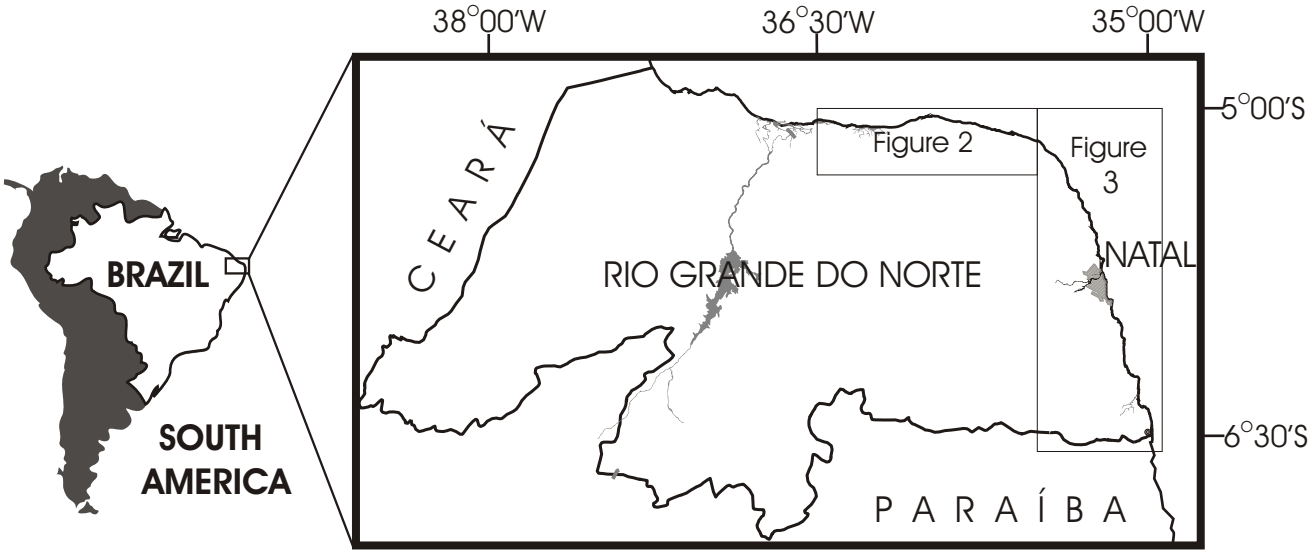
38°00'W
36°30'W
35°00'W
5°00'S
6°30'S
BRAZIL
SOUTH AMERICA
CEARÁ
RIO GRANDE DO NORTE
PARAÍBA
Figure 2
Figure 3
NATAL

Figure 1

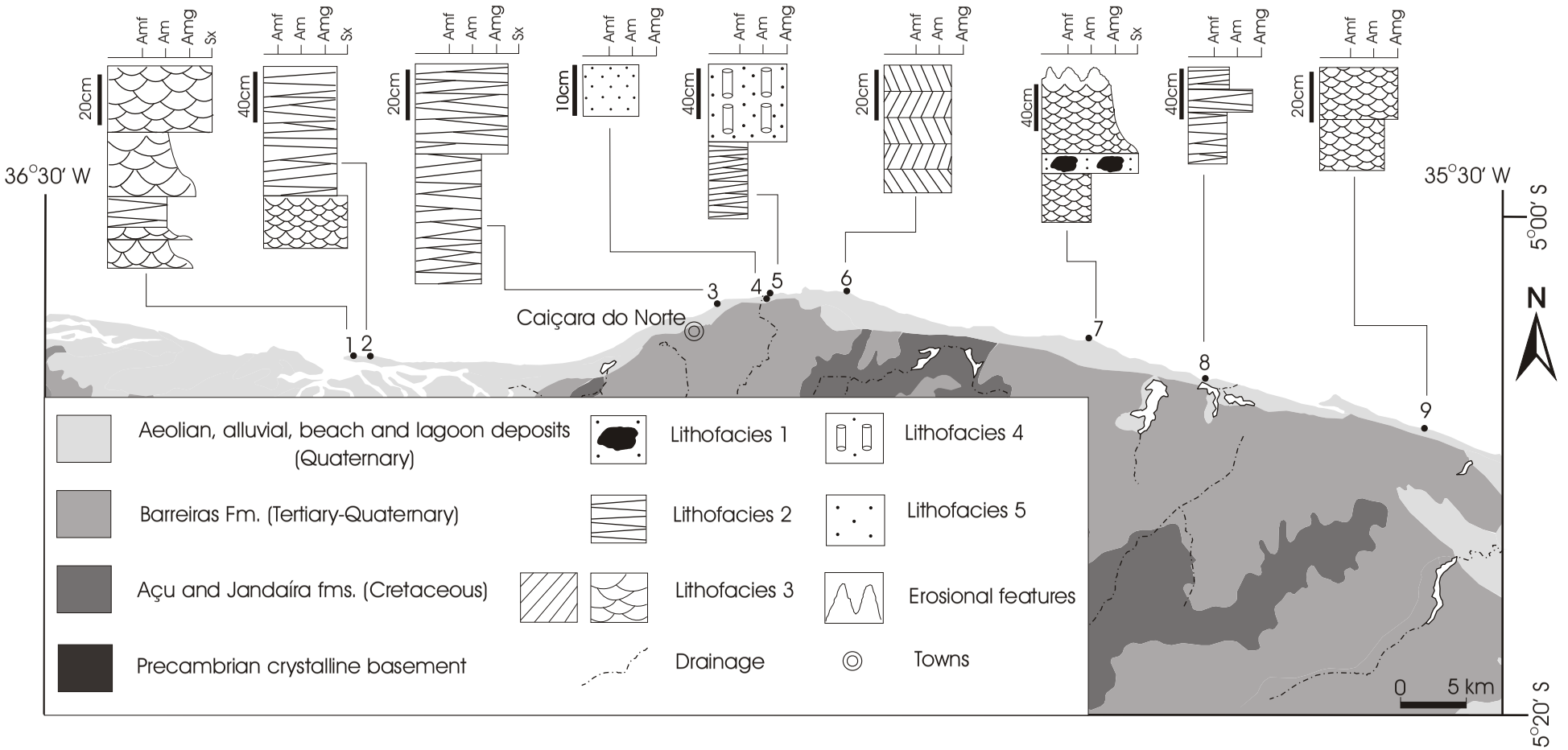
Amf
Am
Amg
Sx
20cm
40cm
10cm
36°30′ W
35°30′ W
5°00′ S
5°20′ S
N
Caiçara do Norte
1
2
3
4
5
6
7
8
9
Aeolian, alluvial, beach and lagoon deposits (Quaternary)
Barreiras Fm. (Tertiary-Quaternary)
Açu and Jandaíra fms. (Cretaceous)
Precambrian crystalline basement
Lithofacies 1
Lithofacies 2
Lithofacies 3
Lithofacies 4
Lithofacies 5
Erosional features
Drainage
Towns
0
5 km

Figure 2

Figure 3A

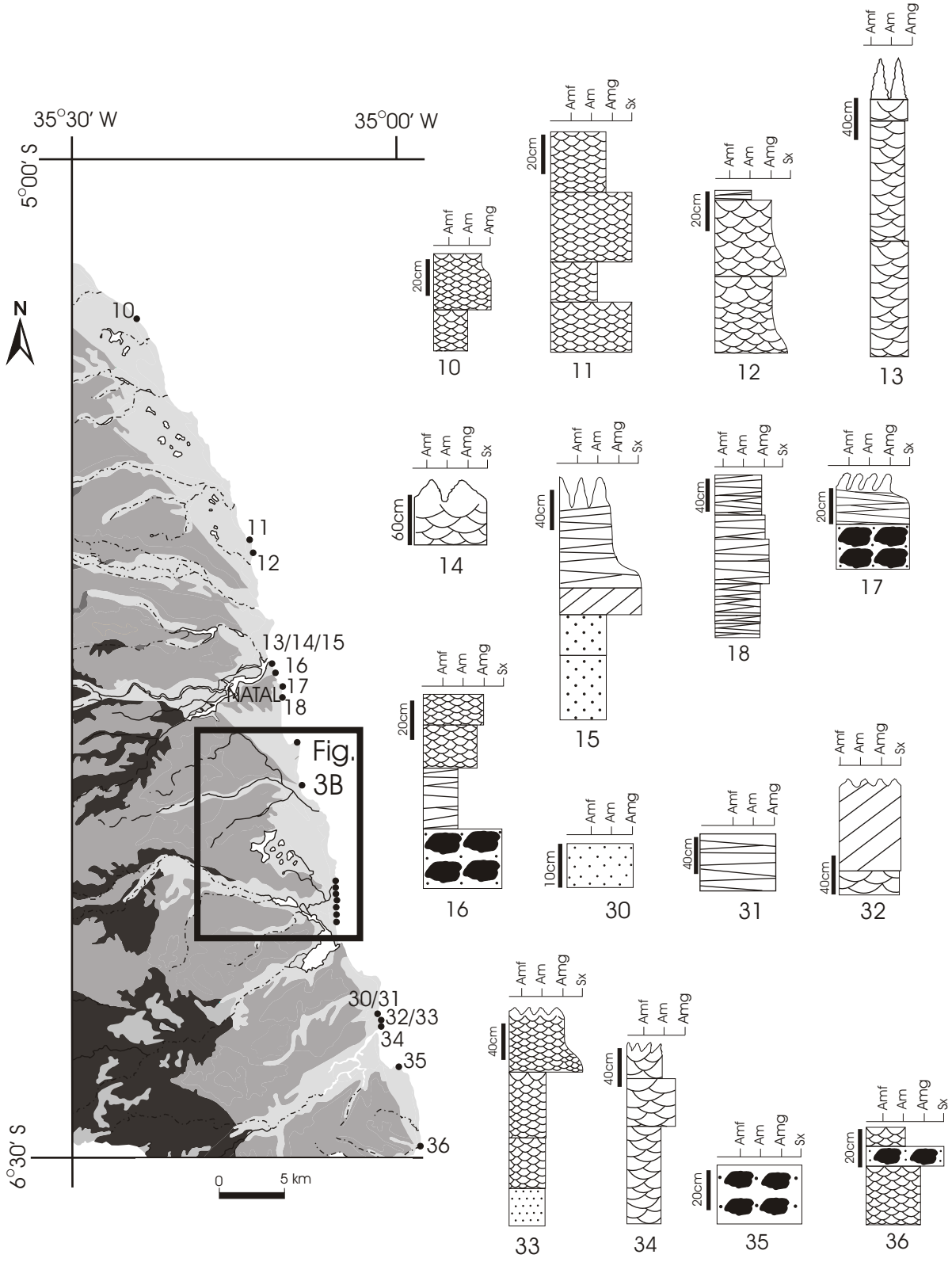
35°30′ W
35°00′ W
5°00′ S
6°30′ S
N
10
11
12
13/14/15
16
17
NATAL
18
Fig. 3B
30/31
32/33
34
35
36
0
5 km
Amf
Am
Amg
Sx
20cm
10
11
12
40cm
13
60cm
14
15
17
18
16
10cm
30
31
32
33
34
35
36

Figure 3B

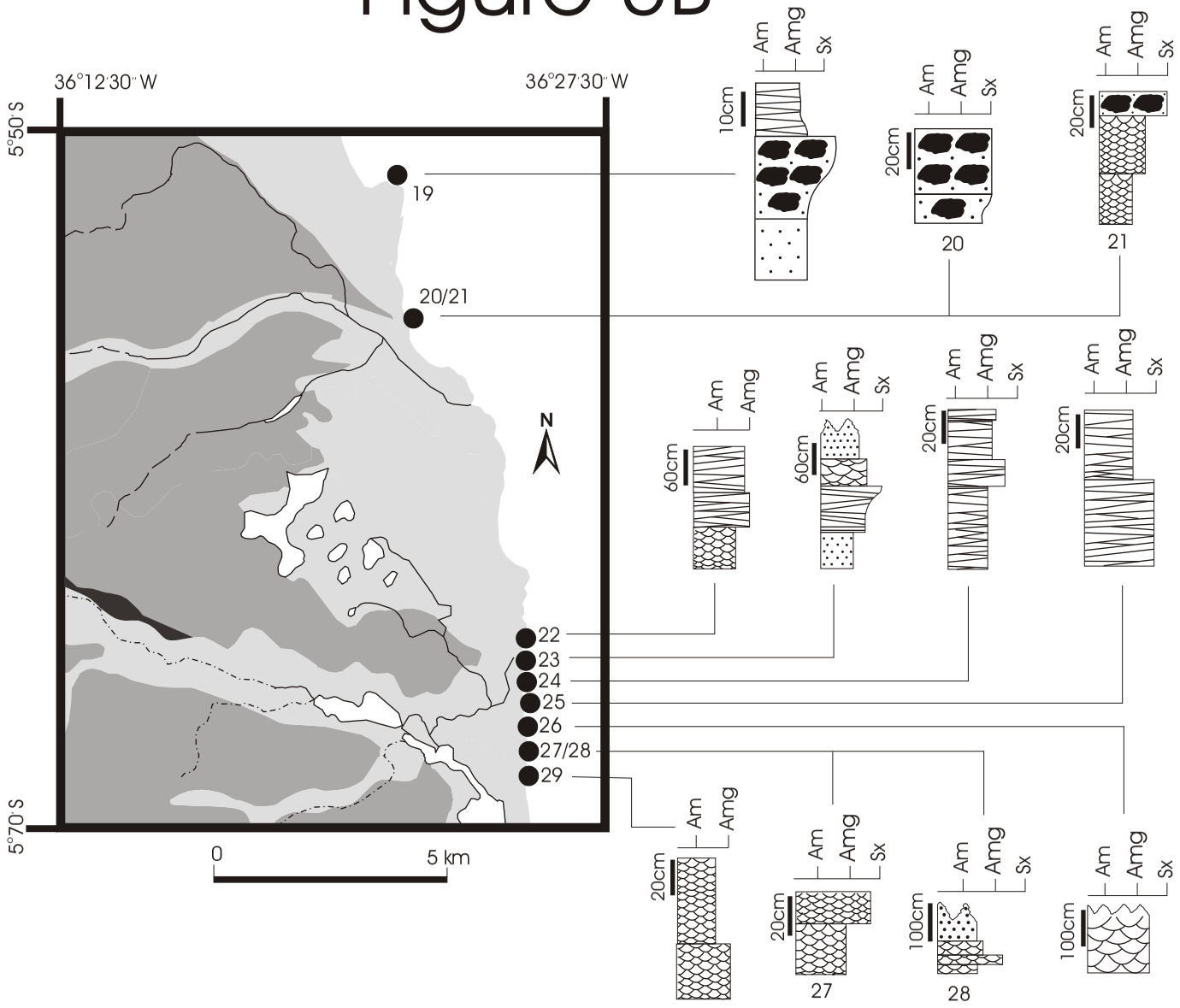
36°12'30" W
36°27'30" W
5°50' S
5°70' S
19
20/21
22
23
24
25
26
27/28
29
N
0
5 km
Am
Amg
Sx
10cm
20cm
60cm
100cm
20
21
27
28

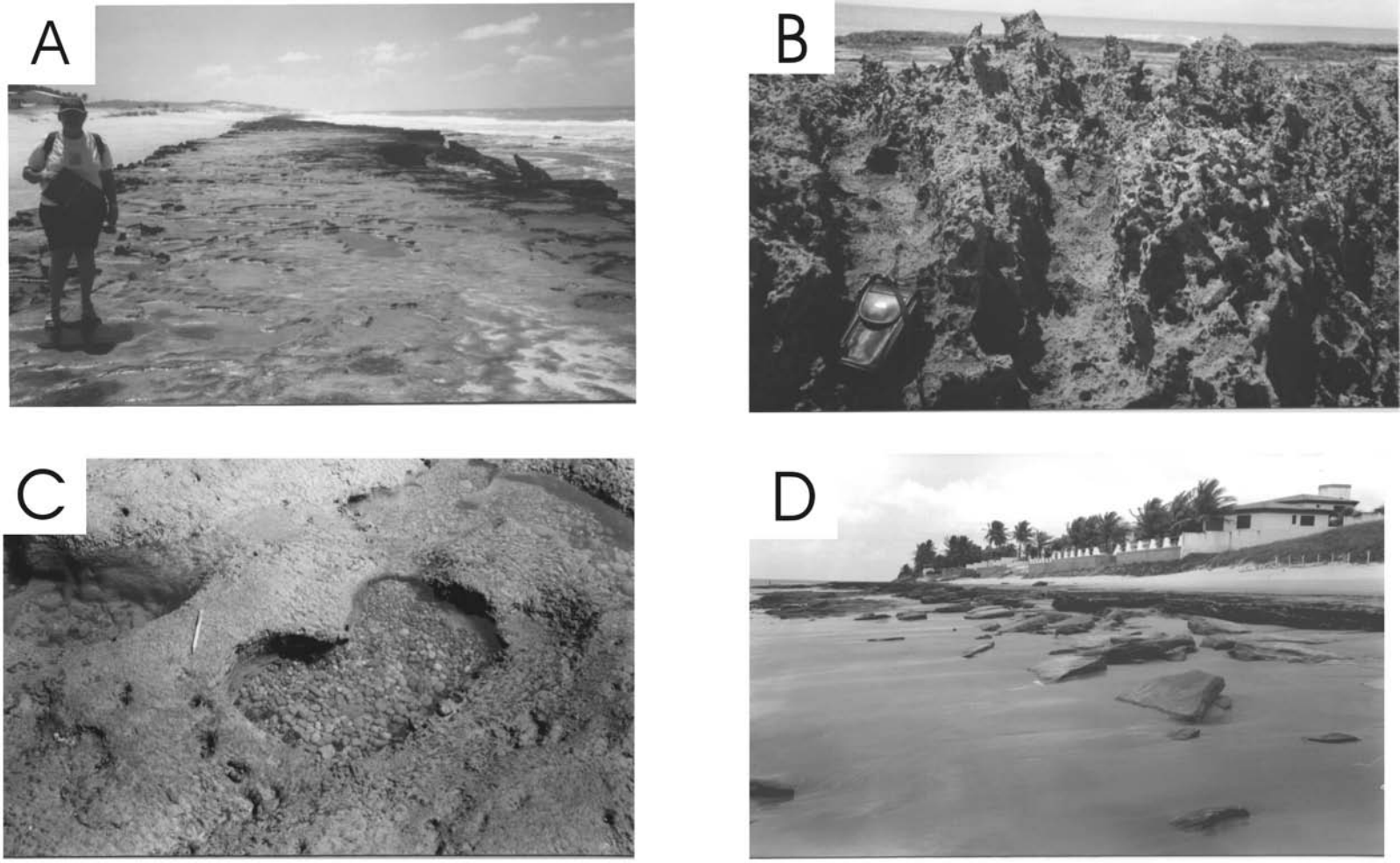

Figure 4

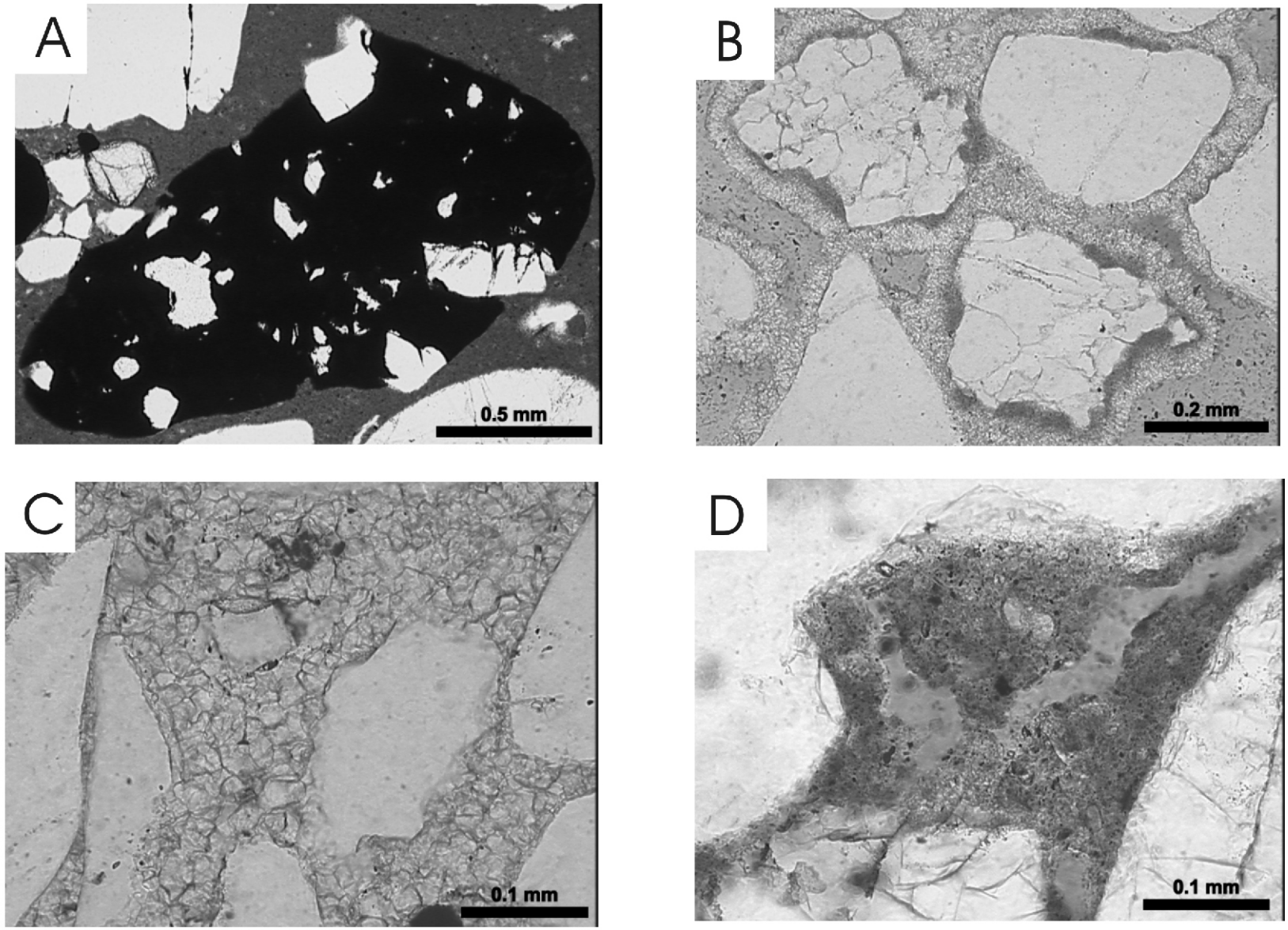

Figure 5

Table 1: Summary of the main characteristics of each lithofacies and paleoenvironmental interpretation

Lithofacies	Description	Interpretation	% relative to total thickness
1	Massive to weakly seaward-dipping stratified, poorly to very poorly sorted, sharp-based conglomerates	Transgressive lag deposit or traction carpet deposit	5%
2	Poorly to well-sorted sandy conglomerate to sandstone with a seaward-dipping low-angle X-stratification	Beachface wave swash or backswash or backwash step vortex	32%
3	Very poorly- to well-sorted sandstones with small- to medium-scale trough cross-stratification with paleocurrents parallel to coastline	Bedload transport by longshore currents on the upper shoreface zone	51%
4	Poorly to very poorly sorted sandstones with numerous vertical tubes densely clustered together	Shelter burrowed on the upper shoreface zone under high wave and current energy	2%
5	Massive poorly to well-sorted sandstones	Higher degree of alteration at the base and top of the outcrops	10%

Table 2: Average and maximum contents of framework grains, cements, infiltrated materials and porosity for lithofacies 1 to 5 and for the studied beachrocks in general .

Lithofacies	1	2	3	4	5	Max.	Gen. Aver.
Monocrystalline quartz	46.90%	54.70%	52.80%	55.80%	49.80%	70.00%	52.00%
Polycrystalline quartz	19.1	6.9	7.3	4.6	6.6	75.5	8.9
Feldspars	0.3	0.4	0.6	0	0.2	2.3	0.3
Heavy minerals	0.2	0.1	0.1	0	1.1	9.6	0.3
Hematite-cemented sandstones	4.2	0.2	0.03	0	0.08	41.4	0.9
Bioclasts	1.2	0.9	2.6	5	1.5	29.6	2.2
Beachrock clasts	0	0.005	0.07	0	0	3.6	0.02
Porosity	6.8	10.3	9.4	7.6	12.9	30.7	9.4
Total cement	20.8	24.5	25.9	25.2	26.5	38.8	24.6
Total infiltrated material	3	1.7	0.2	1.6	0.5	18.7	1.4

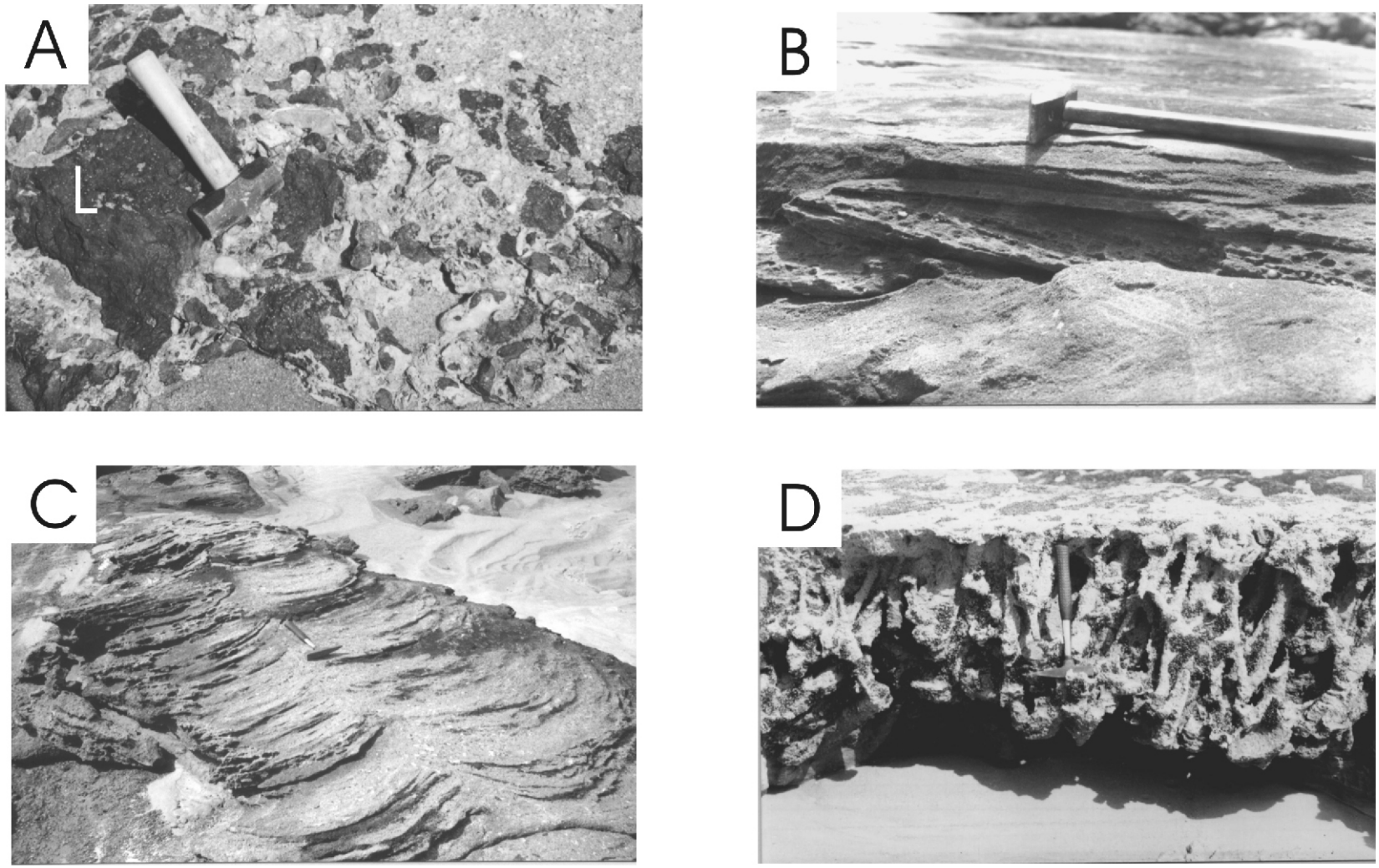

Figure 6

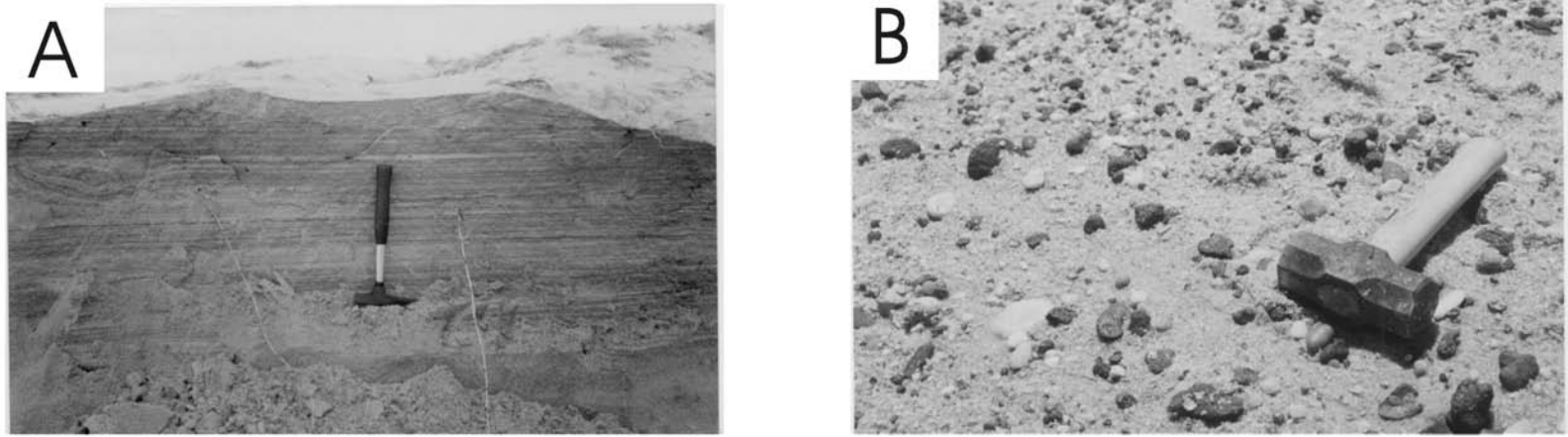

Figure 7

Figure 8

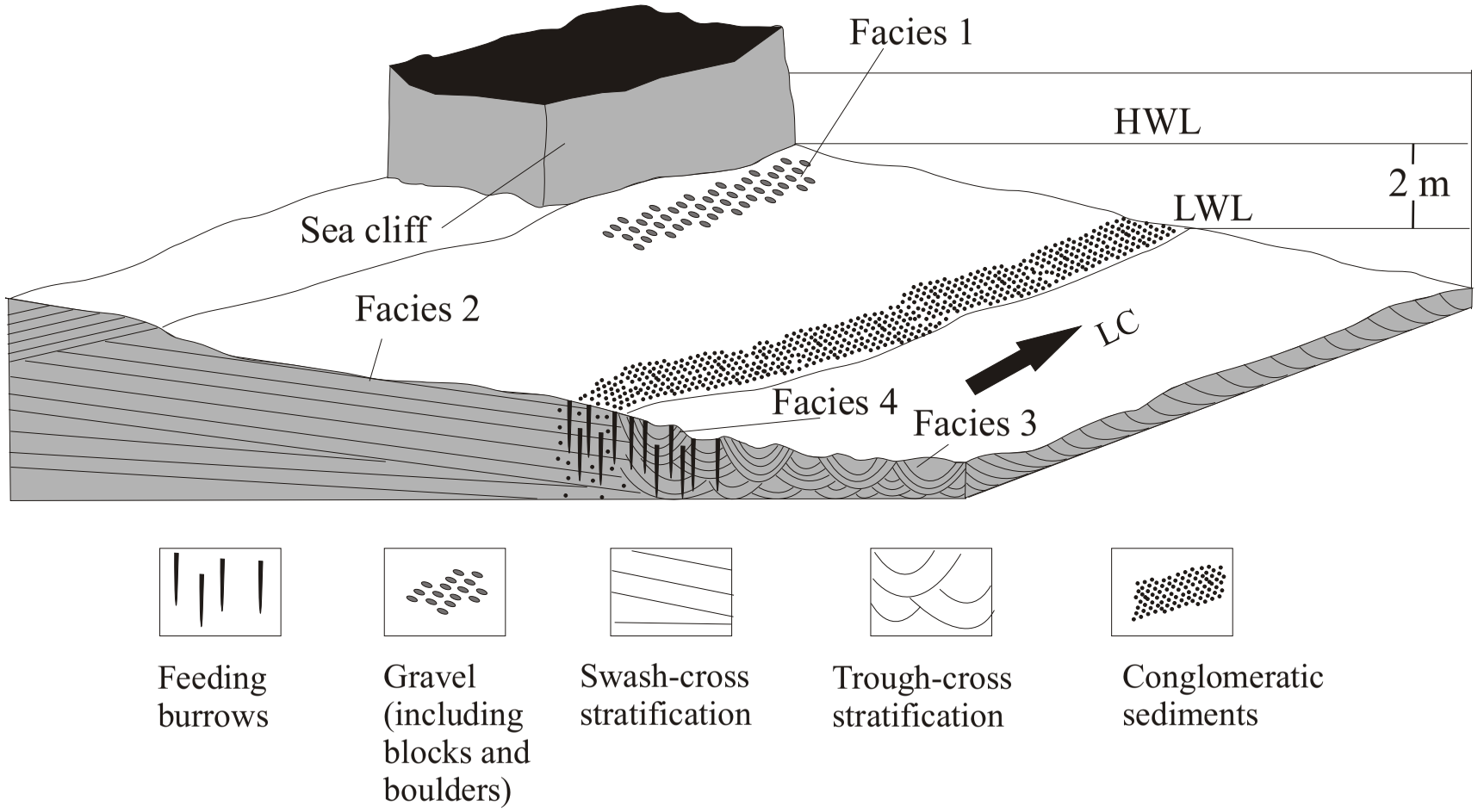
Facies 1
HWL
2 m
LWL
Sea cliff
Facies 2
LC
Facies 4
Facies 3
Feeding burrows
Gravel (including blocks and boulders)
Swash-cross stratification
Trough-cross stratification
Conglomeratic sediments

Figure 9

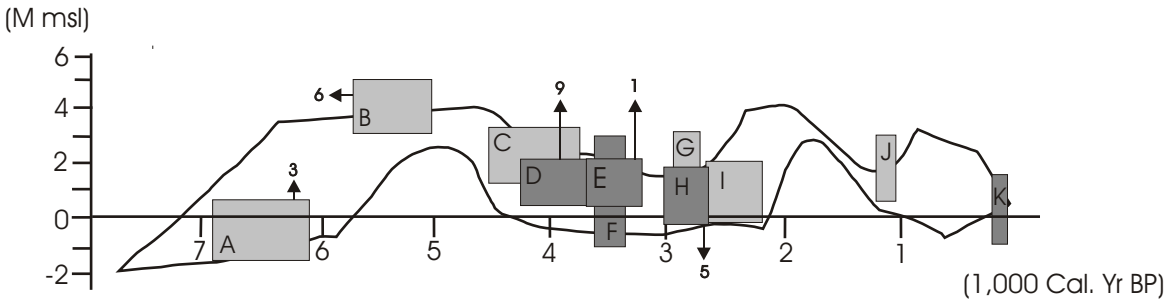

A

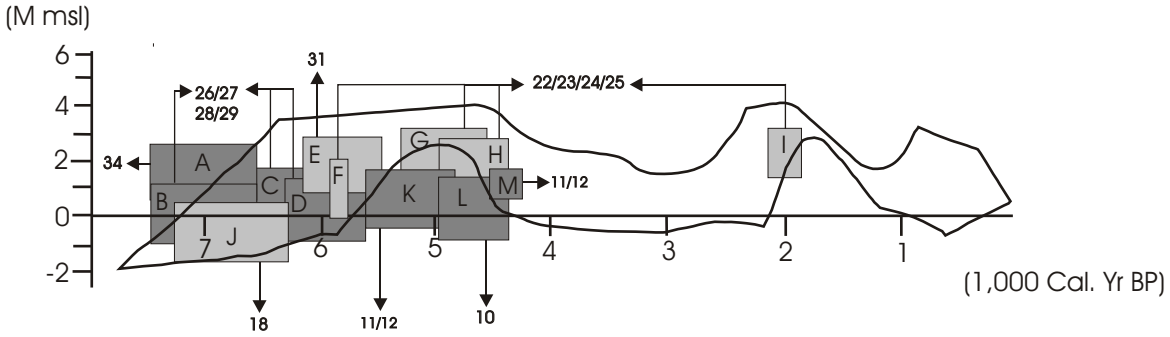

B

Upper and lower foreshore

Upper Shoreface

Table 3: Carbon 14 ages shown in figure 9A. Sample source: (1) Bezerra et al. (1998; 2003); (2), (3), (4) and (5) Stattegger *et al. (2004). These samples were taken from the same beachrock ledges as samples H, A, E and B, respectively, but were not used in the construction of the time-depth diagrams. Abbreviations: msl=mean sea level, mssl=present maximum spring tide sea level, dab= death assemblage of bivalve shells.*

Sample	**Height (m above msl)**	**Sea-level indicator**	**Calibrated age (yr BP at 2σ)**
A[(1)]	-0.5 ± 1.0	dab	6900-6080
B[(1)]	3.9 ± 1.0	dab	5730-5060
C[(1)]	2.1 ± 1.0	dab	4140-3760
D[(1)]	1.2 ± 1.0	dab	4240-3640
E[(1)]	1.1 ± 1.0	dab	3680-3210
F[(1)]	2.0 ± 1.0	dab	3640-3330
G[(1)]	2.1 ± 1.0	dab	2960-2720
H[(1)]	0.6 ± 1.0	dab	3040-2690
I[(1)]	0.6 ± 1.0	dab	2680-2190
J[(1)]	1.8 ± 1.0	dab	1250-1060
K[(1)]	0.2 ± 1.0	dab	160-60
KIA12334[(2)]	0.2	dab	2960-2900
KIA12336[(3)]	-2.5	dab	6830-6750
KIA 14750[(4)]	-1.6	dab	3235-3165
KIA14751[(5)]	+1.0	dab	5945-5875

Table 4: Carbon 14 ages shown in figure 9B. Sample source: (1) Bezerra et al. (1998; 2003); (2) Oliveira et al. (1990). This sample was taken from the same beachrock ledge as samples G and H; (3) Oliveira et al. (1990). These samples were taken from the same beachrock ledge as samples B, C and D. Samples (2) and (3) were not used in the construction of the time-depth diagrams. Abbreviations: msl=mean sea level, dab= death assemblage of bivalve shells.

Sample	**Height (m above msl)**	**Sea-level indicator**	**Calibrated age (yr BP at 2σ)**
A[(1)]	1.5 ± 1.0	dab	7460-6550
B[(1)]	0.0 ± 1.0	dab	7460-6550
C[(1)]	0.7 ± 1.0	dab	6730-5980
D[(1)]	0.2 ± 1.0	dab	6340-5600
E[(1)]	1.7 ± 1.0	dab	6170-5440
F[(1)]	0.8 ± 1.0	dab	5950-5700
G[(1)]	2.2 ± 1.0	dab	5310-4560
H[(1)]	1.8 ± 1.0	dab	4970-4380
I[(1)]	2.1 ± 1.0	dab	2160-1920
J[(1)]	-0.7 ± 1.0	dab	7240-6300
K[(1)]	0.5 ± 1.0	dab	5600-4840
L[(1)]	0.1 ± 1.0	dab	4990-4350
M[(1)]	1.0 ± 0.5	dab	4540-4240
P14[(2)]	+3.0	dab	5310-4640
P20[(3)]	+1.0-2.0	dab	6690-6680
P21[(3)]	+1.0-2.0	dab	6600-6170
P29[(3)]	+3.00	dab	5050-4550

ARTIGO 2

CEMENTATION PATTERNS AND GENETIC IMPLICATIONS OF HOLOCENE BEACHROCKS FROM NORTHEASTERN BRAZIL

Elsevier Editorial System(tm) for Sedimentary Geology

Manuscript Draft

Manuscript Number:

Title: Cementation Patterns and Genetic Implications of Holocene Beachrocks from Northeastern Brazil

Article Type: Research Paper

Section/Category:

Keywords: beachrock; diagenesis; carbonate cement; Brazil

Corresponding Author: Mrs. MARCELA MARQUES VIEIRA,

Corresponding Author's Institution: UNIVERSIDADE FEDERAL DO RIO GRANDE DO NORTE

First Author: MARCELA MARQUES VIEIRA

Order of Authors: MARCELA MARQUES VIEIRA; Luiz Fernando De Ros, PhD

Manuscript Region of Origin:

Abstract: This paper describes the complex patterns of diagenesis in Holocene beachrock ledges located along both the eastern and northern coasts of the state of Rio Grande do Norte, northeastern Brazil. These beachrocks show highly variable diagenetic processes, fabrics, and textures. Carbonate cements are exclusively composed by high-Mg calcite and occur in seven main morphologies: 1) cryptocrystalline coatings; 2) isopachous prismatic rims; 3) equant spar; 4) cryptocrystalline or micritic pore-filling; 5) pseudo-peloidal aggregates; 6) radial aggregates; 7) isolated and randomly oriented clumps of scalenohedral crystals. Other diagenetic features include: a) infiltrated marly hybrid sediment; b) infiltrated micrite; c) authigenic smectitic clay minerals; d) organic films; e) chalcedony pore-filling cement; f) vadose silty internal sediment. The texture and composition of the cements are indicative of precipitation in the active marine phreatic zone. The presence of vadose features and planktonic foraminifers within the infiltrated materials suggest that they were introduced in the backshore sands by muddy waters dislocated from the shelf during

storms. A general succession of diagenetic phases can be recognized, comprising the precipitation of authigenic smectite, micritic coatings, radial fibers, isopachous rims of prismatic crystals or equant spar, cryptocrystalline and pseudo-peloidal pore-filling cements, and vadose infiltration of micritic, marly, or silty materials. The absence of organic structures, such as microbial (bacteria or fungi) filaments and bodies within the cements suggests that the mechanism behind beachrock cementation is essentially inorganic, most probably the evaporation of entrapped seawater in response to the dry climatic conditions.

CEMENTATION PATTERNS AND GENETIC IMPLICATIONS OF HOLOCENE BEACHROCKS FROM NORTHEASTERN BRAZIL

Marcela Marques Vieira[a]

Luiz Fernando De Ros[b]

[a] Departamento de Geologia, Centro de Ciências Exatas e da Terra, Universidade Federal do Rio Grande do Norte, Natal, RN, Brazil; marcela@geologia.ufrn.br; fax number: (84)3215-3806; corresponding author

[b] Instituto de Geociências, Universidade Federal do Rio Grande do Sul, Porto Alegre, RS, Brazil; lfderos@inf.ufrgs.br

ABSTRACT: This paper describes the complex patterns of diagenesis in Holocene beachrock ledges located along both the eastern and northern coasts of the state of Rio Grande do Norte, northeastern Brazil. These beachrocks show highly variable diagenetic processes, fabrics, and textures. Carbonate cements are exclusively composed by high-Mg calcite and occur in seven main morphologies: 1) cryptocrystalline coatings; 2) isopachous prismatic rims; 3) equant spar; 4) cryptocrystalline or micritic pore-filling; 5) pseudo-peloidal aggregates; 6) radial aggregates; 7) isolated and randomly oriented clumps of scalenohedral crystals. Other diagenetic features include: a) infiltrated marly hybrid sediment; b) infiltrated micrite; c) authigenic smectitic clay minerals; d) organic films; e) chalcedony pore-filling cement; f) vadose silty internal sediment. The texture and composition of the cements are indicative of precipitation in the active marine phreatic zone. The presence of vadose features and planktonic foraminifers within the infiltrated materials suggest that they were introduced in

the backshore sands by muddy waters dislocated from the shelf during storms. A general succession of diagenetic phases can be recognized, comprising the precipitation of authigenic smectite, micritic coatings, radial fibers, isopachous rims of prismatic crystals or equant spar, cryptocrystalline and pseudo-peloidal pore-filling cements, and vadose infiltration of micritic, marly, or silty materials. The absence of organic structures, such as microbial (bacteria or fungi) filaments and bodies within the cements suggests that the mechanism behind beachrock cementation is essentially inorganic, most probably the evaporation of entrapped seawater in response to the dry climatic conditions.

Keywords: beachrock, diagenesis, carbonate cement, Brazil.

I - INTRODUCTION

The term *beachrock* refers to the calcium carbonate-cemented sediments that result from lithification in the intertidal (beaches, tidal flats, and windward reef-shingle ridges) and spray zones of mainly tropical coasts. The latitudinal limits of most contemporary beachrocks are approximately 35^{o}N and 35^{o}S (Scoffin & Stoddart, 1983). The lithified material includes sandstones, breccias, and conglomerates with different proportions of siliciclastic and carbonate grains. The importance of beachrocks is based upon three main aspects: their impact upon coastal evolution (Cooper, 1991); their significance as former sea-level indicators (Hopley, 1986); and their evidence on the processes of shallow carbonate cementation (Longman, 1980).

The specific processes responsible for cementation in beachrocks are still doubtful. Mixing of marine and meteoric waters (Schmalz, 1971; Moore, 1973), evaporation (Taylor & Illing, 1969; Moore & Billings, 1971), CO_2 degassing of shallow groundwater (Hanor, 1978;

Binkley et al., 1980; Gischler & Lomando, 1997), and direct or indirect activity of organisms (Webb et al., 1999; Neumeier, 1999) have been pointed out as the most common processes responsible for the precipitation of beachrock cements.

Beachrocks have been studied in different regions around the world, such as south Florida (Ginsburg, 1953); Hawaii (Meyers, 1987); the Mediterranean (Alexandersson, 1969; El-Sayed, 1988; Strasser et al., 1989; Sanlaville et al., 1997); the Red Sea (Holail & Rashed, 1992); Sri Lanka (Cooray, 1968); the Persian Gulf (Taylor & Illing, 1969; Khalaf, 1988); Central America (Russel, 1959; Sibley & Murray, 1972; Beier, 1985; Kindler & Bain, 1993); Africa (Siesser, 1974; Ramsay, 1994; Amieux et al., 1989), and Australia (Maxwell, 1962; Chivas et al., 1986).

Extensive beachrock ledges are a common feature along the northeastern coastline of Brazil. Most of the ledges are nearly parallel to the shoreline and are located on the present intertidal zone, but a few are permanently submerged or emerged. Both the eastern and northern shores of the state of Rio Grande do Norte, northeastern corner of the Brazilian coast (Fig. 1), are characterized by the presence of gently seaward dipping ($<10^{o}$) beachrock ledges, with up to 8 km of continuous extension. Radiocarbon dating of samples collected at various sites between the towns of Macau and Baia Formosa yielded ages from *c*. 7460 to 110 cal. yr. BP (calibrated years before Present; Bezerra et al., 2003).

Despite their great extension and influence in the present shoreline, the beachrocks of Rio Grande do Norte have been relatively infrequently studied. Branner (1904) was the first to describe the geometry, grain size, and encrusting fauna of two ledges located on the eastern coast of the state. For the next seventy years, the sparse works on these beachrocks have emphasized their fossiliferous content (Maury, 1934; Campos e Silva et al., 1964; Mendonça, 1966) or the interpretation of their sedimentary structures (Bigarella, 1975; Oliveira, 1978). More recently, beachrocks have been used for the reconstruction of the Holocene coastal

evolution of Rio Grande do Norte state (Vianna et al., 1993; Amaral, 1999; Caldas, 2002) and for the investigation of neotectonic movements (Bezerra et al., 1998; Bezerra et al., 2003; Bezerra et al., 2004).

Except for the work of Oliveira et al. (1990), who studied the diagenetic evolution of the beachrock ledges located to the south of Natal (Fig. 1), the petrologic and geochemical aspects of the cementation in the beachrocks of Rio Grande do Norte state have never been analyzed. Therefore, the aim of this paper is to describe the complex patterns of beachrock diagenesis in different ledges located on both the eastern and northern coasts of the state of Rio Grande do Norte and to investigate their distribution with regard to depositional facies, age, and position in relation to the current intertidal zone.

II – GEOLOGICAL SETTING

The study area has a tropical climate with typical air temperatures of 30°C and average rainfall between 600 and 1,000 mm/year (Nimer, 1989). Both northern and eastern coasts present a semidiurnal mesotidal regime. Strong longshore currents flow to the north along the eastern coast, and to the west along the northern coast. There is a predominance of intermittent medium to small rivers whose discharge is insignificant for most of the year, while a few perennial large rivers, including some estuaries, commonly drain into lagoons and tidal flats.

The beachrock ledges studied in this work were formed by cementation of Quaternary sediments deposited in two distinct geological provinces (Fig. 1): the Potiguar Basin, with a NE-SW general direction, which received the sedimentation along the northern coast and part of the eastern coast; and the N-S trending Pernambuco-Paraíba-Rio Grande do Norte Basin, which covers the remainder of the state's eastern coast. Both basins lie on a Precambrian

basement composed mainly of schists, marble, quartzites, migmatites, and gneisses (Jardim de Sá, 1994).

The pre-Quaternary stratigraphy of the study area includes sequences that outcrop exclusively along the northern coast (Fig. 1), comprising siliciclastic rocks of the Açu Formation (Albian-Turonian), carbonate rocks of the Jandaíra Formation (Turonian-Campanian), and silty/muddy sandstones of the Tibau Formation (Campanian-Pliocene). Carbonate rocks and calciferous/fossiliferous sandstones of the Guamaré Formation (Campanian-Pliocene) outcrop on both the northern and eastern coasts, as well as the conglomerates, sandstones, and mudrocks of the alluvial Barreiras Formation (Miocene-Pleistocene).

The conglomerates, sandstones, and mudrocks of the Barreiras Formation form cliffs along the entire coast of the state, which are in some places overlain by raised marine terraces formed during Late Pleistocene transgressions (ages from 220 ± 2 ka to 110 ± 10 ka BP; Barreto et al., 2002). Quaternary units also include beachrocks, fixed dunes, peat, diatomite, and travertine, as well as Recent beach, aeolian, alluvial, and mangrove swamp sediments (Silva & Nogueira, 1995).

III – SAMPLING AND METHODS

For the present study, Holocene beachrocks were sampled from different lithofacies exposed in 36 vertical sections described along several ledges located on the eastern and northern coasts of Rio Grande do Norte state. The total rock thickness described at the various sites was approximately 41 m. Impregnated thin sections were made from 112 samples and examined in conventional petrographic microscopes in order to determine the textural features and framework composition of the beachrocks and to identify the diagenetic processes that

they underwent during lithification. Permanently submerged beachrock horizons were not sampled.

Staining methods described by Warne (1962) and Friedman (1971) were used to study carbonate mineralogy of constituent particles and cements. The samples were treated with Feigl's solution for the distinction between calcite and aragonite. Three hundred points were counted in every thin section, along evenly spaced traverses across their depositional orientation.

Additional petrographic investigations included the examination of freshly broken, carbon-, and gold-coated samples in a SHIMADZU SSX-550 scanning electron microscope (accelerating voltage of 20kV), complemented by the determination of elemental composition by energy-dispersive spectroscopy (EDS). The beachrock ages quoted in this study are from Bezerra et al. (1998; 2003) and were determined through conventional radiocarbon (^{14}C) dating of marine shells. With the purpose of detecting contamination of the shells by old and young carbon and identifying appropriate pretreatment procedures, the authors applied special techniques such as microscopic inspection, X-ray diffraction, scanning electron microscopy, and stable isotope analysis (Bezerra et al., 2000).

IV – DEPOSITIONAL CONDITIONS

The beachrocks are discontinuously exposed along the eastern and northern shorelines of Rio Grande do Norte state. Some of the ledges can be followed for up to 8 km parallel to the beach, while others are isolated bodies just a few meters long. They range in thickness from a few centimeters to nearly 3 m and in width from 2 to 50 m. Most of beachrock ledges occur close to current sea level; nevertheless, a few can be found 10 km inland from the beach (Silva, 1991) and 5.7 km offshore (Vianna et al., 1993).

Most beachrocks are made up of gently seaward dipping (<10^{o}) tabular beds that are 5 to 150 cm thick and light-brown in color. Their lower and upper contacts with adjacent beds are abrupt. The upper surface of the studied beachrocks is rarely smooth (Pereira & Bezerra, 2001). Most of them present erosional features similar to those described in South African beachrocks and aeolianites (Miller & Mason, 1994). *Spitzkarren* (upward-pointing pyramids separated by clefts or solution basins) and near-circular depressions (solution basins and potholes) are the most common erosional features.

Beachrock ledges are composed mainly of monocrystalline quartz grains (average: 52% of bulk rock volume; maximum: 70%) and, to a lesser extent, of polycrystalline quartz grains (average: 8.9%; maximum: 75.5%), feldspar grains (mainly K-feldspar; average: 0.3%; maximum: 2.3%), heavy minerals (mostly opaque Ti and Fe oxides, but also epidote, tourmaline, staurolite, kyanite, and titanite; average: 0.3%; maximum: 9.6%), bioclasts (gastropods, bivalves, foraminifers, red algae, and equinoids; average: 2.2%; maximum: 29.6%), and fragments of hematite-cemented sandstones of the Barreiras Formation (average: 0.9%; maximum: 41.4%). Reworked beachrock fragments of various sizes are commonly found, not only as intraclasts within the studied ledges (average: 0.02%; maximum: 3.6%), but also as slabs of up to 2.0 m long, which accumulate in the intertidal or shallow subtidal zones as a result of coastal erosion and onshore wave action. The average amounts of framework grains, cement, infiltrated materials, and porosity are 64.6% (maximum: 80%), 24.6% (maximum: 38.8%), 1.4% (maximum: 18.7%) and 10% (maximum: 30.7%), respectively, in the studied rocks.

Textural characteristics and sedimentary structures were used to group the studied beachrocks into five lithofacies: (1) Massive to Weakly Stratified Conglomerate; (2) Low-Angle Cross-Stratified Conglomerate and Sandstone; (3) Medium-Scale, Tabular-Planar and Trough Cross-Stratified Sandstone; (4) Skolithos-Bioturbated Conglomeratic Sandstone; and

(5) Massive Sandstone. A summary of the main characteristics of each lithofacies and their paleoenvironmental interpretation is shown in Table 1.

The textural characteristics and sedimentary structures identified in each of these lithofacies are diagnostic of deposition in the shallow marine coastal environment. Most of the studied beachrocks were deposited on the upper shoreface zone, represented by facies with trough and tabular cross-stratification, occasionally with ichnofossils. Facies deposited on the foreshore zone—which are characterized by the presence of low-angle cross-stratification—are subordinate, as revealed by the percentage of the lithofacies in relation to the total thickness of rock described at the various sites (Table 1).

V – DIAGENETIC FEATURES

The studied beachrocks show a wide variability in diagenetic processes, fabrics, and textures. They include not only features generated by the precipitation of different types of carbonate cements, but also mechanical infiltration of carbonate and hybrid siliciclastic/carbonate fine-grained sediments. The carbonate cements are composed exclusively of high-Mg calcite, as revealed by staining and confirmed by energy dispersive spectroscopy (EDS) analyses. The Mg-calcite cements occur in seven main morphologies, namely: 1) cryptocrystalline coatings; 2) isopachous prismatic rims; 3) equant spar; 4) cryptocrystalline or micritic pore-filling; 5) pseudo-peloidal aggregates; 6) radial aggregates; 7) isolated and randomly oriented clumps of scalenohedral crystals.

5.1 - Cryptocrystalline coatings

Many framework grains in the studied beachrocks are covered by cryptocrystalline ("micritic"; crystal size < 5 μm) coatings, which are in turn commonly covered by isopachous prismatic rims (Fig. 2*A*). These coatings are predominantly discontinuous, brown, and variable in thickness (maximum of 150 μm and average of 26 μm). Both siliciclastic and carbonate grains are covered by the cryptocrystalline coatings. Micritization—i.e., alteration of carbonate grains by endolithic algi, bacteria, or fungi (*sensu* Bathurst, 1966)—is rarely observed. In a few thin sections, double cryptocrystalline coatings are separated by isopachous prismatic rims. Cryptocrystalline coatings constitute on average 3.7 of bulk volume percent of the described beachrocks (maximum value: 14.5%, at Location 10, Lithofacies 3, Fig. 6A).

5.2 – Isopachous prismatic rims

The most common carbonate cement in the studied beachrocks (average: 12.2 of bulk volume percent; maximum value: 33.6%, at Location 34, Lithofacies 3, Fig. 6C) are isopachous rims composed of prismatic crystals standing perpendicular to grain surfaces (Figs. 2*B* and 2*C*). In places, isopachous rims fill the intraparticle pores in bioclasts, or, rarely, the intergranular pores, generating polygonal boundaries among the interlocking rims (Fig. 2*D*).

Although the rims non-selectively cover both siliciclastic and carbonate grains, the texture of the crystals and their orientation in relation to each substrate is different. The crystals of the rims are arranged perpendicularly to the surface of the carbonate grains, and sub-perpendicularly to chaotically on the surface of siliciclastic grains. When the rims are developed around siliciclastic particles, they commonly present an inner portion composed of smaller equant crystals up to 4 μm size, from which the prismatic crystals grow and widen

sufficiently to show distinct rhombic terminations. The elongate crystals average, in this case, 9.6 μm in width (maximum value: 50 μm) and 47.4 μm in length (maximum value: 200 μm; length/width ratio of approximately 5). The rims developed over carbonate grains are predominantly constituted by lathlike crystals with flat terminations and average 5.9 μm in width (maximum: 20 μm) and 49.2 μm in length (maximum: 200 μm; length/width ratio of 8.3). According to Harris et al. (1985), these dimensions characterize the prismatic crystals around siliciclastic and carbonate grains as bladed and fibrous, respectively. The rims are thicker in coarser-grained beachrocks.

5.3 - Equant spar

The equant spar consists of mainly equigranular, anhedral to subhedral crystals that line or completely fill the pores (Fig. 2*E*). Equant spar cement also fills intraparticle pores within bioclasts and fractures in the siliciclastic grains. Equant spar shows in places a drusiform habit, with the crystals coarsening from the walls toward the centers of the pores. Equant cement is also found as discrete crystals partially filling the pores.

The size of the equant crystals varies from microcrystalline to mesocrystalline. When the length/width ratio is about 1, their diameter averages 20 μm (maximum: 40 μm). When the length/width ratio is up to 2 (maximum value for equant crystals, cf. Harris et al., 1985), long and short dimensions average 36.4 μm (maximum: 64 μm) and 24.5 μm (maximum: 56 μm), respectively. Occasionally, more elongated crystals, commonly scalenohedral, are found within the equant pore-filling cement or projecting from the equant rims. In a few samples, the equant spar occurs in association with rims of stubby crystals.

The average volume of equant spar in the studied beachrocks is 4.4% (maximum value: 34.4%, at Location 8, Lithofacies 2, Fig. 5). In the SEM, the equant spar appears as interlocking, subhedral crystals (Fig. 2*F*).

5.4 - Cryptocrystalline or micritic pore-filling cement

This cement consists of cryptocrystalline carbonate ("micritic" *sensu* Alexandersson, 1972a) distributed in two modes of occurrence: (1) small isolated irregular masses, forming patches between the grains; (2) abundant cement, which completely fill the pores (Fig. 3*A*). Micritic pore-filling cement constitutes on average 0.6% of the studied rocks (maximum value: 15.7%, at Location 35, Lithofacies 1, Fig. 6C).

Closer examination of this precipitate with SEM discloses that it is composed of tiny anhedral crystals (average size less than 1.0 μm) dispersed or clustered together forming structures similar to baguettes (cf. Bathurst, 1983) or grape bunches (Fig. 3*B*).

5.5 – Pseudo-peloidal aggregates

Pseudo-peloidal cement texture (Fig. 3*C*) consists of subspherical (average diameter: 36.9 μm; maximum: 120 μm) to elliptical bodies (average long and short axis: 48.7 and 31.6 μm; respective maximum values: 88 and 75 μm). These pseudo-peloids are commonly surrounded by a mosaic of equant crystals with 4.7 μm of average diameter (maximum: 8 μm) or by rims of prismatic crystals (Figs. 3*D* and 3*E*) averaging 4 μm in width and 12 μm in length (maximum: 20 μm).

The pseudo-peloidal aggregates are frequently associated with massive micritic pore-filling cement. The average amount of pseudo-peloidal cement in the described beachrocks is 1.3% (maximum value: 38.8%, at Location 17, Lithofacies 1, Fig. 6A).

5.6 – Infiltrated micrite

This material consists of micrite (lime mud with crystal size less than 2 μm, according to measurements made in SEM) sediment containing angular silt-sized terrigenous grains (mainly quartz) and microfossils (mostly coccoliths, planktonic, and benthonic foraminifers) (Figs. 3*E* and 3*F*). As a general rule, the fabric of this micrite matrix is massive, although in one sample, bioturbation has resulted in a crude arrangement of the microfossils in circles (Location 36, Fig. 6C). At Location 25 (Fig. 6B), the micritic sediment occurs as menisci, indicative of infiltration in the vadose zone (cf. Dunham, 1971).

In most of the samples where it occurs, the infiltrated micritic material fills the interparticle porosity and, to a lesser extent, intraparticle voids in bioclasts. Infiltrated micritic sediment constitutes on average 0.6% of the described beachrocks (maximum value: 18.7%, at Location 25, Lithofacies 2, Fig. 6B).

5.7 – Infiltrated marl hybrid sediment

This constituent consists of carbonate and siliciclastic mud mixed in different proportions. In plane-polarized light, this material presents a greenish-brown color, while under crossed polarizers, evenly dispersed points of high birrefringence colors are dispersed in an almost opaque mass. This hybrid internal sediment occurs in three different geometries,

namely: (1) coatings on the framework grains, (2) irregular, pore-filling masses, and (3) menisci bridging between the grains (Fig. 4*A*).

The coatings are predominantly discontinuous and anisopachous, averaging 40.8 μm in thickness (maximum: 112 μm). The masses fill the intergranular pores and, less frequently, intraparticle pores within bioclasts. The marly sediment frequently contains abundant angular silt-sized siliciclastic grains (chiefly quartz and opaque minerals) and carbonate particles (mainly planktonic foraminifers). Features of shrinkage of this hybrid sediment, such as detachment of the coatings and reduced replicas of the intergranular space are present in most of the samples. The average content of infiltrated marl sediment in the studied beachrocks is 0.8% (maximum value: 10.9%, at Location 18, Lithofacies 2, Fig. 6A).

5.8 – Isolated and randomly oriented clumps of scalenohedral crystals

In a few samples, isolated scalenohedral crystals with random orientation, project away from the surface of carbonate and siliciclastic grains (Fig. 4B). In other samples, the scalenohedral crystals occur as irregular, randomly oriented clumps of two to five elements. The scalenohedral crystals average 28.5 μm in width (maximum: 60 μm) and 89.3 μm in length (maximum: 200 μm; length/width ratio of approximately 3.1). The average amount of scalenohedral cement in the studied beachrocks is 0.6% (maximum value: 16.3%, at Location 27, Lithofacies 3, Fig. 6B).

5.9 – Radial aggregates

This type of cement is mostly present as prismatic crystals arranged radially from nuclei that in places are pseudo-peloidal bodies, isolated or rarely arranged in groups of two or three. Less commonly, the radial aggregates radiate from equant crystals (Figs. 4C and 4D).

The prismatic crystals of aggregates radiating from pseudo-peloidal bodies average 11.4 μm in width (maximum: 40 μm) and 69.9 μm in length (maximum: 250 μm; average length/width ratio of approximately 6.1). Around equant crystals or in the absence of nuclei, the crystals' width and length average 21.4 μm (maximum: 80 μm) and 91.7 μm (maximum: 240 μm), respectively (average length/width ratio of approximately 4.3). These dimensions indicate that the prismatic crystals belong to the fibrous and bladed shape classes, respectively (cf. Harris et al., 1985). In both situations, the crystals are predominantly rhombic-, and to a lesser extent, flat-terminated.

The radial aggregates occur isolated or in groups, directly on the surfaces of the grains or on previous rim or coating cements. More rarely, they fill intraparticle pores within bioclasts. The radial cements constitute on average 1% of the described beachrocks (maximum value: 22.8 %, at Location 13, Lithofacies 3, Fig. 6A).

5.10 – Authigenic Smectite Clay Mineral

Authigenic smectite clay minerals present a greenish-brown color under uncrossed polarizers, and an almost isotropic nature under crossed polarizers. It occurs in three situations: (1) around grains, as discontinuous envelopes with variable thickness (maximum of 64 μm and average of 40 μm); (2) replacing grains along the cleavages of feldspars, intercrystalline boundaries in polycrystalline quartz, and fractures; (3) pore-filling. In conjunction with the cement, rounded to sub-rounded grains with the same optical characteristics are locally found. Energy dispersive spectroscopy (EDS) analyses have shown that this material consists essentially of smectite clay minerals (identified by the occurrence of Si, Al, and Mg peaks) mixed, at certain points, with microcrystalline carbonate, iron oxide, titanium oxide or silica. It is most abundant in samples from Lithofacies 1, where it attains a

maximum amount of 13.5% at the base of vertical section 20 (Fig. 6B). This phase averages only 0.6% in the described beachrocks.

5.11 – Other diagenetic features

Minute quantities of other diagenetic products that constitute significantly less than 1% of the studied beachrocks were also identified. They include: (1) siliceous cement; (2) vadose silt internal sediment; (3) organic films.

Chalcedony pore-filling cement was identified only in one thin section from Lithofacies 1 (vertical section 36; 0.6%; Fig. 6C). Vadose silt internal sediment consists of angular to sub-angular siliciclastic silt grains (mainly quartz), mixed with lesser amounts of bioclasts and micrite (Fig. 4*E*). It occurs in trace amounts as irregular masses, in a few thin sections from lithofacies 1, 2, 3, and 5. Organic films occur as brown envelopes, constant in thickness (average value: 16 μm), that coat rims of bladed or fibrous crystals (Fig.4*F*). They occur as trace amounts in a few samples of lithofacies 2 and 3, reaching a maximum of 5% at Location 32, Lithofacies 3, Fig. 6C.

VI –DISTRIBUTION OF DIAGENETIC FEATURES

In contrast with the low-Mg calcite cements characteristic of freshwater environments, the cements generated under shallow marine phreatic conditions are composed of metastable carbonate phases: aragonite, generally as irregularly distributed needles, isopachous fibers or botryoids; and magnesian calcite (more than 5 mole% $MgCO_3$), most commonly with a micritic, eventually pseudo-peloidal texture or as isopachous rims of bladed or fibrous crystals (Longman, 1980). Even after many decades of controversy, it is still not fully understood

which factors control the mineralogy and crystalline habit of the marine carbonate cements. This variation is ascribed to several parameters, including the concentration of Mg^{2+} (Folk, 1974), phosphate and sulphate (Burton & Walter, 1990; Busenberg & Plummer, 1985), temperature (Katz, 1973; Morse & Mackenzie, 1990), as well as total salinity (Zhong & Mucci, 1989), partial pressure of CO_2 (Burton & Walter, 1991), presence of organic compounds (Kitano & Hood, 1965; Berner et al., 1978), and the participation of bacteria (Neumeier, 1999).

The most common cements of Recent beachrocks are isopachous rims of aragonite needles and/or micritic high-Mg calcite (e.g., Ginsburg, 1953; Alexandersson, 1969; Taylor & Illing, 1969; Alexandersson, 1972b; Sibley & Murray, 1972; Beier, 1985; El-Sayed, 1988; Khalaf, 1988; Strasser et al., 1989; Whittle et al., 1993; Gischler & Lomando, 1997). The types and relative amount of the diagenetic constituents identified in each vertical section from the studied area are displayed in Figures 5 and 6. These histograms show that the distribution of the diagenetic features is extremely variable along each vertical section, even at a centimetric scale, as well as in large scale, along the northern and eastern coasts. With the exception of the base of vertical section 20 (Fig. 6B), different types of diagenetic constituents always occur in combination of at least two and up to six elements (Location 30, Fig. 6C).

Modal petrographic data of total framework, porosity, cements and infiltrated materials of each lithofacies identified in the study area are displayed in Table 2. From these data, the following patterns concerning the framework composition of each lithofacies can be recognized:

A) The largest relative amounts of polycrystalline quartz grains and fragments of hematite-cemented sandstones are found in Lithofacies 1, as a consequence of the coarser grain size of this lithofacies and of its proximity to the sea cliffs undercutting the Barreiras Formation;

B) The largest volume percent of monocrystalline quartz grains is found in Lithofacies 4, probably as a result of the lower accumulation rate of this Lithofacies, which allowed an intense reworking, both by waves and currents and by the extensive organic activity that promoted distinctive bioturbation, leading to the relative decrease in the amount of unstable grains.

C) The largest content in feldspar grains and bioclasts is found in Lithofacies 3 due to its deposition on the upper shoreface zone, where limited reworking has resulted in deposition of more immature sediments.

D) The largest relative amount of heavy minerals is found in Lithofacies 5, probably owing to the higher degree of weathering that affected this lithofacies, promoting enrichment with some of the more stable heavy mineral grains, such as ilmenite and tourmaline.

E) The largest volume of reworked beachrock intraclasts is found in Lithofacies 3, as a consequence of their preferential transport by longshore currents after being brought by waves that break against beachrock ledges.

The distribution of porosity among the lithofacies reveals the following patterns:

A) The largest relative amount of porosity is found in Lithofacies 5, as a result of the higher degree of alteration that affected this lithofacies, leading to the dissolution of some constituents (particularly of bioclasts) and consequent porosity enhancement.

B) The smallest volume percent of porosity is found in Lithofacies 1, due to its poorer sorting.

Concerning the distribution of total cement and infiltrated materials in the described lithofacies, the following observations can be made:

A) The largest volume percent of cement is found in Lithofacies 5, probably as a consequence of the higher dissolved carbonate concentration at the top of each precipitation zone, due to the more intense evaporation and CO_2 loss.

B) The smallest cement content is found in Lithofacies 1, as a consequence of its poorer sorting and original smaller porosity and permeability.

C) The largest relative amount of infiltrated materials occurs in Lithofacies 1, probably owing to its frequent exposure to storms, which infiltrate muddy waters into the coarse sediments.

D) The lesser volume percent of infiltrated materials is found in Lithofacies 3, possibly due to the intense winnowing on the shoreface zone, which has removed the fine sediments. The non-exposure of this zone to storms along the backshore could be another probable explanation.

The relative amounts of each diagenetic constituent (cements and infiltrated materials) in the lithofacies are displayed in Table 3. As in other beachrocks (e.g., Ginsburg, 1953; Sibley & Murray, 1972; Beier, 1985; Khalaf, 1988; Strasser et al., 1989; Schmalz, 1971; Multer, 1971), isopachous prismatic rims predominate in the study area. The predominance of this type of cement is considered indicative of precipitation in the active marine phreatic zone, where seawater is conducted into sediments mainly by tides, waves, and currents (Longman, 1980). Similar rims, in calcareous Mediterranean beachrocks (Alexandersson, 1972b) and in Bermuda Pleistocene beachrocks (Vollbrecht & Meischner, 1993) were also interpreted as a product of marine cementation.

The regular orientation and uniform size of the rims are a result of the simultaneous crystal nucleation at a multitude of sites on grain surfaces (cf. Alexandersson, 1972a). The presence of an inner portion composed of smaller equant crystals is explained in the described samples by high carbonate concentration during the initial stages of rapid precipitation (cf.

Scoffin, 1987). With the decrease of concentration, precipitation decelerates and crystals develop prismatic forms.

The second most abundant cement type in the studied beachrocks is equant pore-lining and pore-filling spar. The same cement fabric has been identified in Holocene beachrocks from Togo (West Africa; Amieux et al., 1989) and Pleistocene beachrocks from Bermuda (Land, 1970), Salvador Island (Bahamas; Beier, 1985); Lee Stocking and Iguana islands (Bahamas Platform; Whittle et al., 1993); and Belize (Gischler & Lomando, 1997). Other terms that have been applied to the equant spar texture are granular cement (Al-Hashimi, 1977) and drusy spar or mosaic (Friedman, 1964; Gavish & Friedman, 1969). The abundance of equant spar in the studied beachrocks, and in above referred cases, contrasts with most Holocene beachrocks, where the second cement in abundance is micritic Mg-calcite. Apart from beachrocks, the pore space between Pleistocene skeletal sands from the Bermuda Islands (Friedman, 1964); reef-tract sediments on the south coast of Barbados (Steinen, 1974); and sediments associated with Quaternary and modern coral-built terraces along the coast of Red Sea, Gulf of Suez and Gulf of Aqaba (Moursi & Montaggioni, 1994) have also been partially or completely filled by equant spar.

The high-Mg calcite composition of the equant spar in the study area indicates precipitation in a predominantly shallow marine environment (Longman, 1980). This contrasts with the equant spar cements described in some of the studies cited above, which are composed of low-Mg calcite and therefore ascribed to the effect of freshwater diagenesis. In those occurrences, the meteoric interpretation for the intergranular and intraparticle equant spar cementation is supported by the replacement of high-Mg calcite and aragonite by low-Mg calcite, and by the dissolution of marine aragonitic bioclasts and cements. An explanation for the precipitation of high-Mg calcite equant spar in a Recent beach environment was given by Al-Hashimi (1977), who identified high-Mg equant spar within voids of Carboniferous

dolostone beds exposed on the present-day intertidal zone of northeastern England. This author suggests that the precipitation of equant spar cement is purely inorganic and originated from seawater evaporation during low tides, and that the poisoning effect of magnesium ions over calcite growth (Folk, 1974) may be minimized at slow precipitation rates. In the case of the studied beachrocks, the high ambient temperatures should favor a rapid rate of precipitation and carbonate growth from numerous nuclei. The reasons for the reduced nucleation and Mg-poisoning inferred for the necessary conditions for cementation by high-Mg equant spar in the studied beachrocks remain intriguing.

Cryptocrystalline high-Mg calcite coatings are the third cement morphology in abundance in the studied beachrocks. In other beachrock occurrences (e.g., Beier, 1985; Amieux et al., 1989; Strasser et al., 1989; Holail & Rashed, 1992; and Bernier et al., 1997), most of the cryptocrystalline coatings occur around carbonate allochems and have been interpreted as a product of micritization of carbonate substrates by blue-green bacteria and algae (Bathurst, 1966). Conversely, the cryptocrystalline coatings in the studied beachrocks are chemically precipitated both on siliciclastic and carbonate grains and show no relict cellular or laminar structures suggestive of algae activity (Steinen, 1974). Therefore, the presence of this cement texture in the described samples is not indicative of low-energy, stagnant settings with intense bacterial or algal activity, but of rapid supersaturation of pore waters and multiple nucleation (cf. Scoffin, 1987). Micritic cements in submarine crusts (*hardgrounds*) are more abundant closer to the water-sediment interface, whereas rims of fibrous and bladed cements are found away from the interface (Harris et al., 1985). Double cryptocrystalline coatings in beachrocks from San Salvador and the Red Sea have been interpreted as a product of two separate stages of algal activity by Beier (1985) and Holail & Rashed (1992), respectively. Conversely, the double cryptocrystalline coatings identified in the studied beachrocks probably represent phases of faster precipitation that have alternated

with slightly lower rates of precipitation, responsible for the generation of isopachous prismatic rims.

Pseudo-peloidal high-Mg calcite aggregates are the fourth most abundant cement morphology in the study area. The origin of this cement texture has been ascribed to repeated nucleation of submicrocrystalline calcite crystals around centers of growth (Macintyre, 1985). This type of cement has been identified in beachrock samples from Rhodes (Greece; Alexandersson, 1972b), Grand Cayman (West Indies; Moore, 1973), Togo (West Africa; Amieux et al., 1989), Maui (Hawaii; Meyers, 1987), Belize (Gischler & Lomando, 1997), and the Canary Islands (Calvet et al., 2003). While Alexandersson (1972b) attributed the presence of pseudo-peloidal cement exclusively to physico-chemical processes, owing to the absence of structures suggestive of an organic origin, Moore (1973) suggested a biological participation in the precipitation of this type of cement.

The fifth predominant cement type identified in the study area is of radial aggregates. Textures similar to the ones that radiate from pseudo-peloidal bodies have been interpreted as incrustation by high-Mg calcite around algal filaments in Pleistocene beaches from Bermuda, (Vollbrecht & Meischner, 1993). However, we found no recognizable remnants of algal filaments in the studied beachrocks. It is more reasonable to conclude that this cement is a product of limited nucleation on siliciclastic substrates, in contrast with carbonate substrates, which favor the precipitation of continuous fringes. From this limited initial nuclei, prismatic or lathlike crystals of high-Mg calcite would have grown in a radial disposition.

The micritic pore-filling cement results from rapid near-surface precipitation and multiple nucleation, such as the cryptocrystalline coatings. Its frequent coexistence with the pseudo-peloidal cement would result from continued nucleation and growth of crystals on exposed surfaces in an open framework, without variation in crystal morphology (cf. Alexandersson, 1972b). Some authors (Moore, 1973; Kneale & Viles, 2000; Calvet et al., 2003), based on the

presence of filaments and boreholes produced by different types of micro-organisms in micritic pore-filling cements, have attributed the precipitation of this cement type to intense microbial activity. However, in the studied beachrocks no such evidence for the presence of micro-organisms is found in the cryptocrystalline pore-filling cement, what indicates its precipitation by dominantly inorganic, physicochemical processes. This is also suggested by the larger amounts of both the cryptocrystalline and pseudo-peloidal pore-filling cements in Lihofacies 1, which is coarser-grained and therefore originally more permeable than the other lithofacies. Cryptocrystalline pore-filling cements have also been reported in beachrocks from the Mediterranean coast of Israel (Gavish & Friedman, 1969), Mozambique (Siesser, 1974), Belize (Gischler & Lomando, 1997), Heron Island (Great Barrier Reef; Webb et al., 1999), Kuwait (Khalaf, 1988), and Grand Cayman Island (Moore, 1971).

The isolated nature of scalenohedral crystals suggests that they are mainly produced under very slow rates of precipitation, as a result of a drastic decrease in the number of nucleation sites. This type of cement has also been reported in beachrocks from southeastern Tunisia (Strasser et al., 1989).

Infiltrated micrite and marl hybrid sediments are commonly arranged as irregular aggregates and meniscus bridges between the grains. This indicates that these sediments resulted from processes of infiltration of muddy waters through the sandy sediments in the vadose zone. The silt-sized grains that are associated with the micrite and silicilastic mud are mostly composed of angular quartz and planktonic foraminifers, a microfauna typical of deeper waters at about the platform edge of the upper slope (Scoffin, 1987). Muddy waters dislocated from the platform into the backshore by storms would best explain the presence of vadose features associated with extraneous fossiliferous content. Similar infiltrated micritic sediments have been interpreted as cement in other beachrocks (e.g., Alexandersson, 1972b; Moore, 1973; Meyers, 1987; Gischler & Lomando, 1997; Webb et al., 1999; Calvet et al.,

2003). In those cases, evenly dispersed particles have been interpreted as a product of interstitial transport during micritic cement growth. We believe that infiltration is a simpler interpretation for those cases as well, as interpreted for other occurrences by Sibley & Murray (1972), Steinen (1974), and Khalaf (1988). Similarly to the studied case, Alexandersson (1972b) interpreted the presence of sponge spicules and foraminifers dispersed in micritic "matrix" of Mediterranean beachrocks as the product of infiltration of muddy shelf sediments.

The siltic internal sediment infiltrated into the studied beachrocks, commonly called "vadose silt" (cf. Dunham, 1969), forms when silt settles out of water percolating through the sediment. A similar diagenetic feature has also been identified in the larger pores of beachrocks from the eastern shore of Ore Lake in Michigan (Binkley et al., 1980), in borings found in submarine-cemented rocks from the Persian Gulf (Shinn, 1969), and in marginal facies of shallow Belize barrier and atoll reefs (James et al., 1976).

Authigenic smectite is characteristic of the eodiagenesis of siliciclastic sediments both under marine and dry continental conditions (e.g., Mathisen, 1984; McKinley et al., 2003; Ketzer et al., 2003). Therefore, its formation before the high-Mg calcite cementation of the studied beachrocks may be related either to the early meteoric alteration of feldspars and unstable heavy minerals in backshore conditions, or to a very early marine alteration of these labile grains.

Sparse chalcedony pore-filling cement is covered by high-magnesium calcite isopachous prismatic rim at Location 36 (Fig. 6C). This suggests that a phase of meteoric diagenesis, responsible for the precipitation of siliceous cement, has pre-dated cementation under marine conditions. The silica for chalcedony precipitation may have been released from replacement and/or dissolution of silicates within contemporaneous alluvial sediments or in the beachrock itself. The same hypothesis for silica precipitation has been proposed by Mathisen, 1984; McKinley et al., 2003; Ketzer et al., 2003

Moursi and Montaggioni (1994) in reef-associated sediments from the red Sea coastal plain (Egypt). Since that siliceous bioclasts (e.g., sponge spicules; Lima and De Ros, 2002) are absent from the Recent shallow marine sediments of the studied area, it is unlikely that such chalcedony cementation may have occurred under marine conditions.

Coatings of dark, organic matter have been described in beachrocks from Heron Island (Great Barrier Reef; Webb et al., 1999) and in calcrete profiles developed on the surface of the eastern Canary Islands (Alonso-Zarza & Silva, 2002). In both situations, these organic residues are associated with obvious microbial structures (i.e., bacteria and/or fungi filaments and bodies) and appear to have favored the precipitation of carbonate crystals (aragonite isopachous fringes and needle-fiber calcite crystals, respectively). The inverse situation occurs in the study area, where organic films have locally coated isopachous prismatic rims. This suggests that, after a phase of intense water movement into the sediment, in which carbonate cementation occurred, stagnant conditions have locally prevailed, allowing the necessary circumstances for preservation of microbial organic mater.

Table 3 illustrates the large variability on the average content of each diagenetic material in the defined lithofacies 1 to 5. The isopachous prismatic crystal rims, equant spar, and micrite envelopes are the predominant diagenetic products in the described beachrocks, particularly in lithofacies 2 to 5. In Lithofacies 1, on the other hand, the most common diagenetic material is the pseudo-peloidal micrite cement, followed by the elongated crystal rim and equant spar. Other differential aspects concerning Lithofacies 1 are that it presents the largest volumes of cryptocrystalline pore-filling cement, infiltrated marly sediment, authigenic smectite clay mineral, and siliceous cements. The preferential occurrence of these constituents in this lithofacies is probably related to its coarser grain size, therefore larger original permeability, and to its more frequent exposure than the other lithofacies, due to its closer proximity to the continent.

VII – DIAGENETIC SEQUENCE

The different textures of high-Mg calcite cements were not always precipitated in a repeated order during the diagenesis of the studied beachrocks. Even so, a general, statistical succession of diagenetic phases can be proposed for the studied beachrocks, which is schematically displayed in Figure 7. As a general rule, the cementation by authigenic smectite clay mineral was the first diagenetic event to affect the studied beachrocks, followed by a first generation of micritic coating. In most cases, radial fibers precipitated after the micritic coating and before the isopachous prismatic crystal rims or equant spar. Isopachous prismatic crystal rims predominantly precipitated before the cryptocrystalline pore-filling cement, the pseudo-peloidal micrite cement, and the infiltrated micrite. Nevertheless, in a few cases, a single rim formed around these fine-grained materials (Figs. 3*E* and 3*F*). The infiltration of micritic, marly, or silty sediments under vadose conditions was the last event to occur in the samples in which these materials are present (Figs. 3*E*, 3*F*, 4*A,* and 4*E*). Organic films typically occur around previously precipitated cements (Fig. 4*F*).

VIII – BEACHROCK DISTRIBUTION IN RELATION TO SEA LEVEL

The generation of beachrocks is apparently related to sea-level oscillations. However, it is still not clear whether the preferential conditions for beachrock formation are attained during sea-level rise (Russell, 1959; Alexandersson, 1972b), fall (Siesser, 1974; Beier, 1985), or stillstand (Cooray, 1968). The small thickness of the vertical sections of the study area limits direct inferences on sea-level changes from the depositional sequences. Long-term changes can be seen in the sea-level envelope curve constructed by Bezerra et al. (2003) for

the state of Rio Grande do Norte (Fig. 8), which is based on radiocarbon data obtained from sea-level indicators found on beachrocks (death assemblage of bivalve shells, vermetid, and coral reef); peat deposits (bivalve shell in living position and fragments of wood and oyster); Barreiras Formation outcrops (oyster and coral reef); and tidal flats (death assemblage of bivalve shells and oyster). The rectangles shown in Figures 8A and 8B represent the radiocarbon ages obtained from beachrock samples of the northern and eastern coasts, respectively. Their values are displayed in Tables 4 and 5.

The sea-level envelope curve obtained by Bezerra et al. (2003) provides a minimum age for the deposition of the sands cemented in each ledge. Figure 8 shows that the deposition of the sediments from the studied beachrocks occurred under variable conditions, comprising relatively rapid sea-level rise, high sea-level stands, sea-level drop, and low sea-level stands, in the same way as the examples described in the literature. The comparison of Figure 8A with Figure 8B reveals that, along the northern coast, the beach sediments were predominantly deposited between ~4140-2190 cal. yr. BP, when sea level dropped, and during low sea-level stands. Conversely, the beach deposits distributed along the eastern coast were preferentially formed between ~7460-4240 cal. yr. BP, during rapid sea-level rise and high sea-level stand.

The combination of the lithofacies identified in this study (Table 1) with the sea-level envelope curve shown in Figure 8 suggests that, on the northern coast, the shoreface sedimentation zone, represented by lithofacies 3 and 4, is preferentially distributed during sea-level drop and low sea-level stand phases (Fig. 8A), while the foreshore sedimentation zone, represented by Lithofacies 2, can be found along the whole curve. In the case of the eastern coast, both preferential sedimentation zones (shoreface and foreshore) are equally concentrated in the first stages of rapid sea-level rise and high sea-level stand (Fig. 8B).

To what extent the time lapse between the deposition of a beach sediment and its subsequent cementation can be considered negligible, is still controversial. First of all, the period between the death of an organism and the cementation of a beachrock may be hundreds and even thousands of years (Hopley, 1986). Secondly, the cement may form by slow, continuous growth at levels of moderate supersaturation or grow only occasionally, under extremely favorable conditions (Alexandersson, 1972a). In view of these facts, the age yielded by the dating of a constituent organism can only be regarded as the maximum possible age for beachrock cementation (Hopley, 1986). This uncertainty in time of framework deposition relative to time of cementation, together with potential problems with application of ^{14}C dating to beachrock (e.g. difficulty of selecting suitable material for dating), makes any attempt to correlate sea-level change and beachrock diagenesis limited and with a significant element of conjecture. Despite these facts, the following observations can be made, concerning the diagenetic phases in relation to sea-level change along the eastern coast (Fig. 8B):

A) Cryptocrystalline pore-filling cement and pseudo-peloidal aggregates attain larger relative amounts during high sea-level stand (vertical section 31).

B) Infiltrated marly hybrid sediment attains larger relative amounts during sea-level rise (vertical section 18).

C) Infiltrated micrite attains larger relative amounts during sea-level rise (vertical section 18) and high sea-level stand (vertical section 25).

D) Radial aggregates and isolated / randomly oriented clumps of scalenohedral crystals attain larger relative amounts during sea-level rise (vertical sections 27 and 28) and during high sea-level stand (vertical sections 22, 23 and 24).

E) Equant spar attains larger relative amounts mainly during sea-level rise (vertical sections 27, 28 and 34).

F) Cryptocrystalline coating attains larger relative amounts mainly during high sea-level stand (vertical sections 10, 11 and 12).

G) Isopachous prismatic rim attains larger relative amounts in any portion of the sea-level envelope curve.

Concerning the northern coast, the only remark that can be made is the predominance of equant spar during low sea-level stand (vertical sections 1 and 9).

IX – IMPLICATIONS FOR THE COASTAL EVOLUTION OF NE BRAZIL

The foregoing data afford no direct observational evidence of the specific processes responsible for beachrock genesis in the study area. The absence of organic structures, such as microbial (bacteria or fungi) filaments and bodies, as revealed by petrographic and scanning electron microscopes, suggests that the mechanism behind beachrock cementation is essentially inorganic. Similar conclusions have been reached by Alexandersson (1972b) and Gischler & Lomando (1997) for the beachrocks along the Mediterranean and Belize shores, respectively. Evaporation of entrapped seawater seems to be the most probable explanation for precipitation of the described beachrock cements. This interpretation is based chiefly on the climatic conditions of the study area and agrees with conclusions reached elsewhere by Ginsburg (1953), Taylor & Illing (1969), and Khalaf (1988).

As shown in sections V and VI, multiple and irregularly distributed diagenetic features characterize the studied beachrocks. This indicates that their lithification occurred under the influence of rapidly shifting parameters that have changed even in the thin-section scale. Similar conclusions have been reached by Taylor & Illing (1969) for the beachrocks surrounding the Qatar Peninsula (Persian Gulf), where the variability of cements was attributed to a great influence of micro-environments on the cementation. These changes have been attributed to drainage and evaporation rates, which are in turn influenced by percolating

rain, dew, and fluctuating loose-sand cover. Other authors have advocated the temporal and spatial change of the parameters controlling beachrock cementation, such as sea-level fluctuations, as the main cause of their complex cementation patterns (e.g., Taylor & Illing, 1971; Strasser et al., 1989; Holail & Rashed, 1992).

Data presented in section VIII suggest that the driving force of these shifting conditions should be the diversity of sea-level positions under which the beachrocks have been generated. As a general rule, beachrock cementation starts soon after sedimentation and may proceed for a long time, continuously or episodically. The role played by local advances and retreats of the sea or by lower-order sea-level oscillations in these patterns is still not clear. Individual radiocarbon dating of carbonate cements may shed some light on this question; nevertheless, difficulties in obtaining sufficient cement, without contamination by older bioclastic materials, as well as by younger fluids, make the precise dating of beachrock cementation a difficult task (Hopley, 1986). In summary, further investigation appears to be necessary to better understand the extension and amplitude by which sea-level changes have influenced the variety of cement textures detected in the studied beachrocks.

X – CONCLUSIONS

1) The beachrock ledges studied along the coast of northeastern Brazil are composed mainly of monocrystalline quartz grains and, to a lesser extent, polycrystalline quartz grains, feldspar grains, heavy minerals, bioclasts (gastropods, bivalves, foraminifers, red algae and equinoids), and fragments of Tertiary hematite-cemented sandstones of the Barreiras Formation. Reworked beachrock fragments of various sizes are commonly found, not only as intraclasts within the studied ledges, but also as slabs of up to 2.0 m long, which accumulate in the present intertidal or shallow subtidal zones as a result of coastal erosion and onshore wave action. The average amounts of framework grains, cement, infiltrated materials, and porosity

are 64.6 (maximum: 80%), 24.6 (maximum: 38.8%), 1.4 (maximum: 18.7%), and 10% (maximum: 30.7%), respectively.

2) The studied beachrocks show a wide variability in diagenetic processes, fabric, and texture. The carbonate cements are composed exclusively of high-Mg calcite and occur in seven main morphologies, namely: 1) cryptocrystalline coatings; 2) isopachous prismatic rims; 3) equant spar; 4) cryptocrystalline or micritic pore-filling; 5) pseudo-peloidal aggregates; 6) radial aggregates; 7) isolated and randomly oriented clumps of scalenohedral crystals. Other diagenetic features include: 1) infiltrated marly hybrid sediment; 2) infiltrated micrite; 3) authigenic smectite clay mineral; 4) organic films; 5) chalcedony pore-filling cement; 6) vadose silt internal sediment.

3) The distribution of diagenetic features is extremely variable along the 36 vertical sections described in the study area, not only at a centimetric scale, but at a large scale as well. Different types of cement and infiltrated material occur in combination of at least two, and up to six elements. This multiplicity and irregular distribution of diagenetic constituents indicate that lithification of the studied beachrocks occurred under the influence of rapidly shifting parameters that have changed even in the thin-section scale.

4) The textures of the carbonate cements, together with their high-magnesium calcite composition, are indicative of precipitation in the active marine phreatic zone. Concerning the infiltrated micrite and marly hybrid sediment, muddy waters dislocated from the platform into the backshore by storms would best explain the presence of vadose features and planktonic foraminifers. Authigenic smectite clay mineral may be related either to the early meteoric alteration of feldspars and less stable heavy minerals in backshore conditions, or to the very

early marine alteration of these labile grains. Chalcedony pore-filling cement may be attributed to meteoric waters that have replaced carbonate cement or filled voids created by carbonate dissolution. The vadose silt internal sediment was created when silt formed during beachrock exposure settled out of water percolating through the sediments. Local prevalence of stagnant conditions provided the suitable micro-environment for preservation of microbial organic matter as organic films coating the calcite cements.

5) The isopachous prismatic crystal rims, equant spar, and micrite envelopes are the predominant diagenetic products in the described beachrocks, particularly in lithofacies 2 to 5 (2-Low-Angle Cross-Stratified Conglomerate and Sandstone; 3-Medium-Scale, Tabular-Planar, and Trough Cross-Stratified Sandstone; 4-Skolithos-Bioturbated Conglomeratic Sandstone; 5-Massive Sandstone). In Lithofacies 1 (Massive to Weakly Stratified Conglomerate), on the other hand, the most common diagenetic material is the pseudo-peloidal micrite cement, followed by the elongated crystal rim and equant spar. Other differential aspects concerning Lithofacies 1 are that it presents the largest volumes of cryptocrystalline pore-filling cement, infiltrated marly, authigenic smectite clay mineral, and siliceous cements. The preferential occurrence of these constituents in this lithofacies is probably related to its coarser grain size, therefore larger original permeability, and to its more frequent exposure than the other lithofacies.

6) A general succession of diagenetic phases can be proposed for the studied beachrocks. As a general rule, the cementation by authigenic smectite clay mineral was the first diagenetic event to affect the studied beachrocks, followed by the first generation of micritic coating. In most cases, radial fibers precipitated after the micritic coating and before the isopachous prismatic crystal rims or equant spar. Isopachous prismatic crystal rims predominantly

precipitated before the cryptocrystalline pore-filling cement, the pseudo-peloidal micrite cement, and the infiltrated micrite. Nevertheless, in a few cases, a single rim formed around these fine-grained materials. The infiltration of micritic, marly, or silt under vadose conditions was the last event to occur in the samples in which these materials occur. Organic films typically occur around previously precipitated cements.

7) The absence of organic structures suggests that the mechanism behind beachrock cementation is essentially inorganic, most probably through the evaporation of entrapped seawater, in response to the dry climatic conditions. The variety of cement textures demonstrates that diagenetic parameters have changed through time and space. The driving force of these shifting conditions appears to be the diversity of sea-level positions under which beachrocks have been generated. Further investigation appears necessary to better understand the extension and amplitude by which local advances and retreats of the sea or lower-order sea-level oscillations have been responsible for the variety in cement textures.

ACKNOWLEDGMENTS

This work is part of M.M. Vieira's Ph.D. thesis research carried out at the Instituto de Geociências of the Universidade Federal do Rio Grande do Sul, Porto Alegre, Brazil. Partial support for this work was provided by a scholarship granted by CAPES, an organ of the Ministry of Education and Culture of Brazil. The authors thank Dr. F.A. Vieira for his assistance in the scanning electron microscope investigation and Dr. R.F.S. Lima for her help in the staining procedures. Thanks are extended to the Geology Department of the Universidade Federal do Rio Grande do Norte for providing equipment and support.

REFERENCES

Al-Hashimi, W.S., 1977. Recent carbonate cementation from seawater in some weathered dolostones, Northumberland, England. Journal of Sedimentary Petrology 47(3), 1375–1391.

Alexandersson, T., 1969. Recent littoral and sublittoral high-Mg calcite lithification in the Mediterranean. Sedimentology 12, 47–61.

Alexandersson, T., 1972a. Intragranular growth of marine aragonite and Mg-calcite: evidence of precipitation from supersaturated seawater. Journal of Sedimentary Petrology 42(2), 441–460.

Alexandersson, T., 1972b. Mediterranean beachrock cementation: marine precipitation of Mg-calcite. In: D.J. Stanley (Ed.), The Mediterranean Sea: A natural sedimentation laboratory. Dowden, Hutchinson & Ross, Stroudsburg, Penn., pp. 203–223.

Alonso-Zarza, A.M., Silva, P.G., 2002. Quaternary laminar calcretes with bee nests: evidences of small-scale climatic fluctuations, Eastern Canary Islands, Spain. Palaeogeography, Palaeoclimatology, Palaeoecology 178, 119–135.

Amaral, R.F., 1999. Contribuição ao estudo da evolução morfodinâmica do litoral oriental sul do Rio Grande do Norte, entre Ponta de Búzios e Baía Formosa. Ph.D. Thesis. Universidade Federal do Rio Grande do Sul, Porto Alegre, RS, Brazil.

Amieux, P., Bernier, P., Dalongeville, R., Medwecki, V., 1989. Cathodoluminescence of carbonate-cemented Holocene beachrock from the Togo coastline (West Africa): an approach to early diagenesis. Sedimentary Geology 65, 261–272.

Barreto, A.M.F., Bezerra, F.H.R., Suguio, K., Tatumi, S.H., Yee, M., Paiva, R.P., Munita, C. S., 2002. Late Pleistocene marine terrace deposits in northeastern Brazil: sea-level change and tectonic implications. Palaeogeography, Palaeoclimatology, Palaeoecology 179, 57–69.

Bathurst, R.G.C., 1966. Boring algae, micrite envelopes and lithification of molluscan biosparites. Journal of Geology 5, 15–32.

Bathurst, R.G.C., 1983. Early diagenesis of carbonate sediments. In: A. Parker and B.W. Selwood (Eds.), Sediment diagenesis. D. Reidel, pp. 349–377.

Beier, J.A., 1985. Diagenesis of Quaternary Bahamian beachrock: petrographic and isotopic evidence. Journal of Sedimentary Petrology 55(5), 755–761.

Berner, R.A., Westrich, R.G., Smith, J., Martens, C., 1978. Inhibition of aragonite precipitation from supersaturated seawater; a laboratory and field study. American Journal of Science 278, 816–837.

Bernier, P., Guidi, J.B., Böttcher, M.E., 1997. Coastal progradation and very early diagenesis of ultramafic sands as a result of rubble discharge from asbestos excavations (northern Corsica, western Mediterranean). Marine Geology 144, 163–175.

Bezerra, F.H.R., Lima-Filho, F.P., Amaral, R.F., Caldas, L.H.O., Costa-Neto, L.X., 1998. Holocene coastal tectonics. In: I.S. Stewart and C. Vita-Finzi (Eds.), Coastal tectonics. Geological Society, London. Special Publications 146, pp. 279–293.

Bezerra, F.H.R., Vita-Finzi, C., Lima-Filho, F.P., 2000. The use of marine shells for radiocarbon dating of coastal deposits. Revista Brasileira de Geociências 30(1), 211–213.

Bezerra, F.H.R., Barreto, A.M.F., Suguio, K., 2003. Holocene sea-level history on the Rio Grande do Norte State coast, Brazil. Marine Geology 196, 73–89.

Bezerra, F.H.R., Amaral, R.F., Lima-Filho, F.P., Ferreira Jr., A.V., Sena, E.S., Diniz, R.F., 2004. Beachrock fracturing in Brazil, Journal of Coastal Research, Special Issue 42, 169–182.

Bigarella, J.J., 1975. Reef sandstones from northeastern Brazil (A survey on sedimentary structures). Anais da Academia Brasileira de Ciências 47, 395–409.

Binkley, K.L., Wilkinson, B.H., Owen, R.M., 1980. Vadose beachrock cementation along a southeastern Michigan Marl Lake. Journal of Sedimentary Petrology 50(3), 953–962.

Branner, J.C., 1904. The stone reefs of Brazil, their geological and geographical relations, with a chapter on the coral reefs. Museum of Comparative Zoology, Harvard College, Cambridge, Mass., Geological Series 7.

Burton, E.A., Walter, L.M., 1990. The role of pH in phosphate inhibition of calcite and aragonite precipitation rates in seawater. Geochimica et Cosmochimica Acta 54, 797–808.

Burton, E.A., Walter, L.M., 1991. The effects of P_{CO2} and temperature on magnesium incorporation in calcite in seawater and MgCl2-CaCl2 solutions. Geochimica et Cosmochimica Acta 55, 777–785.

Busenberg, E., Plummer, L.N., 1985. Kinetic and thermodynamic factors controlling the distribution of SO_4^{2-} and Na^+ in calcites and selected aragonites. Geochimica et Cosmochimica Acta, 49, 713–725.

Caldas, L.H.O., 2002. Late Quaternary coastal evolution of the northern Rio Grande do Norte coast, NE Brazil. Ph.D. Thesis, University of Kiel, Kiel, Germany.

Calvet, F., Cabrera, M.C., Carracedo, J.C., Mangas, J., Pérez-Torrado, F.J., Recio, C., Trave, A., 2003. Beachrocks from the island of La Palma (Canary Islands, Spain). Marine Geology 197, 75–93.

Campos e Silva, A., Silva, D.D., Vasconcelos, M.D.T., 1964. Informação sobre a malacofauna dos beach rocks de Touros e São Bento do Norte. Arquivos do Instituto de Antropologia, 50(2), 79–90.

Chivas, A., Chippell, J., Polach, H., Pillans, B., Flood, P., 1986. Radiocarbon evidence for the timing and rate of island development, beachrock formation and phosphatization at Lady Elliot Island, Queensland, Australia. Marine Geology 69, 273–287.

Cooper, J.A.G., 1991. Beachrock formation in low latitudes: implications for coastal evolutionary models. Marine Geology 98, 145–154.

Cooray, P.G., 1968. A note on the occurrence of beachrock along the west coast of Ceylon. Journal of Sedimentary Petrology 38, 650–654.

Dunham, R.J., 1969. Early vadose silt in Townsend Mound (reef), New Mexico. In: G.M. Friedman (Ed.), Depositional environments in carbonate rocks, a symposium. SEPM Special Publication 14, 139–181.

Dunham, R.J., 1971. Meniscus cement. In: O.P. Bricker (Ed.), Carbonate cements. Johns Hopkins University Press, Baltimore, Md., pp. 297–300.

El-Sayed, M.M., 1988. Beachrock cementation in Alexandria, Egypt. Marine Geology 80, 29–35.

Folk, R.L., 1974. The natural history of crystalline calcium carbonate; effect of magnesium content and salinity. Journal of Sedimentary Petrology 44, 40–53.

Friedman, G.M., 1964. Early diagenesis and lithification in carbonate sediments. Journal of Sedimentary Petrology 34(4), 777–813.

Friedman, G.M., 1971. Staining. In: R.E. Carner (Ed.), Procedures in sedimentary petrology. Wiley, New York, pp. 511–530.

Gavish, E., Friedman, G.M., 1969. Progressive diagenesis in Quaternary to Late Tertiary carbonate sediments: sequence and time scale. Journal of Sedimentary Petrology 39(3), 980–1006.

Ginsburg, R.N., 1953. Beachrock in south Florida. Journal of Sedimentary Petrology 23(2), 85–92.

Gischler, E., Lomando, A.J., 1997. Holocene cemented beach deposits in Belize. Sedimentary Geology 110, 277–297.

Hanor, J.S., 1978. Precipitation of beach rock cements: mixing of marine and meteoric waters vs. CO_2 degassing. Journal of Sedimentary Petrology 48, 489–502.

Harris, P.M., Kendall, C.G. St. C., Lerche, I., 1985. Carbonate cementation: a brief review. In: N. Schneidermann and P.M. Harris, (Eds.), Carbonate cements. SEPM Special Publication 36, pp. 79–95.

Holail, H., Rashed, M., 1992. Stable isotopic composition of carbonate-cemented recent beachrock along the Mediterranean and Red Sea Coasts of Egypt. Marine Geology 106, 141–148.

Hopley, D., 1986. Beachrock as a sea-level indicator. In: O. Van de Plassche (Ed.), Sea-level research. Galliard Printers, Great Yarmouth, pp. 157–173.

James, N.P., Ginsburg, R.N., Marszalek, D.S., Choquette, P.W., 1976. Facies and fabric specificity of early subsea cements in shallow Belize (British Honduras) reefs. Journal of Sedimentary Petrology 46, 523–544.

Jardim De Sá, E.F., 1994. A Faixa Seridó (Província Borborema) e seu significado geodinâmico na Cadeia Brasiliana/Panafricana. Ph.D. Thesis, Universidade de Brasília, Brazil.

Katz, A., 1973. The interaction of magnesium with calcite during crystal growth at 25–30^{o}C and one atmosphere. Geochimica et Cosmochimica Acta 37, 1563–1586.

Ketzer, J.M., Morad, S., and Amorosi, A., 2003. Predictive diagenetic clay-mineral distribution in siliciclastic rocks within a sequence stratigraphic framework. In: R.H. Worden and S. Morad (Eds.), Clay cements in sandstones. IAS Special Publication 34. International Association of Sedimentologists, Blackwell Scientific Publications, Oxford, UK, pp. 42–59.

Khalaf, F.I., 1988. Quaternary calcareous hard rocks and the associated sediments in the intertidal and offshore zones of Kuwait. Marine Geology 80, 1–27.

Kindler, P., Bain, R.J., 1993. Submerged upper Holocene beachrock on San Salvador island, Bahamas: implications for recent sea-level history. Geol. Rundsch 82, 241–247.

Kitano, Y., Hood, D.W., 1965. The influence of organic material on the polymorphic crystallization of calcium carbonate. Geochimica et Cosmochimica Acta 29, 29–41.

Kneale, D., Viles, H.A., 2000. Beach cement: incipient $CaCO_3$-cemented beachrock development in the upper intertidal zone, North Uist, Scotland. Marine Geology 132, 165–170.

Land, L.S., 1970. Phreatic versus vadose meteoric diagenesis of limestones: evidence from a fossil water table. Sedimentology 14, 175–185.

Lima, R.D., De Ros, L.F., 2002. The role of depositional setting and diagenesis on the reservoir quality of Late Devonian sandstones from the Solimões Basin, Brazilian Amazonia. Marine and Petroleum Geology 19, 1047–1071.

Longman, M.W., 1980. Carbonate diagenetic textures from nearsurface diagenetic environments. The American Association of Petroleum Geologists Bulletin 64, 461–487.

Macintyre, I.G., 1985. Submarine cements: the peloidal question. In: N. Schneidermann and P.M. Harris (Eds.), Carbonate cements. SEPM Special Publication 36, pp. 109–116.

McKinley, J.M., Worden, R., Ruffell, A.H., 2003. Smectite in sandstones: a review of the controls on occurrence and behaviour during diagenesis. In: R.H. Worden and S. Morad (Eds.), Clay cements in sandstones. IAS Special Publication 34. International Association of Sedimentologists, Blackwell Scientific Publications, Oxford, UK, pp. 109–128.

Mathisen, M.E., 1984. Diagenesis of Plio-Pleistocene non-marine sandstones, Cagayan Basin, Philippines: early development of secondary porosity in volcanic sandstones. In: R. Surdam and D.A. McDonald (Eds.), Clastic diagenesis. AAPG Memoir 37. American Association of Petroleum Geologists, Tulsa, Ok., pp. 177–193.

Maury, C.J., 1934. Fossil invertebrata from northeastern Brazil. American Museum of Natural History Bulletin 67(4), 123–179.

Maxwell, W.G.H., 1962. Lithification of carbonate sediments in the Heron Island Reef, Great Barrier Reef. Journal of the Geological Society of Australia 8, 217–238.

Mendonça, M.I., 1966. O recife de arenito de Tibau. Arquivos do Instituto de Antropologia, 2, 343–346.

Meyers, J.H., 1987. Marine vadose beachrock cementation by criptocrystalline magnesian calcite–Maui, Hawaii. Journal of Sedimentary Petrology 57, 558–570.

Miller, W.R., Mason, T.R., 1994. Erosional features of coastal beachrock and eolianite outcrops in Natal and Zululand, South Africa. Journal of Coastal Research 10(2), 394–414.

Moore Jr., C.H., 1971. Beachrock cements, Grand Cayman Island, B.W.I. In: O.P. Bricker (Ed.), 1971. Carbonate cements. Johns Hopkins University, Baltimore, Md. Studies in Geology 19, pp. 9–12.

Moore Jr., C.H., 1973. Intertidal carbonate cementation, Grand Cayman, West Indies. Journal of Sedimentary Petrology 43, 591–602.

Moore Jr., C.H., Billings, G.K., 1971. Preliminary model of beachrock cementation, Grand Cayman Island, B.W.I. In: O.P. Bricker (Ed.), 1971. Carbonate cements. Johns Hopkins University, Baltimore, Md., Studies in Geology 19, pp. 40–43.

Morse, V., Mackenzie, F.T., 1990. Geochemistry of sedimentary carbonates. Developments in Sedimentology 48, Elsevier, 707p.

Moursi, M., Montaggioni, L.F., 1994. Diagenesis of Pleistocene reef-associated sediments from the Red Sea coastal plain, Egypt. Sedimentary Geology 90, 49–59.

Multer, H.G., 1971. Holocene cementation of skeletal grains into beachrock, Dry Tortugas, Florida. In: O.P. Bricker (Ed.), Carbonate cements. Johns Hopkins University, Baltimore, Md., Studies in Geology, 19, pp. 17–24.

Neumeier, U., 1999. Experimental modelling of beachrock cementation under microbial influence. Sedimentary Geology 126, pp. 35–46.

Nimer, E., 1989. Climatologia do Brasil. Instituto Brasileiro de Geografia e Estatística, Departamento de Recursos Naturais e Ambientais. Rio de Janeiro, RJ, Brazil.

Oliveira, M.I.M., 1978. Os recifes de Natal. MSc Thesis, Universidade Federal de Pernambuco. Recife, PE, Brazil.

Oliveira, M.I.M., Bagnoli, E., Farias, C.C., Nogueira, A.M.B., Santiago, M., 1990. Considerações sobre a geometria, petrografia, sedimentologia, diagênese e idades dos *beachrocks* do Rio Grande do Norte. XXXVI Congresso Brasileiro de Geologia. Sociedade Brasileira de Geologia. Natal, RN, Brazil. Boletim de Resumos 2, pp. 621–34.

Pereira, M.M.V., Bezerra, F.H.R., 2001. Feições erosionais em beachrocks do Rio Grande do Norte. XIX Simpósio de Geologia do Nordeste. Sociedade Brasileira de Geologia, Núcleo Nordeste. Natal, RN, Brazil. Boletim de Resumos 17, pp. 77–78.

Ramsay, P.J., 1994. Marine geology of the Sodwana Bay shelf, southeast Africa. Marine Geology 120, 225–247.

Russel, R.J., 1959. Caribbean beachrock observations. Z. Geomorphol. 3, 227–236.

Sanlaville, P., Dalongeville, R., Bernier, P., Evin, J., 1997. The Syrian coast: a model of Holocene coastal evolution. Journal of Coastal Research 13(2), 385–396.

Schmalz, R.F., 1971. Formation of beachrock at Eniwetok Atoll. In: O.P. Bricker (Ed.), Carbonate cements. Johns Hopkins University, Baltimore, Md., Studies in Geology 19, pp. 17–24.

Scoffin, T.P., 1987. An introduction to carbonate sediments and rocks. Blackie, Glasgow and Hall, New York, 274p.

Scoffin, T.P., Stoddart, D.R., 1983. Beachrock and intertidal cements. In: A.S. Goudie and K. Pye (Eds.), Chemical sediments and geomorphology: precipitates and residua in the near-surface environment. Academic Press, pp. 401–425.

Shinn, E.A., 1969. Submarine lithification of Holocene carbonate sediments in the Persian Gulf. Sedimentology 12, 109–144.

Sibley, D.F., Murray, R.C., 1972. Marine diagenesis of carbonate sediment, Bonaire, Netherlands Antilles. Journal of Sedimentary Petrology 42(1), 168–178.

Siesser, W.G., 1974. Relict and recent beachrock from southern Africa. Geological Society of America Bulletin 85, 1849–1854.

Silva, C. G., 1991. Holocene stratigraphy and evolution of the Açu River Delta, Rio Grande do Norte State, northeastern Brazil. PhD thesis, Duke University, Durham, NC.

Silva, R.L.C., Nogueira, A.M.B., 1995. Estratigrafia da porção emersa da costa do Rio Grande do Norte. 1º Simpósio sobre Processos Sedimentares e Problemas Ambientais na Zona Costeira Nordeste do Brasil. Recife, Pernambuco, Brazil, pp. 144–147.

Steinen, R.P., 1974. Phreatic and vadose diagenetic modification of Pleistocene limestone: petrographic observations from subsurface of Barbados, West Indies. The American Association of Petroleum Geologists Bulletin 58(6), 1008–1024.

Strasser, A., Davaud, E., Jedoui, Y., 1989. Carbonate cements in Holocene beachrock: example from Bahiret el Biban, southeastern Tunisia. Sedimentary Geology, 62, 89–100.

Taylor, J.C.M., Illing, L.V., 1969. Holocene intertidal calcium carbonate cementation, Qatar, Persian Gulf. Sedimentology 12, 69–107.

Taylor, J.C.M., Illing, L.V., 1971. Variation in recent beachrock cements, Qatar, Persian Gulf. In: O.P. Bricker (Ed.), Carbonate cements. Johns Hopkins University, Baltimore, Md., Studies in Geology 19, pp. 40–43.

Vianna, M.L., Cabral, A.P., Gherardi, D.F.M., 1993. TM-Landsat imagery applied to study of the impact of global climate change on a tropical coastal environment during the last deglaciation. International Journal of Remote Sensing 14(14), 2971–2983.

Vollbrecht, R., Meischner, D., 1993. Sea level and diagenesis: a case study on Pleistocene beaches, Whalebone Bay, Bermuda. Geol Rundsch 82, 248–262.

Warne, S. St. J., 1962. A quick field or laboratory staining scheme for the differentiation of the major carbonate minerals. Journal of Sedimentary Petrology 32(1), 29–38.

Webb, G.E., Jell, J.S., Baker, J.C., 1999. Cryptic intertidal microbialites in beachrock, Heron Island, Great Barrier Reef: implications for the origin of microcrystalline beachrock cement. Sedimentary Geology 126, 317–334.

Whittle, L.G., Kendall, C.G. St. C., Dill, R.F., Rouch, L., 1993. Carbonate cement fabrics displayed: A traverse across the margin of the Bahamas Platform near Lee Stocking Island in the Exuma Cays. Marine Geology 110, 213–243.

Zhong, S., Mucci, A., 1989. Calcite and aragonite precipitation from seawater solutions of various salinities: precipitation rates and overgrowth compositions. Chemical Geology 78, 283–299.

Fig. 1: Location and simplified geological map of the study area.

Fig. 2: (A) Quartz grain cemented by an inner band of thick, dark micrite envelope and an outer, lighter band of elongated crystal rim. Note irregular thickness of the fine-grained coating; uncrossed polarizers (//P); Location 19. (B) Regular and isopachous elongated crystal rims lining monocrystalline quartz grains. Note perfectly perpendicular orientation of crystals with respect to grain surfaces and occurrence of two generations of elongated crystal rims (center of the photograph); crossed polarizers (XP); Location 24. (C) Scanning electron

microscopy (SEM) image of the same sample, showing detail of the prismatic shape of the crystals. (D) Polygonal sutures formed by elongated crystal rims that have grown from micritic coatings to compromise boundaries; //P; Location 24. (E) Mesocrystalline anhedral to subhedral equant spar completely filling the pore space between quartz grains; //P; Location 16. (F) Close-up view of subhedral, Mg-calcite equant spar filling pore-space; note the step-sided, defective crystals; SEM; Location 32.

Fig. 3: (A) Dark, cryptocrystalline cement completely filling the pore space between quartz grains; note the very fine-grain size of the cement and lack of any previous crystalline cements; //P; Location 35. (B) SEM image of the same sample, showing detail of the cryptocrystalline cement, formed by subhedral Mg-calcite crystals. (C) Pseudo-peloidal, micritic pore-filling cement; //P; Location 17. (D) SEM image of the same sample, showing detail of radial structure of pseudo-peloids. (E) Pseudo-peloidal micrite cement (left) covered by a rim of elongated crystals; an infiltrated micritic sediment with bioclasts of different sizes occupies the remaining pore space; //P; Location 30. (F) SEM image of the same sample, showing quartz and feldspar grains (top) covered by a rim of elongated crystals, and this in turn by infiltrated micrite sediment.

Fig. 4: (A) Meniscus of infiltrated marly sediment bridging between elongated crystal rims that cover quartz grains; //P; Location 18. (B) Close view of a scalenohedral crystal projecting from the surface of a quartz grain; //P; Location 15. (C) Radial aggregate encrusting a previous, equant pore-filling cement; //P; Location 15. (D) SEM close-up view of a radial aggregate, showing defective crystal faces; Location 23. (E) Multiple pore-filling phases: the upper part of the void between the quartz grains has been filled by pseudo-peloidal micritic cement, and the remaining pore space has been filled by infiltrated micritic and marly

sediments, followed by silty, quartzose, and bioclastic sediment; //P; Location 18. (F) Dark organic film coating rims of bladed and equant crystals; //P; Location 32.

Figure 5: North coast of Rio Grande do Norte state, showing locations of the studied beachrock occurrences (black dots and adjacent numbers). Histograms display the types and relative amounts of the diagenetic constituents identified in each described thin section. The vertical distribution of the histograms corresponds to the position of the samples along the section constructed at each location.

Figure 6: (A) and (C) East coast of Rio Grande do Norte state, showing locations of the studied beachrock occurrences (black dots and adjacent numbers). Histograms display the types and amounts of the diagenetic constituents identified in each described thin section. The vertical distribution of the histograms corresponds to the sample position along each studied section. Legend is the same as in Figure 5. Rectangle corresponds to Fig. 6B. (B) Inset of Fig. 6A with part of the studied sections.

Figure 7: Most usual sequence of diagenetic phases during the evolution of the studied beachrocks.

Figure 8: (A) Samples analyzed for ^{14}C of the North coast, plotted along the sea-level curve for Rio Grande do Norte state (Bezerra et al., 2003). Radiocarbon data were obtained from shells within beachrocks, and this curve resulted from the intersection of two others obtained for the North and East coasts. Numbers in rectangles refer to the vertical sections used to interpret the predominant sedimentation zone (foreshore or shoreface) of the beachrock ledges

from which the ^{14}C samples were obtained. (B) Distribution of the ^{14}C samples from the East coast.

Table 1

Click here to download Table: Table 1.doc

Table 1: Summary of the main characteristics of each lithofacies and paleoenvironmental interpretation

Lithofacies	Description	Interpretation	% relative to total thickness
1	Massive to weakly seaward-dipping stratified, poorly to very poorly sorted, sharp-based conglomerates	Transgressive lag deposit or traction carpet deposit	5%
2	Poorly to well-sorted sandy conglomerate to sandstone with a seaward-dipping low-angle X-stratification	Beachface wave swash or backswash or backwash step vortex	32%
3	Very poorly- to well-sorted sandstones with small- to medium-scale trough cross-stratification with paleocurrents parallel to coastline	Bedload transport by longshore currents on the upper shoreface zone	51%
4	Poorly to very poorly sorted sandstones with numerous vertical tubes densely clustered together	Shelter burrowed on the upper shoreface zone under high wave and current energy	2%
5	Massive poorly to well-sorted sandstones	Higher degree of alteration at the base and top of the outcrops	10%

Table 2

Click here to download Table: Table 2.xls

Table 2: Average and maximum contents of framework grains, cements, infiltrated materials and porosity for lithofacies 1 to 5 and for the studied beachrocks in general .

Lithofacies	1	2	3	4	5	Max.
Monocrystalline quartz	46.90%	54.70%	52.80%	55.80%	49.80%	70.00%
Polycrystalline quartz	19.1	6.9	7.3	4.6	6.6	75.5
Feldspars	0.3	0.4	0.6	0	0.2	2.3
Heavy minerals	0.2	0.1	0.1	0	1.1	9.6
Hematite-cemented sandstones	4.2	0.2	0.03	0	0.08	41.4
Bioclasts	1.2	0.9	2.6	5	1.5	29.6
Beachrock clasts	0	0.005	0.07	0	0	3.6
Porosity	6.8	10.3	9.4	7.6	12.9	30.7
Total cement	20.8	24.5	25.9	25.2	26.5	38.8
Total infiltrated material	3	1.7	0.2	1.6	0.5	18.7

Gen. Aver.
52.00%
8.9
0.3
0.3
0.9
2.2
0.02
9.4
24.6
1.4

Table 3

Click here to download Table: Table 3.xls

Table 3: Average and maximum content of diagenetic materials in the studied beachrocks

Lithofacies	1	2	3	4	5	Max
isopachous prismatic rims	4.5%	13.2%	10.3%	18.1%	14.9%	33.6%
radial aggregates	0.4	1.0	1.9	0.0	1.8	22.8
equant spar	4.2	5.2	8.6	0.0	4.2	34.4
cryptocrystalline coating	1.4	2.9	3.3	7.1	3.9	14.5
pseudo-peloidal aggregates	5.2	0.4	0.03	0.0	1.1	38.8
cryptocrystalline pore-fill	2.0	0.8	0.1	0.0	0.2	15.7
infiltrated marly hybrid sediment	2.4	0.8	0.09	0.0	0.5	10.9
infiltrated micrite	0.6	0.9	0.09	1.6	0.0	18.7
scalenohedral crystals	0.0	0.9	1.6	0.0	0.4	16.3
organic films	0.0	0.0	0.1	0.0	0.0	5.0
authigenic smectite	3.1	0.01	0.0	0.0	0.0	13.5
siliceous cement	0.05	0.0	0.0	0.0	0.0	0.6

Aver
12.2%
1.0
4.4
3.7
1.3
0.6
0.8
0.6
0.6
0.02
0.6
0.01

Table 4

Click here to download Table: Table 4.xls

Table 4: Carbon 14 ages from Bezerra et al. (1998; 2003) shown in Figure 8A.

Sample	Height (m above msl)	Sea-level indicator	Calibrated age (yr BP)
A	-0.5 ± 1.0	dab	6900-6080
B	3.9 ± 1.0	dab	5730-5060
C	2.1 ± 1.0	dab	4140-3760
D	1.2 ± 1.0	dab	4240-3640
E	1.1 ± 1.0	dab	3680-3210
F	2.0 ± 1.0	dab	3640-3330
G	2.1 ± 1.0	dab	2960-2720
H	0.6 ± 1.0	dab	3040-2690
I	0.6 ± 1.0	dab	2680-2190
J	1.8 ± 1.0	dab	1250-1060
K	0.2 ± 1.0	dab	160-60

Abbreviations: msl = mean sea level; mssl = present maximum spring tide sea level; dab = death assemblage of bivalve shells.

Table 5

Click here to download Table: Table 5.xls

Table 5: Carbon 14 ages from Bezerra et al. (1998; 2003) shown in Figure 8B

Sample	Height (m above msl)	Sea-level indicator	Calibrated age (yr BP)
A	1.5 ± 1.0	dab	7460-6550
B	0.0 ± 1.0	dab	7460-6550
C	0.7 ± 1.0	dab	6730-5980
D	0.2 ± 1.0	dab	6340-5600
E	1.7 ± 1.0	dab	6170-5440
F	0.8 ± 1.0	dab	5950-5700
G	2.2 ± 1.0	dab	5310-4560
H	1.8 ± 1.0	dab	4970-4380
I	2.1 ± 1.0	dab	2160-1920
J	0.7 ± 1.0	dab	7240-6300
K	0.5 ± 1.0	dab	5600-4840
L	0.1 ± 1.0	dab	4990-4350
M	1.0 ± 0.5	dab	4540-4240

Abbreviations: msl = mean sea level; mssl = present maximum spring tide sea level; dab = death assemblage of bivalve shells.

Figure 1

Click here to download high resolution image

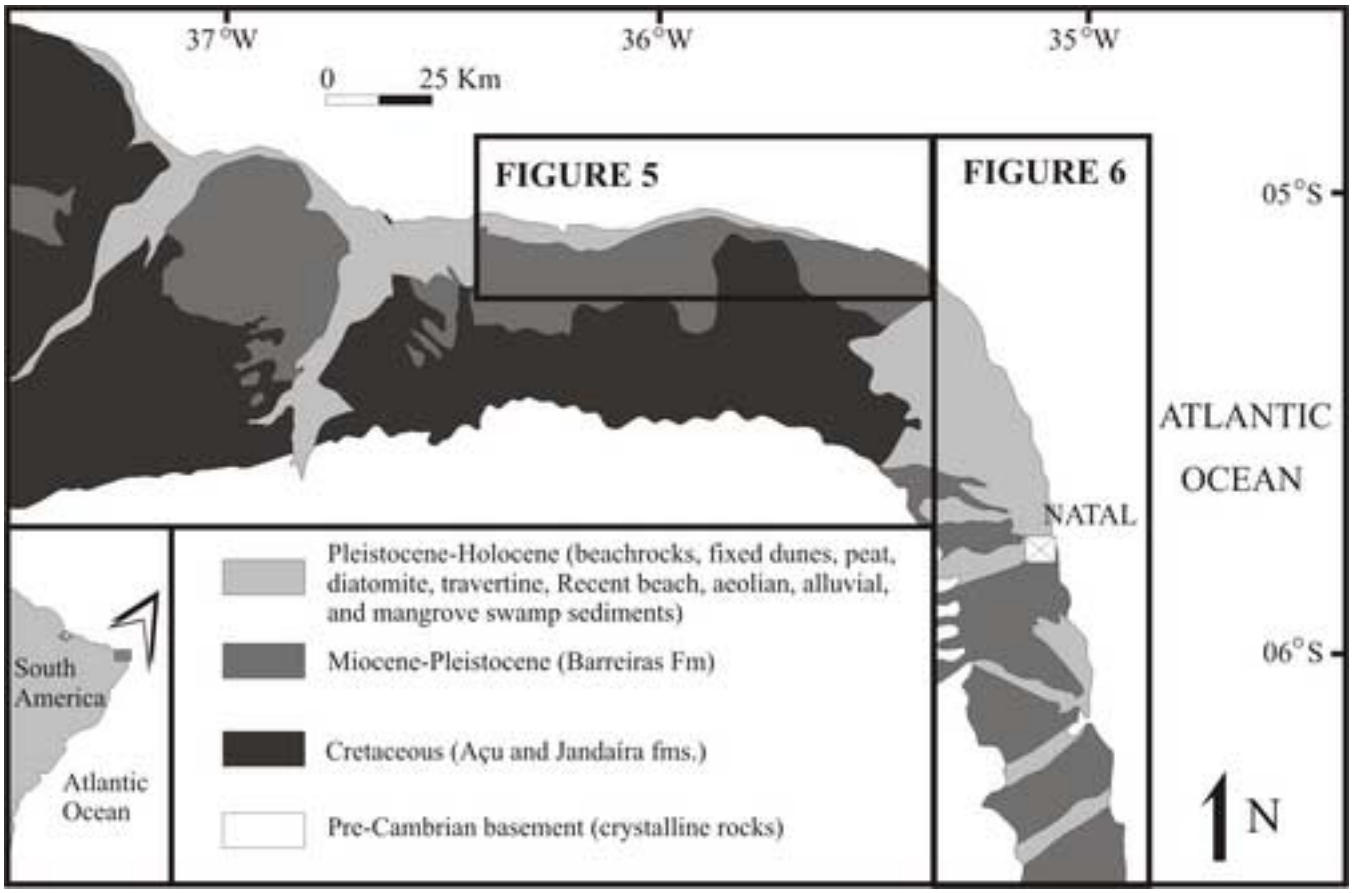

Figure 2

Click here to download high resolution image

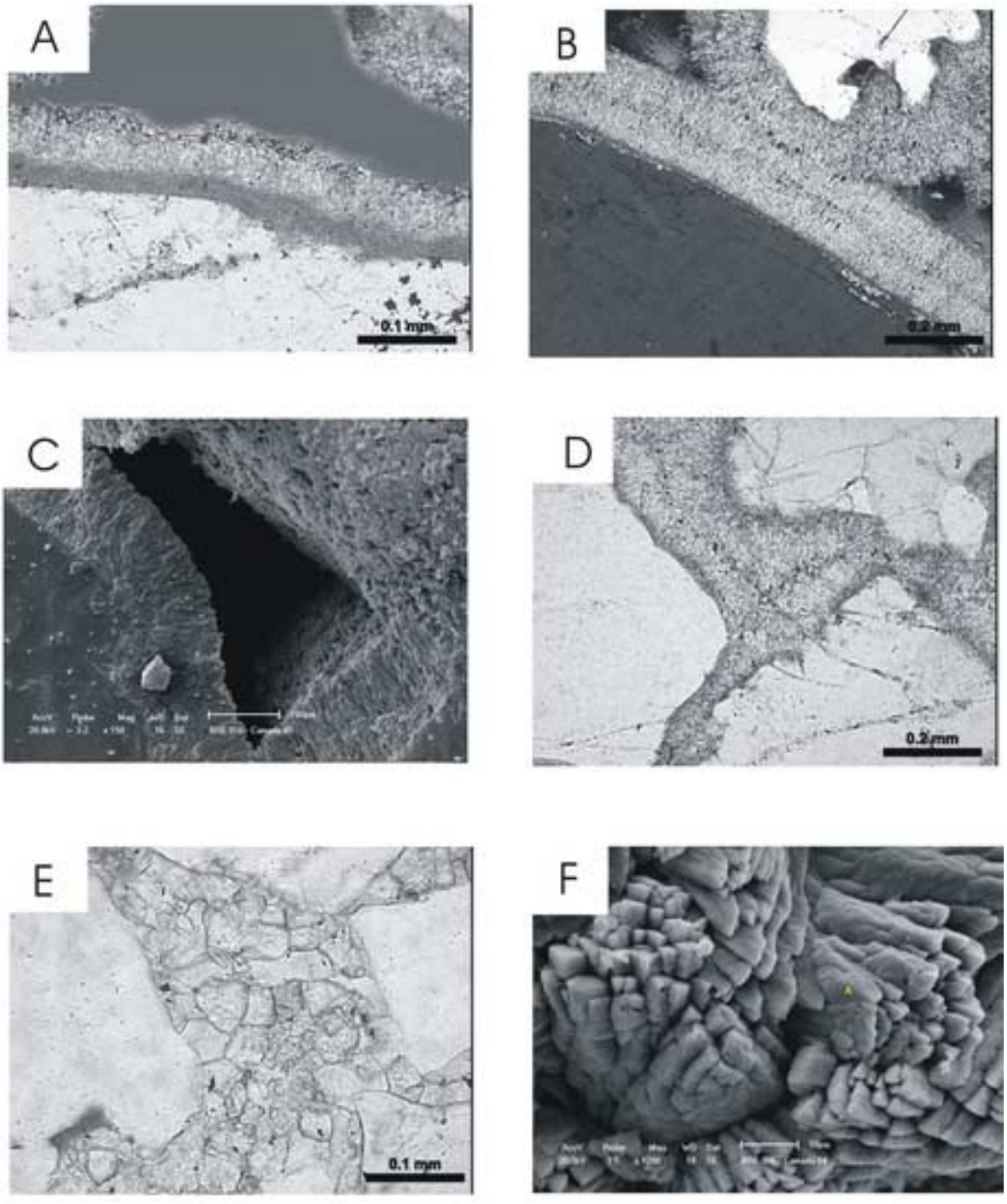

Figure 3

Click here to download high resolution image

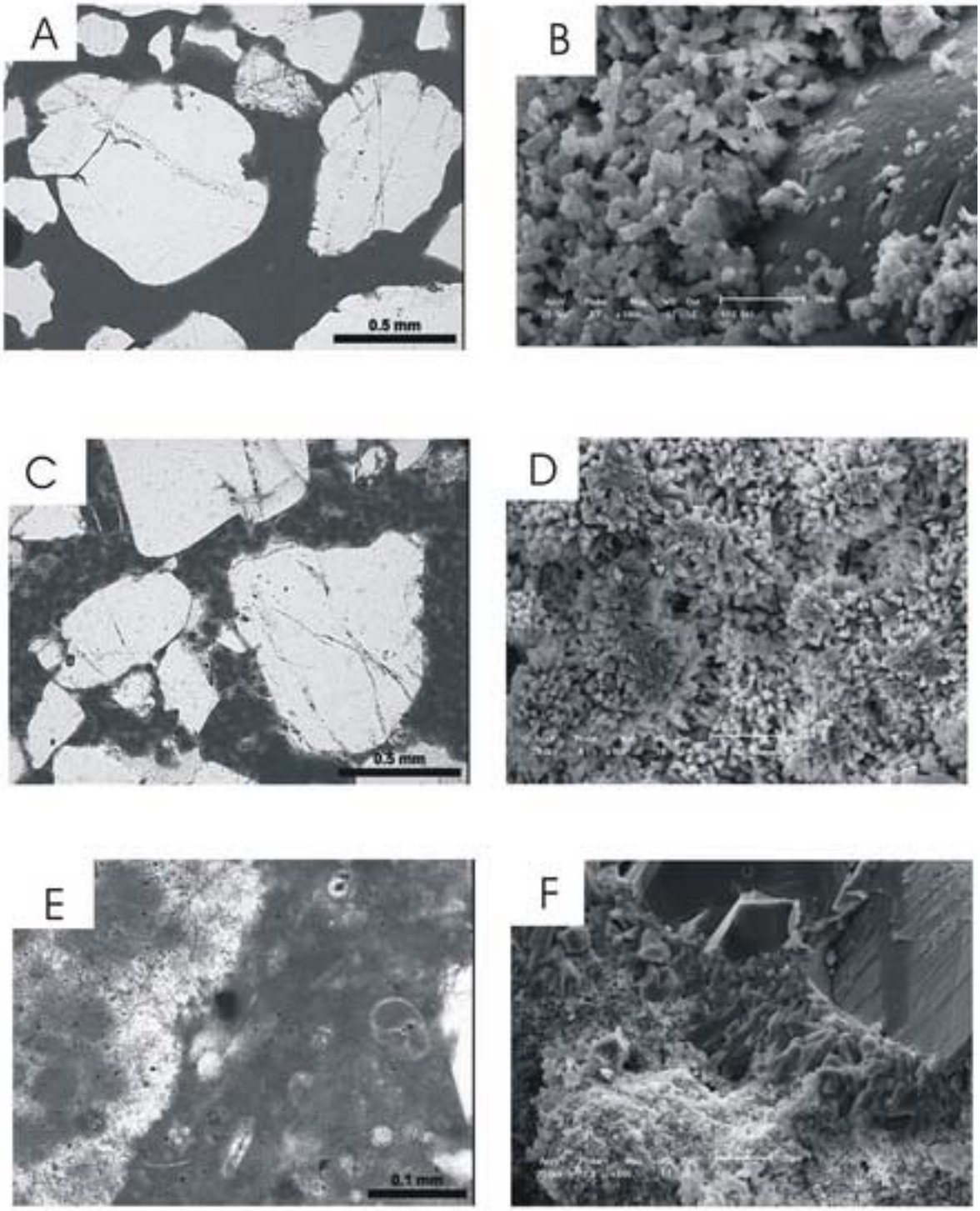

Figure 4

Click here to download high resolution image

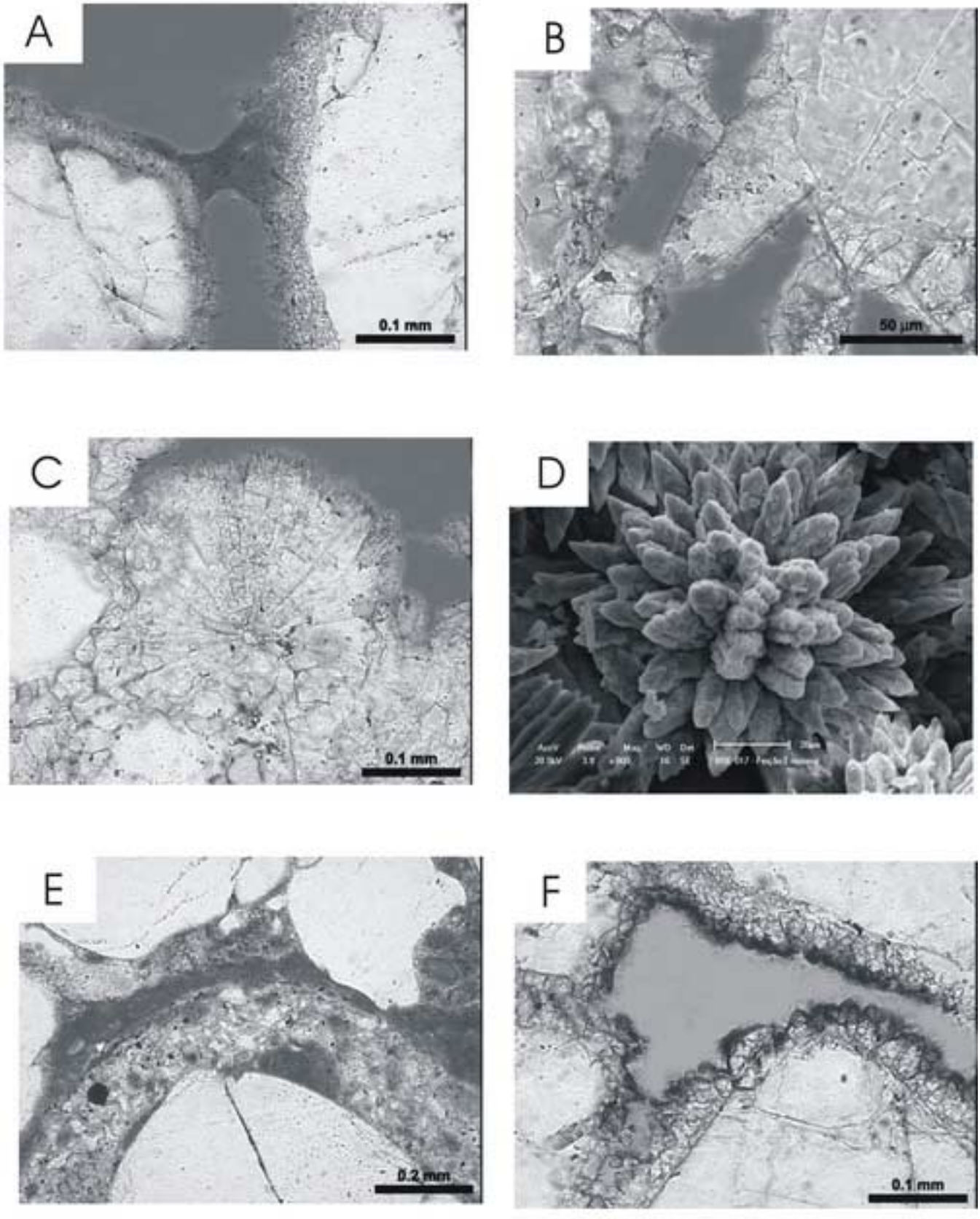

Figure 5

Click here to download high resolution image

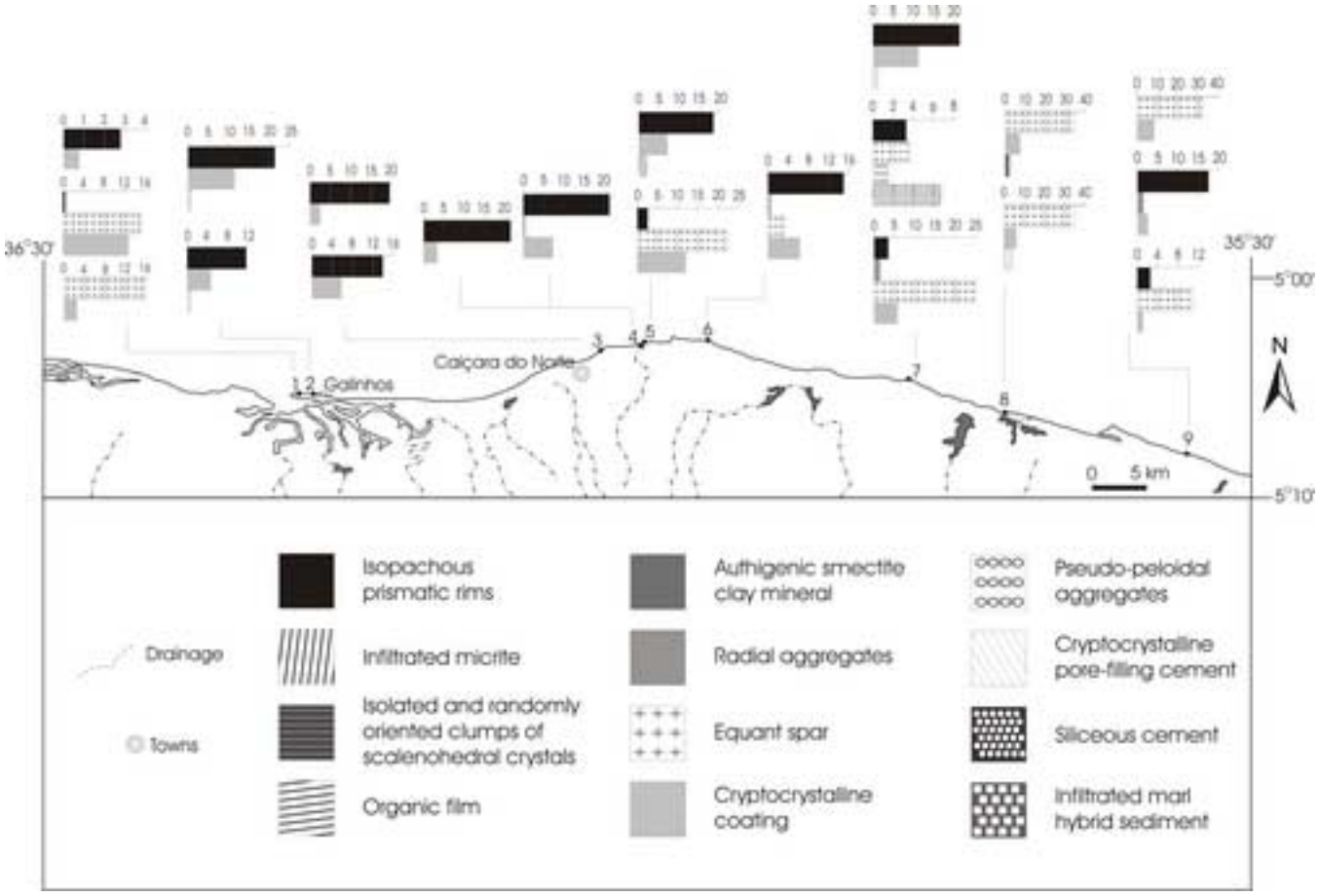

Figure 6A

Click here to download high resolution image

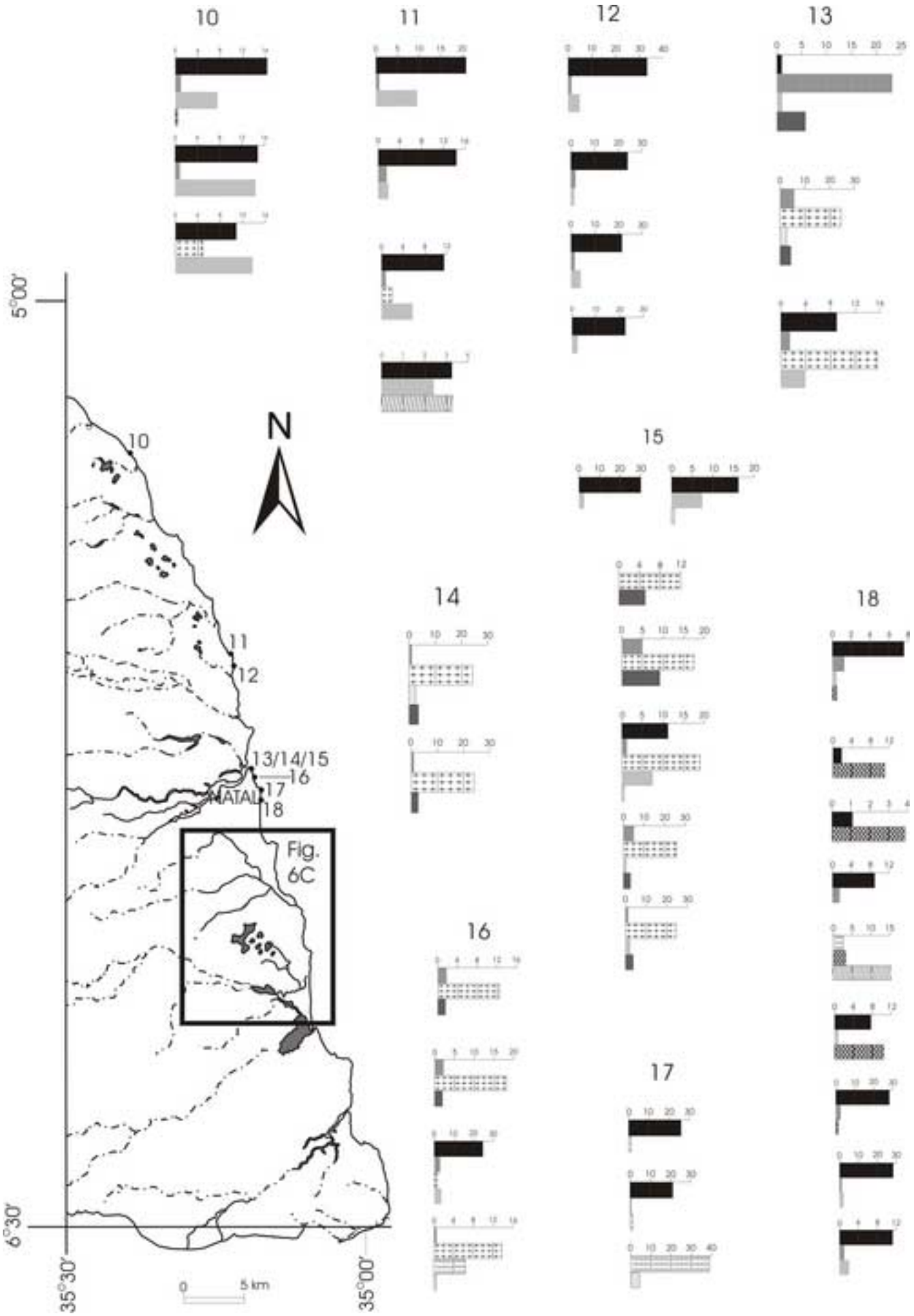

Figure 6B

Click here to download high resolution image

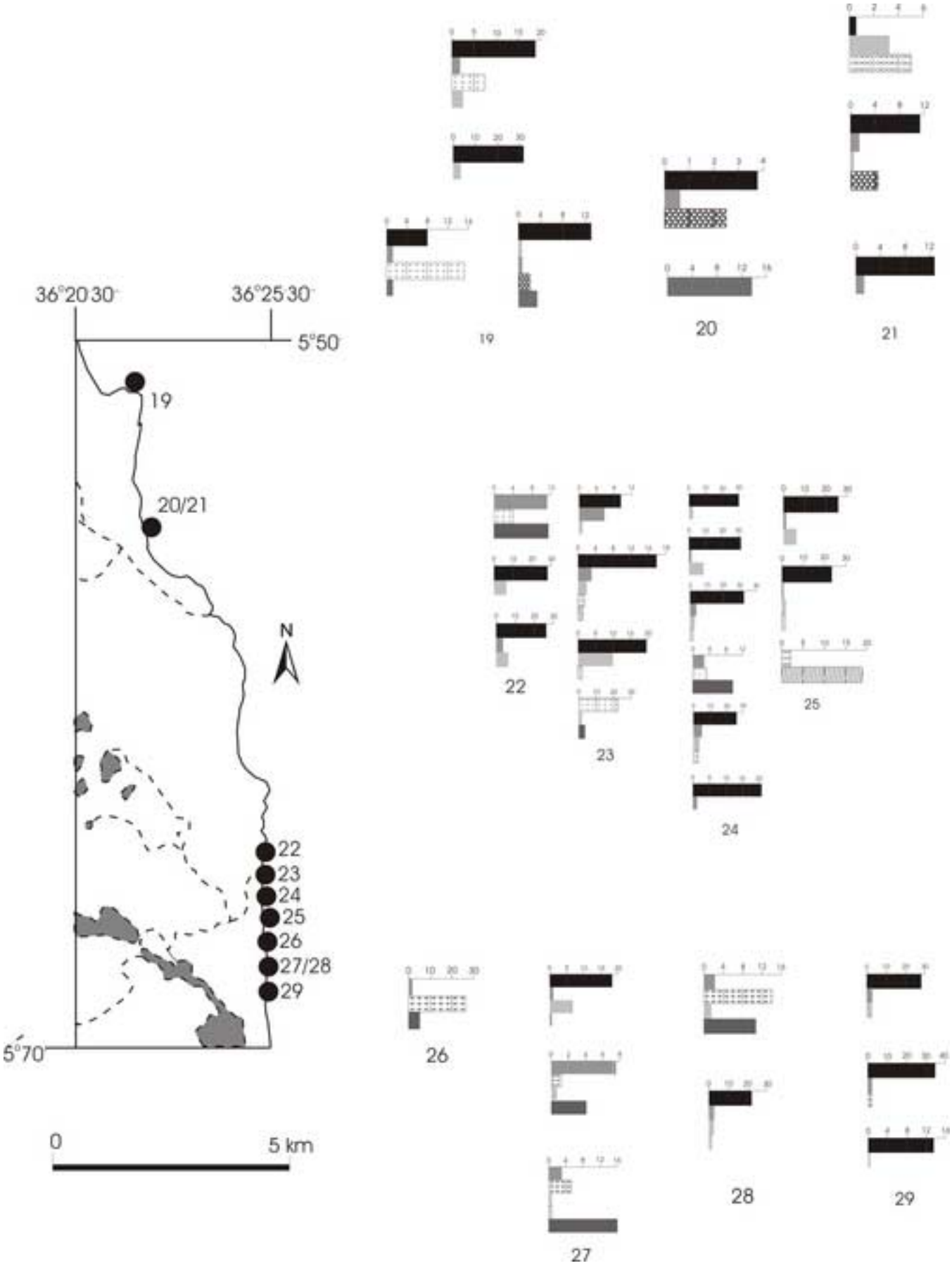

Figure 6C

Click here to download high resolution image

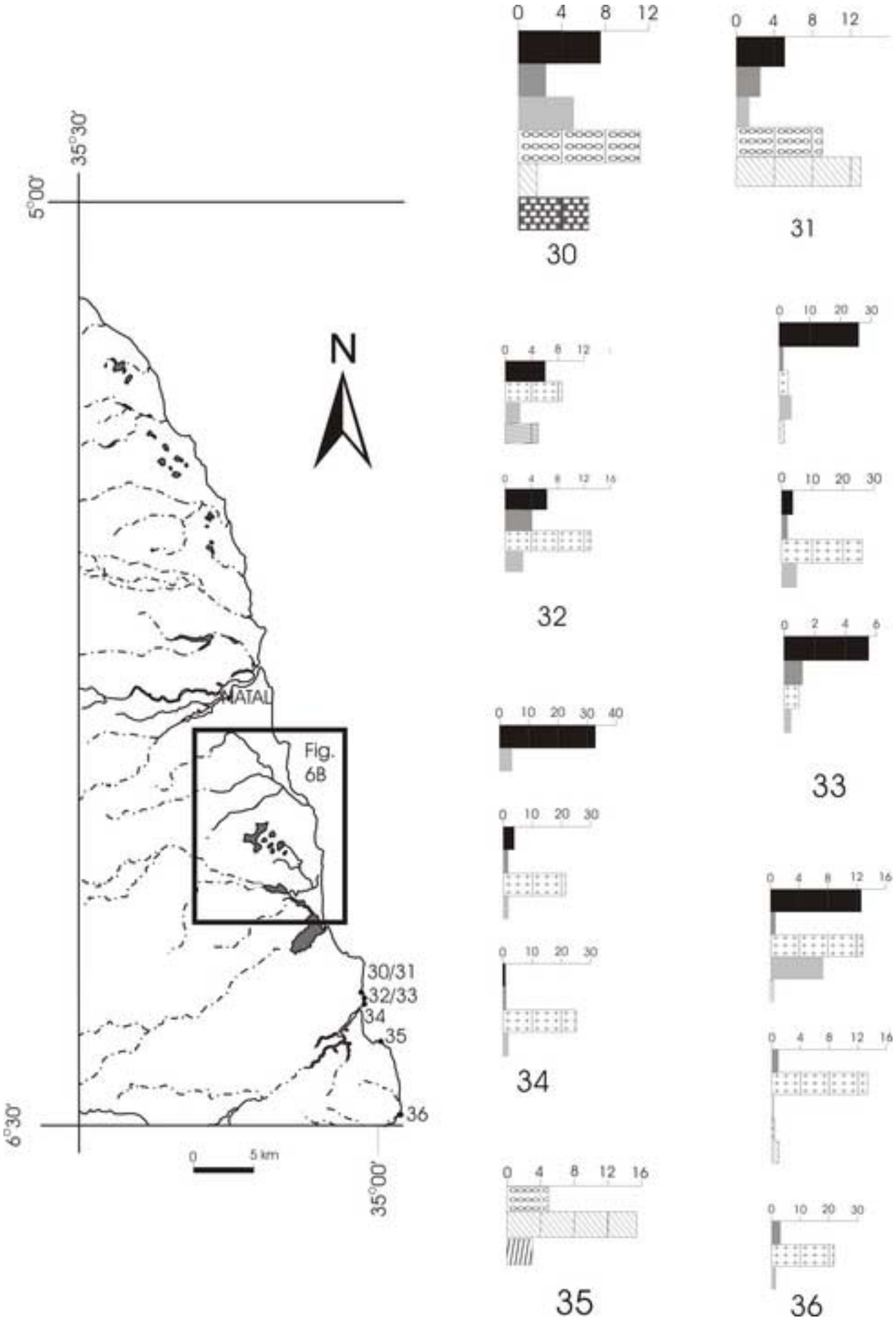

Figure 7

Click here to download high resolution image

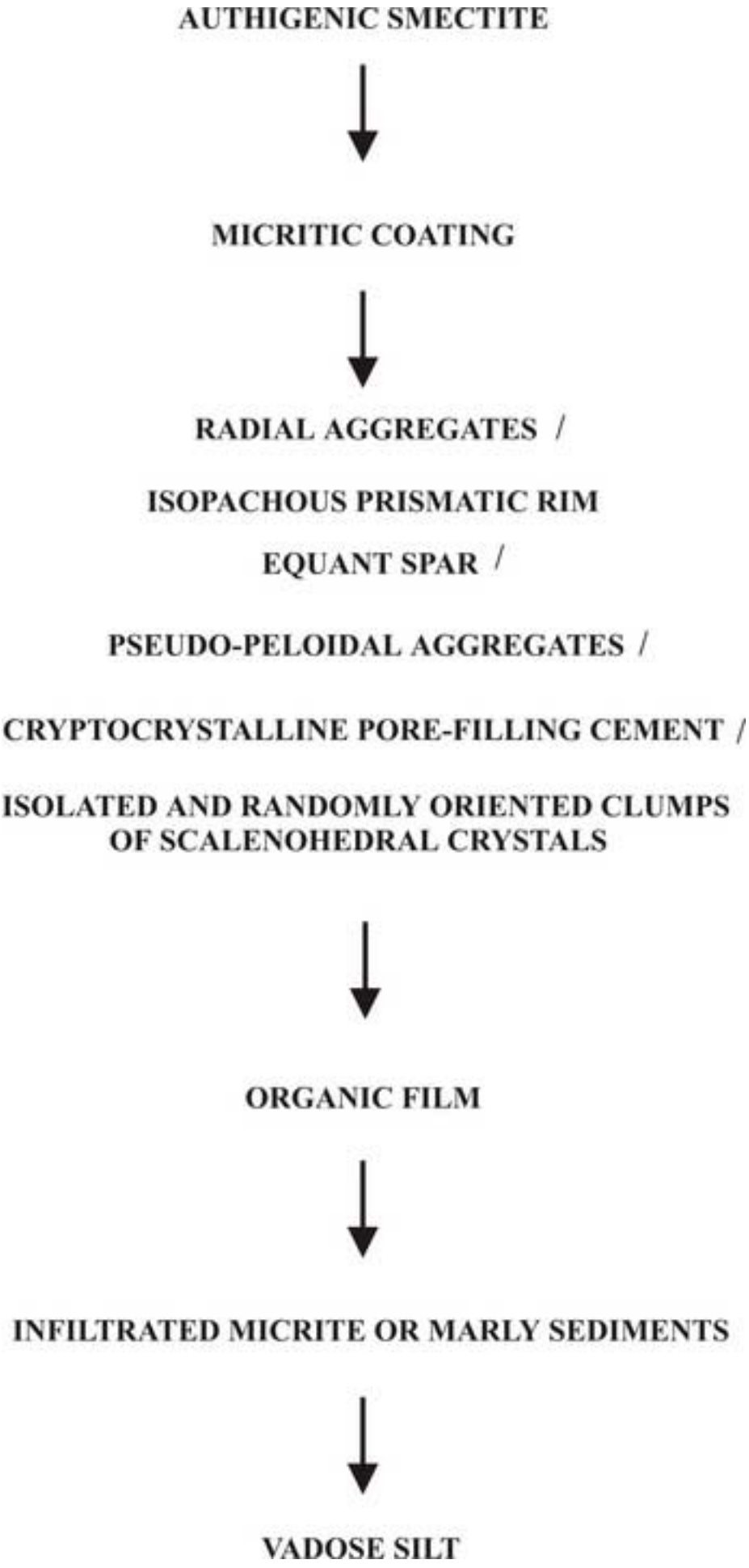

Figure 8A

Click here to download high resolution image

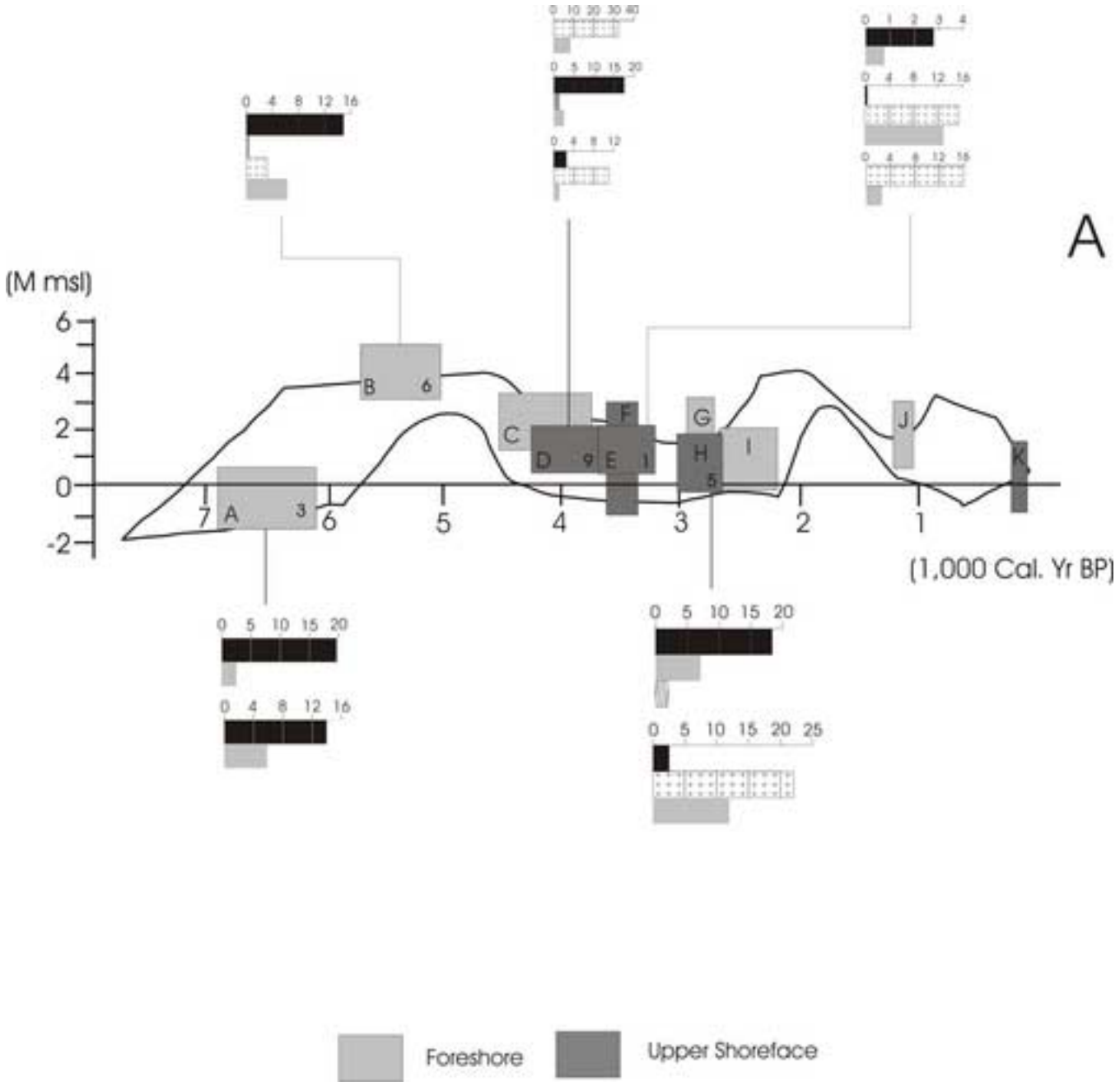

Figure 8B

Click here to download high resolution image

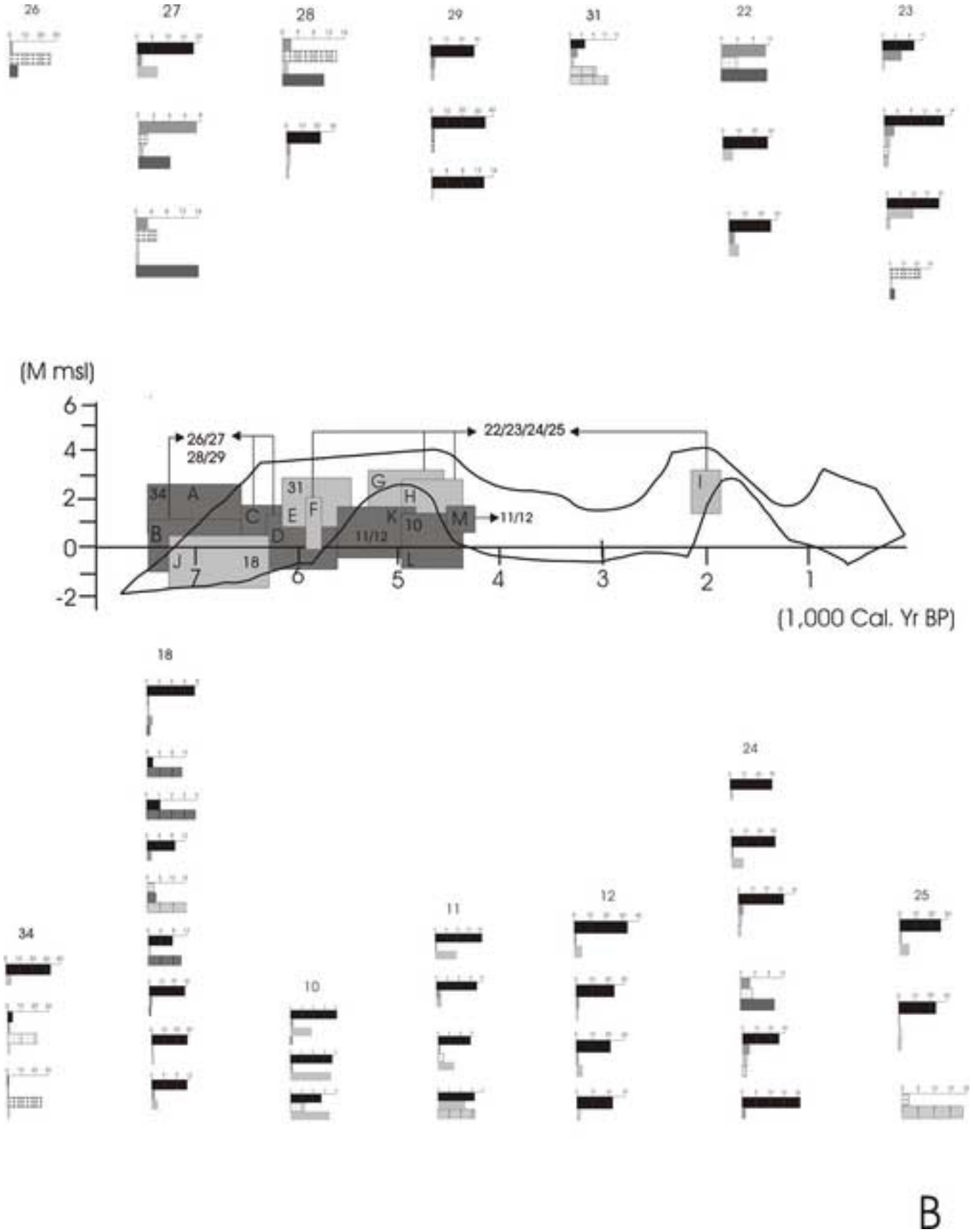

ARTIGO 3

ORIGIN OF HOLOCENE BEACHROCK CEMENTS IN NORTHEASTERN BRAZIL REVEALED BY CARBON AND OXYGEN ISOTOPES

ORIGIN OF HOLOCENE BEACHROCK CEMENTS IN NORTHEASTERN BRAZIL REVEALED BY CARBON AND OXYGEN ISOTOPES

Marcela Marques Vieira[a,d,*]

Alcides Nóbrega Sial[b]

João Marcelo Medina Ketzer[c]

Luiz Fernando De Ros[d]

[a] *Departamento de Geologia, Centro de Ciências Exatas e da Terra, Universidade Federal do Rio Grande do Norte, Natal, RN, Brazil; marcela@geologia.ufrn.br;* [*] *corresponding author*

[b] *NEG-LABISE, Departamento de Geologia, Universidade Federal de Pernambuco, Recife, PE, Brazi; ans@ufpe.br*

[c] *Pontifícia Universidade Católica do Rio Grande do Sul, Porto Alegre, RS, Brazil; jm@ketzer.com.br*

[d] *Programa de Pós-Graduação em Geociências, Universidade Federal do Rio Grande do Sul, Porto Alegre, RS, Brazil; lfderos@inf.ufrgs.br*

ABSTRACT

This study discusses carbon and oxygen isotopic data obtained from Holocene beachrock cements of Rio Grande do Norte State coast, northeastern Brazil. The cements are exclusively constituted of Mg-calcite, with isopachous prismatic rim, equant spar, cryptocrystalline coating or pore-filling, pseudo-peloidal, radial and scalenohedral habits. The $\delta^{18}O_{VPDB}$ values of most (93%) of the samples range from -1.79‰ to 0.54‰ and average 0.06‰ (corresponding to $\delta^{18}O_{SMOW}$ values of 31.41‰, 29.01‰ and 30.94‰, respectively), what is compatible with precipitation from evaporating marine waters. The maximum, minimum and average $\delta^{13}C_{VPDB}$ values of these cements are +3.57‰, 1.73‰ and +3.05‰, respectively. A few samples show strongly negative $\delta^{13}C_{VPDB}$ (-7.35‰ and -7.80‰) and $\delta^{18}O_{VPDB}$ values (-4.41‰ and -4.33‰, corresponding to 26.32‰ and 26.40‰ $\delta^{18}O_{SMOW}$), which probably reflect precipitation from mixed marine-meteoric waters, or recrystallization of marine cements by interaction with meteoric waters. The isotopically abnormal cements are, however, also constituted by Mg-calcite. The precipitation temperatures calculated for the samples with $\delta^{18}O_{VPDB}$ values around 0‰ range from 23.3ºC to 34.9ºC and average 25.7ºC, assuming a $\delta^{18}O_{VPDB}$ value +2‰ for precipitating marine fluids modified by evaporation. If a $\delta^{18}O_{VPDB}$ value of -2‰ is assumed for a mixed meteoric-marine precipitating fluid, temperatures of 27.5 and 27.9ºC are calculated for the abnormal cements, which are compatible to the surface temperatures of the area.

Introduction

Beachrocks are defined as friable to well-cemented rocks, formed in the intertidal zone in tropical or subtropical regions. They consist of sand or gravel (clastic and/or bioclastic) cemented with calcite (Bates and Jackson 1987). Despite the relatively extensive study of beachrocks (Ginsburg 1953; Alexandersson 1969; Taylor and Illing 1969; Chivas et al. 1986; Meyers 1987; Amieux et al. 1989; Holail and Rashed 1992; Kindler and Bain 1993), the specific processes responsible for their generation are still controversial. Mixing of marine and meteoric waters (Schmalz 1971; Moore 1973), evaporation (Taylor and Illing 1969; Moore and Billings 1971), CO_2 degassing of shallow groundwater (Hanor 1978; Binkley et al. 1980; Gischler and Lomando 1997) and direct or indirect activity of organisms (Webb et al. 1999; Neumeier 1999) have been most commonly pointed out as the processes responsible for beachrock cementation.

Branner (1904) was the first to recognize that several beachrock ledges encountered in northeastern Brazil were not coral reefs, but clastic shoreface sediments cemented by calcite, which he called “stone reefs.” Most of Holocene beachrocks occur nearly parallel to the shoreline, within the present-day intertidal zone. Few beachrocks are permanently submerged or emerged. Radiocarbon dating of beachrocks in northeastern Brazil show ages from *c*. 7460 to 110 cal. yr BP (calibrated years Before Present; Bezerra et al. 2003).

Previous studies (Oliveira et al. 1990; M. M. Vieira and L. F. De Ros, unpublished data) revealed that northeastern Brazil beachrocks show a wide variability in diagenetic processes, fabrics and textures, even on a centimeter scale. Such diagenetic processes include not only features generated by different types of calcite

cementation, but also mechanical infiltration of carbonate and hybrid siliciclastic/carbonate fine-grained sediments. Despite the variability of diagenetic process involved in the formation of these beachrocks, their mineralogical composition is surprisingly homogenenous (M. M. Vieira and L. F. De Ros, unpublished data). The aim of this paper is to unravel the complex origin and diagenetic evolution of Holocene beachrocks from northeastern Brazil based on the carbon and oxygen stable isotope values of their cements.

Previous Studies

Despite their great extension and influence on the present shoreline, the northeastern Brazil's beachrocks are still poorly studied. After the pioneer study by Branner (1904), the only works on beachrocks have emphasized their fossiliferous content (Maury 1934; Campos e Silva et al. 1964; Mendonça 1966), sedimentary structures (Bigarella 1975; Oliveira 1978 M. M. Vieira, L. F. De Ros and F.H.R. Bezerrra, unpublished data) and diagenetic evolution (Oliveira et al. 1990; M. M. Vieira and L. F. De Ros, unpublished data). More recently, beachrocks have been used for the reconstruction of the Holocene coastal evolution of Rio Grande do Norte State (Vianna et al. 1993; Amaral 1999; Caldas 2002) and for the investigation of neotectonic movements (Bezerra et al. 1998, 2003, 2004).

Only two previous studies have focused on the stable isotopic signature of the beachrocks. Bezerra et al. (2000) have applied stable isotope analyses to detect and reduce (or eliminate) the effects of contamination by old and young carbon when using radiocarbon dating method. In this case, the isotopic data were helpful to distinguish shells that had not been transported from continental shelf or from the continent. Caldas

(2002) performed isotopic measurements in carbonate cements from beachrocks with the purpose of recognizing the processes evolved during their formation and their post-depositional stabilization.

Geological Setting

The study area has a tropical climate with typical air temperatures of 30°C and average rainfall between 600 and 1,000 mm/year (Nimer 1989). Both northern and eastern coasts present a semidiurnal mesotidal regime in which the tide interval varies from 3.2 m to 0.8 m, along the northern coast, and from 2.7 m to 0.1 m, along the eastern coast. Throughout most of the year, southeasterly and northeasterly winds that blow towards the eastern and northern coast, respectively, result in longshore currents that flow to the north along the eastern coast, and to the west along the northern coast (Bittencourt et al. 2002).

The studied beachrocks were formed by cementation of Quaternary sediments deposited in two distinct geological provinces (fig. 1): the Potiguar Basin, with a NE-SW general direction, along the northern coast and part of the eastern coast; and the N-S trending Pernambuco-Paraíba-Rio Grande do Norte Basin, along the remaining eastern coast. The pre-Quaternary stratigraphy of the studied area includes sequences that outcrop exclusively along the northern coast (fig. 1): (1) Albian-Turonian siliciclastic rocks of Açu Formation; (2) Turonian-Campanian carbonate rocks of the Jandaíra Formation and silty/muddy sandstones of the Tibau Formation, (3) Campanian-Pliocene carbonate rocks and calciferous/fossiliferous sandstones of the Guamaré Formation and (4) Miocene-Pleistocene conglomerates, sandstones, and mudrocks of the alluvial

Barreiras Formation. The latter form cliffs along the entire coast of the state, which are in some places overlain by marine terraces formed during Late Pleistocene transgressions (220 ± 2 ka to 110 ± 10 ka BP; Barreto et al. 2002). Quaternary units also include beachrocks, dunes, peat, diatomite, and travertine, as well as Recent beach, aeolian, alluvial, and mangrove swamp sediments (Silva and Nogueira 1995).

Sampling and Methods

For the present study, Holocene beachrocks were sampled from different lithofacies exposed in 36 vertical sections described along several ledges located on the eastern and northern coasts of Rio Grande do Norte State (fig.1). The total rock thickness described at the various sites was approximately 41 m. Permanently submerged beachrock horizons were not sampled.

Blue resin impregnated thin sections were made from 112 samples and examined under conventional petrographic microscope. Samples were treated with Feigl's solution for the distinction between calcite and aragonite. Additional petrographic investigations included the examination of freshly broken, carbon-, and gold-coated samples in a SHIMADZU SSX-550 scanning electron microscope (accelerating voltage of 20kV), complemented by the determination of elemental composition of 24 samples by energy-dispersive spectroscopy (EDS).

A total of thirty bulk-rock samples, selected based on the large quantity of only one type of cement enclosing the grains, were assayed for $\delta^{13}C$ and $\delta^{18}O$ isotopic composition. To avoid bioclastic contamination, shell fragments were gently scrapped off the samples with the help of a binocular stereoscopic microscope. Between 20 and

50 mg of powdered samples were reacted with a 100% orthophosphoric acid, in a high vacuum line, at 25°C, for one day. The released CO_2 gas, after cryogenically cleaning, was analyzed in a double inlet, triple collector mass spectrometer (VG-ISOTECH SIRA II) at the Stable Isotopes Laboratory (LABISE – Federal University of Pernambuco) at Recife, Brazil. All the values are reported in parts per mil (‰) notation (δ) relative to the VPDB (Vienna Pee Dee Belemnite) international standard (Urey et al. 1951; Craig 1957). The $\delta^{18}O$ SMOW (Standard Mean Ocean Water) standard (Craig 1961) is also used.

Depositional Setting

The beachrocks are discontinuously exposed along the eastern and northern shorelines of Rio Grande do Norte State. Some of the ledges can be followed for up to 8 km parallel to the coast, while others are isolated bodies only a few meters long. They range in thickness from a few centimeters to nearly 3 m and in width from 2 to 50 m. Most of beachrock ledges occur close to present-day sea-level, within the intertidal zone; nevertheless, a few can be found 200 m inland from the beach and 5.7 km offshore (Vianna et al. 1993).

Most beachrocks gently dip seaward (<10°) and form tabular beds that are 5 to 150 cm thick and light-brown in color. Their lower and upper contacts with adjacent deposits are abrupt. The upper surface of the beachrocks is rarely smooth (Pereira and Bezerra 2001). Most of them present erosional features similar to those described in South African beachrocks and aeolianites (Miller and Mason 1994). *Spitzkarren*

(upward-pointing pyramids separated by clefts or solution basins) and near-circular depressions (solution basins and potholes) are the most common erosional features.

Beachrock ledges are composed mainly of monocrystalline quartz grains (average: 52% of bulk rock volume; maximum: 70%) and, to a lesser extent, of polycrystalline quartz grains (average: 8.9%; maximum: 75.5%), feldspar grains (mainly K-feldspar; average: 0.3%; maximum: 2.3%), heavy minerals (average: 0.3%; maximum: 9.6%), bioclasts (gastropods, bivalves, foraminiferans, red algae, and equinoids; average: 2.2%; maximum: 29.6%), and fragments of hematite-cemented sandstones of the Barreiras Formation (average: 0.9%; maximum: 41.4%). Reworked beachrock fragments of various sizes are commonly found, not only as intraclasts within the studied ledges (average: 0.02%; maximum: 3.6%), but also as slabs of up to 2.0 m long, which accumulate in the intertidal or shallow subtidal zones as a result of coastal erosion and onshore wave action. The average amounts of framework grains, cement, infiltrated materials and porosity are 64.6 (maximum: 80%), 24.6 (maximum: 38.8%), 1.4 (maximum: 18.7%) and 10% (maximum: 30.7%), respectively.

Textural characteristics and sedimentary structures were used to group the studied beachrocks into five lithofacies, named 1 to 5 (M. M. Vieira, L. F. De Ros and F. H. R. Bezerra, unpublished data): (1) Massive to Weakly Stratified Conglomerate; (2) Low-Angle Cross-Stratified Conglomerate and Sandstone; (3) Medium-Scale, Tabular-Planar and Trough Cross-Stratified Sandstone; (4) Bioturbated (Skolithos) Conglomeratic Sandstone; and (5) Massive Sandstone. A summary of the main characteristics of each lithofacies and their paleoenvironmental interpretation is shown in Table 1.

The textural characteristics and sedimentary structures identified in each of these lithofacies are diagnostic of deposition in the shallow marine coastal environment. Most of the studied beachrocks were deposited in the shoreface, represented by facies with

trough and tabular cross-stratification, occasionally with skolithos ichnofossils. Facies deposited in the foreshore zone, which are characterized by the presence of low-angle cross-stratification are subordinate, as revealed by the percentage of lithofacies in relation to the total thickness of rock described at the various sites (Table 1).

Long-term sea-level changes along the coast of Rio Grande do Norte State can be seen in the relative sea-level curve constructed by Bezerra et al. (2003). The rectangles shown in this curve represent the samples of the northern (fig. 2A) and eastern (fig. 2B) coasts. Radiocarbon ages used in the construction of both figures are displayed in tables 2 and 3. They were obtained from sea-level indicators found on beachrocks (death assemblage of bivalve shells, vermetid, and coral reef); peat deposits (bivalve shell in living position, fragments of wood, and oyster); Barreiras Formation outcrops (oyster and coral reef); and tidal flats (death assemblage of bivalve shells and oyster).

The diagram by Bezerra et al. (2003) for Rio Grande do Norte State indicates that deposition of beachrock sediments occurred during different stages, comprising rapid sea-level rise, high sea-level stands, sea-level drop, and low sea-level stands. Along the northern coast, the beach sediments were predominantly deposited between ~4140-2190 cal. yr BP, during sea-level falling and lowstand. Conversely, the beach deposits in the eastern coast were preferentially accumulated between ~7460-4240 cal. yr BP, during rapid sea-level rise and highstand. Beachrock exposure and erosion occurred during the present-day lowstand, if we take into account that the present relative sea-level is approximately 2 to 3m shorter than ~5000 cal. yr BP. The lack of relation between beachrock radiocarbon ages and a definite position along the sea-level curve is partly due to the dating of bioclasts not cements.

Carbonate Cementation

The studied beachrocks show a wide variability in diagenetic processes, fabrics and textures. High-Mg calcite is the only carbonate cement found, as revealed by energy dispersive spectroscopy (EDS) techniques. Mg-calcite occurs as: 1) cryptocrystalline coatings (fig. 3A); 2) isopachous prismatic rims (figs. 3B and 3C); 3) equant spar (Figs. 3D and 3E); 4) cryptocrystalline or micritic pore-filling (figs. 3F and 4A); 5) pseudo-peloidal aggregates (figs. 4B and 4C); 6) radial aggregates (figs. 4D and 4E); 7) isolated to randomly oriented clumps of scalenohedral crystals (fig.4F). The wide variability of the average content of each diagenetic material in the total studied beachrocks and in each of the defined lithofacies is shown on Table 4.

Cryptocrystalline (< 5μm) coatings are discontinuous, brown, and variable in thickness (maximum of 150 μm and average of 26 μm). They cover both siliciclastic and carbonate grains. Isopachous rims, which are composed of prismatic crystals standing perpendicular to grain surfaces, are the most common cement texture in the studied beachrocks. These elongate crystals average 7.8 μm in width (maximum value: 50 μm) and 48.3 μm in length (maximum value: 200 μm).

The equant spar cement consists of mainly anhedral to subhedral crystals that line or completely fill the pores. When the length/width ratio is about 1, their diameter averages 20 μm (maximum: 40 μm). When the length/width ratio is up to 2 (maximum value for equant crystals, cf. Harris et al. 1985), long and short dimensions average 36.4 μm (maximum: 64 μm) and 24.5 μm (maximum: 56 μm), respectively. Cryptocrystalline or micritic pore-filling cement consists of micritic (*sensu* Alexandersson 1972) calcite occurring as: (1) small, isolated irregular masses, forming patches between grains; and (2) abundant cement, which completely fill the pores.

The pseudo-peloidal aggregate texture consists of subspherical (average diameter: 36.9 μm; maximum: 120 μm) to elliptical particles (average long and short axis: 48.7 and 31.6 μm; respective maximum values: 88 and 75 μm). These pseudo-peloids are commonly surrounded by a mosaic of equant crystals or by rims of prismatic crystals. Radial aggregates commonly present nuclei formed by pseudo-peloidal sub-spherical bodies, isolated or arranged in groups of two or three (less frequent). These aggregates occur isolated or in groups, directly on the surfaces of the grains or on previous rim or coating cements. The crystals are predominantly rhombic-, and to a lesser extent, flat-terminated, averaging 11.4 μm in width (maximum: 40 μm) and 69.9 μm in length (maximum: 250 μm).

Scalenohedral crystals, isolated or arranged in randomly oriented clumps, project away from the surface of carbonate and siliciclastic grains. The scalenohedral crystals average 28.5 μm in width (maximum: 60 μm) and 89,3 μm in length (maximum: 200 μm).

Other Diagenetic Features

Other diagenetic features ocurring in the studied beachrocks include: 1) infiltrated marly sediment; 2) infiltrated micrite; 3) authigenic smectite; 3) chalcedony pore-filling cement; 4) vadose silt internal sediment; 5) organic films.

Mechanically infiltrated marl and micrite are commonly arranged as irregular aggregates and meniscus bridges (cf. Dunham 1971) between the grains. Angular silt-sized terrigenous grains (mainly quartz) and microfossils typical of deep waters (mostly coccoliths, planktonic and benthonic foraminifers) are frequently present.

Smectite clay minerals mixed, at certain points, with microcrystalline carbonate, iron oxide, titanium oxide or silica, as identified by EDS analyses, occurs as: (1), discontinuous envelopes around grains with variable thickness (maximum of 64 μm and average of 40 μm); (2) replacing grains along cleavages of feldspars, intercrystalline boundaries in polycrystalline quartz, and fractures; (3) pore-filling aggregates.

Vadose silt internal sediment consists of angular to sub-angular siliciclastic silt grains (mainly quartz), mixed with carbonate bioclasts and micrite. Organic films occur as brown envelopes, constant in thickness (average value: 16μm), that coat rims of bladed or fibrous crystals.

Carbon and Oxygen Isotopic Data

The isotopic values ($\delta^{13}C_{VPDB}$ and $\delta^{18}O_{VPDB}$) for 30 beachrock samples are shown in Table 5. The maximum, minimum and average $\delta^{13}C_{VPDB}$ values are +3.57‰, –7.80‰ and +2.34‰, respectively. The $\delta^{18}O_{VPDB}$ values range from –4.41‰ to 0.54‰ (average: –0.22‰). The plot of $\delta^{13}C_{VPDB}$ versus $\delta^{18}O_{VPDB}$ (fig. 5A) shows a significant positive correlation, with a coefficient of determination (R^2) of 0.8783.

The isotopic values are also analyzed considering the predominant type of cement present in the each sample. Equant spar has $\delta_{13CVPDB}$ values ranging from -7.80‰ to +3.53‰ (average: +1.57‰), $\delta^{18}O_{VPDB}$ values ranging from -4.41‰ to +0.54‰ (average: -0.56‰), and $\delta^{18}O_{SMOW}$ values ranging from +26.32‰ to +31.41‰ (average: +30.28‰). Samples in which isopachous prismatic rims predominate present $\delta^{13}C_{VPDB}$ values ranging from +1.73‰ to +3.57‰ (average: +2.95‰), $\delta^{18}O_{VPDB}$ values ranging from -0,44‰ to +0,43‰ (average: +2.95‰), and $\delta^{18}O_{SMOW}$ values ranging

from +30.40‰ to +31.30‰ (average: +30.94‰). Isolated to randomly oriented clumps of scalenohedral crystals show $\delta^{13}C_{VPDB}$ values ranging from +3.15‰ to +3.52‰ (average: +3.31‰), $\delta^{18}O_{VPDB}$ values ranging from +0.01‰ to +0,30‰ (average: +0.14‰), and $\delta^{18}O_{SMOW}$ values ranging from +30.87‰ to +31.17‰ (average: +31.0‰). The only sample analyzed in which pseudo-peloidal cement predominates shows $\delta^{13}C_{VPDB}$, $\delta^{18}O_{VPDB}$ and $\delta^{18}O_{SMOW}$ values of +2.89‰, 0‰ and +30.86‰, respectively.

Individual plots of the carbon and oxygen isotope values were constructed for the samples in which equant spar and isopachous prismatic rims predominate (figs. 5B and 5C, respectively). In both graphs, $\delta^{13}C_{VPDB}$ and $\delta^{18}O_{VPDB}$ are positively correlated, but the determination coefficients (R^2) differ widely ($R^2 = 0.8869$, in the case of equant spar, and $R^2 = 0.2454$, for the isopachous prismatic rims). As to the other two cements (isolated to randomly oriented clumps of scalenohedral crystals and pseudo-peloidal aggregates), the number of samples is insufficient to calculate R^2.

Discussion

The high-Mg calcite composition of the cements of the studied beachrocks suggests a significant influence of seawater in their precipitation (Longman 1980). This inference is corroborated by the distribution of the $\delta^{18}O$ and $\delta^{13}C$ isotopic data, which plot in the marine cement field (fig. 6). This includes all the samples with isopachous prismatic rims, scalenohedral crystals and pseudo-peloidal pore-filling, and most of the samples with equant spar.

The Z value calculated for the studied samples confirm a marine origin for the cements. This parameter has been proposed by Keith and Weber (1964) with the

purpose of distinguishing between marine and fresh-water limestones. It is applicable to Jurassic and younger samples and is given by the equation:

$$Z = a(\delta^{13}C + 50) + b(\delta^{18}O + 50)$$

where a and b are 2.048 and 0.498, respectively. Limestones with a Z value above 120 would be classified as marine, and those with Z below 120 as fresh-water types. The Z values obtained for the studied samples range from 109.17 to 134.69 (average: 131.98). Concerning each type of cement individually, the following Z ranges were obtained: 1) equant spar, 109.17 to 134.67 (average: 130.23); 2) prismatic isopachous rim, 130.74 to 134.69 (average: 133.38); and 3) isolated to randomly oriented clumps of scalenohedral crystals, 133.75 to 134.66 (average: 134.15). The single analyzed sample with pseudo-peloidal pore-filling has a Z value calculated to be 133.22.

Plots of Z versus $\delta^{18}O$ were constructed for the total studied samples (fig. 7A) and separately, for each type of cement (figs. 7B and 7C). In all the plots, the correlation of the variables are positive. The coefficient of determination (R^2) for all the samples is 0.8995. In the first two graphs, R^2 attains similar values for all the samples ($R^2 = 0.8995$) and for the samples with equant spar ($R^2 = 0.9067$). The only weakly positive correlation is for the samples in which prismatic isopachous rims predominate, which present a coefficient of determination of 0.3253. Statistically, this means that only 33% of the variation in Z is explained by the $\delta^{18}O$ variation.

The values of $\delta^{13}C$ also present a significant positive correlation with Z calculated for all the samples and each type of cement, as well (figs. 8A, 8B and 8C). The coefficients of determination are 0.9989 for all the studied samples (fig. 8A), 0.9989 for samples with equant spar (fig. 8B) and 0.9922 for samples with prismatic isopachous rims (fig. 8C).

The exclusive high-magnesium calcite composition of the studied beachrock cements provides a probable explanation for the observed isotopic homogeneity of the samples. Oxygen and carbon isotope compositions are different for coexisting aragonite and high-magnesium calcite cements in beachrocks distributed along the coast of Israel (Magaritz et al. 1979), as well as in Holocene carbonates from Enewetak, Bikini, Bermuda and Belize (González and Lohmann 1985). The small range of precipitation temperatures and the uniformity of water composition during the cementation of the analyzed samples have also certainly played a role in their uniform isotopic signature. Similarly, the oxygen isotopic homogeneity within the beachrock cements of Mediterranean and Red Sea is explained by Holail and Rashed (1992) as related to the absence of changes the in temperature or composition of precipitation waters during cement growth.

Two samples with predominance of equant spar cement (locations 7 and 8) show anomalous isotopic compositions. Their $\delta^{13}C_{VPDB}$ values (-7.35 and –7.80 ‰, respectively) are approximately 4 times lower than the limit (-2 ‰) established for modern marine carbonates (Magaritz 1983). In addition, these samples are depleted in ^{18}O relatively to the seawater ($\delta^{18}O_{VPDB}$ values of -4.41 and –4.33 ‰, respectively). This relative depletion of ^{18}O and ^{13}C suggests that the cements at locations 7 and 8 were precipitated under the influence of isotopically lighter meteoric waters or submitted to post-precipitation isotopic exchange with them. Both situations can be attributed to three causes: (a) freshwater influx during low tide; (b) contact with a freshwater lens; (c) dissolution by rainwater. The $\delta^{18}O$ *versus* $\delta^{13}C$ diagram (fig. 6) confirms these observations as both samples plot in close proximity to the Barbados meteoric cement field.

These lighter isotopic fractionation values are in contradiction with the high-Mg calcite composition of the cements in both samples, which suggests that their precipitation occurred from marine water. Friedman (1964) shows an increase in the lighter carbon (^{12}C) and oxygen isotopes (^{16}O) with an increase in low-magnesium calcite, in marine carbonates of Bermuda Islands subjected to fresh water alteration as a result of exposure to subaerial environment. An exception to this mineralogical trend are the metastable carbonates along the shoreline cliffs of these islands, which must have been exposed to fresh water during the Pleistocene, but have not been converted to low-magnesium calcite. This appears to be the case of both samples with anomalous isotopic compositions described above in which the cements have survived in the metastable phase, despite their interaction with meteoric water. No explanation was suggested for the anomalous samples from Bermuda. As to the beachrocks described in this study, which are holocenic, one probable explanation for the apparent contradiction in the mineralogical composition could be insufficient time for magnesium to be leached by fresh water or for high-magnesium calcite to be removed and low-magnesium calcite emplaced by solution-deposition. Another possibility could be the composition of the water, more specifically the degree of saturation. The absence of organic structures, such as microbial (bacteria or fungi) filaments and bodies, within the cements of the studied beachrocks, suggests that the mechanism behind beachrock cementation is essentially inorganic, most probably the evaporation of entrapped seawater in response to the dry climatic conditions (M. M. Vieira and L. F. De Ros, unpublished data). Under these extreme conditions, besides temperature, which is the critical factor in governing the precipitated Mg content of calcite, the absolute value of the Mg^{2+}/Ca^{2+} ratio can also play a role (Scoffin 1987).

Relative depletion of ^{18}O and ^{13}C due to contact with meteoric interstitial water have been described in beachrocks distributed along other coastal areas of northeastern Brazil by Assis et al. (1990), Chaves and Sial (1998), Guerra and Sial (2003) and Barros et al. (2003). Lowering of sea-level, uplift correlated to quaternary tectonic activity and interception of sea-level by phreatic level**,** near the surface, have been pointed out by these authors as the causes of the freshwater influx. Concerning the samples with strongly negative $\delta^{18}O$ values analyzed in this study, they were taken from two locations situated east of the Carnaubais Fault (fig. 1), which has been active during the Holocene (Bezerra and Vita-Finzi, 2000). The presence of uplifted blocks southeast of the fault, as attested by ^{14}C dating of a marine bivalve fauna in beachrocks and tidal flats, may have provided the access for the percolation of meteoric waters through the studied beachrocks.

The oxygen isotopic equilibrium fractionation between a carbonate and the water from which it has precipitated is a function of temperature. In this paper, the following thermometric equation by Irwin et al. (1977) was applied to estimate the ambient water temperature prevailing during the precipitation of beachrock cements:

$$T = 16.9 - 4.21(\delta_c - \delta_w) + 0.14\ (\delta_c - \delta_w)^2$$

where $(\delta_c - \delta_w)$ is the measured difference in $\delta^{18}O$ between calcite and water.

The precipitation temperatures calculated for the samples with $\delta^{18}O_{VPDB}$ values around 0‰ range from 23.3ºC to 34.9ºC and average 25.7ºC, assuming a $\delta^{18}O_{VPDB}$ value +2‰ for precipitating marine fluids modified by evaporation. If a $\delta^{18}O_{VPDB}$ value of -2‰ is assumed for a mixed meteoric-marine precipitating fluid, temperatures of 27.5 and 27.9ºC are calculated for the abnormal cements, which are compatible to the surface temperatures of the area.

As to each type of cement individually, the following temperature ranges were obtained:

1) equant spar: 23,3 a 34,9°C (mean value: 26,1°C);

2) prismatic isopachous rim: 23,8 a 28,0°C (mean value: 25,5°C);

3) isolated to randomly oriented clumps of scalenohedral crystals: 25,4 a 25,8°C (mean value: 25,6°C).

Concerning the single sample with pseudo-peloidal pore-filling, the temperature during its precipitation has been calculated to be 25,9°C.

Conclusions

1) The maximum, minimum and mean $\delta^{13}C_{VPDB}$ values for the beachrock samples analyzed are +3,57‰, –7,80‰ and +2,34‰, respectively. As to the $\delta^{18}O$ values, they range from –4,41‰ to 0,54‰ relative to VPDB standard (mean value: –0,22‰) and from 26,32‰ to 31,41‰ relative to SMOW standard (mean value: 30,64‰);

2) The $\delta^{18}O_{VPDB}$ values of most (93%) of the samples range from –1.79‰ to 0.54‰ and average 0.06‰(corresponding to $\delta^{18}O_{SMOW}$ values of 31.41‰, 29.01‰ and 30.94‰, respectively), what is compatible with precipitation from evaporating marine waters. The maximum, minimum and average $\delta^{13}C_{VPDB}$ values of these cements are +3.57‰, 1.73‰ and +3.05‰, respectively. This includes the greater part of samples with equant spar and all the ones with isopachous prismatic rims, isolated to randomly oriented clumps of scalenohedral crystals and pseudo-peloidal pore-filling. The exclusive high-magnesium calcite composition of the studied beachrock cements provides a probable

explanation for the observed isotopic homogeneity of the samples, as well as the uniformity of physiochemical parameters controlling beachrock cementation, attested by the small variety of paleotemperature values calculated for the studied samples;

4) A few samples show strongly negative $\delta^{13}C_{VPDB}$ (-7.35‰ and -7.80‰) and $\delta^{18}O_{VPDB}$ values (-4.41‰ and -4.33‰, corresponding to 26.32‰ and 26.40‰ $\delta^{18}O_{SMOW}$), which probably reflect precipitation from mixed marine-meteoric waters, or recrystallization of marine cements by interaction with meteoric waters. Uplift of blocks correlated to holocenic tectonic activity of the Carnaubais Fault may have provided the access for the percolation of meteoric waters through the studied beachrocks;

5) The precipitation temperatures calculated for the samples with $\delta^{18}O_{VPDB}$ values around 0‰ range from 23.3°C to 34.9°C and average 25.7ºC, assuming a $\delta^{18}O_{VPDB}$ value +2‰ for precipitating marine fluids modified by evaporation. If a $\delta^{18}O_{VPDB}$ value of -2‰ is assumed for a mixed meteoric-marine precipitating fluid, temperatures of 27.5 and 27.9ºC are calculated for the abnormal cements, which are compatible to the surface temperatures of the area.

ACKNOWLEDGMENTS

This work is part of M.M. Vieira doctorate research carried out at the Geosciences Institute of the Federal University of Rio Grande do Sul, Porto Alegre, Brazil. Partial support for this work was provided by a scholarship granted by CAPES, an organ of the Ministry of Education and Culture of Brazil. The authors thank the Stable Isotopes

Laboratory (LABISE – Federal University of Pernambuco) for performing the stable isotope analyses. Thanks are extended to the Geology Department of the Federal University of Rio Grande do Norte for providing equipment and support.

REFERENCES CITED

Alexandersson, T. 1969 Recent littoral and sublittoral high-Mg calcite lithification in the Mediterranean: Sedimentology. 12: 47-61.

Alexandersson, T. 1972. Intragranular growth of marine aragonite and Mg-calcite: evidence of precipitation from supersaturated seawater: Journal of Sedimentary Petrology. 42(2): 441-460.

Amaral, R. F. 1999. Contribuição ao estudo da evolução morfodinâmica do litoral oriental sul do Rio Grande do Norte, entre Ponta de Búzios e Baía Formosa. PhD Thesis, Universidade Federal do Rio Grande do Sul.

Amieux, P.; Bernier, P.; Dalongeville, R.; and Medwecki, V. 1989. Cathodoluminescence of carbonate-cemented Holocene beachrock from the Togo coastline (West Africa): an approach to early diagenesis: Sedimentary Geology. 65: 261-272.

Assis, H.M.B.; Amaral, R.F.; and Manso, V.A.V. 1990. Caracterização dos beachrocks do litoral sul de Pernambuco com base em evidências petrográficas e isotópicas. XXXVI Congresso Brasileiro de Geologia. Sociedade Brasileira de Geologia. 2: 635-646.

Barreto, A.M.F.; Bezerra, F.H.R.; Suguio, K.; Tatumi, S.H.; Yee, M.; Paiva, R.P.; and Munita, C. S. 2002. Late Pleistocene marine terrace deposits in northeastern Brazil:

sea-level change and tectonic implications: Palaeogeography, Palaeoclimatology, Palaeoecology. 179: 57-69.

Barros, S.D.S.; Sial, A.N.; and Cunha, I.S. 2003. Carbon and oxygen isotope composition of carbonate cements of beachrocks at the Lagoinha and Uruau beaches, State of Ceará, Northeastern Brazil. IV South American Symposium on Isotope Geology, Salvador (BA), Brazil. Short Papers. 1: 38-40.

Bates, R. L.; and Jackson, J. A. 1987. Glossary of Geology, 3rd Edition. American Geological Institute, Alexandria, VA.

Bezerra, F. H. R.; Lima-Filho, F. P.; Amaral, R. F.; Caldas, L. H. O.; and Costa-Neto, L. X. 1998. Holocene coastal tectonics. In: Stewart, I. S. & Vita-Finzi, C., eds. Coastal Tectonics. Geological Society, London. Special Publication 146. p. 279-293.

Bezerra, F.H.R.; and Vita-Finzi, C. 2000. How active is a passive margin? Paleoseismicity in northeastern Brazil. Geology. 28(7): 591-594.

Bezerra, F.H.R.; Vita-Finzi, C.; and Lima-Filho, F.P. 2000. The use of marine shells for radiocarbon dating of coastal deposits. Revista Brasileira de Geociências. 30(1): 211-213.

Bezerra, F.H.R.; Barreto, A.M.F.; and Suguio, K. 2003. Holocene sea-level history on the Rio Grande do Norte State coast, Brazil: Marine Geology. 196: 73-89.

Bezerra, F.H.R.; Amaral, R.F.; Lima-Filho, F.P.; Ferreira Jr., A.V.; Sena, E.S.; and Diniz, R.F. 2004. Beachrock fracturing in Brazil: Journal of Coastal Research, Special Issue. 42: 169-182.

Bigarella, J.J. 1975. Reef sandstones from northeastern Brazil (A survey on sedimentary structures): Anais da Academia Brasileira de Ciências. 47: 395-409.

Binkley, K.L.; Wilkinson, B.H.; and Owen, R.M. 1980. Vadose beachrock cementation along a southeastern Michigan Marl Lake: Journal of Sedimentary Petrology. 50(3): 953-962.

Bittencourt, A.C.S.P.; Martin, L.; Dominguez, J.M.L.; Silva, I.R.; and Sousa D.L. 2002. A significant longshore transport divergence zone at Northeastern Brazilian coast: implications on coastal Quaternary evolution. Anais da Academia Brasileira de Ciências. 74(3): 505-518.

Branner, J.C. 1904. The stone reefs of Brazil, their geological and geographical relations, with a chapter on the coral reefs. Museum of Comparative Zoology, Harvard College, Cambridge, Geological Series 7.

Caldas, L.H.O. 2002. Late Quaternary coastal evolution of the northern Rio Grande do Norte coast, NE Brazil. PhD Thesis, University of Kiel.

Campos E Silva, A.; Silva, D.D.; and Vasconcelos, M.D.T. 1964. Informação sobre a malacofauna dos beach rocks de Touros e São Bento do Norte: Arquivos do Instituto de Antropologia. 50(2): 79-90.

Chaves,N.S.; and Sial, A.N. 1998. Mixed oceanic and freshwater depositional conditions for beachrocks of northeast Brazil: evidence form carbon and oxygen isotopes: International Geology Review. 40: 748-754.

Chivas, A.; Chippell, J.; Polach, H.; Pillans, B.; and Flood, P. 1986. Radiocarbon evidence for the timing and rate of island development, beachrock formation and phosphatization at Lady Elliot Island, Queensland, Australia: Marine Geology. 69: 273-287.

Craig, H. 1957. Isotopic standards for carbon and oxygen correction factors for mass spectrometric analysis of carbon dioxide. Geochimica et Cosmochimica Acta. 12: 133-149.

Craig, H. 1961. Standard for reporting concentrations of deuterium and oxygen-18 in natural water: Science. 133: 1833-1834.

Dunham, R.J. 1971. Meniscus cement. In: Bricker, O.P., ed. Carbonate Cements. Johns Hopkins University Press, Baltimore, p. 297-300.

Epstein, S.; Buchsbaum, R.; Lowestan, H.A.; and Urey, H.C. 1953. Revised carbonate-water Folk, R.L., 1974, The natural history of crystalline calcium carbontate; effect of magnesium content and salinity: Journal of Sedimentary Petrology. 44: 40-53.

Friedman, G.M. 1964. Early diagenesis and lithification in carbonate sediments: Journal of Sedimentary Petrology. 34(4): 777-813.

Ginsburg, R.N. 1953. Beachrock in south Florida: Journal of Sedimentary Petrology. 23(2): 85-92.

Gischler, E.; and Lomando, A.J. 1997. Holocene cemented beach deposits in Belize: Sedimentary Geology. 110: 277-297.

González, L.A.; and Lohmann, K.C. 1985. Carbon and oxygen isotopic composition of Holocene reefal carbonates: Geology. 13: 811-814.

Guerra, N.C.; and Sial, A.N. 2003. Diagenetic model for beachrocks of the Alagoas State, Northeastern Brazil: isotopic and petrographic evidence. IV South American Symposium on Isotope Geology, Salvador (BA), Brazil, Short Papers. 1: 357-358.

Hanor, J. S. 1978. Precipitation of beach rock cements: mixing of marine and meteoric waters vs. CO_2 degassing: Journal of Sedimentary Petrology. 48: 489-502.

Harris, P.M.; Kendall, C.G. St. C.; and Lerche, I. 1985. Carbonate cementation: a brief review. In: N. Schneidermann and P.M. Harris, eds. Carbonate cements. SEPM Special Publication 36, p. 79–95.

Holail, H.; and Rashed, M. 1992. Stable isotopic composition of carbonate-cemented recent beachrock along the Mediterranean and Red Sea Coasts of Egypt: Marine Geology. 106: 141-148.

Irwin, H.; Curtis, C.; and Coleman, M. 1977. Isotopic evidence for source of diagenetic carbonates formed during burial of organic-rich sediments: Nature. 269: 209-213.

Keith, M.L.; and Weber, J.N. 1964. Carbon and oxygen isotopic composition of selected limestones and fossils: Geochimica et Cosmochimica Acta. 28: 1787-1816.

Kindler, P.; and Bain, R. J. 1993. Submerged upper Holocene beachrock on San Salvador island, Bahamas: implications for recent sea-level history: Geol. Rundsch. 82: 241-247.

Longman, M. W. 1980. Carbonate diagenetic textures from nearsurface diagenetic environments: AAPG Bulletin. 64: 461-487.

Magaritz, M. 1983. Carbon and oxygen isotope composition of Recent and ancient coated grains. In: Peryt, T.M., ed. Coated Grains. Springer-Verlag, Berlin, Heildelberg, p. 27-37.

Magaritz, M.; Gavish, E.; Bakler, N.; and Kafri, U. 1979. Carbon and oxygen isotope composition – indicators of cementation environment in Recent, Holocene, and Pleistocene sediments along the coast of Israel: Journal of Sedimentary Petrology. 49(2): 401-412.

Maury, C.J. 1934. Fossil invertebrata from northeastern Brazil: American Museum of Natural History Bulletin, V. LXVII, art. IV, p. 123-179, pl. IX-XIX. New York.

Mendonça, M.I. 1966. O recife de arenito de Tibau: Arquivos do Instituto de Antropologia, 2: 343-346.

Miller, W.R.; and Mason, T.R. 1994. Erosional features of coastal beachrock and eolianite outcrops in Natal and Zululand, South Africa: Journal of Coastal Research. 10(2): 394-414.

Meyers, J. H. 1987. Marine vadose beachrock cementation by criptocrystalline magnesian calcite – Maui, Hawaii: Journal of Sedimentary Petrology. 57: 558-570.

Moore Jr., C. H. 1973. Intertidal carbonate cementation, Grand Cayman, West Indies: Journal of Sedimentary Petrology. 43: 591-602.

Moore Jr., C.H.; and Billings, G.K. 1971. Preliminary model of beachrock cementation, Grand Cayman Island, B. W. I. In: Bricker, O. P., ed. Carbonate Cements. Johns Hopkins University, Studies in Geology 19, p. 40-43.

Neumeier, U. 1999. Experimental modelling of beachrock cementation under microbial influence: Sedimentary Geology. 126: 35-46.

Nimer, E. 1989. Climatologia do Brasil. Instituto Brasileiro de Geografia e Estatística, Departamento de Recursos Naturais e Ambientais, Rio de Janeiro.

Oliveira, M.I.M. 1978 Os recifes de Natal. MSc Thesis, Universidade Federal de Pernambuco, Recife.

Oliveira, M. I. M.; Bagnoli, E.; Farias, C. C.; Nogueira, A. M. B.; and Santiago, M. 1990. Considerações sobre a geometria, petrografia, sedimentologia, diagênese e idades dos *beachrocks* do Rio Grande do Norte. XXXVI Congresso Brasileiro de Geologia. Sociedade Brasileira de Geologia. 2: 621-634.

Pereira, M.M.V.; and Bezerra, F.H.R. 2001. Feições erosionais em beachrocks do Rio Grande do Norte. XIX Simpósio de Geologia do Nordeste. Sociedade Brasileira de Geologia, Núcleo Nordeste, Natal, RN, Brazil. Boletim de Resumos. 17: 77-78.

Schmalz, R.F. 1971, Formation of beachrock at Eniwetok Atoll. In: Bricker, O. P., ed. Carbonate Cements. Johns Hopkins University, Studies in Geology, 19, p. 17-24.

Scoffin, T.P. 1987. An introduction to carbonate sediments and rocks. Blackie, Glasgow and Hall, New York, 274p.

Silva, R.L.C.; and Nogueira, A.M.B. 1995. Estratigrafia da porção emersa da costa do Rio Grande do Norte. I Simpósio sobre Processos Sedimentares e Problemas Ambientais na Zona Costeira Nordeste do Brasil, Recife, Pernambuco, Brazil, p. 144 -147.

Taylor, J.C.M.; and Illing, L.V. 1969. Holocene intertidal calcium carbonate cementation, Qatar, Persian Gulf: Sedimentology. 12: 69-107.

Urey, H.C.; Lowestam, H.A.; Epstein, S.; and McKinney, C.R. 1951. Measurements of paleotemperatures and temperatures of the Upper Cretaceous of England, Denmark and the southeastern United States: Geological Society of American Bulletin. 62: 399-416.

Vianna, M.L.; Cabral, A.P.; and Gherardi, D.F.M. 1993. TM-Landsat imagery applied to study of the impact of global climate change on a tropical coastal environment during the last deglaciation: International Journal of Remote Sensing. 14 (14): 2971-2983.

Webb, G.E.; Jell, J.S.; and Baker, J.C. 1999. Cryptic intertidal microbialites in beachrock, Heron Island, Great Barrier Reef: implications for the origin of microcrystalline beachrock cement: Sedimentary Geology. 126: 317-334.

LEGENDS FOR ILLUSTRATIONS

Figure 1. Location and simplified geological map of the study area. Black dots and adjacent numbers correspond to the constructed vertical sections.

Figure 2. (A) ^{14}C samples of the E-W trending littoral zone distributed along the final sea-level curve for Rio Grande do Norte State (Bezerra et al. 2003). Radiocarbon data were obtained from shells with beachrocks as host rocks, and this final curve resulted from the intersection of two others obtained for the E-W and N-S coasts. Numbers in rectangles refer to the vertical sections used to interpret the predominant cementation zone (foreshore or shoreface) of the beachrock ledges from which the ^{14}C samples were obtained. Letters in rectangles correspond to the values found in Table 2; (B) ^{14}C samples of the N-S trending littoral zone. Letters in rectangles correspond to the values found in Table 3.

Figure 3. (A) Two generations of elongated crystal fringe separated by a micrite envelope. Thin section, crossed polarizers (XP), Location 3; (B) Regular and isopachous elongated crystal fringes coating monocrystalline quartz grains. Note perfectly perpendicular orientation of crystals with respect to grain surfaces and occurrence of two generations of elongated crystal fringe (right corner of the photograph). Thin section, XP, Location 24; (C) Same sample as the previous one seen through the scanning electron microscope; (D) Rims of stubby crystals lining the pore space between quartz grains. Thin section, uncrossed polarizers (//P), Location 34; (E) Euhedral Mg-calcite equant spar filling pore-space. Note the square-sided crystals. Scanning electron micrograph, Location 32; (F) Dark colored cryptocrystalline cement completely filling the pore space between quartz grains. Note the fine-grain size of the cement and lack of any clear sparry carbonate. Thin section, //P, Location 37.

Figure 4. (A) Cryptocrystalline pore-filling cement (on the right) around quartz grain. Notice the presence of irreducible porosity between both. Scanning electron micrograph, Location 12; (B) Quartz grains (on the left side and on the bottom right) coated by isopachous prismatic rims. Pseudo-peloidal micrite cement (centre of the photograph) has occupied the remaining pore space. Thin section, //P, Location 17. (C) Pseudo-peloidal micrite cement (centre of the photograph) filling the pore space between quartz grains. Scanning electron micrograph, Location 17; (D) Radial aggregates (centre of the photograph) arranged from pseudo-peloidal subspherical nuclei. Thin section, //P, Location 19; (E) Close-up view of radial fibers. Scanning electron micrograph, Location 23; (F) Close view of isolated scalenohedral crystal projecting away from the surface of a quartz grain. Thin section, //P, Location 15.

Figure 5. (A) Plot of $\delta^{13}C_{VPDB}$ versus $\delta^{18}O_{VPDB}$ obtained for all the samples; (B) Plot of $\delta^{13}C_{VPDB}$ versus $\delta^{18}O_{VPDB}$ obtained for the samples in which equant spar predominates; (C) Plot of $\delta^{13}C_{VPDB}$ versus $\delta^{18}O_{VPDB}$ for the samples in which isopachous prismatic rims predominate.

Figure 6. Oxygen and carbon-isotope plot (PDB, ‰) for beachrock samples from this study. See Table 5 for analyses. Adapted from Moore (1989).

Figure 7. (A) Plot of Z value versus $\delta^{18}O_{VPDB}$ obtained for all the samples; (B) Plot of Z value versus $\delta^{18}O_{VPDB}$ obtained for the samples in which equant spar predominates; (C) Plot of Z value versus $\delta^{18}O_{VPDB}$ obtained for the samples in which isopachous prismatic rims predominate.

Figure 8. (A) Plot of Z value versus $\delta^{13}C_{VPDB}$ obtained for all the samples; (B) Plot of Z value versus $\delta^{13}C_{VPDB}$ obtained for the samples in which equant spar predominates; (C) Plot of Z value versus $\delta^{13}C_{VPDB}$ obtained for the samples in which isopachous prismatic rims predominate.

Table 1. Summary of the main characteristics of each lithofacies and paleoenvironmental interpretation (M. M. Vieira, L. F. De Ros and F.H.R. Bezerra, unpublished data).

Lithofacies	**Description**	**Interpretation**	**% relative to total thickness**
1	Massive to weakly seaward-dipping stratified, poorly to very poorly sorted, sharp-based conglomerates	Transgressive lag deposit or traction carpet deposit	5%
2	Poorly to well-sorted sandy conglomerate to sandstone with a seaward-dipping low-angle X-stratification	Beachface wave swash or backswash or backwash step vortex	32%
3	Very poorly- to well-sorted sandstones with small- to medium-scale trough cross-stratification with paleocurrents parallel to coastline	Bedload transport by longshore currents on the upper shoreface zone	51%
4	Poorly to very poorly sorted sandstones with numerous vertical tubes densely clustered together	Shelter burrowed on the upper shoreface zone under high wave and current energy	2%
5	Massive poorly to well-sorted sandstones	Higher degree of alteration at the base and top of the outcrops	10%

Table 2. Carbon 14 ages shown in figure 2A. Sample source: (1) Bezerra et al. (1998; 2003); (2), (3), (4) and (5) Stattegger et al. (2004). These samples were taken from the same beachrock ledges as samples H, A, E and B, respectively, but were not used in the construction of the time-depth diagrams. Abbreviations: msl=mean sea level, mssl=present maximum spring tide sea level, dab= death assemblage of bivalve shells.

Sample	**Height (m above msl)**	**Sea-level indicator**	**Calibrated age (yr BP at 2σ)**
A[(1)]	-0.5 ± 1.0	dab	6900-6080
B[(1)]	3.9 ± 1.0	dab	5730-5060
C[(1)]	2.1 ± 1.0	dab	4140-3760
D[(1)]	1.2 ± 1.0	dab	4240-3640
E[(1)]	1.1 ± 1.0	dab	3680-3210
F[(1)]	2.0 ± 1.0	dab	3640-3330
G[(1)]	2.1 ± 1.0	dab	2960-2720
H[(1)]	0.6 ± 1.0	dab	3040-2690
I[(1)]	0.6 ± 1.0	dab	2680-2190
J[(1)]	1.8 ± 1.0	dab	1250-1060
K[(1)]	0.2 ± 1.0	dab	160-60
KIA12334[(2)]	0.2	dab	2960-2900
KIA12336[(3)]	-2.5	dab	6830-6750
KIA 14750[(4)]	-1.6	dab	3235-3165
KIA14751[(5)]	+1.0	dab	5945-5875

Table 3: Carbon 14 ages shown in figure 2B. Sample source: (1) Bezerra et al. (1998; 2003); (2) Oliveira et al. (1990). This sample was taken from the same beachrock ledge as samples G and H; (3) Oliveira et al. (1990). These samples were taken from the same beachrock ledge as samples B, C and D. Samples (2) and (3) were not used in the construction of the time-depth diagrams. Abbreviations: msl=mean sea level, dab= death assemblage of bivalve shells.

Sample	Height (m above msl)	Sea-level indicator	Calibrated age (yr BP at 2σ)
A[(1)]	1.5 ± 1.0	dab	7460-6550
B[(1)]	0.0 ± 1.0	dab	7460-6550
C[(1)]	0.7 ± 1.0	dab	6730-5980
D[(1)]	0.2 ± 1.0	dab	6340-5600
E[(1)]	1.7 ± 1.0	dab	6170-5440
F[(1)]	0.8 ± 1.0	dab	5950-5700
G[(1)]	2.2 ± 1.0	dab	5310-4560
H[(1)]	1.8 ± 1.0	dab	4970-4380
I[(1)]	2.1 ± 1.0	dab	2160-1920
J[(1)]	-0.7 ± 1.0	dab	7240-6300
K[(1)]	0.5 ± 1.0	dab	5600-4840
L[(1)]	0.1 ± 1.0	dab	4990-4350
M[(1)]	1.0 ± 0.5	dab	4540-4240
P14[(2)]	+3.0	dab	5310-4640
P20[(3)]	+1.0-2.0	dab	6690-6680
P21[(3)]	+1.0-2.0	dab	6600-6170
P29[(3)]	+3.00	dab	5050-4550

Tabela 4. Average and maximum content of diagenetic material in the studied beachrocks.

Lithofacies	**1**	**2**	**3**	**4**	**5**	**Max**	**Aver**
Isopachous prismatic rims	4.5	13.2	10.3	18.1	14.9	33.6	12.2
Radial aggregates	0.4	1.0	1.9	0.0	1.8	22.8	1.0
Equant spar	4.2	5.2	8.6	0.0	4.2	34.4	4.4
Cryptocrystalline coatings	1.4	2.9	3.3	7.1	3.9	14.5	3.7
Pseudo-peloidal aggregates	5.2	0.4	0.03	0.0	1.1	38.8	1.3
Cryptocrystalline pore-fill	2.0	0.8	0.1	0.0	0.2	15.7	0.6
Infiltrate marl hybrid sediment	2.4	0.8	0.09	0.0	0.5	10.9	0.8
Infiltrated micrite	0.6	0.9	0.09	1.6	0.0	18.7	0.6
Scalenohedral crystals	0.0	0.9	1.6	0.0	0.4	16.3	0.6
Organic films	0.0	0.0	0.1	0.0	0.0	5.0	0.02
Authigenic smectite	3.1	0.01	0.0	0.0	0.0	13.5	0.6
Siliceous cement	0.05	0.0	0.0	0.0	0.0	0.6	0.01

Table 5 - Isotopic values and calculated precipitation temperatures of diagenetic carbonate cements

Sample	Cement	Mineralogy	$\delta^{13}C$(VPDB)	$\delta^{18}O$(SMOW)	$\delta^{18}O$(VPDB)	$\delta^{18}O$water	T (°C)	Z value
1	Isop Prism Rim	Mg-calcite	1,73	30,64	-0,21	2,0	26,9	130,74
2	Isop Prism Rim	Mg-calcite	1,83	30,53	-0,32	2,0	27,4	130,89
4	Isop Prism Rim	Mg-calcite	2,58	31,3	-0,43	2,0	28,0	132,79
8	Equant Spar	Mg-calcite	2,08	30,78	-0,08	2,0	26,3	131,52
12	Isop Prism Rim	Mg-calcite	3,55	31,12	0,25	2,0	24,7	134,69
13	Equant Spar	Mg-calcite	3,43	31,22	0,35	2,0	24,2	134,49
13	Equant Spar	Mg.calcite	3,38	31,16	0,29	2,0	24,5	134,36
14	Equant Spar	Mg-calcite	3,32	31,22	0,35	2,0	24,2	134,27
15	Equant Spar	Mg-calcite	3,24	29,01	-1,79	2,0	34,9	133,05
15	Equant Spar	Mg-calcite	3,53	31,15	-0,28	2,0	27,2	134,67
16	Equant Spar	Mg-calcite	3,25	31,37	0,49	2,0	23,6	134,2
16	Equant Spar	Mg-calcite	3,12	31,41	0,54	2,0	23,3	133,96
17	Pseudo-Pel Aggr	Mg-calcite	2,89	30,86	0	2,0	25,9	133,22
21	Isop Prism Rim	Mg-calcite	3,06	30,4	0,44	2,0	23,8	133,35
22	Isop Prism Rim	Mg-calcite	3,05	31,01	0,15	2,0	25,2	133,62
22	Isop Prism Rim	Mg-calcite	3,42	31,15	0,28	2,0	24,6	134,44
23	Isop Prism Rim	Mg-calcite	3,25	31,22	0,35	2,0	24,2	134,13
24	Isop Prism Rim	Mg-calcite	3,57	30,87	0,01	2,0	25,8	134,61
24	Scalen Crystals	Mg-calcite	3,27	30,97	0,11	2,0	25,4	134,05
24	Isop Prism Rim	Mg-calcite	3,03	30,94	0,08	2,0	25,5	133,55
27	Isop Prism Rim	Mg-calcite	3,2	31,13	0,26	2,0	24,6	133,98
27	Scalen Crystals	Mg-calcite	3,52	31,17	0,3	2,0	25,7	134,66
28	Scalen Crystals	Mg-calcite	3,15	30,87	0,01	2,0	25,8	133,75
29	Isop Prism Rim	Mg-calcite	3,12	30,97	0,1	2,0	25,4	133,74
32	Equant Spar	Mg-calcite	3,07	31,21	0,34	2,0	24,3	133,76
32	Equant Spar	Mg-calcite	3,47	31,04	0,17	2,0	25,1	134,49
34	Equant Spar	Mg-calcite	2,72	30,92	0,06	2,0	25,6	132,9
34	Equant Spar	Mg-calcite	2,48	30,74	-0,11	2,0	26,4	132,33
MAX	"Normal Marine"	Mg-calcite	3,57	31,41	0,54	2,0	34,9	134,69
MIN	"Normal Marine"	Mg-calcite	1,73	29,01	-1,79	2,0	23,3	130,74
AVER	"Normal Marine"	Mg-calcite	3,05	30,94	0,06	2,0	25,7	133,58
7	Abnormal Equant Spar	Mg-calcite	-7,35	26,32	-4,41	-2,0	27,9	110,05
8	Abnormal Equant Spar	Mg-calcite	-7,8	26,4	-4,33	-2,0	27,5	109,17
MAX	Abnormal Equant Spar	Mg-calcite	-7,35	26,4	-4,33	-2,0	27,9	110,05
MIN	Abnormal Equant Spar	Mg-calcite	-7,8	26,32	-4,41	-2,0	27,5	109,17
AVER	Abnormal Equant Spar	Mg-calcite	-7,58	26,36	-4,37	-2,0	27,7	109,61

Figure 1

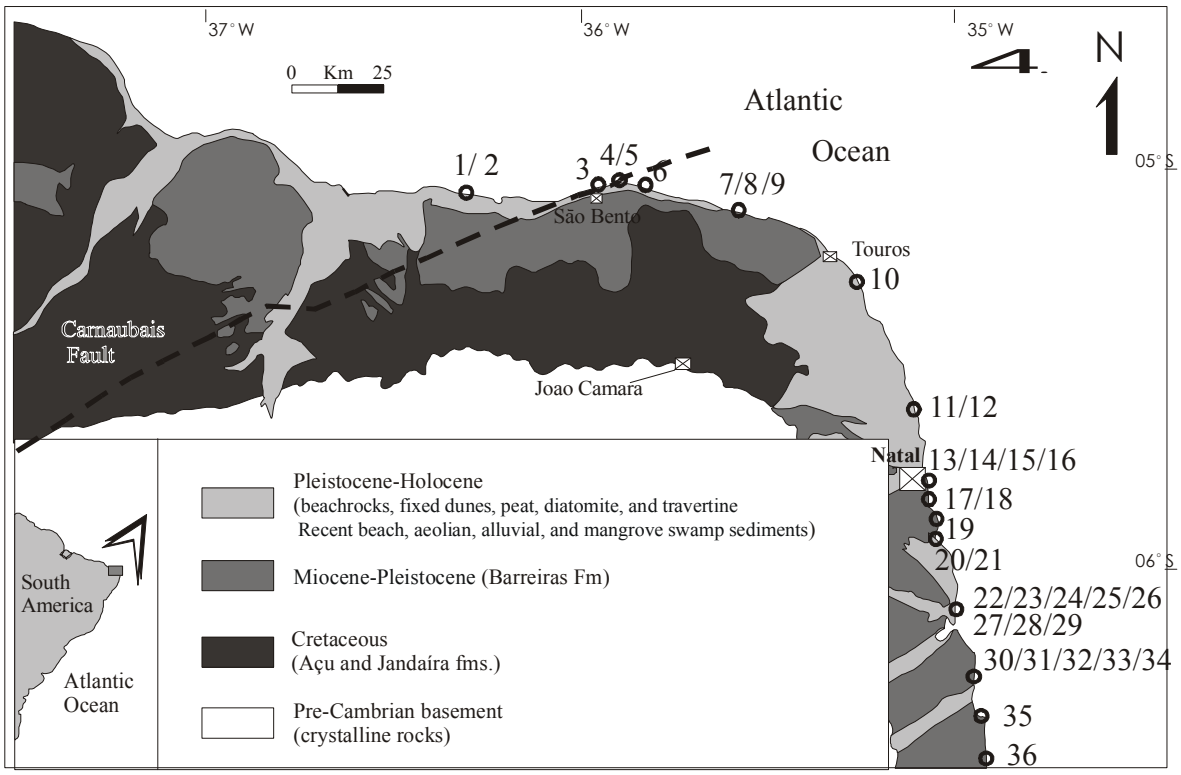
37° W
36° W
35° W
N
0 Km 25
Atlantic
Ocean
1/ 2
3
4/5
6
7/8/9
São Bento
Touros
10
Carnaubais
Fault
Joao Camara
11/12
Natal
13/14/15/16
17/18
19
20/21
22/23/24/25/26
27/28/29
30/31/32/33/34
35
36
05° S
06° S
Pleistocene-Holocene
(beachrocks, fixed dunes, peat, diatomite, and travertine
Recent beach, aeolian, alluvial, and mangrove swamp sediments)
Miocene-Pleistocene (Barreiras Fm)
Cretaceous
(Açu and Jandaíra fms.)
Pre-Cambrian basement
(crystalline rocks)
South
America
Atlantic
Ocean

Figure 2

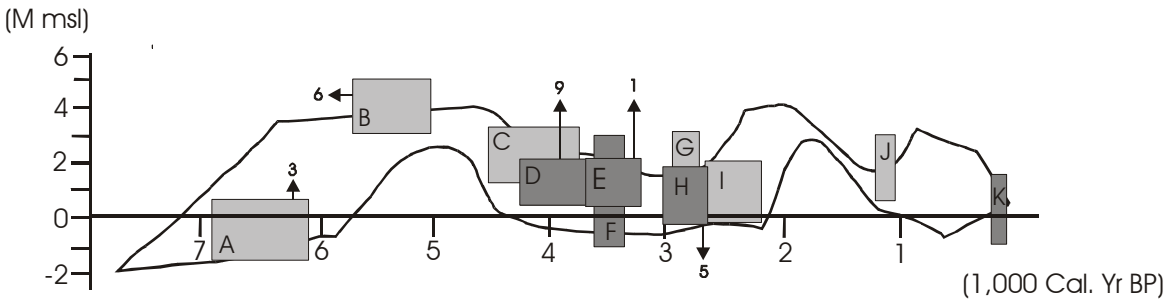

A

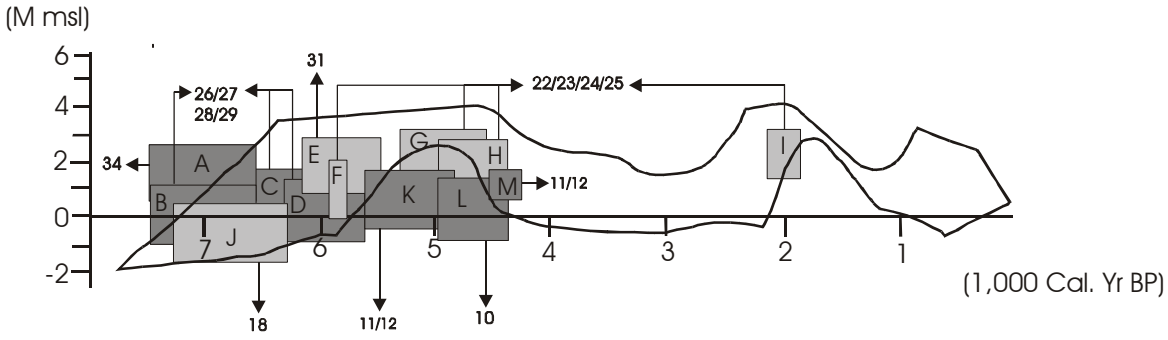

B

Upper and lower foreshore

Upper Shoreface

Figure 3

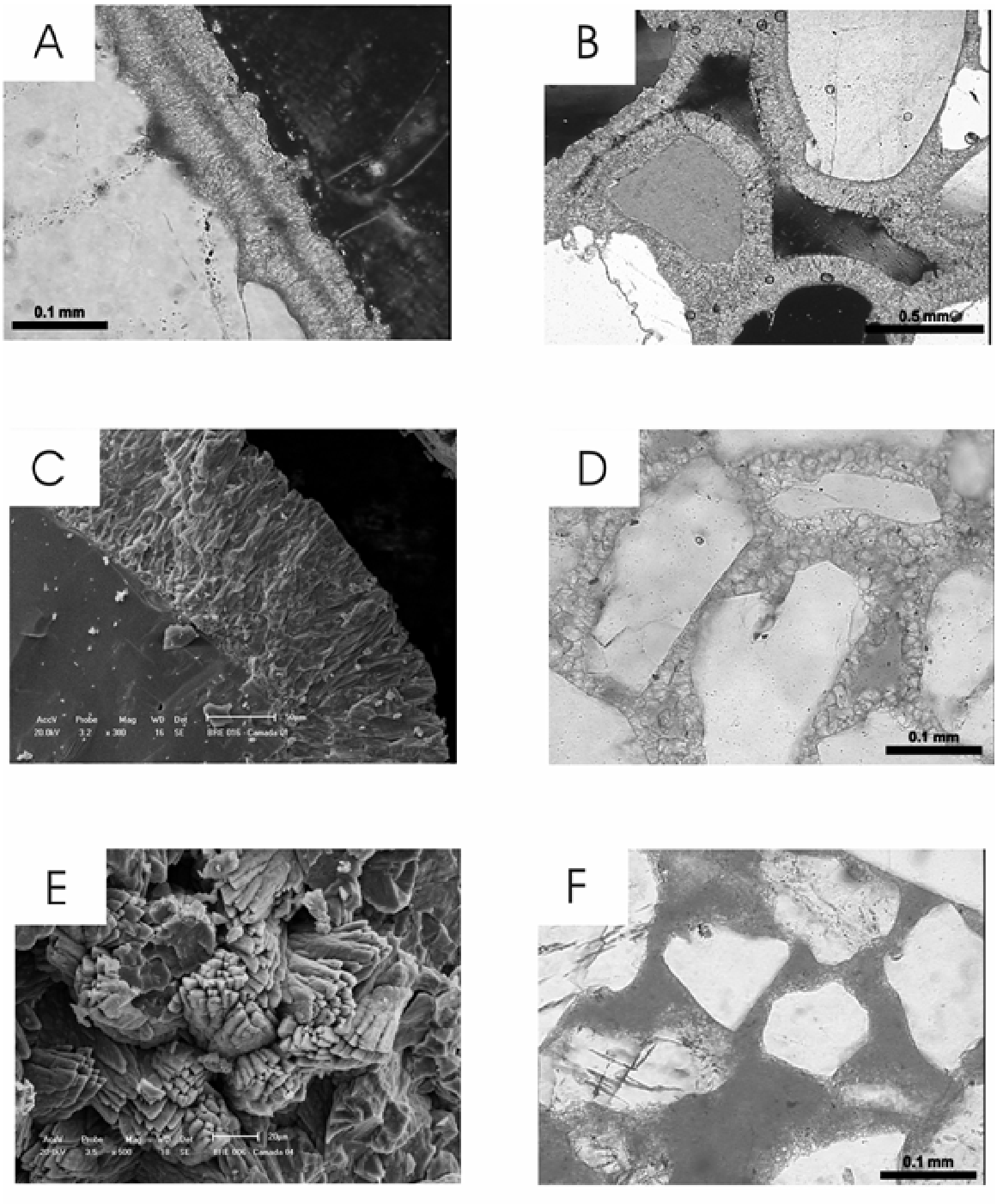

Figure 4

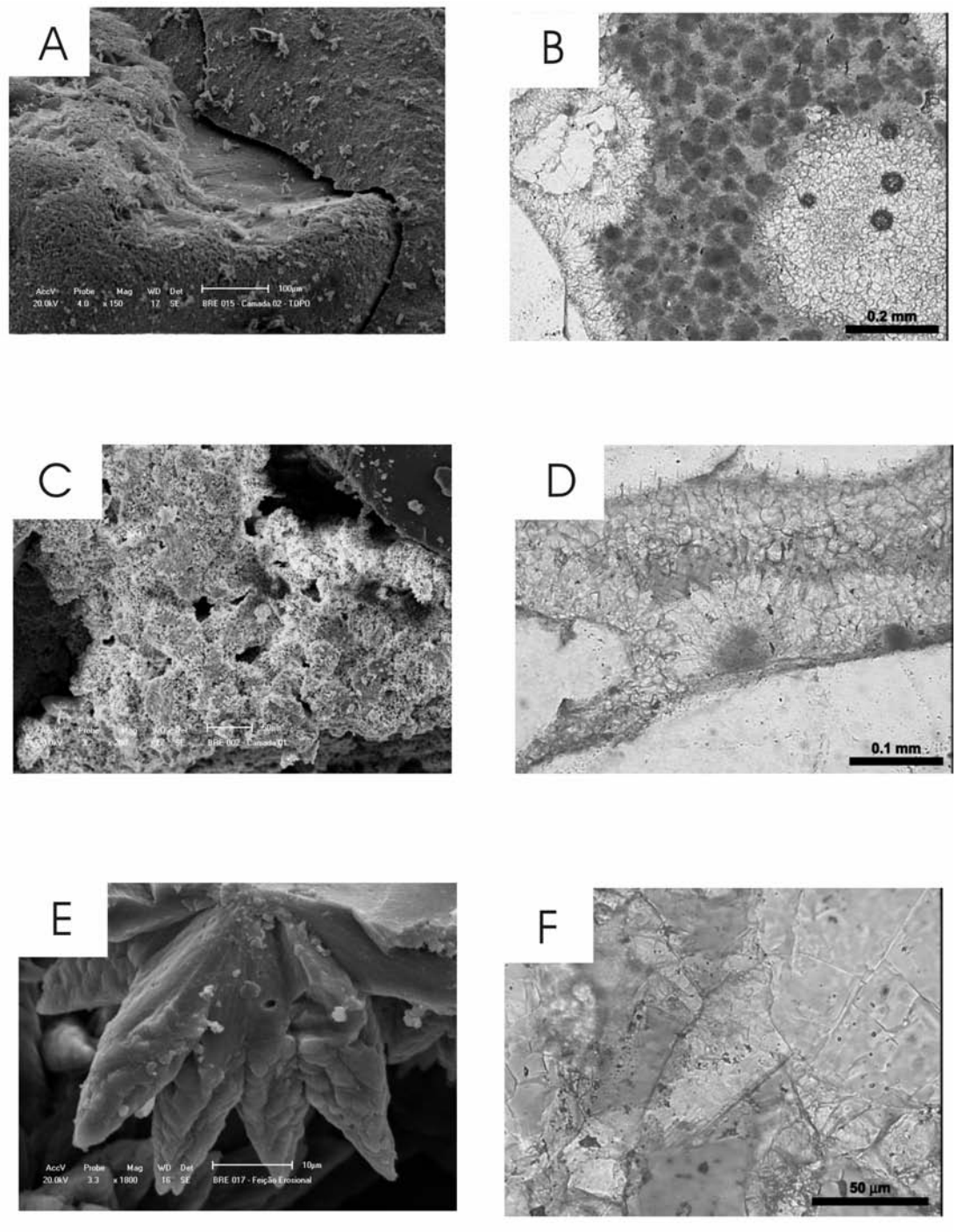

Figure 5

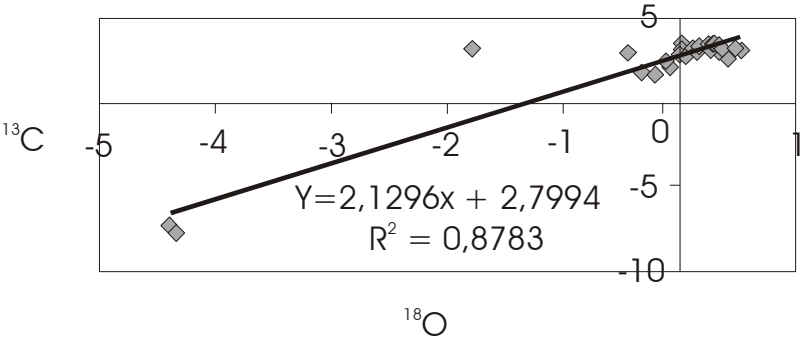
5
0
-5
-10
-5
-4
-3
-2
-1
0
1
Y=2,1296x + 2,7994
R² = 0,8783
13C
18O

A

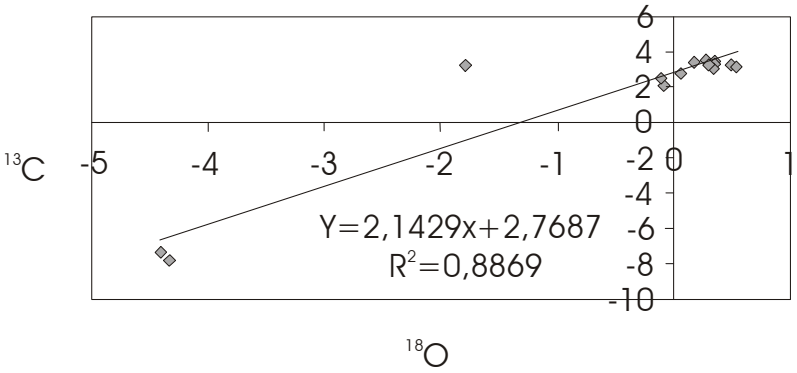
6
4
2
0
-2
-4
-6
-8
-10
-5
-4
-3
-2
-1
0
1
Y=2,1429x+2,7687
R²=0,8869
13C
18O

B

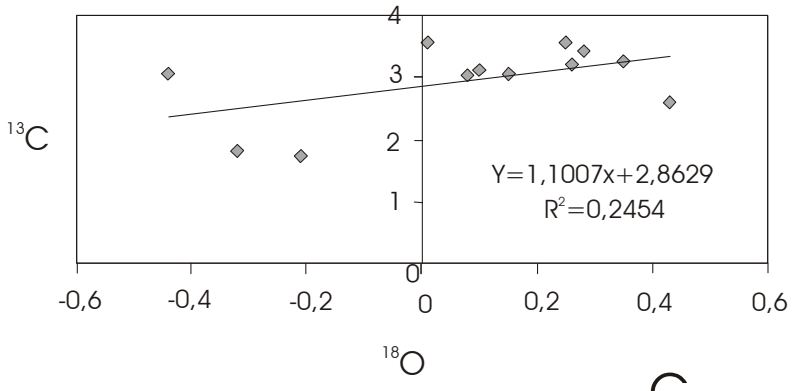
4
3
2
1
0
-0,6
-0,4
-0,2
0
0,2
0,4
0,6
Y=1,1007x+2,8629
R²=0,2454
13C
18O

C

Figure 6

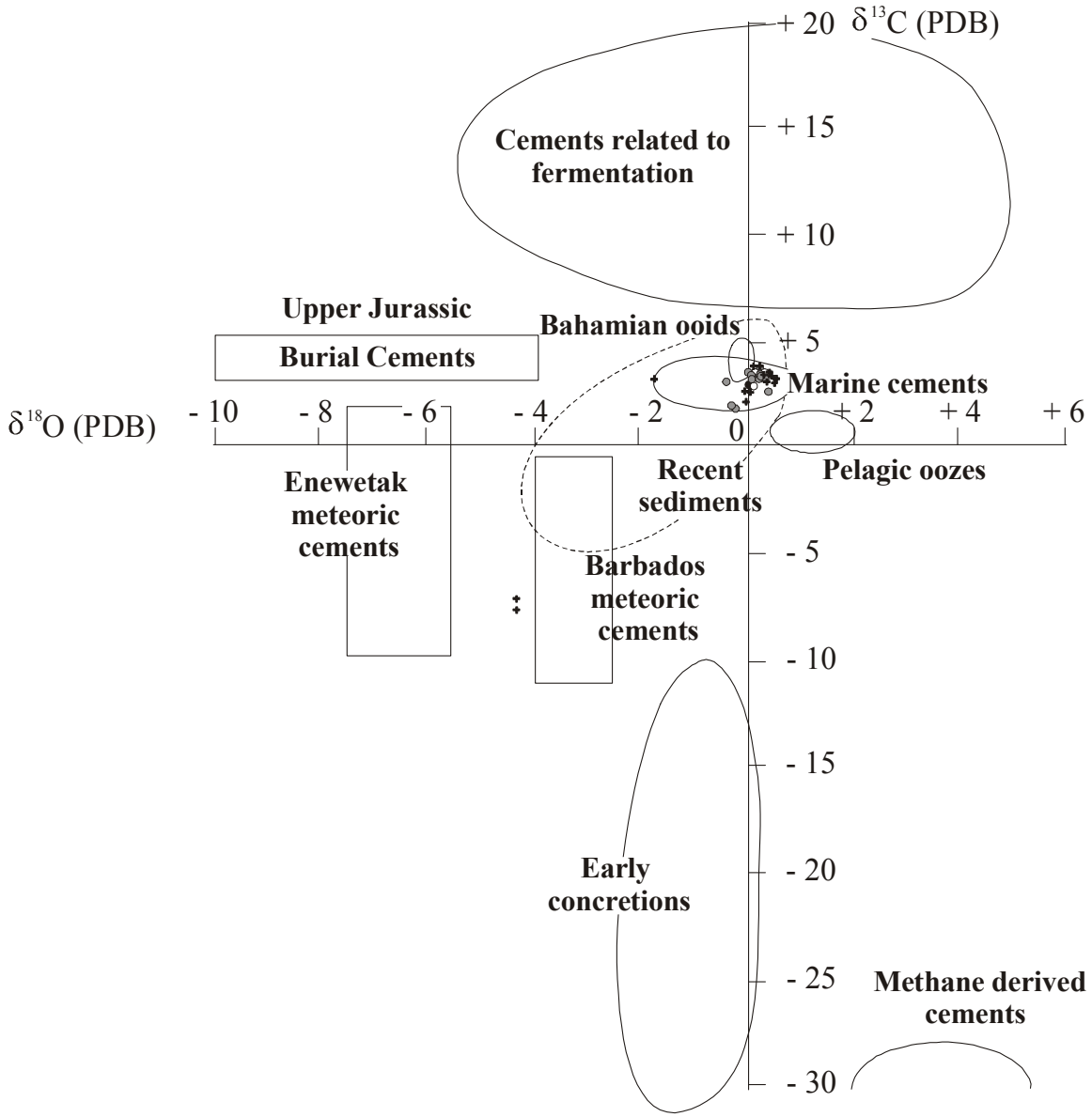

○ Isolated and randomly oriented clumps of scalenohedral crystals

✚ Equant spar

● Isopachous prismatic rims

● Pseudo-peloidal cement

Figure 7

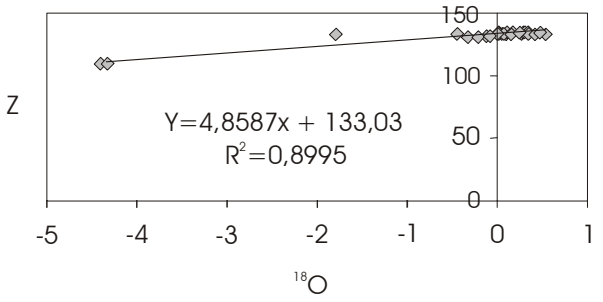
Z
150
100
50
0
Y=4,8587x + 133,03
R²=0,8995
-5
-4
-3
-2
-1
0
1
18O

A

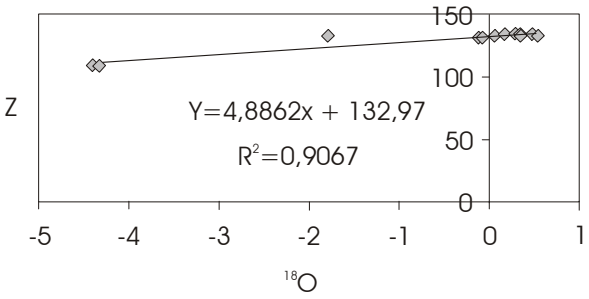
Z
150
100
50
0
Y=4,8862x + 132,97
R²=0,9067
-5
-4
-3
-2
-1
0
1
18O

B

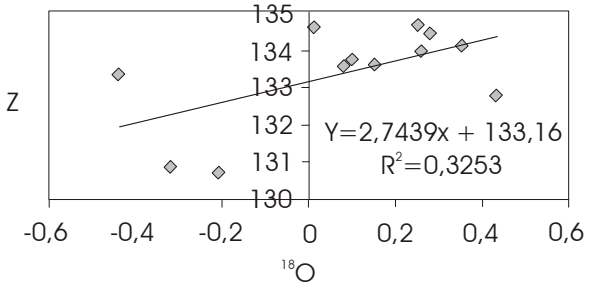
Z
135
134
133
132
131
130
Y=2,7439x + 133,16
R²=0,3253
-0,6
-0,4
-0,2
0
0,2
0,4
0,6
18O

C

Figure 8

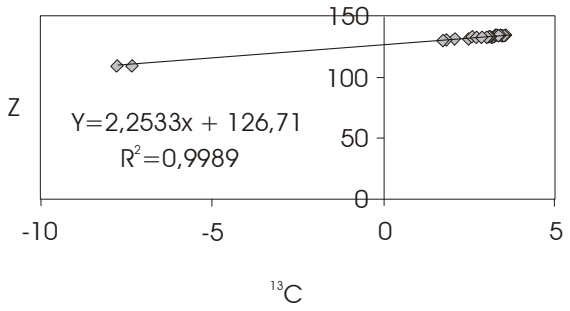
150
100
50
0
Z
Y=2,2533x + 126,71
R²=0,9989
-10
-5
0
5
13C

A

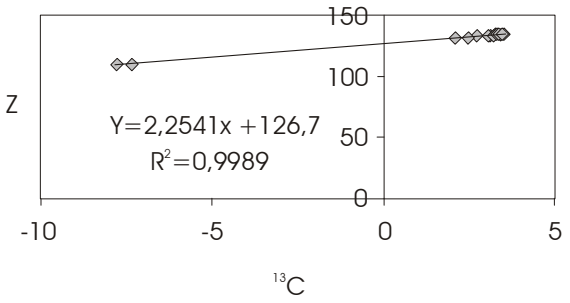
150
100
50
0
Z
Y=2,2541x +126,7
R²=0,9989
-10
-5
0
5
13C

B

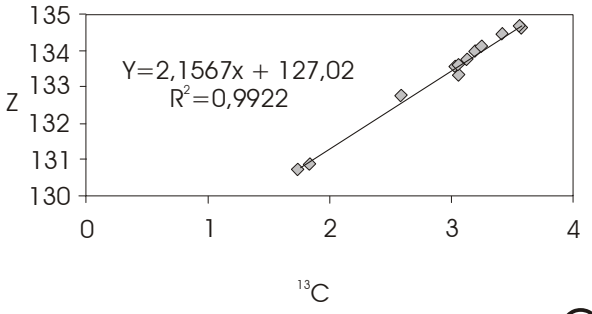
135
134
133
132
131
130
Z
Y=2,1567x + 127,02
R²=0,9922
0
1
2
3
4
13C

C

ANEXO 1

FOTOS DE LÂMINAS DELGADAS

PRANCHA 1: (A) Esmectita autigênica (marrom-claro) ao longo da clivagem de um feldspato. O espaço poroso entre os grãos é ocupado por um mosaico de cristais equantes; polarizadores descruzados (P//); Ponto 19; (B) Espaço intergranular ocupado por mosaico de cristais equantes; polarizadores cruzados (PX); Ponto 16; (C) Franja de cristais prismáticos, regular e isópaca, desenvolvida ao redor de grãos de quartzo monocristalino, após uma primeira fase de cimentação por um envelope micrítico. Notar a orientação perfeitamente perpendicular dos cristais em relação à superfície dos grãos e presença de duas gerações de franjas ao redor do maior grão; PX; Ponto 24; (D) Franja de cristais prismáticos, regular e isópaca, desenvolvida ao redor de grãos de quartzo monocristalino; PX; Ponto 24; (E) Franja de cristais prismáticos, regular e isópaca, desenvolvida ao redor de grãos. Notar presença de envelope micrítico espesso e descontínuo adjacente ao grão (centro da foto); P//; Ponto 28; (F) Espaço intergranular ocupado por agregado pseudo-peloidal; P//; Ponto 17.

PRANCHA 2: (A) Franja de cristais prismáticos seguida de filme orgânico (marrom). Notar orientação sub-perpendicular dos cristais em relação à superfície dos grãos; P//; Ponto 17; (B) Duas gerações de franja de cristais prismáticos separada por envelope micrítico; PX; Ponto 4; (C) Sedimento margoso. Notar a presença de foraminíferos planctônicos; PX; Ponto 18; (D) Sedimento margoso infiltrado na zona vadosa. Notar presença de silte siliciclástico e meniscos (setas); P//; Ponto 18; (E) Sedimento micrítico infiltrado ocupando parte do poro. Notar a presença de foraminíferos planctônicos. O restante da porosidade foi ocupado por um agregado pseudo-peloidal; P//; Ponto 18; (F) Foraminíferos planctônicos em micrita infiltrada; P//; Ponto 18.

PRANCHA 3: (A) Foraminíferos planctônicos em micrita infiltrada; P//; Ponto 18; (B) Espaço poroso ocupado por cimento micrítico seguido de agregado pseudo-peloidal e marga infiltrada (centro da foto); P//; Ponto 18; (C) Franja de cristais prismáticos, regular e isópaca, desenvolvida ao redor de grãos de quartzo monocristalino. Espaço poroso remanescente foi ocupado por silte vadoso composto por grãos predominantemente

quartzosos angulosos a sub-angulosos; P//; Ponto 18; (D) Múltiplas fases diagenéticas. De cima para baixo: envelope micrítico seguido de franja de cristais prismáticos, marga infiltrada, silte vadoso e, novamente, marga infiltrada; P//; Ponto 18; (E) Espaço poroso ocupado por silte vadoso. Notar a presença de cutículas micríticas (marrom) ao redor dos grãos; P//; Ponto 18; (F) Micrita infiltrada contendo grãos angulosos, predominantemente quartzosos, na fração silte e microfósseis. Provável bioturbação resultou em um discreto arranjo circular destes grãos; P//; Ponto 35.

PRANCHA 4: (A) Minerais pesados (P). Cimento micrítico ocupa totalmente o espaço poroso; P//; Ponto 35; (B) Cimento carbonático radiaxial em poro intragranular de um arenito cimentado por hematita da Formação Barreiras; P//; Ponto 35; (C) Cristais escalenoédricos projetando-se a partir da superfície dos grãos de quartzo; PX; Ponto 15; (D) Espaço poroso ocupado por agregado pseudo-peloidal circundado por franjas de cristais prismáticos. Restante do espaço poroso foi ocupado por micrita infiltrada (porção inferior da foto); P//; Ponto 30; (E) Espaço intergranular ocupado por cristais equantes; PX; Ponto 15; (F) Agregado radial (porção superior da foto) e cristal escalenoédrico isolado (porção inferior da foto); P//; Ponto 15.

PRANCHA 5: (A) Agregados radiais (R) dispostos a partir de corpos pseudo-peloidais seguidos de micrita infiltrada. Notar a presença de foraminíferos planctônicos dispersos na mesma; PX; Ponto 30; (B) Franja de cristais prismáticos ao redor de quartzo monocristalino (esquerda da foto). Restante do espaço poroso ocupado por agregado pseudo-peloidal (porção superior da foto) circundado por franja de cristais prismáticos única e micrita infiltrada com microfósseis dispersos; PX; Ponto 30; (C) Espaço intergranular parcialmente ocupado por cristais equantes; P//; Ponto 15; (D) Franjas de cristais equantes ao redor de grãos de quartzo monocristalino; P//; Ponto 34; (E) Foto anterior com polarizadores cruzados.

PRANCHA 1

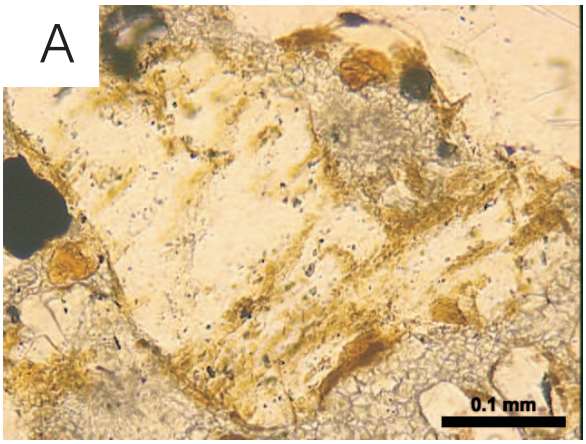

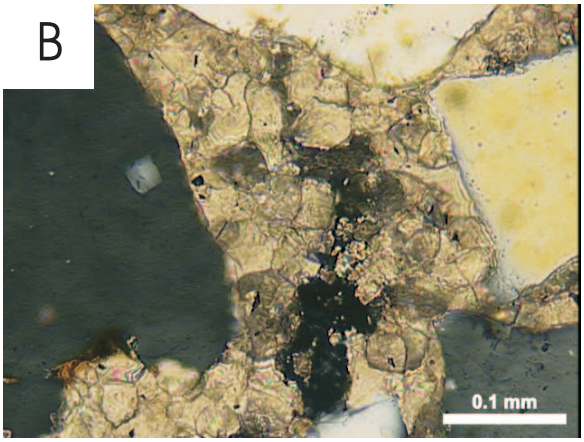

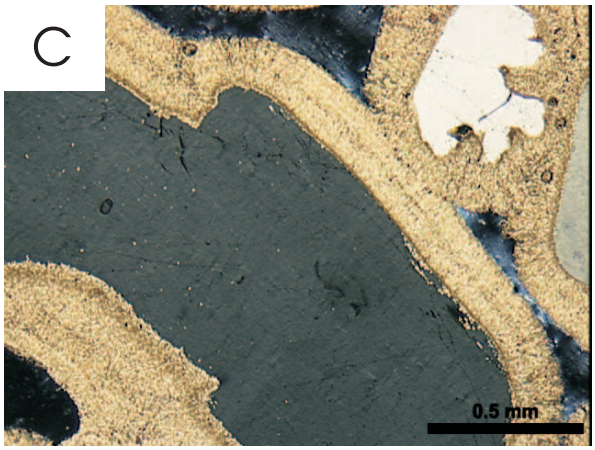

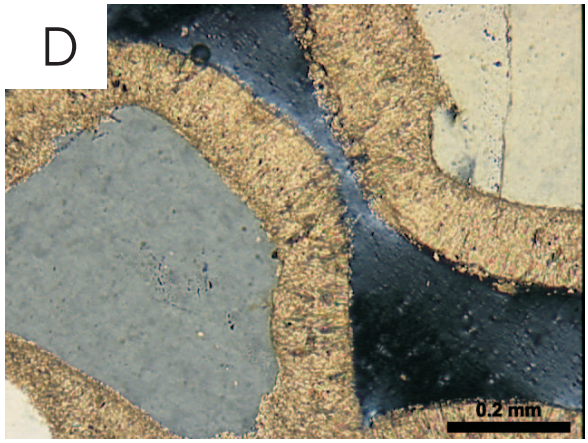

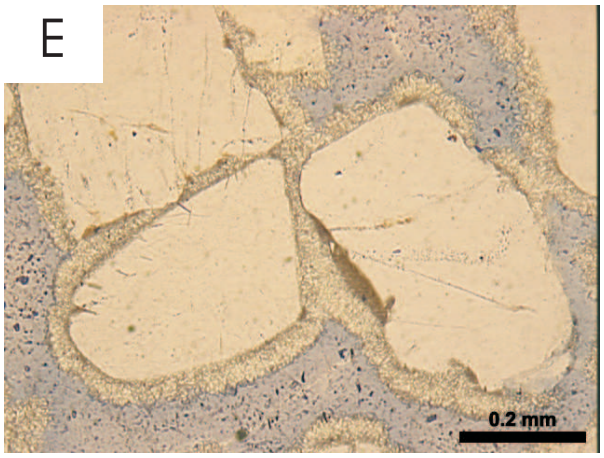

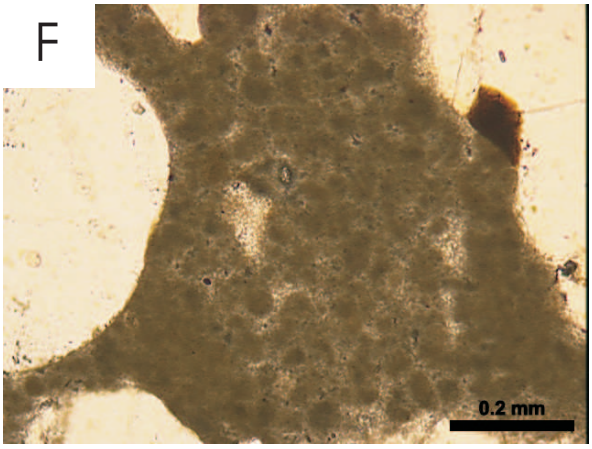

PRANCHA 2

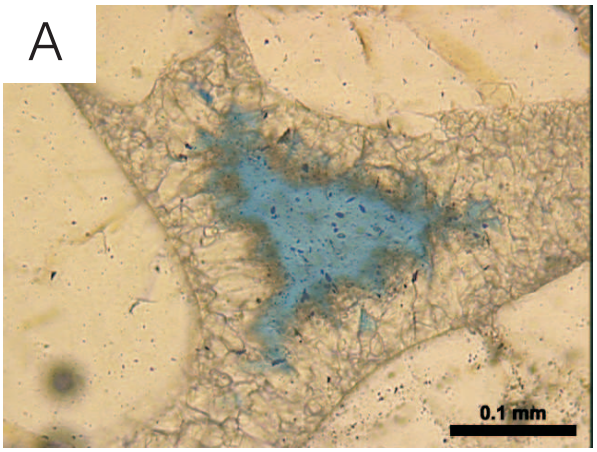

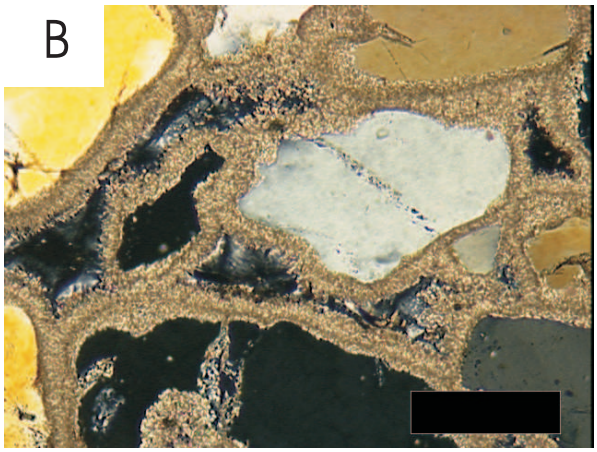

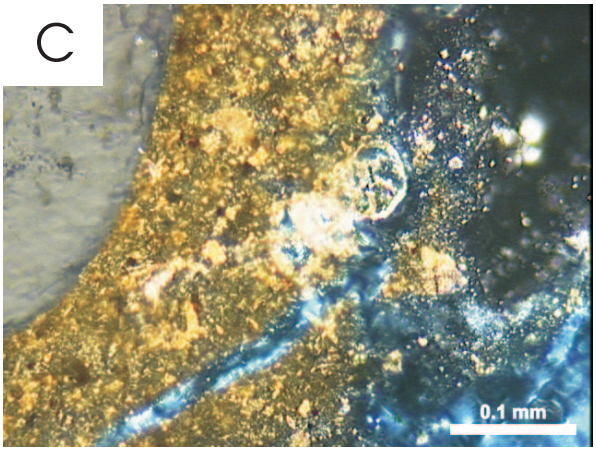

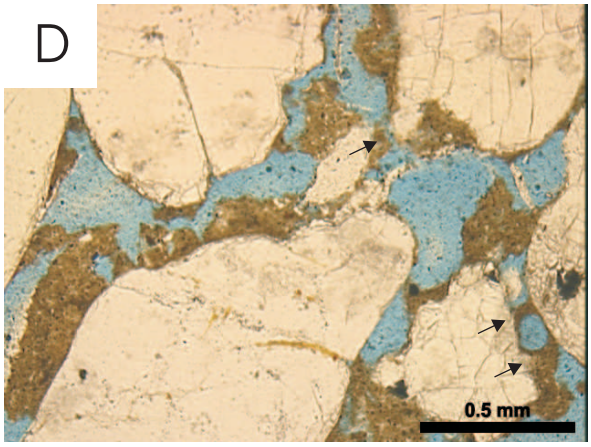

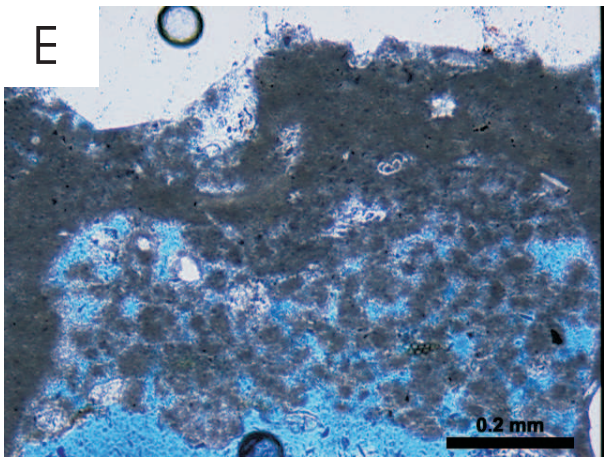

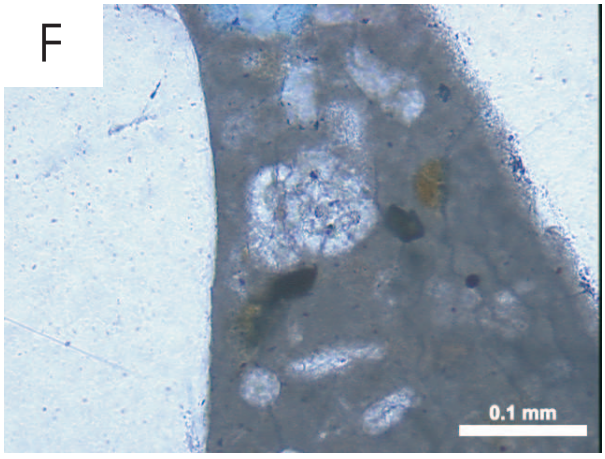

PRANCHA 3

A

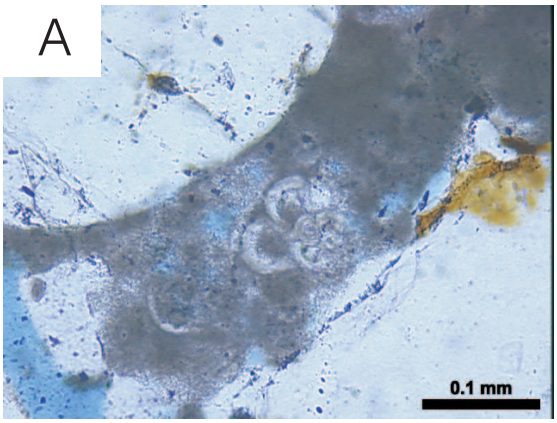

B

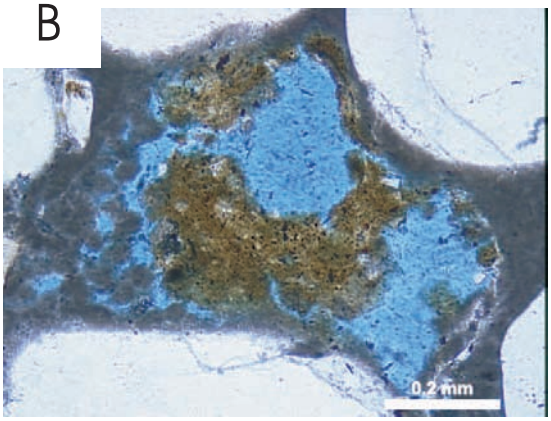

C

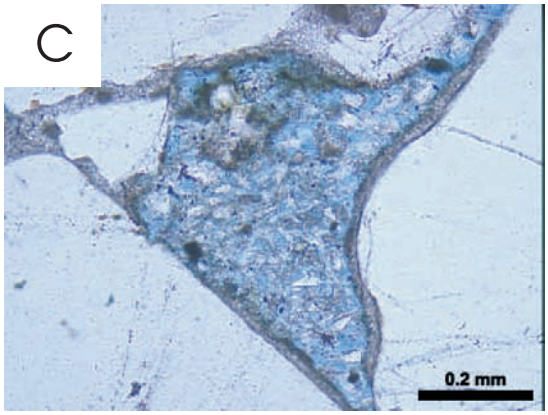

D

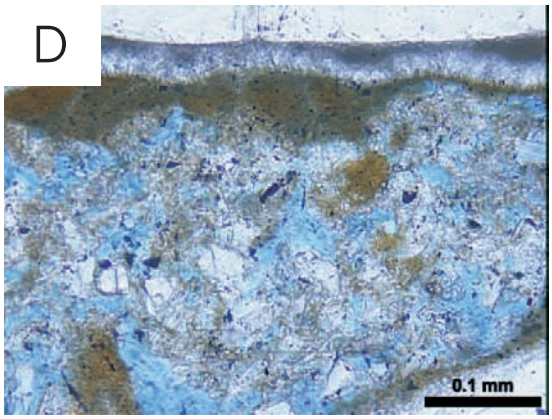

E

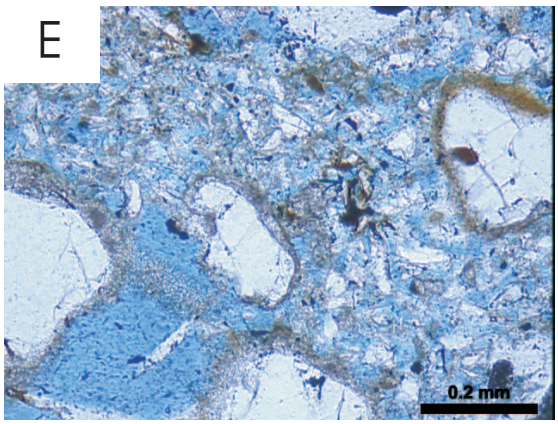

F

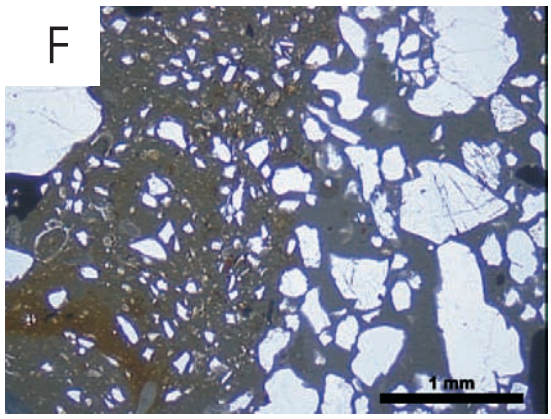

PRANCHA 4

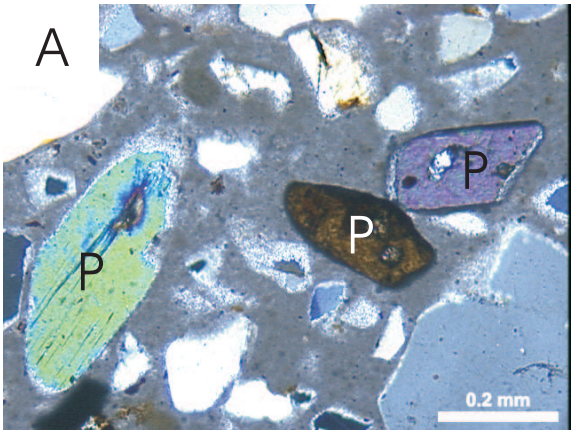

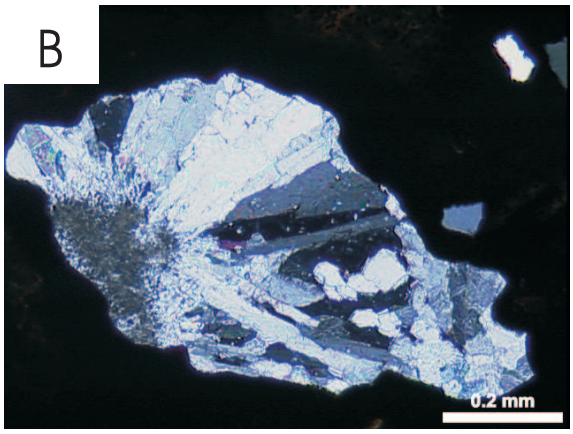

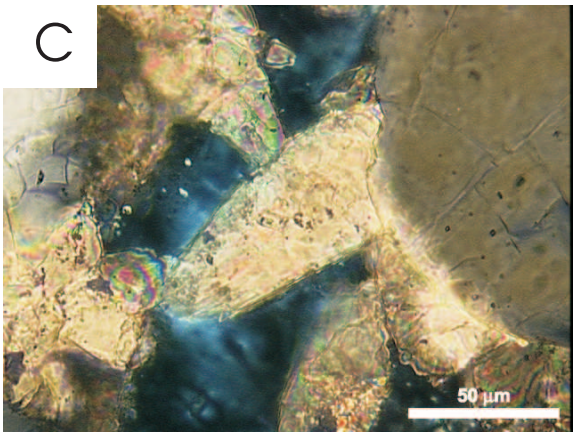

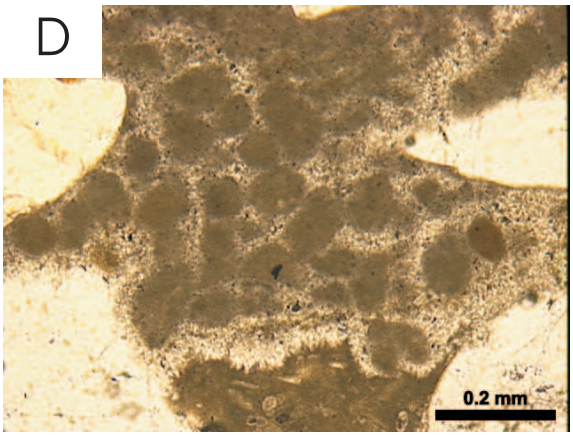

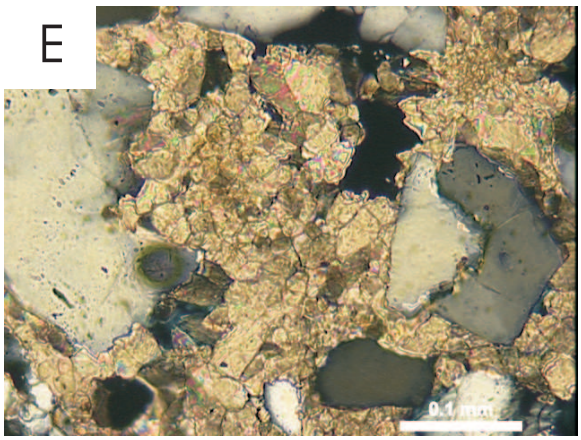

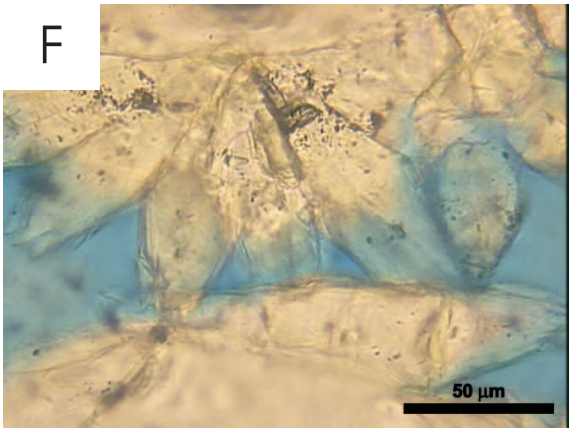

PRANCHA 5

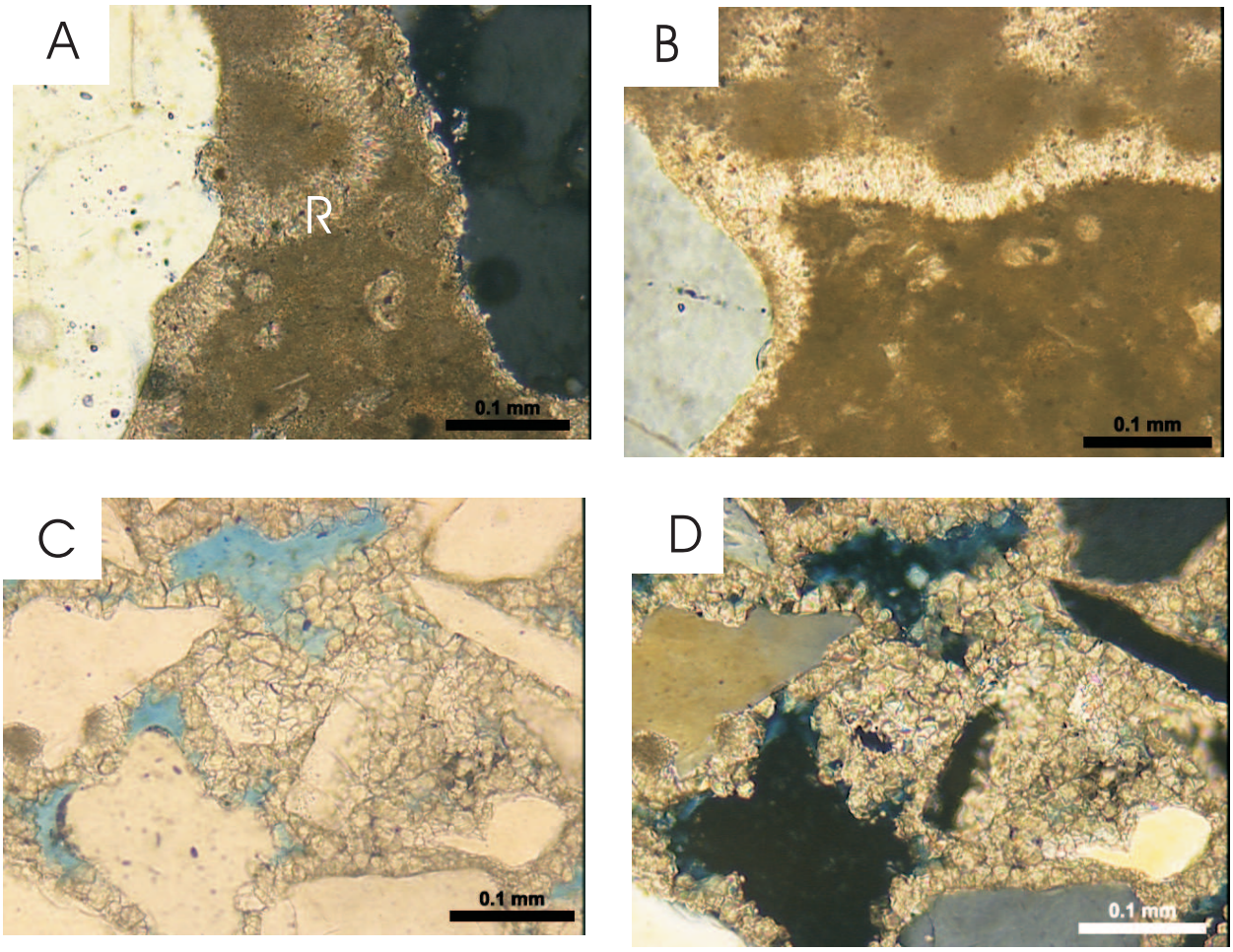

ANEXO 2

FOTOS AO MICROSCÓPIO ELETRÔNICO DE VARREDURA

PRANCHA 6: (A) Detalhe de agregado pseudo-peloidal, mostrando a micro-fábrica de cristais escalenoédricos radialmente dispostos que compõem os pseudo-pelóides. Ponto 17; (B) Fina franja de cristais prismáticos desenvolvida ao redor de grão de quartzo. Notar orientação sub-perpendicular dos cristais em relação à superfície dos grãos. Ponto 18; (C) Detalhe da foto anterior. Letra A corresponde ao ponto em que foi feita a análise dos elementos maiores e traços por microscopia eletrônica de energia dispersada (EDS; Anexo 3); (D) Mesma amostra vista de outro ângulo; (E) Cristais equantes com faces escalonadas, ocupando o espaço poroso entre os grãos. Ponto 32; (F) Mesma amostra vista de outro ângulo.

PRANCHA 7: (A) Grão de quartzo (Canto superior direito) circundado por uma franja de cristais alongados. Espaço poroso restante foi ocupado por uma micrita infiltrada com bioclastos (seta). Ponto 30; (B) Agregado fibro-radial visto em corte. Letra A corresponde ao ponto em que foi feita a análise dos elementos maiores e traços por microscopia eletrônica de energia dispersada (EDS; Anexo 3). Ponto 30; (C) Detalhe de um pseudo-pelóide. Ponto 30; (D) Micrita infiltrada vista em detalhe. Notar formato irregular dos cristais de calcita magnesiana. Ponto 30; (E) Franja de cristais prismáticos desenvolvidas ao redor de grãos do arcabouço. Letra A corresponde ao ponto em que foi feita a análise dos elementos maiores e traços por microscopia eletrônica de energia dispersada (EDS; Anexo 3). Ponto 31; (F) Detalhe da foto anterior. Notar orientação sub-perpendicular dos cristais em relação à superfície do grão de quartzo (à direita).

PRANCHA 8: (A) Visão geral do arcabouço circundado por fina franja de cristais prismáticos. Ponto 21; (B), (C), (D) e (E) Detalhes da foto anterior. Notar o caráter não contínuo das franjas e a não perpendicularidade dos cristais em relação à superfície dos grãos de quartzo monocristalino. Letra A na foto E corresponde ao ponto em que foi feita a análise dos elementos maiores e traços por microscopia eletrônica de energia dispersada (EDS; Anexo 3); (F) Franja de cristais prismáticos, regular e isópaca, desenvolvidas ao redor de grãos de quartzo monocristalino. Ponto 24.

PRANCHA 9: (A) Franja de cristais prismáticos, regular e isópaca, desenvolvida ao redor de grãos de quartzo monocristalino. Notar orientação perfeitamente perpendicular dos cristais em relação à superfície dos grãos. Ponto 24; (B) e (C) Detalhes da foto anterior, evidenciando a regularidade, o caráter isópaco e a grande espessura das franjas. (D) Visão geral do mosaico de cristais equantes euédricos, ocupando o espaço poroso entre os grãos. Ponto 24; (E) e (F) Cimento equante da amostra anterior visto em maior detalhe.

PRANCHA 10: (A) e (B) Visão geral dos agregados fibro-radiais. Ponto 23; (C) Foto B vista em maior detalhe; (D) Visão geral dos agregados fibro-radiais. Ponto 23; (E) Foto anterior vista em detalhe. Letra A corresponde ao ponto em que foi feita a análise dos elementos maiores e traços por microscopia eletrônica de energia dispersada (EDS, Anexo 3); (F) Cimento criptocristalino, preenchendo o espaço poroso entre os grãos de quartzo. Notar formato irregular dos cristais de calcita magnesiana. Ponto 35.

PRANCHA 6

A

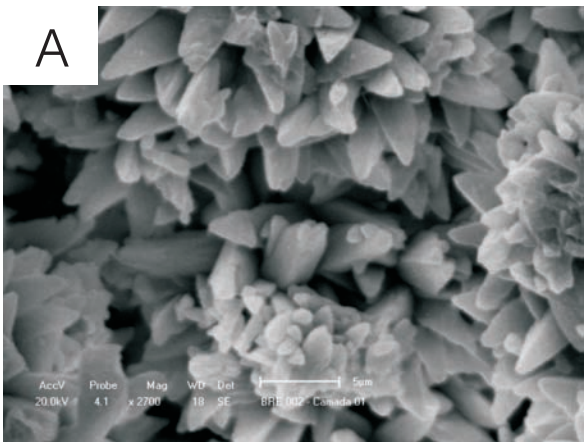

B

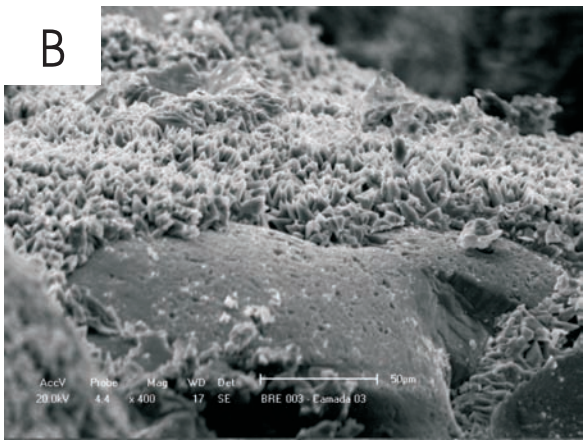

C

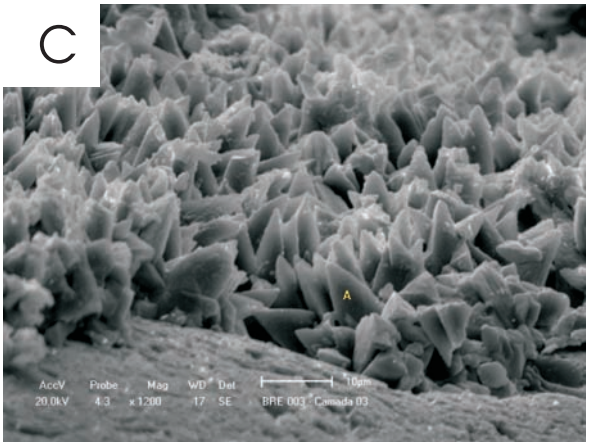

D

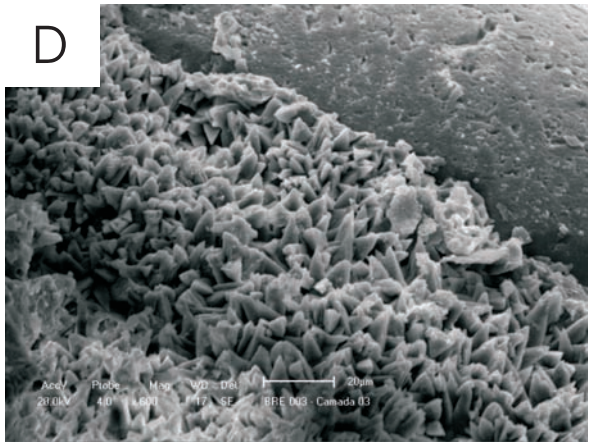

E

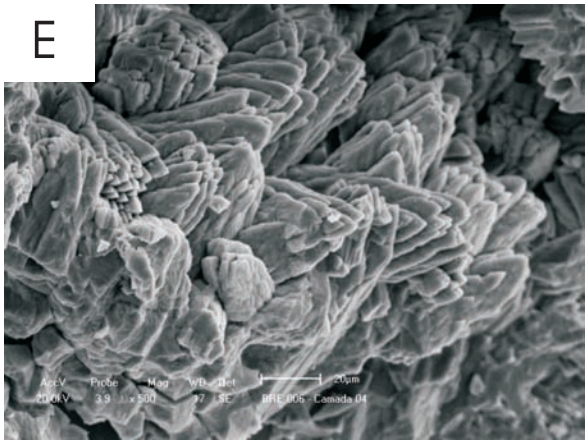

F

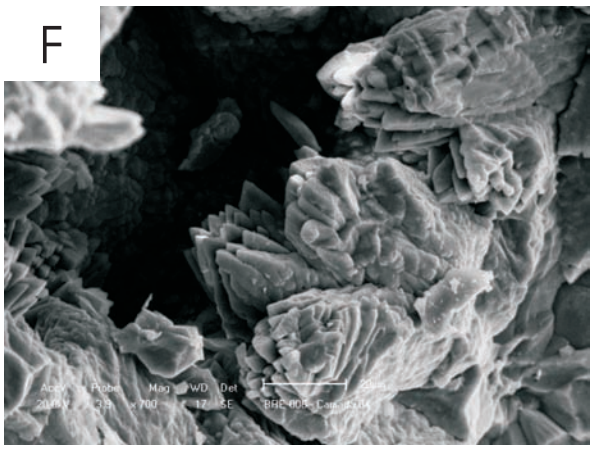

PRANCHA 7

A

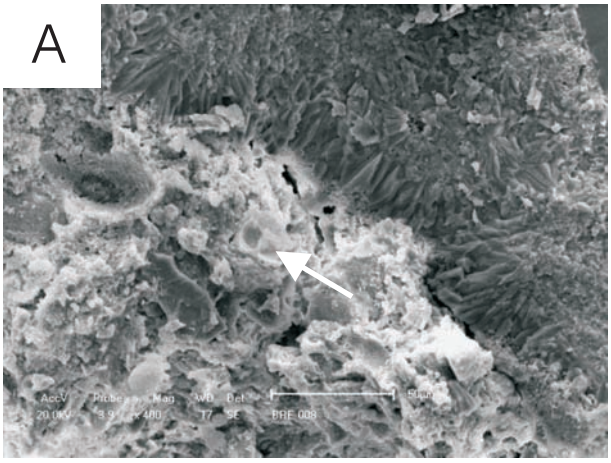

B

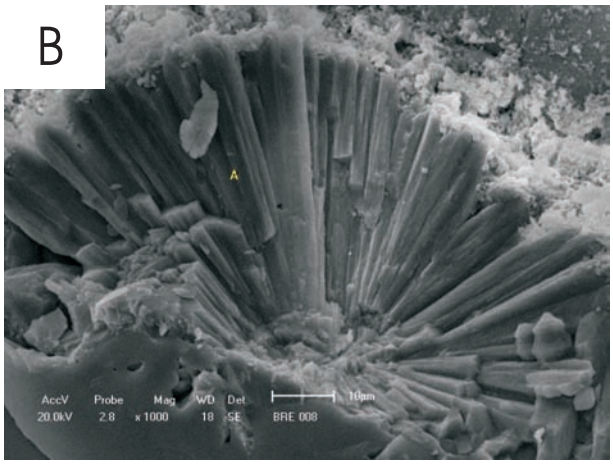

C

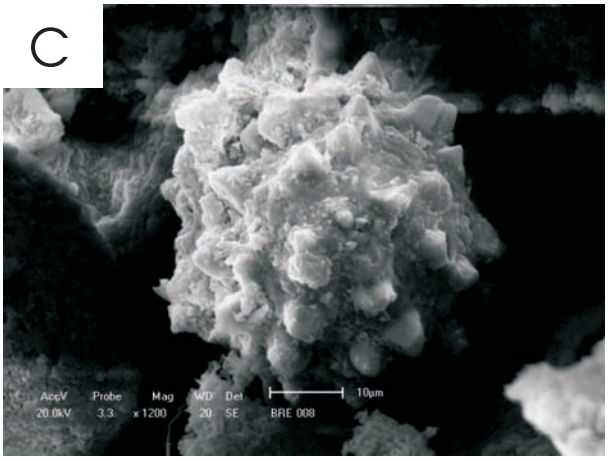

D

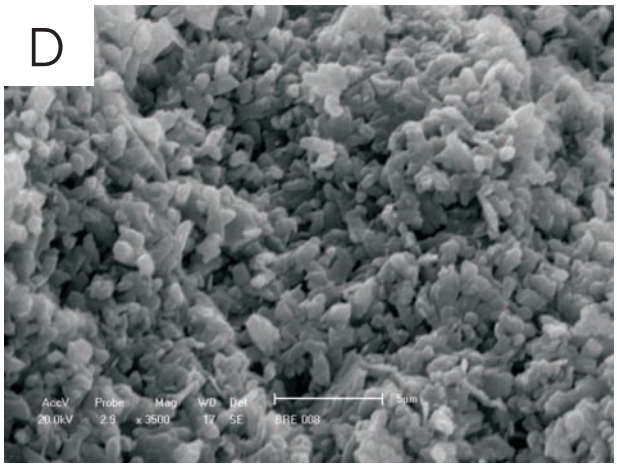

E

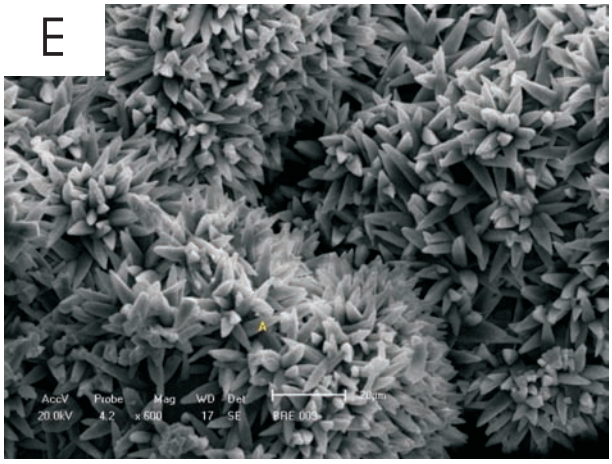

F

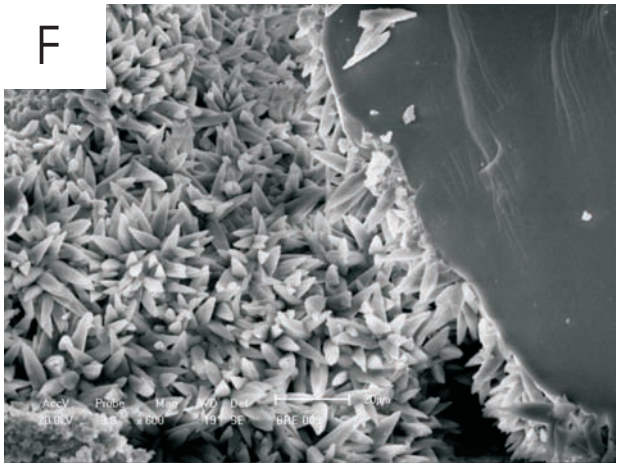

PRANCHA 8

A

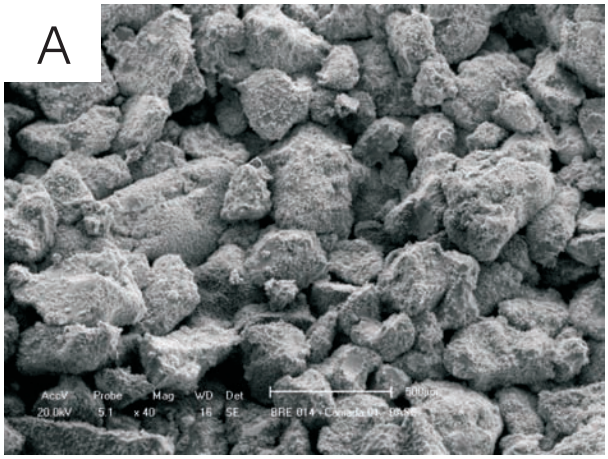

B

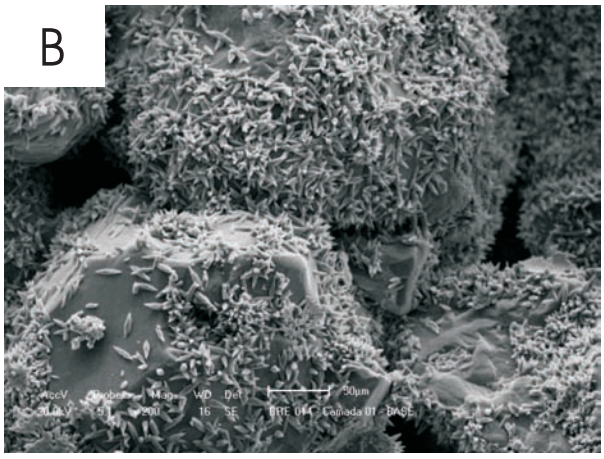

C

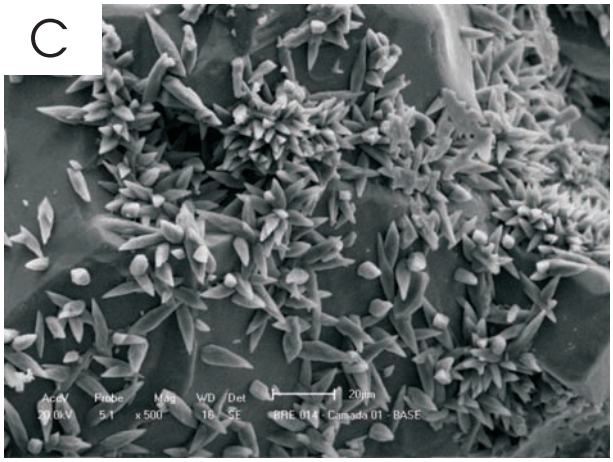

D

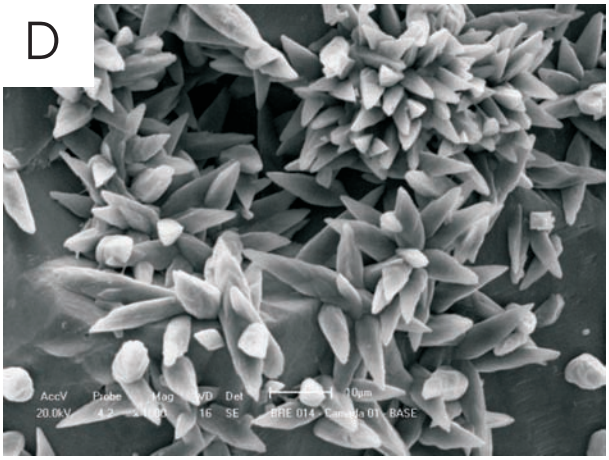

E

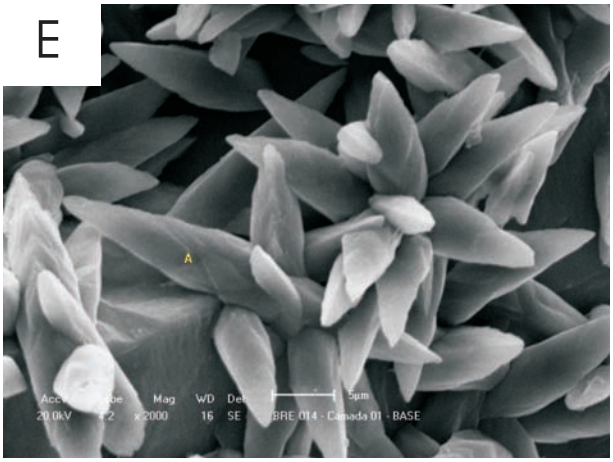

F

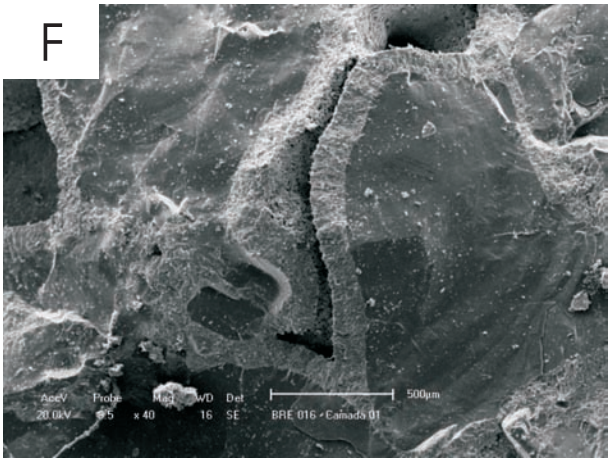

PRANCHA 9

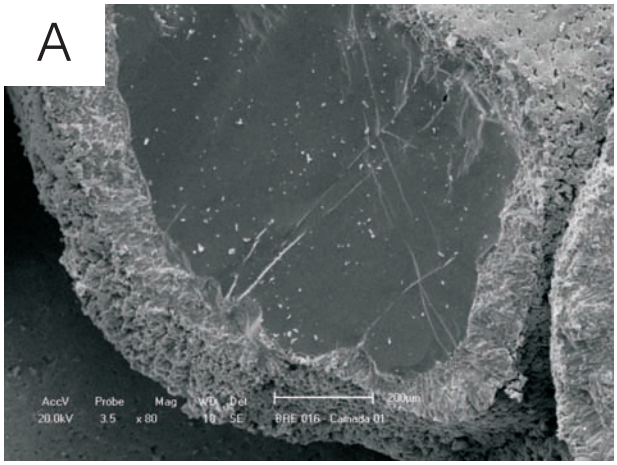
A
AccV Probe Mag WD Det
20.0kV 3.5 x 80 10 SE
200µm
BRE 016 - Camada 01

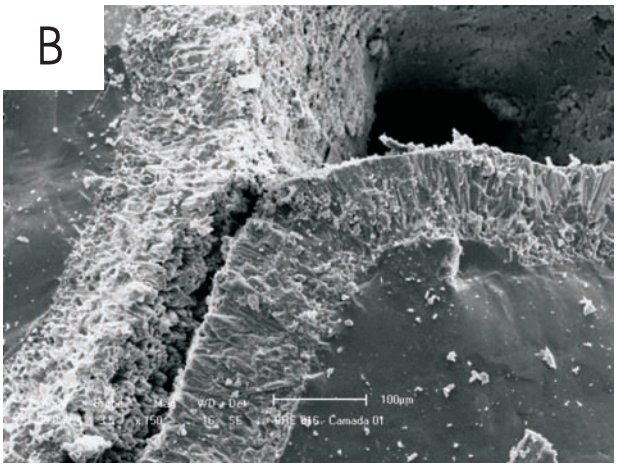
B
100µm

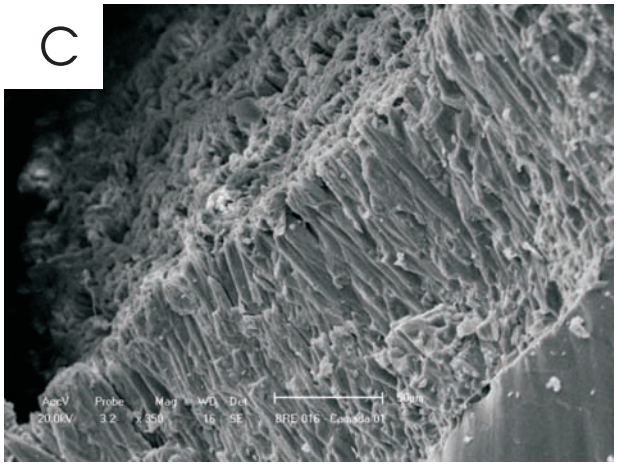
C

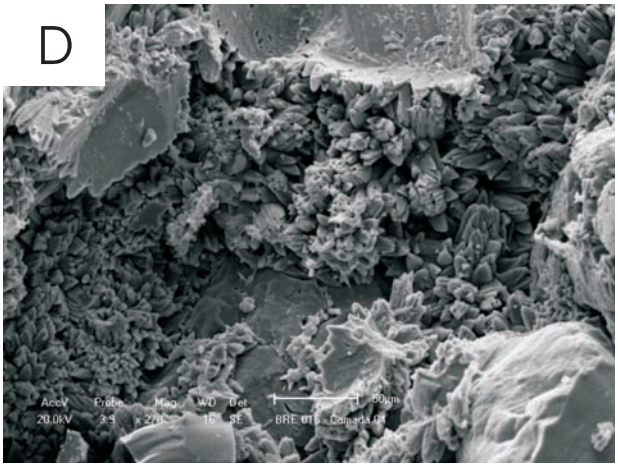
D

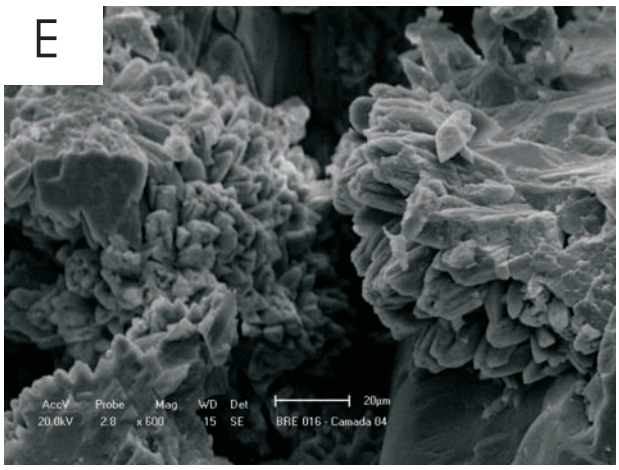
E
AccV Probe Mag WD Det
20.0kV 2.8 x 600 15 SE
20µm
BRE 016 - Camada 04

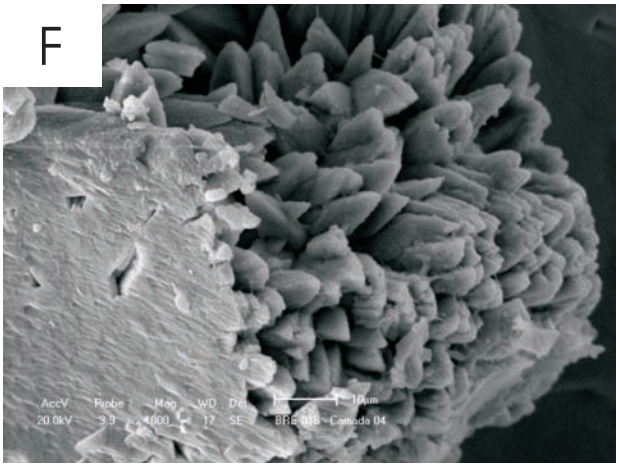
F

PRANCHA 10

A

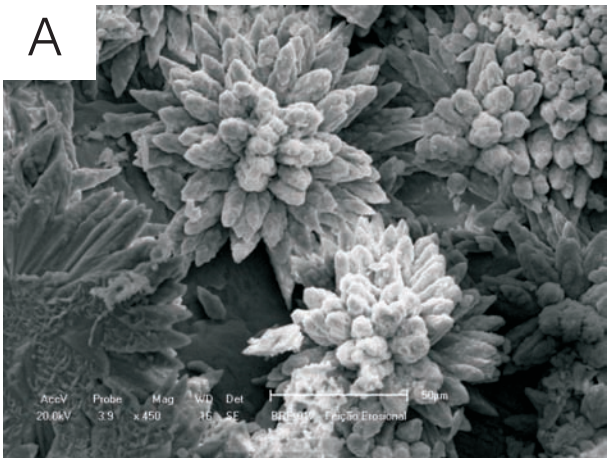

B

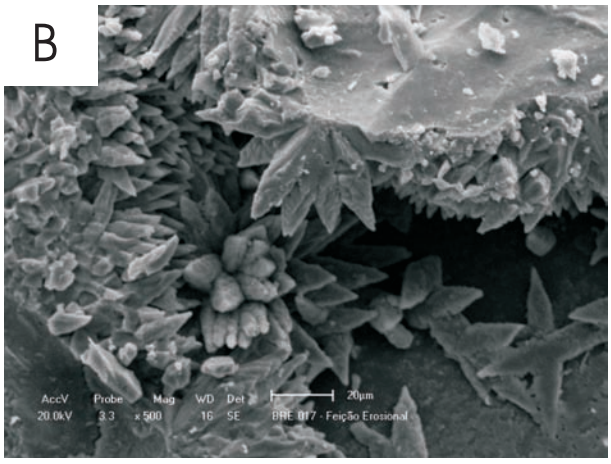

C

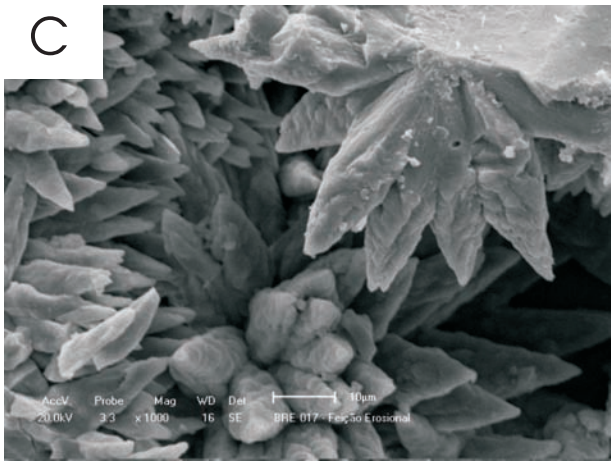

D

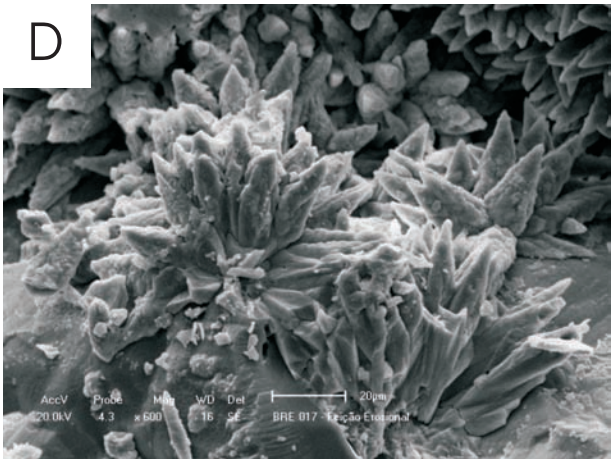

E

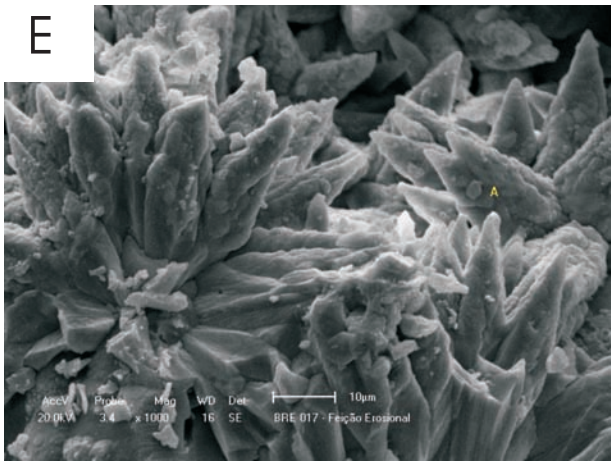

F

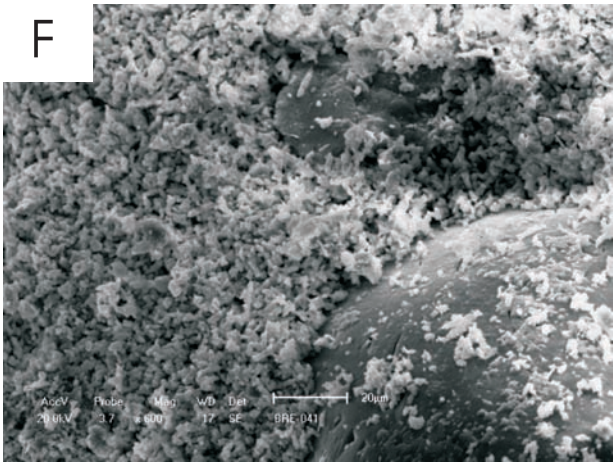

ANEXO 3

ANÁLISES DE ESPECTROSCOPIA DE ENERGIA DISPERSADA (EDS)

Figura 1: Cristais que compõem a estrutura interna dos pseudo-pelóides; Ponto 17.

Figura 2: Discreta franja de cristais prismáticos desenvolvida ao redor de grão de quartzo monocristalino. Notar orientação sub-perpendicular dos cristais em relação à superfície dos grãos; Ponto 18.

Figura 3: Cristais equantes com faces escalonadas complexas, ocupando o espaço poroso entre os grãos; Ponto 32.

Figura 4: Cristais equantes, ocupando o espaço poroso entre os grãos; Ponto 32.

Figura 5: Agregado fibro-radial visto em corte; Ponto 30.

Figura 6: Micrita infiltrada; Ponto 30.

Figura 7: Micrita infiltrada vista em detalhe. Notar formato irregular dos cristais de calcita magnesiana; Ponto 30.

Figura 8: Franja de cristais prismáticos desenvolvidas ao redor de grãos do arcabouço. Notar orientação sub-perpendicular dos cristais em relação à superfície dos grãos; Ponto 31.

Figura 9: Detalhe de fina franja de cristais prismáticos. Notar o caráter não contínuo da mesma e a não perpendicularidade dos cristais em relação à superfície dos grãos; Ponto 21.

Figura 10: Cimento criptocristalino ao redor de grãos de quartzo; Ponto 25.

Figura 11: Cimento criptocristalino ao redor de grãos de quartzo. Notar formato irregular dos cristais de calcita magnesiana; Ponto 25.

Figura 12: Franja de cristais prismáticos, regular e isópaca, desenvolvida ao redor de grãos de quartzo monocristalino. Notar orientação perfeitamente perpendicular dos cristais em relação à superfície dos grãos; Ponto 24.

Figura 13: Cristais escalenoédricos isolados; Ponto 24.

Figura 14: Agregados radiais; Ponto 23.

Figura 15: Cimento criptocristalino; Ponto 35.

FIGURA 1

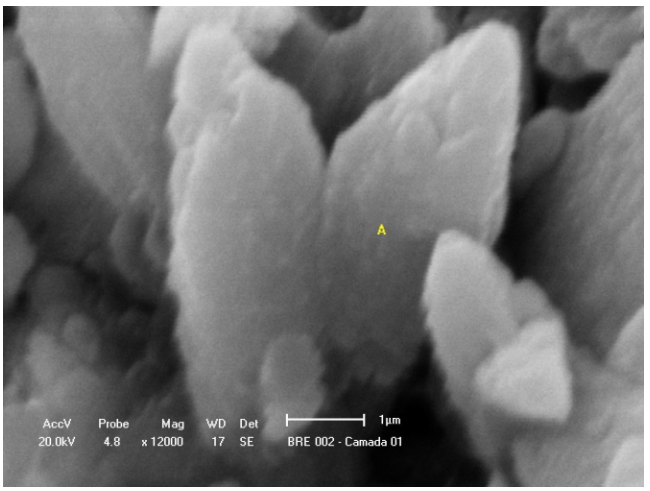

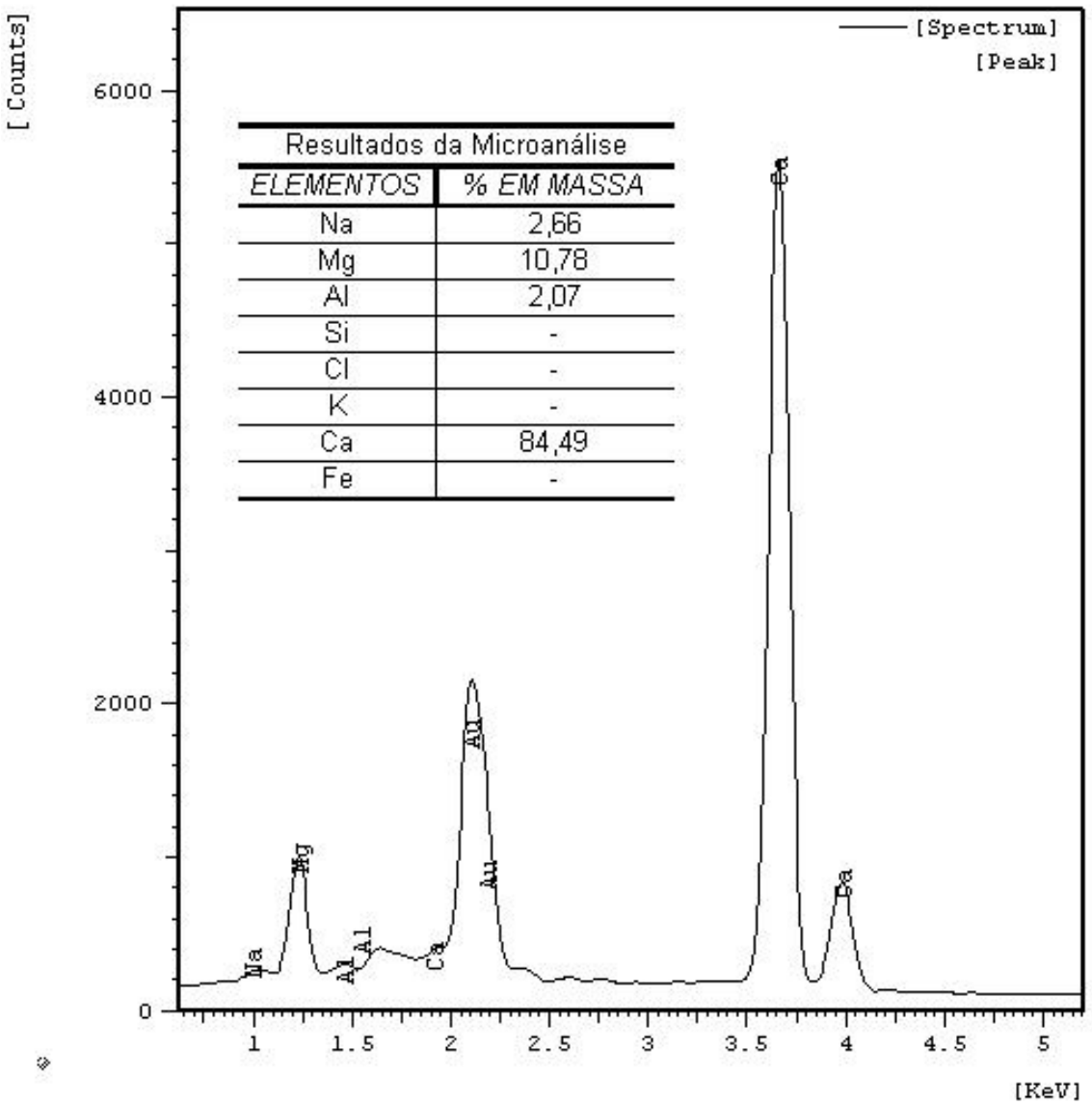

Resultados da Microanálise	
ELEMENTOS	*% EM MASSA*
Na	2,66
Mg	10,78
Al	2,07
Si	-
Cl	-
K	-
Ca	84,49
Fe	-

FIGURA 2

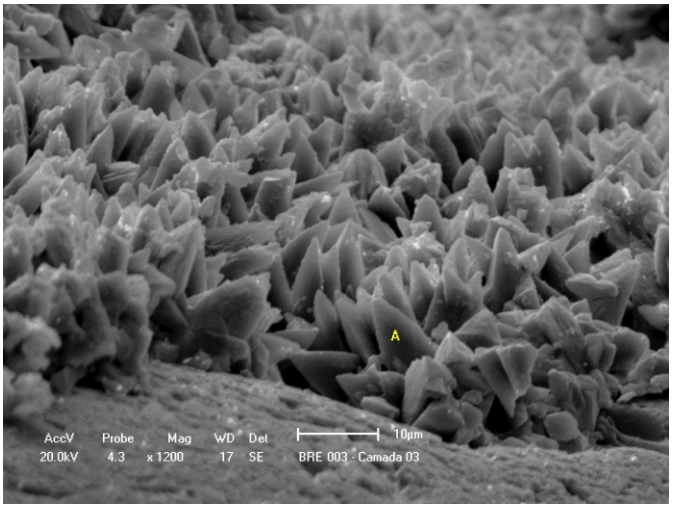

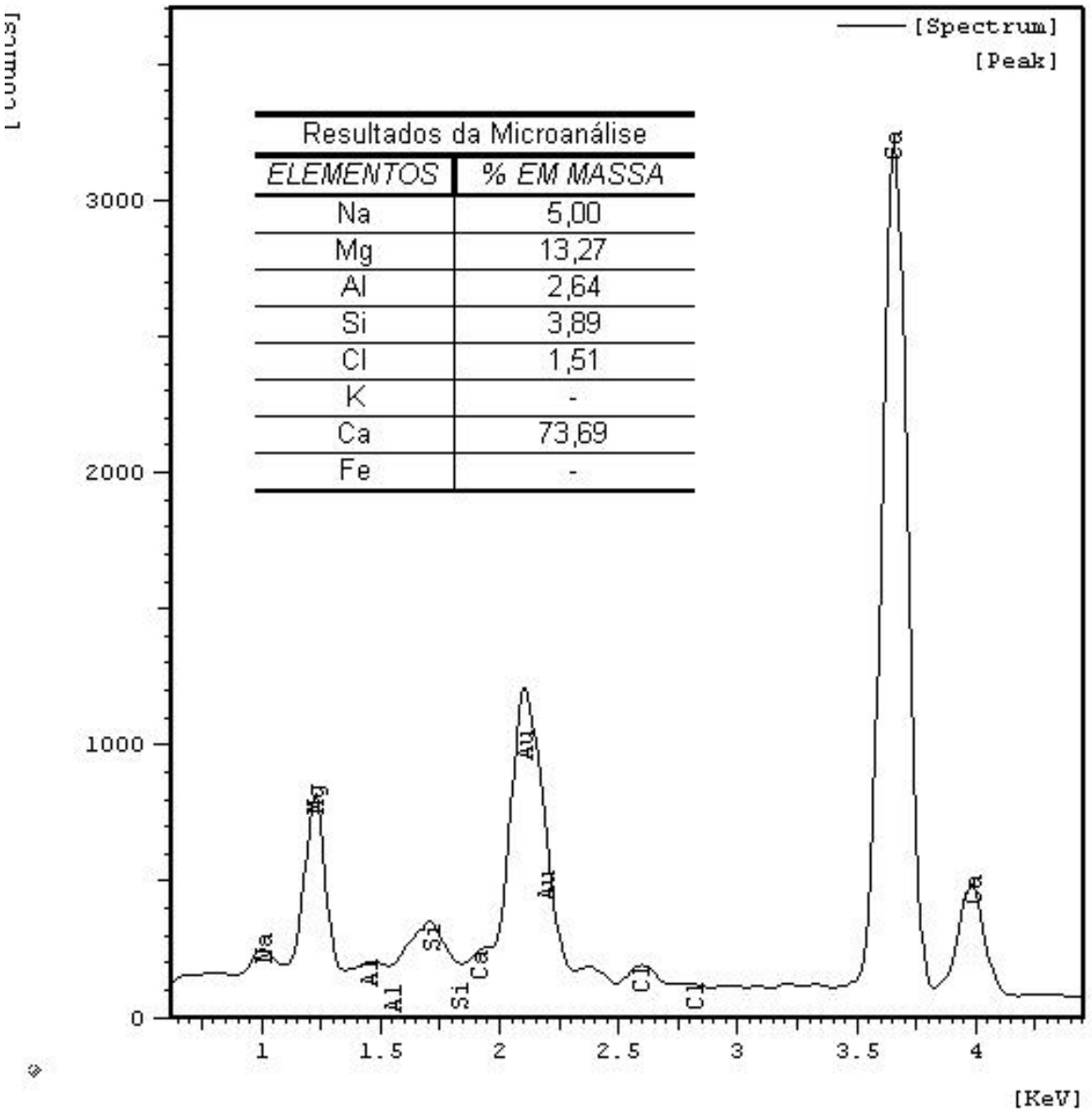

Resultados da Microanálise	
ELEMENTOS	*% EM MASSA*
Na	5,00
Mg	13,27
Al	2,64
Si	3,89
Cl	1,51
K	-
Ca	73,69
Fe	-

FIGURA 3

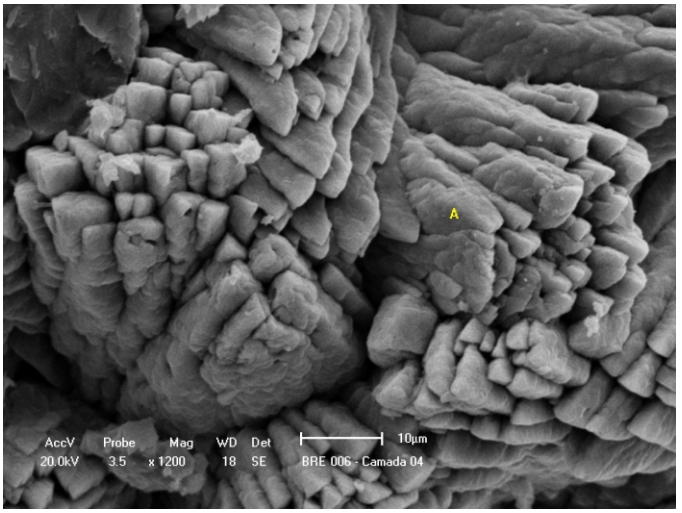

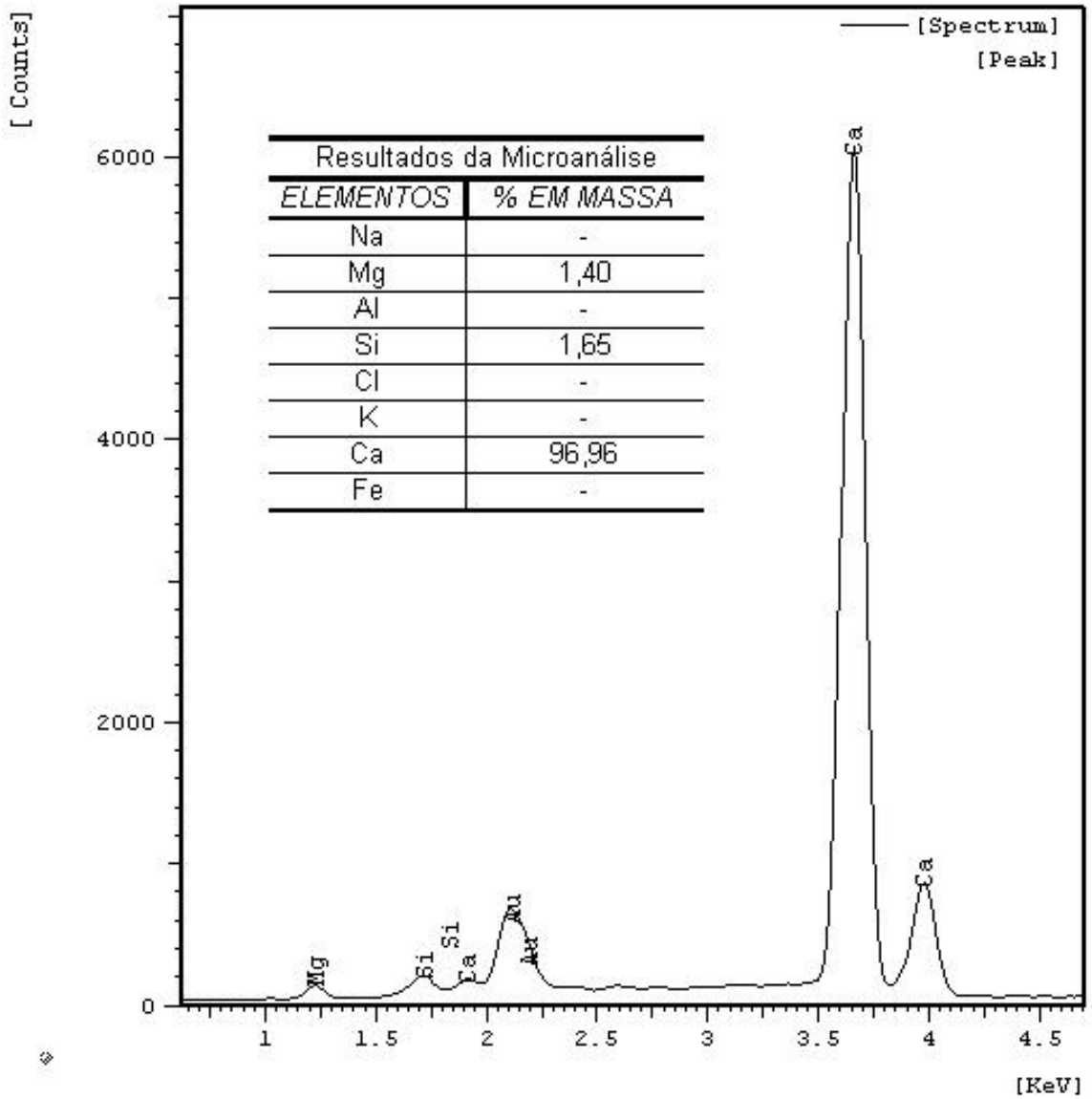

Resultados da Microanálise	
ELEMENTOS	*% EM MASSA*
Na	-
Mg	1,40
Al	-
Si	1,65
Cl	-
K	-
Ca	96,96
Fe	-

FIGURA 4

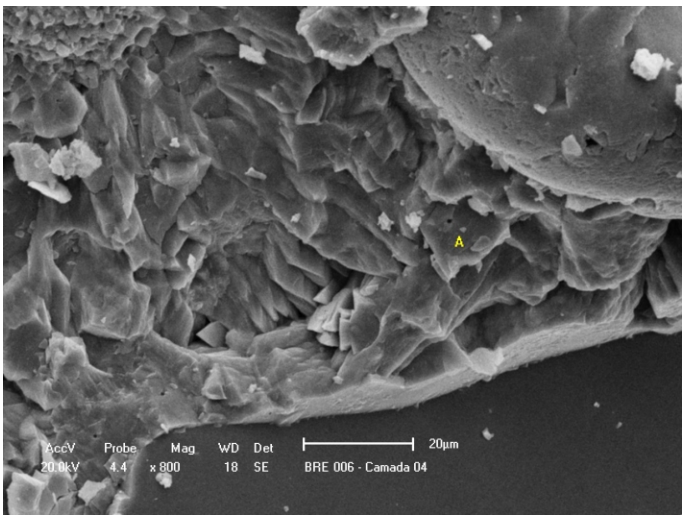

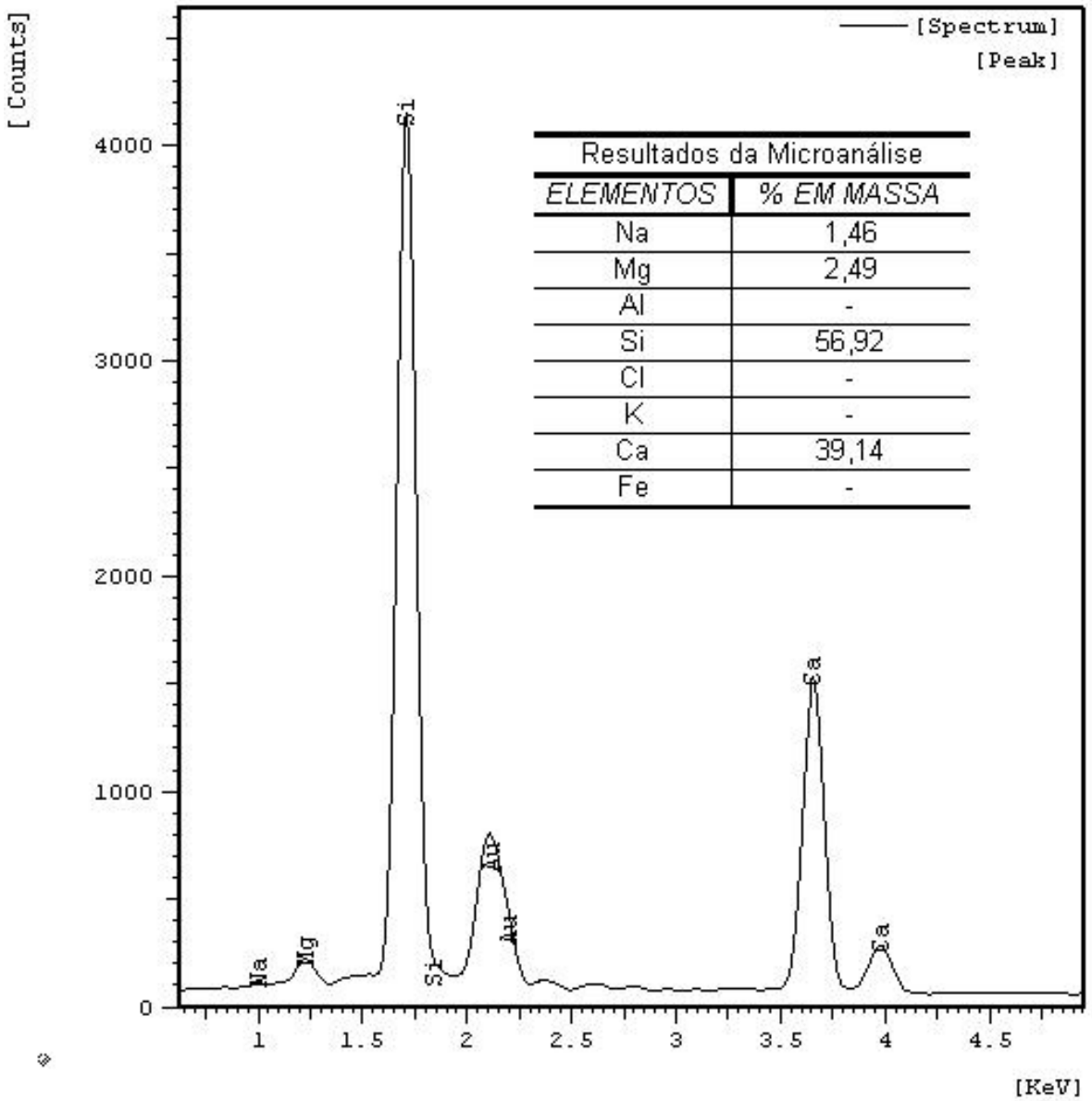

Resultados da Microanálise	
ELEMENTOS	*% EM MASSA*
Na	1,46
Mg	2,49
Al	-
Si	56,92
Cl	-
K	-
Ca	39,14
Fe	-

FIGURA 5

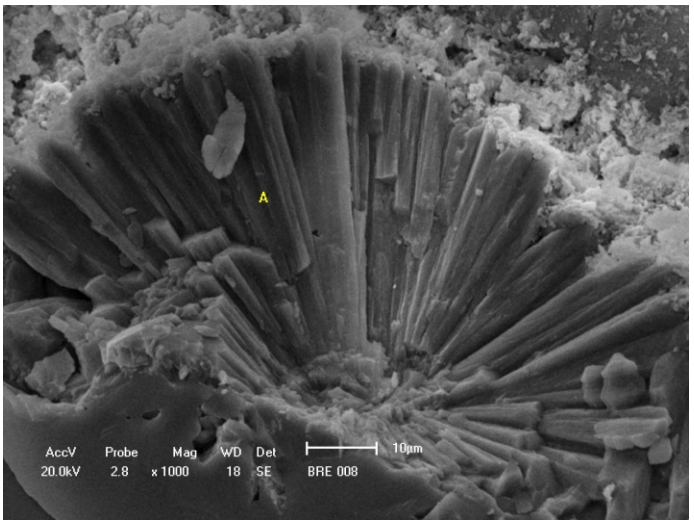

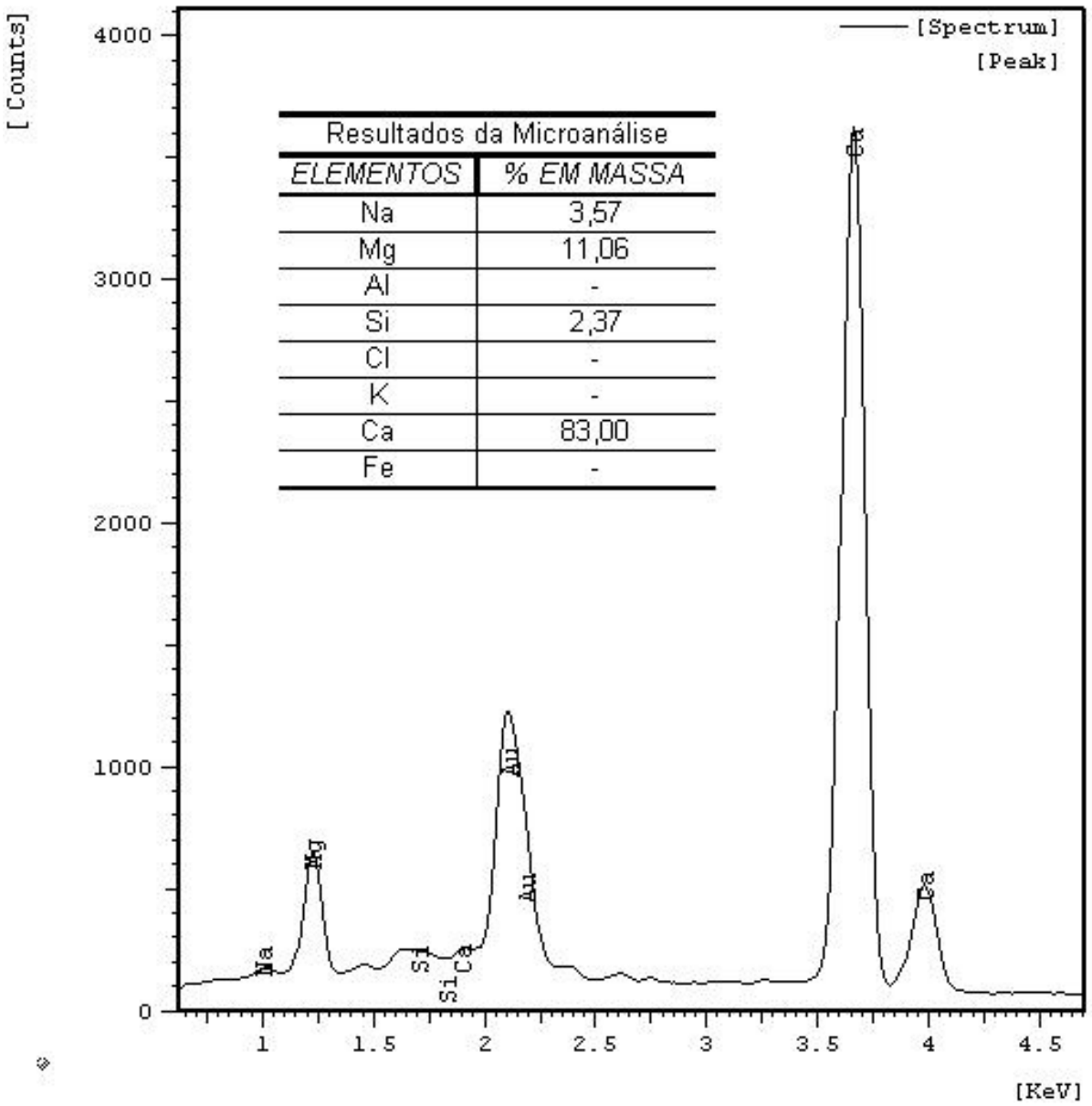

Resultados da Microanálise	
ELEMENTOS	*% EM MASSA*
Na	3,57
Mg	11,06
Al	-
Si	2,37
Cl	-
K	-
Ca	83,00
Fe	-

FIGURA 6

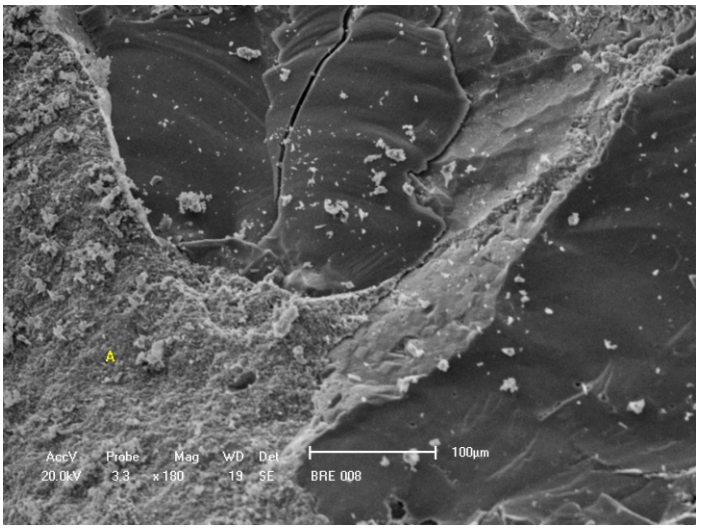

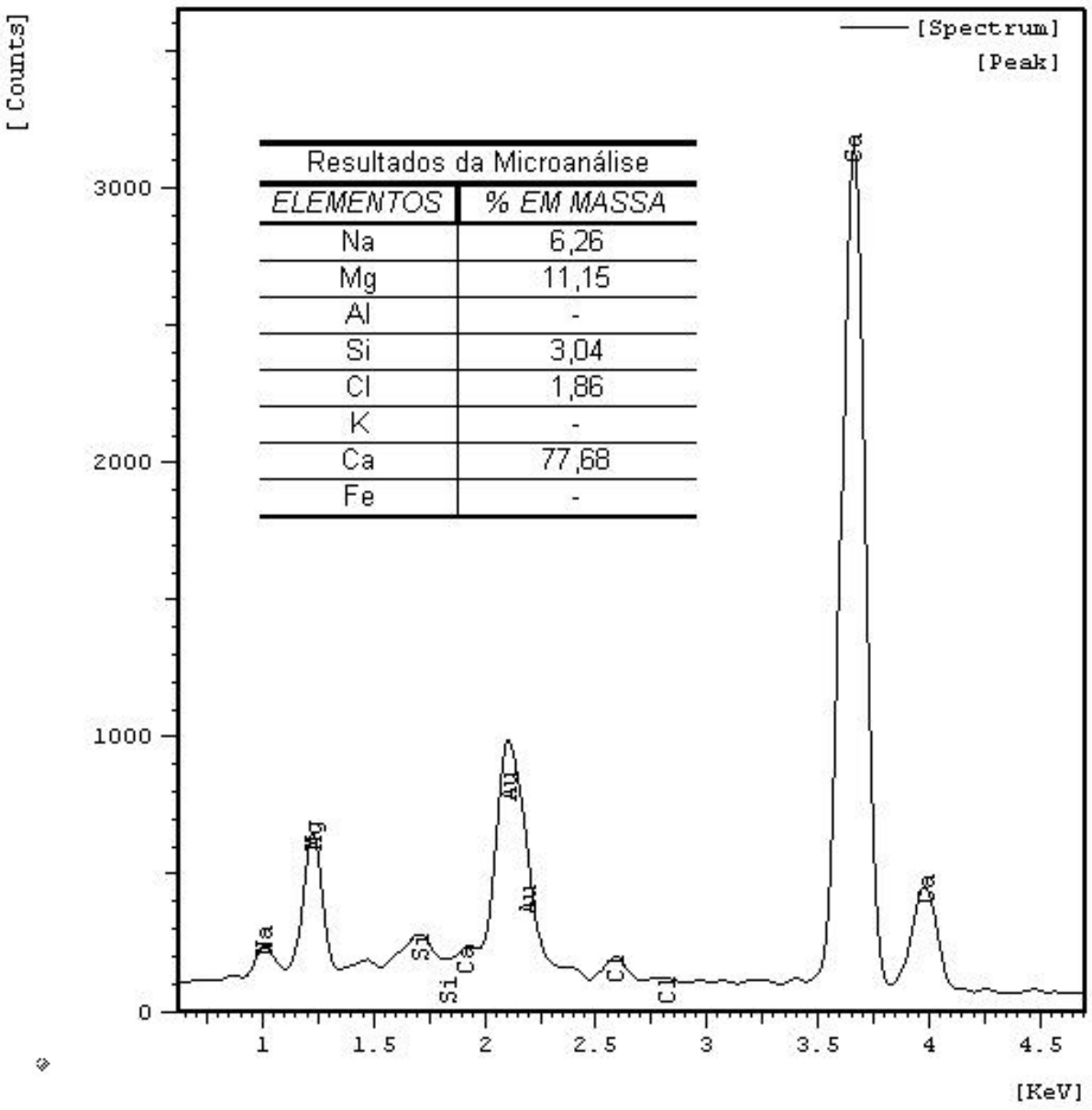

Resultados da Microanálise	
ELEMENTOS	*% EM MASSA*
Na	6,26
Mg	11,15
Al	-
Si	3,04
Cl	1,86
K	-
Ca	77,68
Fe	-

FIGURA 7

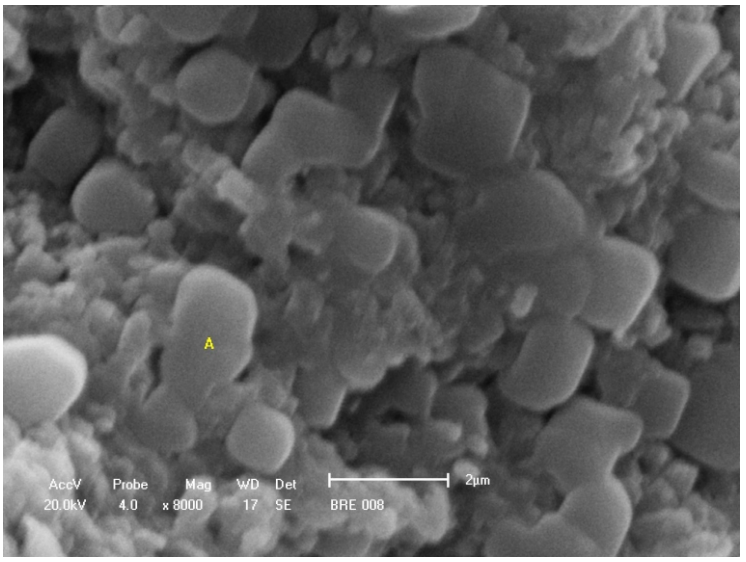

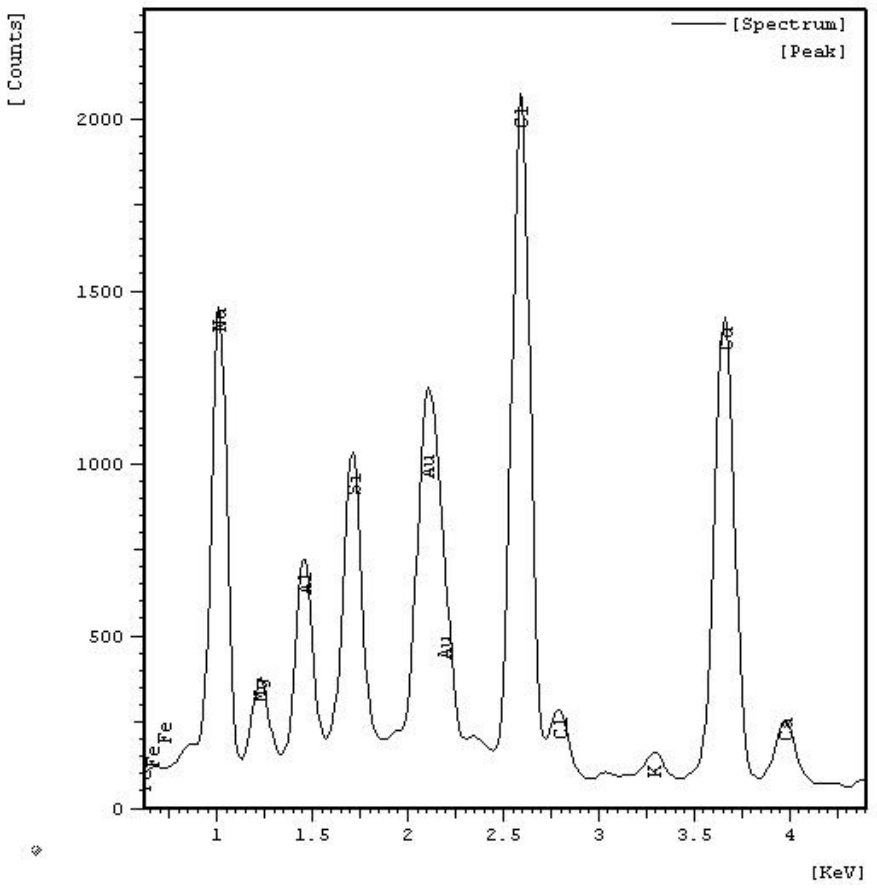

Resultados da Microanálise	
ELEMENTOS	*% EM MASSA*
Na	18,85
Mg	3,84
Al	7,01
Si	9,04
Cl	25,66
K	1,19
Ca	19,73
Fe	14,67

FIGURA 8

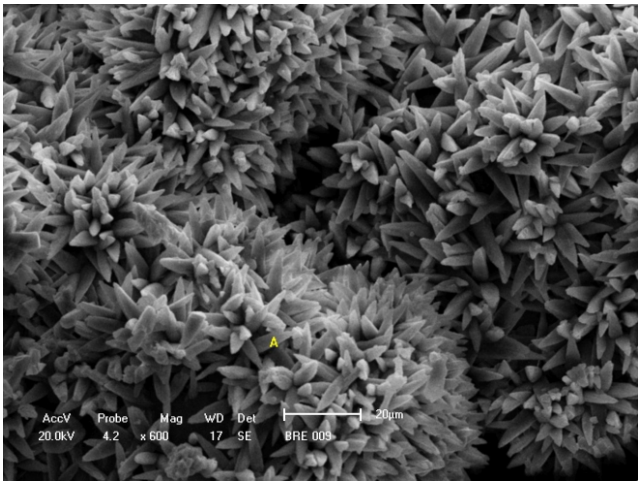

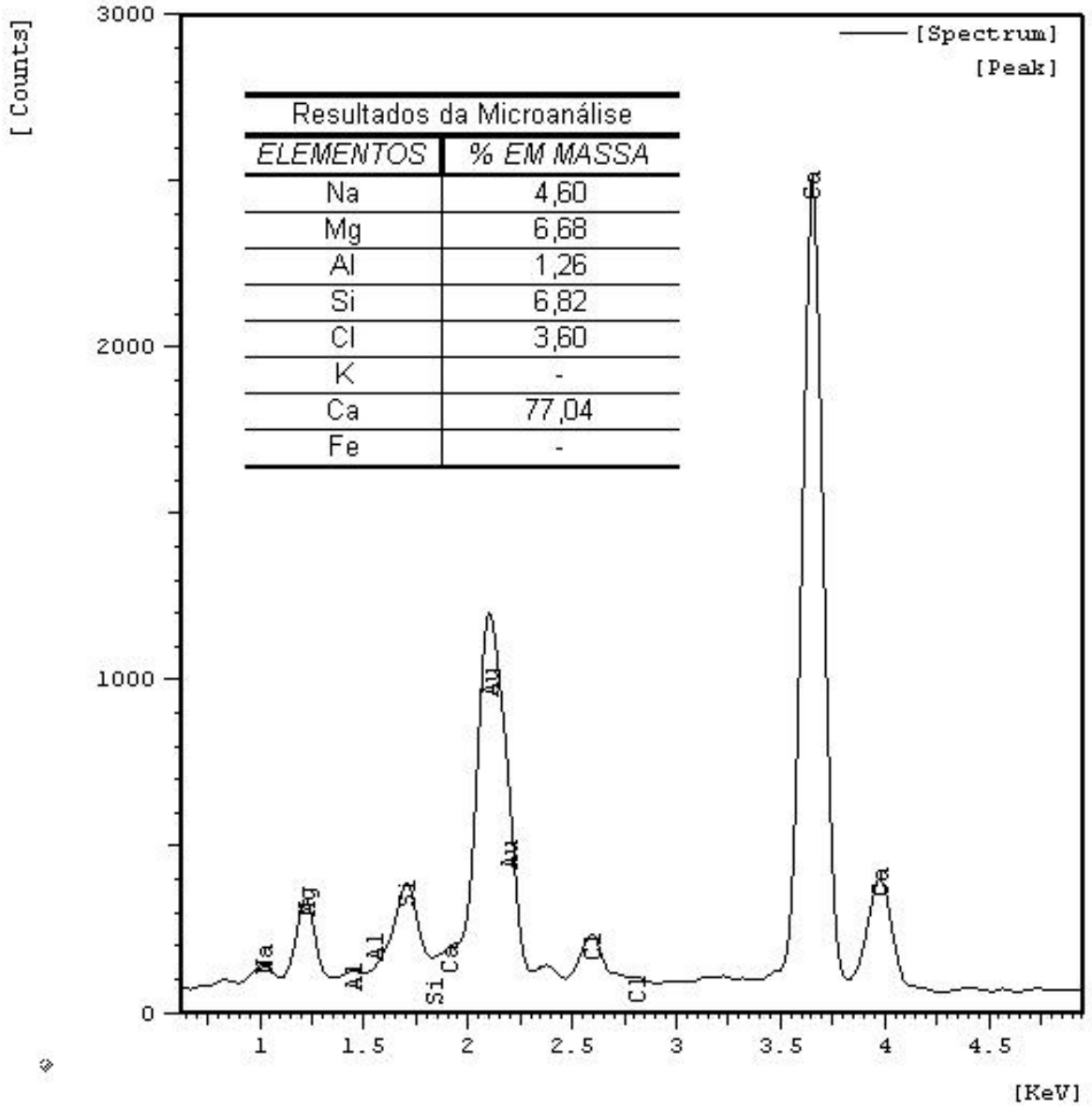

Resultados da Microanálise	
ELEMENTOS	*% EM MASSA*
Na	4,60
Mg	6,68
Al	1,26
Si	6,82
Cl	3,60
K	-
Ca	77,04
Fe	-

FIGURA 9

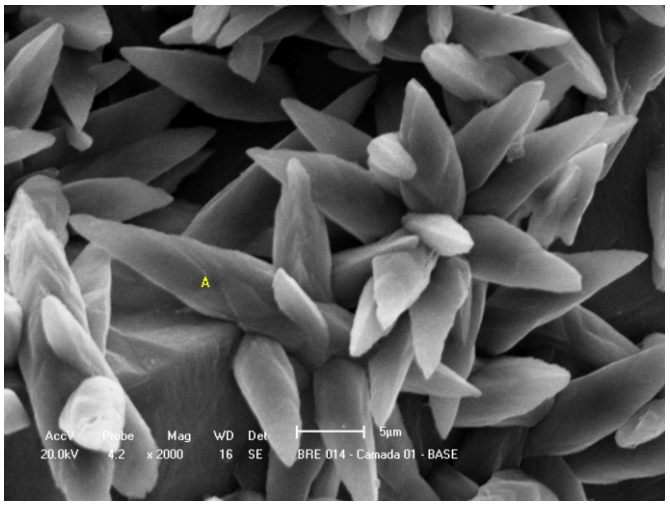

Resultados da Microanálise	
ELEMENTOS	*% EM MASSA*
Na	3,37
Mg	8,82
Al	1,66
Si	16,25
Cl	1,27
K	-
Ca	68,63
Fe	-

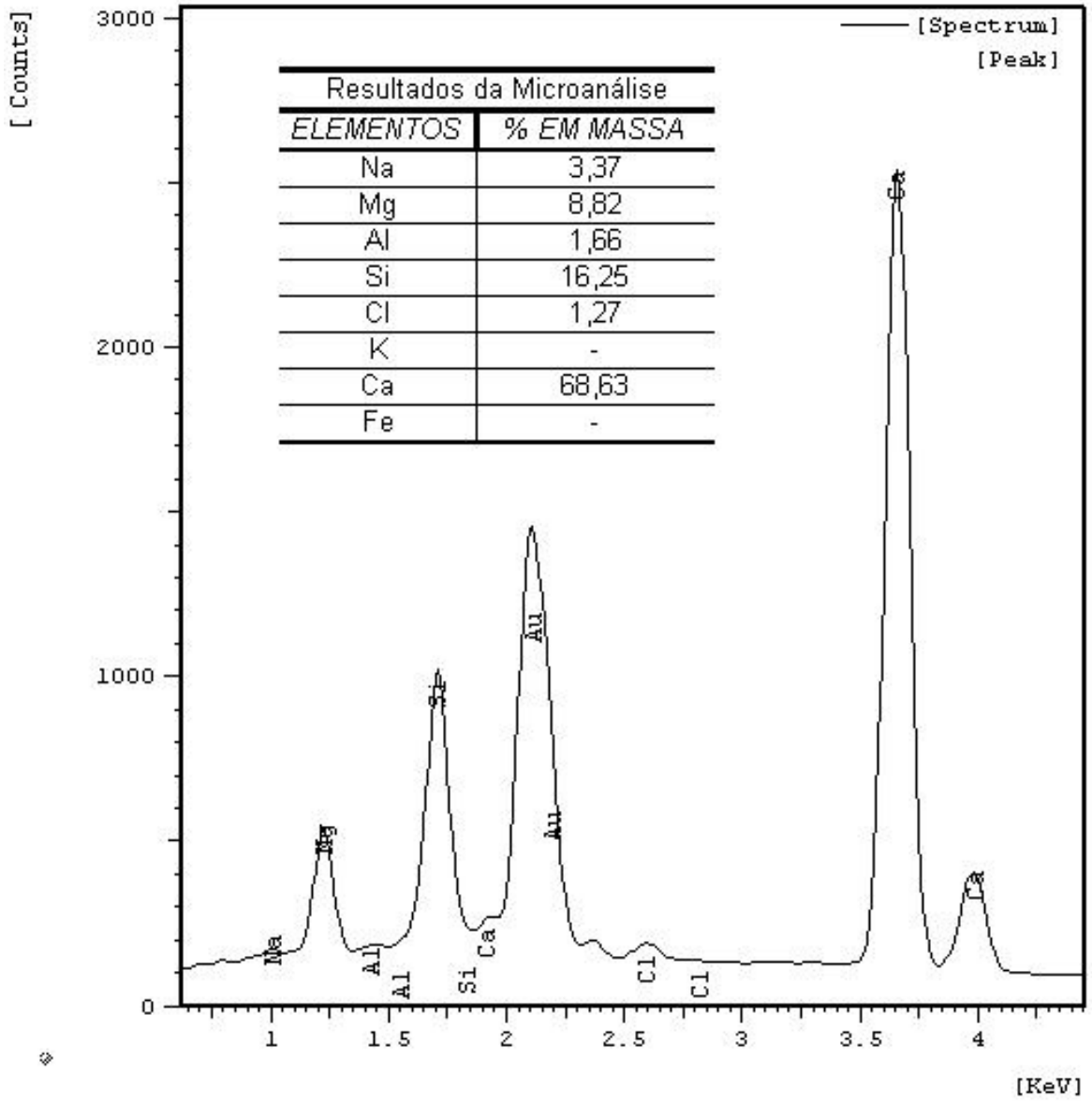

FIGURA 10

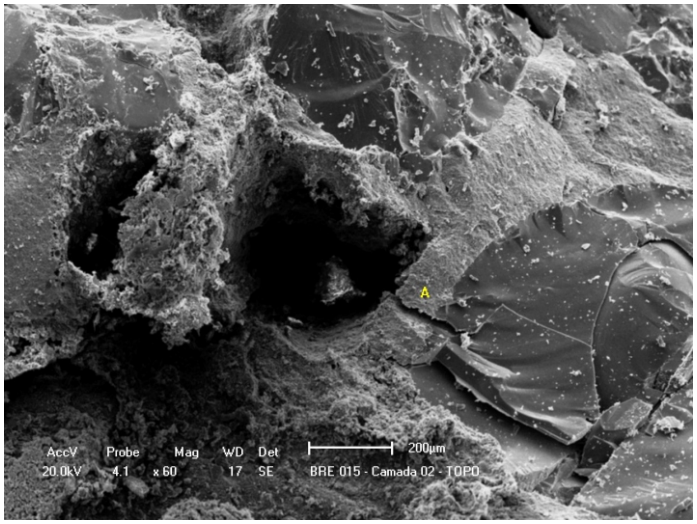

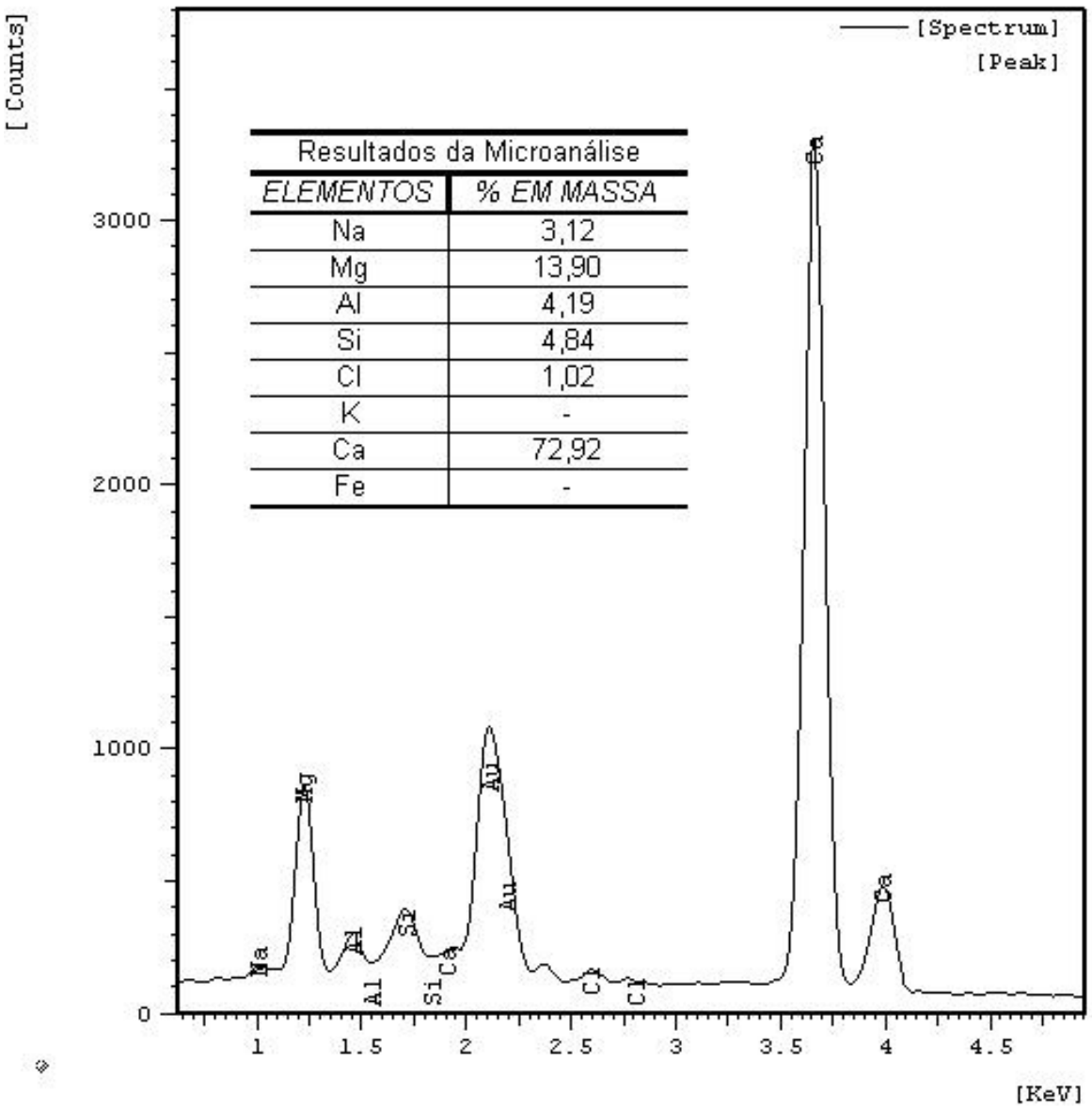

Resultados da Microanálise	
ELEMENTOS	*% EM MASSA*
Na	3,12
Mg	13,90
Al	4,19
Si	4,84
Cl	1,02
K	-
Ca	72,92
Fe	-

FIGURA 11

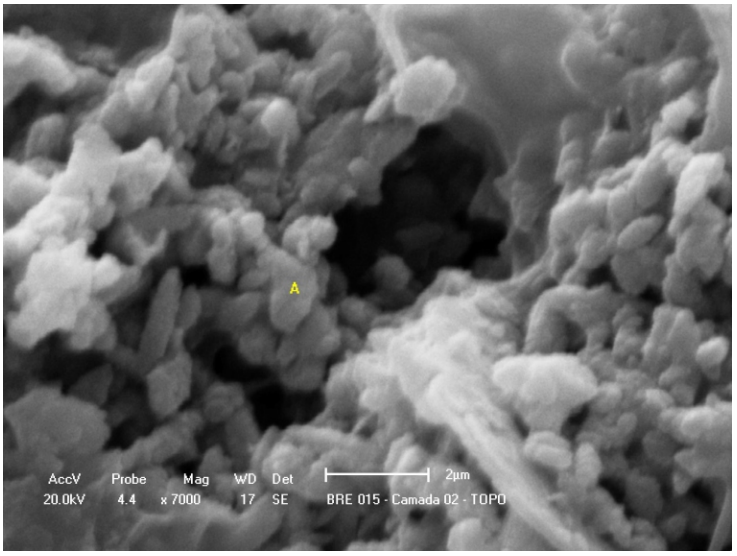

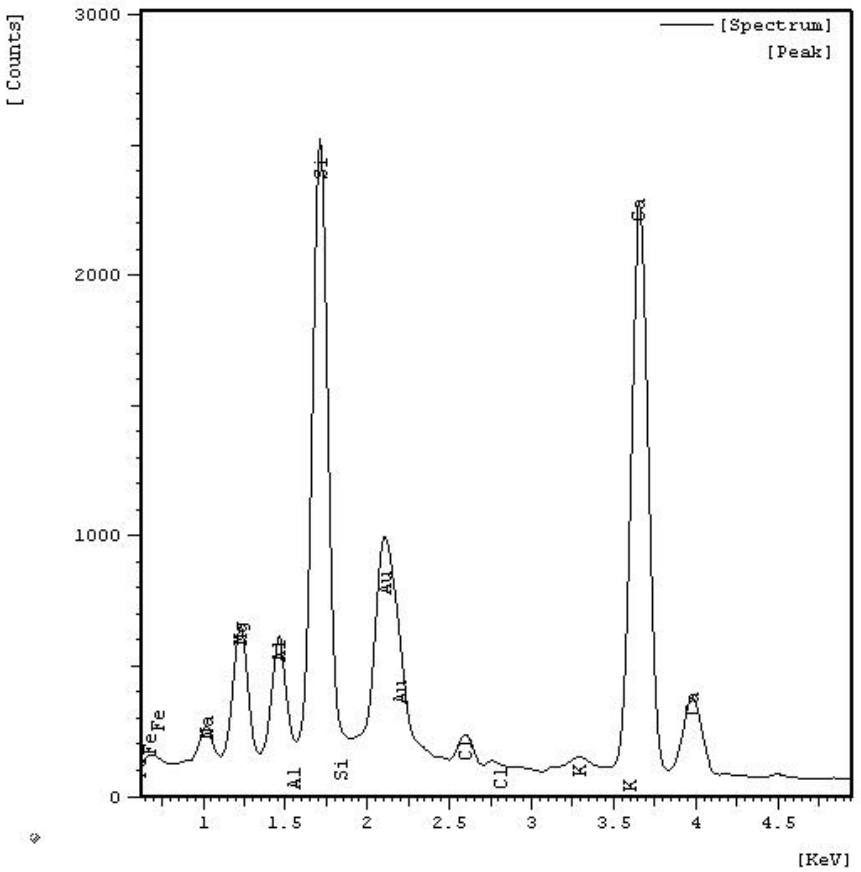

Resultados da Microanálise	
ELEMENTOS	*% EM MASSA*
Na	3,84
Mg	7,19
Al	7,28
Si	29,36
Cl	2,25
K	1,13
Ca	43,47
Fe	5,48

FIGURA 12

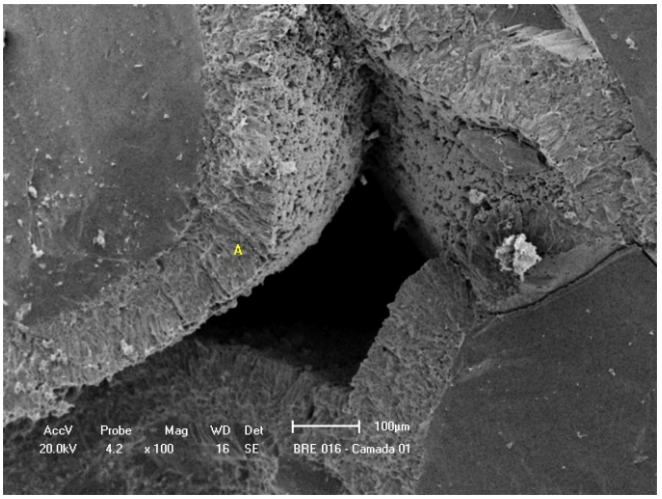

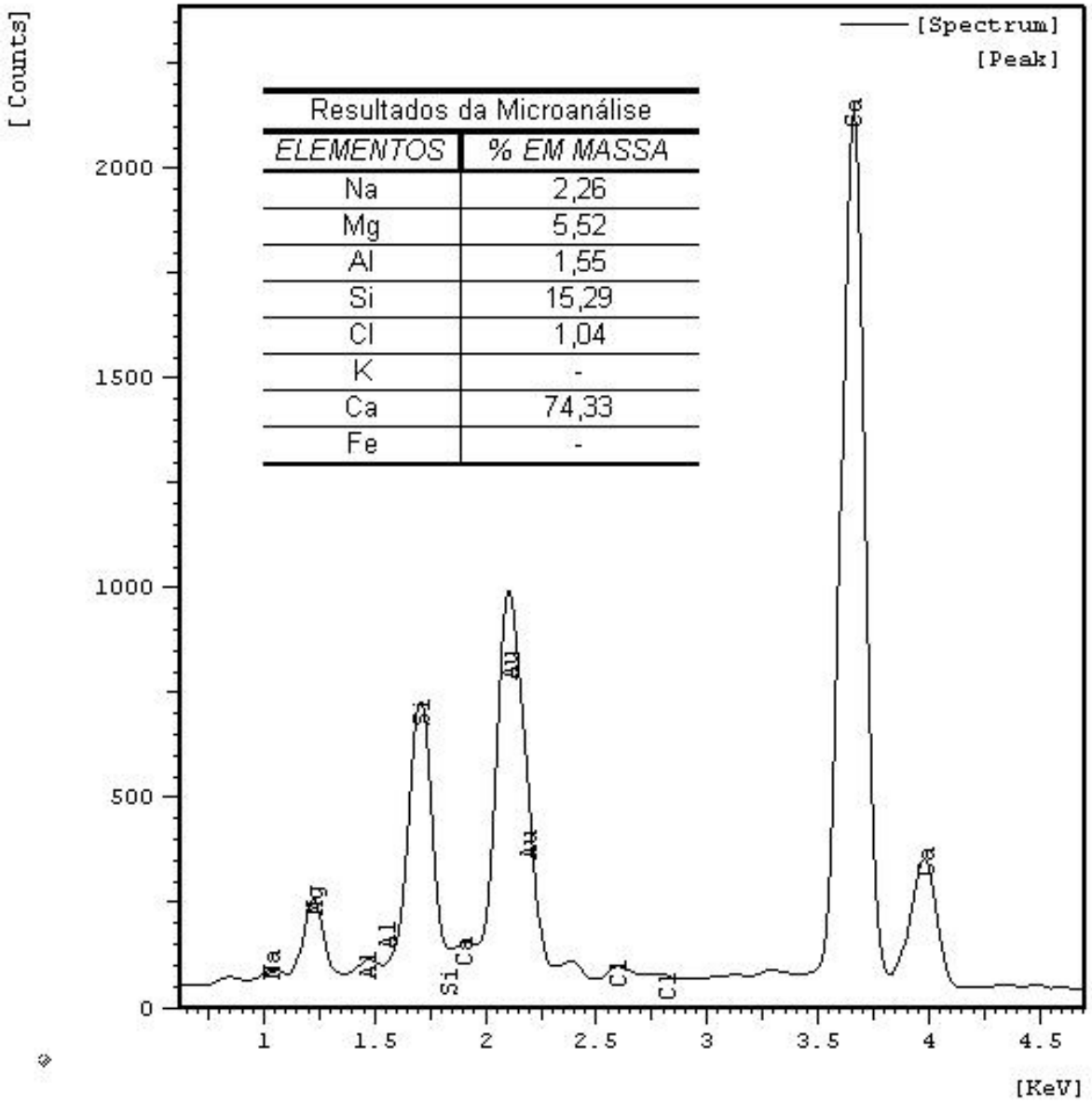

Resultados da Microanálise	
ELEMENTOS	*% EM MASSA*
Na	2,26
Mg	5,52
Al	1,55
Si	15,29
Cl	1,04
K	-
Ca	74,33
Fe	-

FIGURA 13

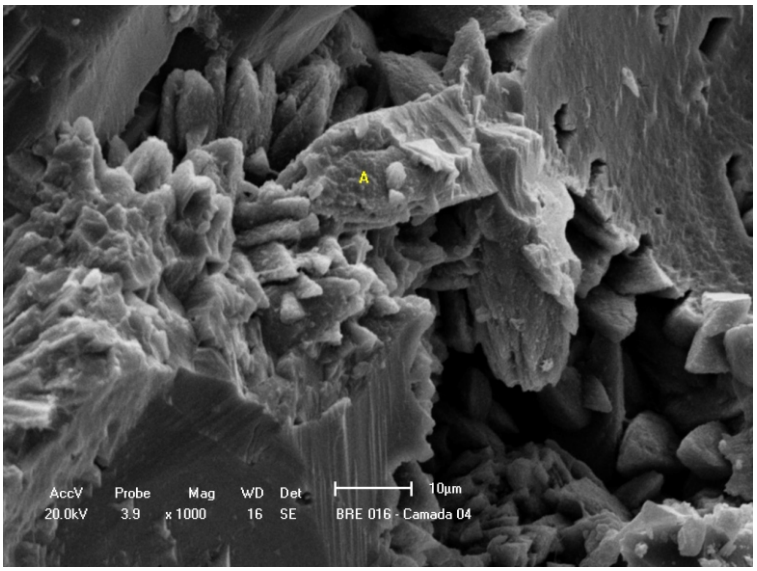

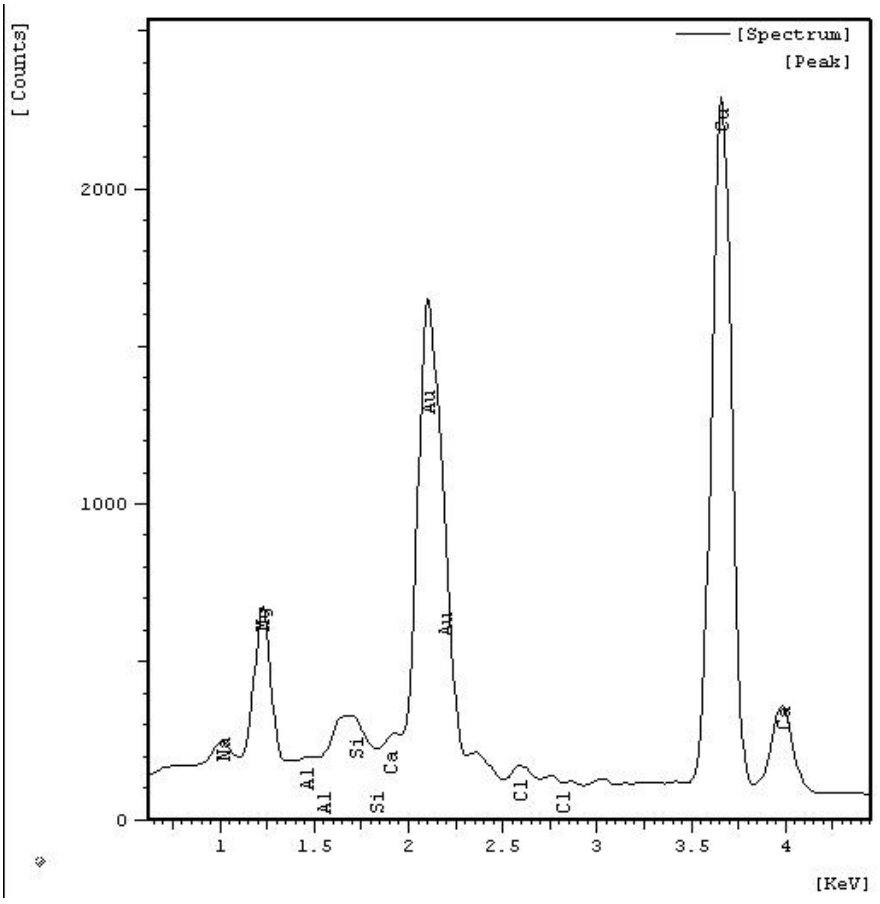

Resultados da Microanálise	
ELEMENTOS	*% EM MASSA*
Na	6,58
Mg	14,85
Al	2,48
Si	4,67
Cl	1,32
K	-
Ca	70,11
Fe	-

FIGURA 14

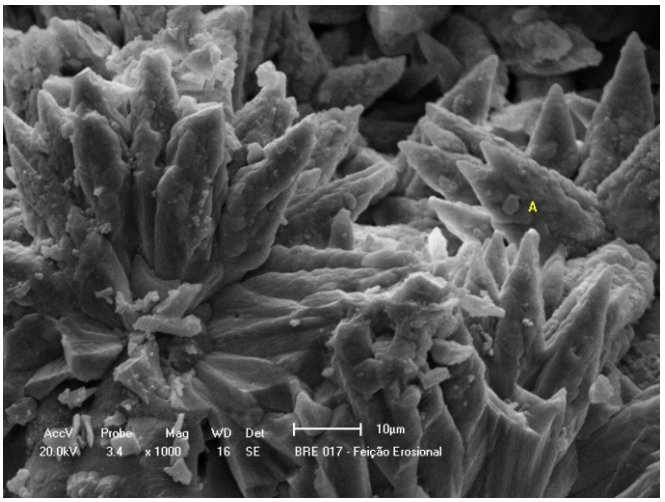

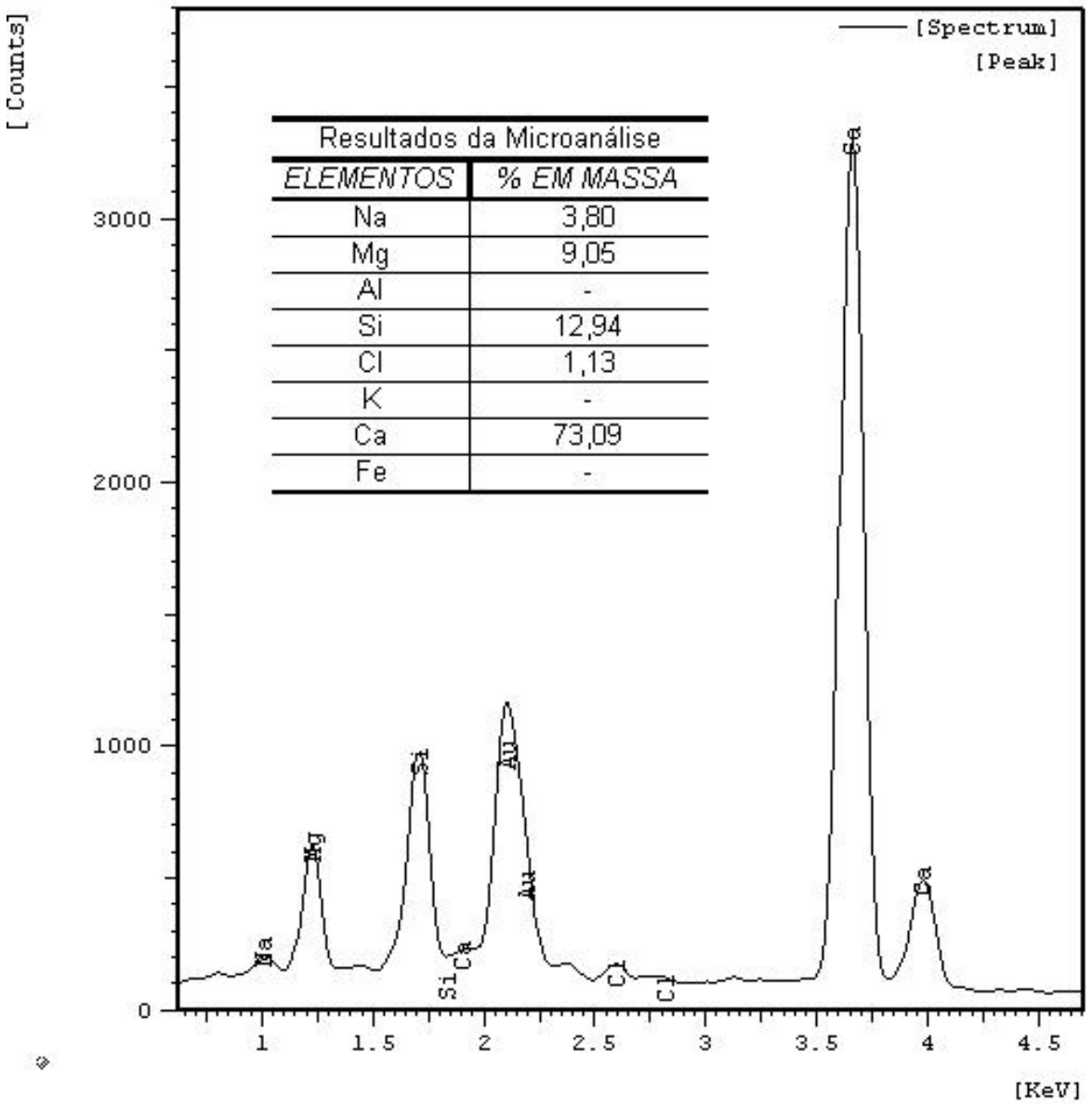

Resultados da Microanálise	
ELEMENTOS	*% EM MASSA*
Na	3,80
Mg	9,05
Al	-
Si	12,94
Cl	1,13
K	-
Ca	73,09
Fe	-

FIGURA 15

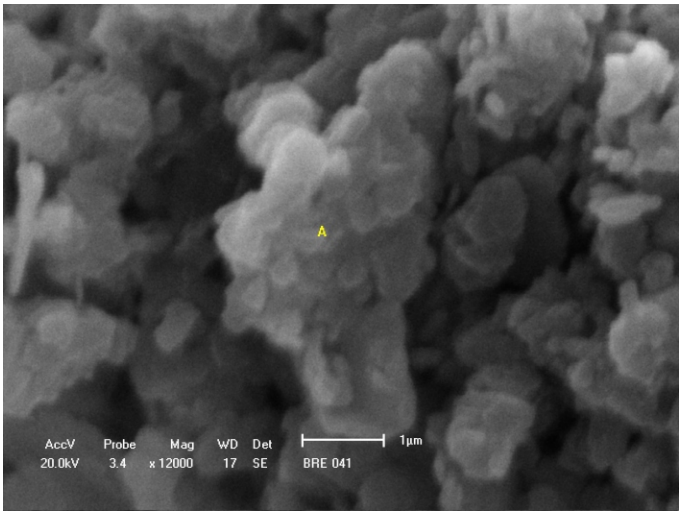

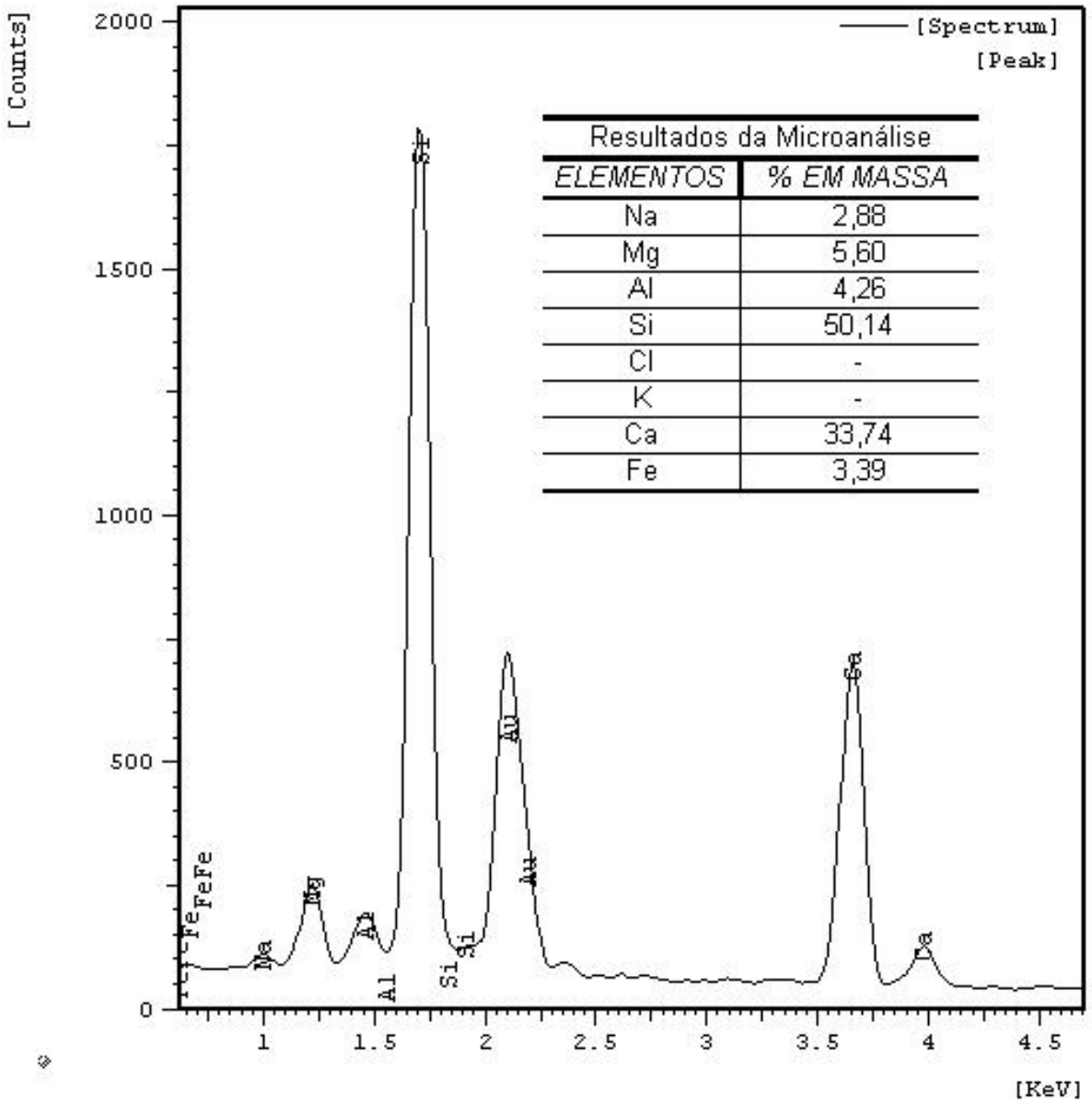

Resultados da Microanálise	
ELEMENTOS	*% EM MASSA*
Na	2,88
Mg	5,60
Al	4,26
Si	50,14
Cl	-
K	-
Ca	33,74
Fe	3,39